Natural variation in nutrient homeostasis mechanisms of *Chlamydomonas reinhardtii*

PhD thesis

Sara Marina Cardoso Esteves

University of Liège

Faculty of Sciences
Department of Life Sciences
InBioS – PhytoSystems
Laboratory of Translational Plant Biology

Natural variation in nutrient homeostasis mechanisms of *Chlamydomonas reinhardtii*

PhD thesis by Sara Marina Cardoso Esteves
Submitted on the 21st of November 2022
To obtain the degree of Doctorat en Sciences
Faculty of Sciences
Department of Life Sciences

Supervisor: Pr. Marc HANIKENNE
Co-supervisor: Dr. Tom DRUET
Jury: Prof. C. REMACLE (ULiège, President), M. AARTS (Wageningen UR), O. DE CLERCK (UGent), H. VANDERSCHUREN (KULeuven), F. BOUCHE (ULiège, Secretary)

Table of Contents

❖ List of figures and tables

❖ Supplemental files

Figure S.III.6 Distribution of the Na, P and Zn accumulation phenotypes of the MAGIC progeny in different media (TAP, TAP-Ca, -S, -Cu, -Fe and –Mn).

Figure S.III.7 Pairwise scatter plot matrix, histogram, and Pearson correlation coefficients between the 8 batches used to phenotype the MAGIC progeny (biomass-related traits).

Figure S.III.8 Pairwise scatter plot matrix, histogram, and Pearson correlation coefficients between the 8 batches used to phenotype the MAGIC progeny ([Ca], [Cu], [Fe]).

Figure S.III.9 Pairwise scatter plot matrix, histogram, and Pearson correlation coefficients between the 8 batches used to phenotype the MAGIC progeny ([K], [Mg], [Mn]).

Figure S.III.10 Pairwise scatter plot matrix, histogram, and Pearson correlation coefficients between the 8 batches used to phenotype the MAGIC progeny ([Na], [P], [Zn]).

Figure S.III.11 Pairwise scatter plot matrix, histogram, and Pearson correlation coefficients between the 8 batches used to phenotype the MAGIC progeny (photosynthesis-related).

Figure S.III.12 Pearson correlation between the 2 replicates used to phenotype the MAGIC progeny, colour-coded by batch.

Figure S.III.13 Heatmap of the scaled phenotypic data, clustered by design. (A) Photosynthesis-related traits, (B) biomass-related traits, (C) ionome traits.

Figure S.III.14 Distribution of each founder's contribution (A) to each F8 line and (B) at each genomic position.

Figure S.III.15 Genetic correlations within each of the 14 phenotypes measured in each of the 6 different media.

Figure S.III.16 Genetic correlations within each of the 6 media used to measure each of the 14 phenotypes. (A) TAP, (B) -Ca, (C) -S.

Figure S.III.17 Genetic correlations within each of the 6 media used to measure each of the 14 phenotypes (A) -Cu, (B) -Fe, (C)-Mn.

Table S.II.1. Description of the 24 Chlamydomonas strain panel.

Table S.II.2. Composition of the single element deficiency TAP media.

Table S.II.3. Deficiency marker gene description and qRT-PCR primers.

Table S.III.1. Summary statistics of length of IBD segments shared between founder strains (length is expressed in kb).

Dataset S.II.1. Descriptive statistics of day 4 optical density measurements in all tested media (Support to Figures 1A and 2A).

Dataset S.II.2. Descriptive statistics of the growth curves in all tested media (Support to Figures S2, S3 and S4).

Dataset S.II.3. Descriptive statistics of the ionome (Support to Figures 1C-D)

Dataset S.II.4. Top and bottom 3 strains for all measured parameters at day 4 (Support to Figure 2B).

Dataset S.II.5. Descriptive statistics of the relative nutrient concentrations under nutrient deficiency (Support to Figure 3).

Dataset S.II.6. Heatmap dataset (Support to Figures 4, S5 and S6)

Dataset S.II.7. Strains CC-1373 and CC-2290 nutrient concentrations in TAP and -Mn (Support to Figure S7).

Dataset S.II.8. Statistic differences for rETR and NPQ for strains CC-1373 and CC-2290 in TAP and -Mn (Support to Figure 5C-D).

Dataset S.II.9. Strains CC-2343 and CC-4414 nutrient concentrations in TAP and -Fe (Support to Figure S9).

Dataset S.II.10. Statistic differences for rETR and NPQ for strains CC-2343 and CC-4414 in TAP and -Fe (Support to Figures 5C-D).

Dataset S.III.1 List of genes present in the confidence interval of the 67 mineral nutrition QTLs mapped. QTL numbers are the same as in Table III.12-13

❖ Thesis motivation and outline

Algae is an umbrella term used to describe, with exceptions, most primary producers in aquatic systems, which have chlorophyll as their main pigment, do oxygenic photosynthesis and lack differentiated tissues.

From their first use as food, feed and fertilisers, to the more recent applications as biomaterials, cosmetics, nutraceuticals and for bioremediation, algae have been exploited for centuries. Yet, despite the identification of more than 150 thousand species of algae, only a small fraction is routinely used in research and industry.

Often, algae are placed under abiotic stress to simply study their response or increase production of compounds of interest. Stress allows not only exploring phenotypic variability, but also the genetic architecture of the stress responses.

This thesis aims to study the influence of natural variation in *Chlamydomonas reinhardtii* (Chlamydomonas) on nutrient homeostasis and is centred on three major axes: the phenotypic differences among individuals of one species (i.e. natural variation in complex traits), how nutrients are balanced during nutrient deficiency and the model microalga Chlamydomonas.

In **Chapter I**, natural variation and nutrient homeostasis will be generally described in the first chapter. The study organism, Chlamydomonas, will be introduced afterwards, and framed in the scope of the previous points.

The **Chapter II** focuses on the description of natural variation when facing nutrient deficiency in Chlamydomonas.

The generation of a recombinant population using a MAGIC design, its phenotyping upon nutrient deficiency and QTL mapping to identify the major determinants of its variation will be approached in **Chapter III**.

A general conclusion and future perspectives will be presented in **Chapter IV**, and the methods used to perform the research presented in this thesis will be described in **Chapter V**. In **Chapter VI** a review article on iron homeostasis in plants and algae is presented **Supplemental figures and data**, due to their size, can be found in a separate file, at the university repository (Orbi).

❖ Abstract

Natural variation in living organisms is essential in stress responses and adaptation to new environments. Many of the traits presenting natural variation are regulated by a complex genetic architecture of genes with small to moderate effects. Consequently, understanding which variants impact traits of medical, industrial or agronomical interest is fundamental. In photosynthetic organisms, the production of biomass is a complex process which results from interactions among mineral nutrition, photosynthesis and the environments. Mineral nutrients in particular, have wide range of functions in the cell, hence cells have evolved an intricate network to maintain intracellular nutrient concentrations within physiological range and avoid nutrient deficiency or excess.

Chlamydomonas reinhardtii (Chlamydomonas) is a unicellular eukaryotic haploid microalga used as a model organism for the study of for instance photosynthesis, nutrient homeostasis, or flagella characterisation. Previous work within the Chlamydomonas community highlighted the extent of genetic and phenotypic variation among strains, making it a suitable species to study natural variation in nutrient homeostasis. This thesis focusses on the study of intraspecific variation in Chlamydomonas nutrient homeostasis, in both field and laboratory isolates, then on creating and leveraging a Multiparent Advanced Generation Inter-Crossing (MAGIC) population to dissect the genetic architecture of traits related to nutrient homeostasis.

First, a 24-strain Chlamydomonas panel was grown under mixotrophy (control), autotrophy, macronutrient (-Ca, -Mg, -N, -P, -S) or micronutrient (-Cu, -Fe, -Mn, -Zn) deficiency, and differences in growth and ionome were quantified. Globally, variation at the growth level was minor compared to that observed at the ionome level, and greater variation could also be found among the field isolates than among the laboratory strains. The comparison of diverging pairs of field strains revealed different strategies to manage nutrient deficiency, as underscored by the differential expression of key marker genes and impact on photosynthesis.

Secondly, taking advantage of the genetic and phenotypic variation observed previously, 8 strains were selected as founder lines of a MAGIC design. Biallelic crosses were performed during 8 generations, during which the contribution of each founder in each progeny was reduced by means of sexual recombination, creating 768 F8 progeny strains which are mosaics of the founders. Progeny lines were then sequenced and phenotyped under mixotrophy and nutrient deficiency (-Ca, -S, -Cu, -Fe, -Mn) to map Quantitative Trait Loci (QTL) related to mineral nutrition. The majority of the mapped QTLs was linked to the ionome (41) or photosynthesis (21) under nutrient deficiency. Many of the mapped QTLs contained a small

number of genes or genes known to be involved in nutrient homeostasis, worth investigating in further studies.

Altogether the work developed in this thesis allowed a deeper understanding of the different strategies applied by field and laboratory strains in the management of nutrient deficiency, as well as the establishment of a MAGIC design using Chlamydomonas, and the mapping of QTLs related to mineral nutrition.

Keywords: *Chlamydomonas reinhardtii*, intraspecific variation, mineral nutrition, nutrient deficiency, ionome, MAGIC design, QTL mapping

I. Introduction

Living organisms present natural variation for several traits as a mean to overcome adverse environments. Studying this phenomenon within a species has proved a powerful tool to examine diverse biological processes, namely nutrient homeostasis.

In this first chapter, natural variation and its implications will be presented in point A, followed by a brief definition of nutrients, their function and homeostasis, as well as a framing in the context of natural variation in point B. Lastly, in point C, *Chlamydomonas reinhardtii* will be introduced in the scope of its establishment as a model microalga used to study cellular processes, such as photosynthesis and nutrient homeostasis, with examples of the importance of considering natural variation in *C. reinhardtii* studies.

A. Natural variation

Individuals within a species are expected to present variations in their genetic make-up. This variation results in an assortment of traits which, in some cases, will help colonize novel environments and resist to stress (Godhe & Rynearson, 2017; Violle et al., 2012). A few examples of complex traits presenting natural variation are skin pigmentation in humans, plant tolerance to polluted sites or the size of a fish.

Intraspecific trait differences can result from genetic variation or phenotypic plasticity (Violle et al., 2012). Phenotypic plasticity can help buffer the effects of selection, acting as a precursor to adaptation, but remains subject to selective pressures (Delker & Quint, 2011; Draghi & Whitlock, 2012; Gulisija et al., 2016). Several authors hypothesize that phenotypic adaptation is a result of independent polygenic adaptation, and that the existing hereditary (i.e. standing) variation will allow the population to adapt to the new environment (Barghi et al., 2020; reviewed in Pritchard & di Rienzo, 2010).

1. Implications for model organisms

In a laboratory context, minimal influence of the genetic background is essential when studying the mechanisms implicated in biological processes, when the goal is not the actual study of genetic variation. Consequently, model organisms, such as bacteria (*Escherichia coli*), yeast (*Saccharomyces cerevisiae*), algae (*Chlamydomonas reinhardtii*), thale cress (*Arabidopsis thaliana*) or zebrafish (*Danio rerio*), with specific genetic backgrounds (i.e. specific strains or accessions) are chosen when conducting research. In addition, gene-environment interactions are minimized in such laboratory set-ups leading all individuals to have the same sensitivity to the environmental pressure (Crusio, 2007). In contrast, heritable traits linked to fitness are subject to selective pressures in nature, leaving only the most favourable variants (Fischer, 1930).

Model strains can, however, fail to represent their species, by artificial selection or accumulation of mutations advantageous to laboratory life (Gasch et al., 2016) during domestication. An example of this is the study by Warringer et al., (2011), where the universal *S. cerevisiae* type strain represents, in fact, an outlier among both wild and industrial isolates, despite studying strains with different population histories and wide trait variation.

The integration of natural variation in experimental designs, from the detection of the frequency of an allele for a gene of interest to the incorporation of strains with different genetic backgrounds (Gasch et al., 2016), can help shed a light on how much the laboratory strains represent the species. Furthermore, the utilisation of new strains with different phenotypes may offer a workaround to some research bottlenecks.

2. Study of natural variation

Some complex traits, which are influenced by many polymorphisms (in many genes) with small or moderate effects, stand out as being noteworthy in a variety of fields, such as agriculture (e.g., Faralli & Lawson, 2020 - crop yield), industry (e.g., Cubillos, 2016 - fermentation in yeast) and medicine (e.g., Siao et al., 2020 - malaria parasite resistance). Prior to taking advantage of traits of interest however, it is important to characterize their genetic architecture.

Screening individuals with different genotypes for phenotypes of interest, in a forward genetics approach, has proven to be a powerful mean to study trait heritability as well as variation. While mapping from genotype to phenotype (mutants, reverse genetics) represents a possible middle ground for quantitative and molecular genetics, mapping from phenotype to genotype (forward genetics) applies statistical methods to identify chromosomal regions contributing the variation observed (Mauricio, 2001). Two powerful tools connect genotype and phenotype: Genome-Wide Association Studies (GWAS) and Quantitative Trait Loci (QTL) (GWAS: Jorde, 2000; Kruglyak, 1999; QTL: Lander & Botsteins, 1989; Paterson et al., 1988; GWAS/QTL: Plissonneau et al., 2017).

QTL mapping (**Figure I.1. A-C**) focuses on the detection of genomic regions associated with phenotypes and requires the generation of an experimental mapping population (see below) (**Figure I.1. A**) (Alonso-Blanco et al., 2006; Miles & Wayne, 2008). The connection between the quantitative trait and a genetic marker can be made using statistical methods with different degrees of complexity, ranging from single marker tests to interval mapping and multiple QTL mapping, to test if the observed phenotype is independent of the genotype (reviewed in Doerge, 2002). The strength of association can be assessed with a logarithm of the odds (LOD) score, comparing the likelihoods of the data in models with or without QTL at the tested position (**Figure I.1. B**) (van Ooijen, 1999). The mapping resolution depends on the number of recombinations in the design and can be improved by

increasing the size of the mapping population or the number of generations, so that it contains a number of genes small enough for functional studies (Glazier et al., 2002).

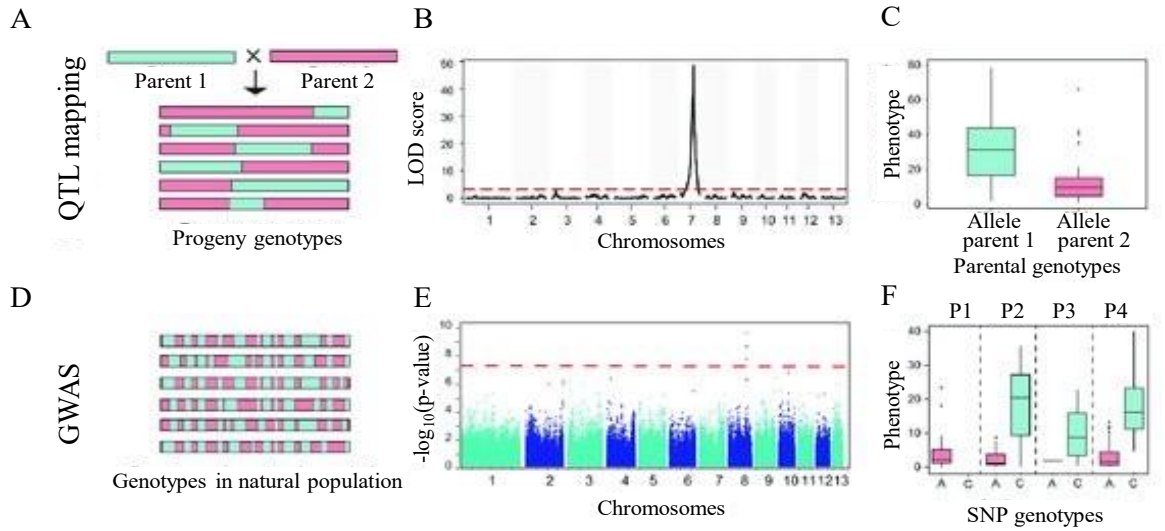

Figure I.1 Identifying genes underlying phenotypic traits using QTL mapping (A-C) and GWAS (D-F). Chromosomes in QTL mapping are composed of large blocks inherited from crossing different parents (A). The block length is determined by the amount of recombination between the parental chromosomes. In contrast, chromosomes in field populations underwent numerous rounds of recombination (D). Due to this, linkage disequilibrium decays rapidly in GWAS mapping populations. (B) Result of a QTL mapping with a QTL with a high logarithm of the odds (LOD) ratio located on chromosome 7. The red dashed line shows the significance threshold. (E) In this example of GWAS mapping, the Manhattan plot shows a significant association on chromosome 8 above the Bonferroni significance threshold. Association of phenotypes and genotypes at a significant QTL (C) and a GWAS SNP (F). The GWAS included populations from four different populations (P1-4). [Adapted from Plissonneau et al., 2017].

GWAS (**Figure I.1.D-F**), on the other hand, is used to map genetic variants associated with phenotypes of interest in unrelated individuals (Figure I.1.D) and relies on linkage disequilibrium (LD) to establish a correlation between these traits and a candidate polymorphism. Linkage disequilibrium refers to the fact that two alleles at different loci are not independently associated (not randomly associated) and is minimal in the absence of selection pressure when genes are expected to recombine at random (Sved & Hill, 2018). GWAS p-values are usually shown in the y-axis of a Manhattan plot, following a $-\log_{10}$ transformation, in function of the SNP position along the chromosome in the x-axis (**Figure I.1.E**), and SNPs whose p-value are below a "genome-wide significance" threshold (Ehret, 2010) indicate the presence of a true association in the vicinity. Nonetheless, GWAS does not allow the distinction of the causative polymorphism, and is influenced by the variant effect, mapping panel size and composition, quality of the genotyping, relatedness of the panel and the population structure (reviewed in Korte & Farlow, 2013). Despite using different methodologies to identify genome regions correlating with the phenotype of interest and the consequent limitations (summarized in **Table I.1**), QTL mapping and GWAS can be used together to minimize their limitations. This approach has been used in diverse research, such as study of flowering time of *A. thaliana* in nature (Brachi et al., 2010; Zhao et al., 2007), capsaicinoid content in *Capsicum spp* (Han et al., 2018), branch number in *Brassica napus* (He et al., 2017) or to test lung cancer susceptibility in mice (Manenti et al., 2009), where it allowed the selection of relevant loci by

narrowing QTL intervals, as well as reducing the discovery rate of both false-negatives and false-positives.

Table I.1 Comparison between QTL and GWAS mapping.

QTL	GWAS
Polymorphic variation markers [e.g., single nucleotide polymorphism (SNP), copy number variation (CNV), small insertions and deletions (Indels)]	
Linkage mapping	Linkage disequilibrium
Quantitative (continuous) traits	Qualitative (discrete) and quantitative traits
Recombinant populations	Unrelated individuals
Limitations	
Mapping ability related to the amount of recombination	Selection of suitable populations
Limited to polymorphisms in parental lines	Related individuals reduce resolution / create artifacts
	Rare variants are less often detected

a) Quantitative trait variation

Many traits of interest, such as biomass and metabolite production, or fitness disorders, are the result of variation in multiple genes, gene-gene or gene-environment interactions. Unlike classical Mendelian traits, these interactions result in quantitative traits, a non-discrete gradient of phenotypes (Crusio, 2007). The biometric attributes were broadly unified according to Mendel's discrete inheritance scheme by Fisher (1919), who became one the parents of modern evolutionary quantitative genetics.

Mapping populations designed for QTL studies are obtained by crossing at least two genetically diverse lines and divide in two types: *primary*, cross of two homozygous lines with different phenotypes and/or geographic origins, and *secondary*, cross of lines issued from a mapping design (better suited for fine mapping). According to Singh & Singh (2015), there are 12 types of primary mapping populations, 6 of which are summarised in **Table I.2**. The strategy choice is usually based on the type of reproduction, time available, as well as traits and resolution of interest.

Table I.2 Examples of primary mapping populations for diploid organisms [as described by Singh & Singh (2015)]

Population	Generation	Use	Remarks
F_2	Selfing or sib-mating of the F_1 individuals from a cross between the selected parents	Preliminary mapping of markers and oligogenes (genes that produce or significantly affect the expression of a qualitative heritable characteristic)	Each F_2 population is genetically different from the others Cannot be evaluated in replicated trials* Ephemeral* *unless asexually propagated
F_2-derived F_3 ($F_{2:3}$)	Selfing the F_2 individuals for a single generation	Mapping of both oligogenes and QTLs	Heterogeneous due to segregation of one or more genes Ephemeral
Recombinant inbred lines (RILs)	Homozygous lines produced by continuous inbreeding/selfing of individual F_2	Mapping of both oligogenes and QTLs	Inbred 5-8 generations Homozygous Only additive genetic variances can be estimated Perpetual
Near-isogenic lines (NILs)	Produced by BC in which a donor parent (DP) having the trait/allele of interest is crossed with a recurrent parent (RP)	QTL mapping Functional genomics	Pairs of homozygous lines identical in genotype, except for a single gene/locus Homozygous Perpetual
Advanced intercross lines (AIL)	Intermating of the F_2 individuals and subsequent generations	QTL mapping	Maintains heterozygosity in the population Improves mapping resolution

These mapping populations can then be used to identify a QTLome: the collection of all QTLs mapped for a determined trait in a species (Salvi & Tuberosa, 2015). For each trait, the number of QTLs, their mapping position, as well as the size, type and interactions of the genetic effects are recorded. Following the discovery of the QTLome and the creation of a database, this should be characterized in terms of QTL/gene (G) combinations relevant to optimize traits in specific environments (E) and management strategies (M) (GxExM interactions, see Cooper et al., 2021 for a review on crops), expected behaviour of the genotype (QTL-based modelling), and isogenic hybrid behaviour (QTL isogenization). A fully characterized QTLome can then be used for molecular marker-assisted breeding and strain improvement, or locus of interest can be cloned for further studies, such as genetic engineering and discovery of new alleles. The different steps are summarized in **Figure I.2**.

b) Multiparent Advanced Generation Inter-Cross (MAGIC) design

The MAGIC concept currently applied to plants is based on the "heterogeneous stock" used to map traits in mice (Churchill et al., 2004; Valdar et al., 2006a). This "heterogeneous stock", first used by Mott et al., (2000a), was established by making an 8-way cross of inbred laboratory mice

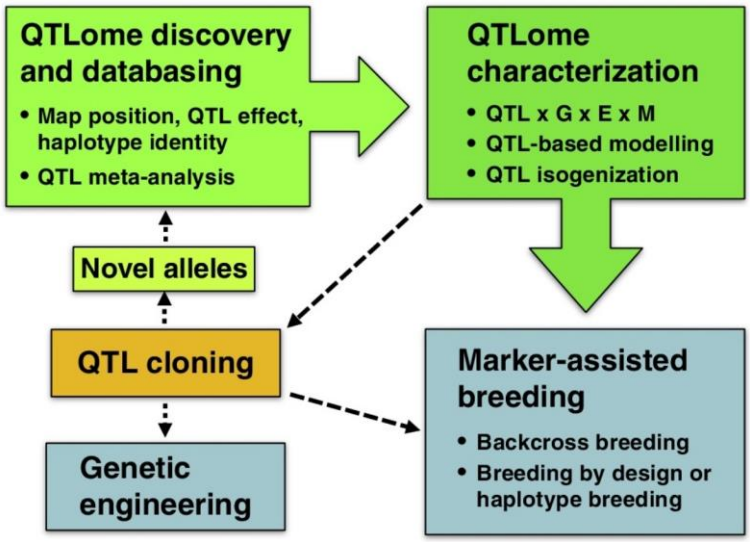

Figure I.2 QTLome indexation workflow. The QTLs related to a trait are first discovered and described after which they are characterized regarding their interactions and effects. Following their characterization, QTLs can be used directly in marker-assisted breeding or cloned before further studies. [Retrieved from Salvi & Tuberosa 2015].

whose ancestry was known, in order to increase QTL mapping resolution compared to an F_2 intercross. The concept was then adapted for crops by Mackay and Powel (2007), and applied to the model *Arabidopsis thaliana* by Kover et al., (2009) shortly after, following the crossing scheme described by Cavanagh et al., (2008). In the past decade, many crops have had MAGIC populations made available and many others are ongoing (reviewed in Arrones et al., 2020; Huang et al., 2015; Samantara et al., 2021; Yang et al., 2021). Some examples are included in **Table I.3**.

Table I.3 Examples of MAGIC designs in crops.

	Species	Reference
Cereals	Rice *Oryza sativa* (*japonica* & *indica*)	Bandillo et al., (2013)
	Corn *Zea mays*	Dell'acqua et al., (2011)
	Wheat *Triticum aestivum*	Huang et al., (2012)
Legumes	Cowpea *Vigna unguiculata*	Huynh et al., (2018)
	Faba bean *Vicia faba*	Sallam & Martsch, (2015)
Fruits	Tomato *Solanum lycopersicum*	Pascual et al., (2015)
	Strawberry *Fragaria* × *ananassa*	Wada et al., (2017)

Traditionally, MAGIC designs are an association of RILs (diploid homozygous lines produced by inbreeding/ selfing of progeny encompassing contributions of all parents for several generations to obtain an almost homozygous final population) obtained by extension of AIL (advanced intercross of the F_2 originated and successive generations from the chosen crosses) (Singh & Singh, 2015). The development of a MAGIC design in crops can be divided in four steps: (i) choice of the parents, (ii) crossing of the parents, (iii) advanced intercrosses, and (iv) inbreeding. The result is a "funnel"

(**Figure I.3 A**) or a "diallelic" (**Figure I.3 B**) crossing scheme, with terminal lines that are mosaics of the founding lines.

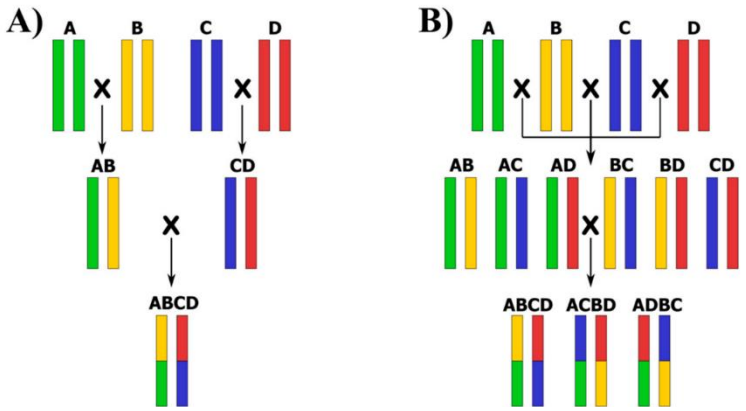

Figure I.3 Crossing scheme-of a 4-way MAGIC population with parents A-D: (A) "funnel" design vs (B) "diallel" design. Given the number of parents (n=4), the number of generations needed to ensure all parents contribute to the progeny is 2 ($^{n}/_{2}$) in diploid organisms, several rounds (6-8) of selfing ensue, to generate homozygote individuals [Adapted from Arrones et al. (2020)].

In the "funnel" scheme, *n* parent lines are crossed 2 at a time, generating $^{n}/_{2}$ F_1 recombinant strains which will then be intercrossed sequentially until the fragments of the genome of all parents is present in the progeny. In the "diallelic" approach, *n* parent lines are crossed in a pairwise fashion to generate $^{n(n-1)}/_{2}$ unique F_1 which will also be intercrossed until all parents contribute to the progeny. In both cases, $^{n}/_{2}$ generations are necessary, so all founders contribute in similar proportions to the progeny. Further generations are then obtained by selfing (inbreeding).

Using MAGIC designs in the study of natural variation in diverse plant species has led to the identification of genomic regions related with quantitative traits, such as:

- In *A. thaliana*, a design initiated with 19 parent accessions led to the identification of 25 QTL From these 25, 4 explained 63% of the phenotypic variance for traits such as days to bolt, 2 were related to flowering time, 4 related to vegetative growth and 2 others related to germination time (Kover et al., 2009). The 90% confidence intervals for the QTLs obtained were smaller than 6 Mb, and some contained good candidate genes, such as the *FRIGIDA* gene, known for affecting flowering time;
- In *Brassica juncea*, a design using 8 parents was used to study glucosinolate content (Yan et al., 2020). One QTL regarding indole glucosinolate as well as two overlapping QTLs related to total and aliphatic glucosinolate were detected, all containing glucosinolate metabolism-related genes.

B. Nutrition

1. Nutrient definition

Humans have been changing soil mineral composition, by adding ash, lime, bonemeal (among others) with the goal to improve crop yield since the early days of agriculture. However, it was not until the 19th century that a connection between minerals and their role as nutrients was made. Through observation, Liebig (1803-1873) concluded that some elements, such as nitrogen and phosphorus, are fundamental for plant growth (Kirkby, 2011). Sprengel's "Law of the minimum", stating that if one of the essential nutrients is deficient, growth will be poor even when all other essential nutrients are abundant, was popularized by Liebig for crops and an equivalent for marine algae was proposed by Brandt (de Baar, 1994). This law of the minimum can be pictured as a barrel with uneven stave length, in which each stave represents a nutrient, with the most limiting nutrient being represented by the shortest stave, the one limiting water rise (i.e., yield/growth). The concept of critical concentrations, i.e. the lowest and highest concentrations that ensure 90% of maximum yield/growth (Jones et al., 1991), is based on the "Law of minimum", dividing nutrients into deficient, sufficient or in excess, often disregarding nutrient interactions (e.g., Römheld, 2011).

Besides their concentration in the medium, elements can also be classified regarding the plant's needs. According to Arnon & Stout (1939), minerals can be classified as essential if they meet 3 conditions: (i) the plant cannot complete its life cycle when the element is absent, (ii) the function of element cannot be replaced by another, (iii) the element must be directly involved in plant metabolism. Similar to the "Law of minimum", this nutrient classification also ignores crosstalks among nutrients (e.g., Hanikenne et al., 2020). Additionally, essential nutrients can be divided according to the plant's needs: the ones required and present in cells in relatively large quantity, are designated macronutrients; and the ones required and present in cells in smaller amounts, micronutrients (Mengel et al., 2001a).

2. Nutrient functions

Carbon-based life, as we know it, is dependent on 6 major non-metal elements:

- Carbon (C), hydrogen (H) and oxygen (O), which form H_2O and CO_2, as well as the backbone of all organic (macro)-molecules via photo/chemosynthesis;
- Nitrogen (N), phosphorus (P) and sulphur (S), which are incorporated in biomolecules (e.g., ATP, DNA, amino acids) to expand the range of their biochemical reactions.

Land plants and algae have different needs of the different minerals, with some species requiring specific elements, but they can be generally grouped as described in **Table I.4** (Burstrom, 1948; Gerloff, 1963; Hunter & Provasoli, 1964; Kirkby, 2011).

Table I.4 Essential nutrients and their general function

Nutrients	Uptake	General function
C, H, O, N, S	CO_2, HCO_3, H_2O, O_2, NO_3, NH_4, SO_4^{2-}, SO_2 ions from the (soil) solution or gases from the atmosphere	Major constituents of organic material. Essential elements of atomic groups involved in enzymatic processes. Assimilation by oxidation-reduction reactions.
P, B, Si	PO_4^{3-}, H_3BO_3, $Si(OH)_4$ from the (soil) solution	Esterification with alcohol groups. Phosphate esters involved in energy transfer reactions. Silicon involved in some microalgae structural components (e.g., diatom's frustula).
K, Na, Ca, Mg, Mn, Cl	Ions from the (soil) solution	Non-specific functions establishing osmotic potential. More specific functions for optimal conformation of enzymes (enzyme activation). Bridging of reaction partners. Balancing anions. Controlling membrane permeability and electrochemical potentials.
Fe, Cu, Zn, Mo	Ions or chelates from the (soil) solution	In chelated form in prosthetic groups of enzymes. Enable electron transport by valence change. (except Zn)

In addition to those 6 major non-metal elements, the alkaline earth metals calcium (Ca) and magnesium (Mg) are macronutrients in photosynthetic organisms and have specific roles in addition to regulating pH and the ionic balance. Ca is a ubiquitous signalling molecule, playing a key role in flagella movement in swimming photosynthetic eukaryotes but also in fast membrane signalling (Verret et al., 2010). Other roles of Ca include water-binding and stabilization of the Oxygen Evolving Complex (OEC) (Shen, 2015). Moreover, Ca is stored with other cations (Mg, Na, K, Zn and Fe), phosphate and basic amino acids in acidocalcisomes (Docampo et al., 2005; Goodenough et al., 2019). Mg occupies a central role in chlorophyll, but it can also bind substrates and proteins, and act as a co-factor, playing an important role in ribosome and replisome stabilisation (Hawkesford et al., 2012; Marchand et al., 2018). Since Mg binds weakly with its interactors, the cytosolic and compartment concentrations of Mg are tightly regulated (Hawkesford et al., 2012).

Alkali metals K and Na also play important roles in plant cells. Unlike animals, potassium (K) is the main electrolyte in plants. Additionally, K intervenes in several parts of the translation process,

and the conformational changes it induces (as well as other monovalent cations) are required for enzyme activation (Hawkesford et al., 2012). The K content of the cell has a direct influence on photosynthesis, namely at the RuBisCO synthesis and efficiency levels (Mengel et al., 2001b), and on photorespiration (Hawkesford et al., 2012).

Sodium (Na) cannot be called an essential nutrient, in the sense described by Arnon and Stout (1939). In fact, despite being chemically and structurally similar to K, Na cannot replace it and plants actively discriminate between the two cations. The term "functional nutrient" for Na has been proposed, since in some land plants (mainly C4) it reduces the requirement of essential nutrients or increases yield (Subbarao et al., 2003). Certain microalgae have also been reported to increase lipid production with Na supplementation or to use Na^+ in the symport of organic and inorganic phosphate (H_2PO_4 and P_i) (Borowitzka, 2016).

Other nutrients, like copper (Cu), iron (Fe), manganese (Mn) and zinc (Zn), are required in smaller quantities than macronutrients. These micronutrients, or trace elements, are involved in protein stabilization (e.g., Zn) and reduction and oxidation reactions (e.g., Fe), increasing the array of reactions happening inside the cell (Williams, 2015). Iron's reactivity and high bioavailability preceding water oxygenation earned it a major role in photosynthesis and respiration, but also in reactive oxygen species (ROS) production and scavenging (Hänsch & Mendel, 2009). The chloroplast is the biggest Fe user in the cell, and employs the three main Fe forms -heme, non-heme and FeS clusters- along the photosynthetic electron transport chain (Kroh & Pilon, 2020).

Similarly to Fe, Cu has a significant role in electron transport during photosynthesis and respiration, ROS detoxification, among other metalloproteins. In particular, Cu high affinity with molecular oxygen makes it a suitable prosthetic group, acting as a catalyst in several oxidases (e.g., cytochrome *c* oxidase) (Hänsch & Mendel, 2009). Mn, and its redox potential, is known for its role as the catalytic centre of the photosynthetic OEC (Shen, 2015). In algae, Mn is also used to maintain chloroplast membrane structure, in superoxide dismutases, acid phosphatases, and ribonucleotide reductases and in transfers across chloroplast membranes (Borowitzka et al., 2016). Zn, unlike the previous metals, is not used for its redox features but rather for its electrophile properties and is part of up to 10% of all eukaryotic proteins (Clemens, 2021). Zn metalloenzymes in particular can be found in all enzyme classes (oxidoreductases, transferases, hydrolases, lyases, isomerases, or ligases) (Andreini et al., 2008), comprising (together with Fe) the biggest portion of the proteome (Zhang et al., 2022a). Nonetheless, most Zn proteins participate in nucleic acid-related processes (synthesis, transcription, translation and regulation) (Hänsch & Mendel, 2009).

3. Nutrient homeostasis

Every cell, regardless of the complexity degree, has an intricate network set in place in order to keep their elemental composition within a physiological range in response to the surrounding environment (Tamás & Martinoia, 2006). It is composed of mechanisms to uptake, distribute and store nutrients into the cell, but also for the chelation and detoxification of excess metals. The response to varying environmental concentrations depends on whether the element is essential or non-essential (Maret & Copsey, 2012). In the case of essential elements, outside of the optimal concentration range, there are 2 zones where growth is impaired (**Figure I.4-A**)(Frieden, 1984; Frunzo et al., 2019; Römheld, 2011):

- the deficiency, observed when element supply is below the lower critical concentration and element supplementation leads to a positive effect (e.g., biomass increase). Depending on the available amount of element, the effects may be hidden (e.g., growth limitation) or severe (e.g., survival without growth or lethality);
- the toxicity, observed when element supply is above the upper critical concentration and increase in element concentration leads to a negative effect (e.g., biomass decrease). Again, depending on the available amount of element, the effects may be hidden (e.g., growth inhibition) or severe (e.g., survival without growth or lethality).

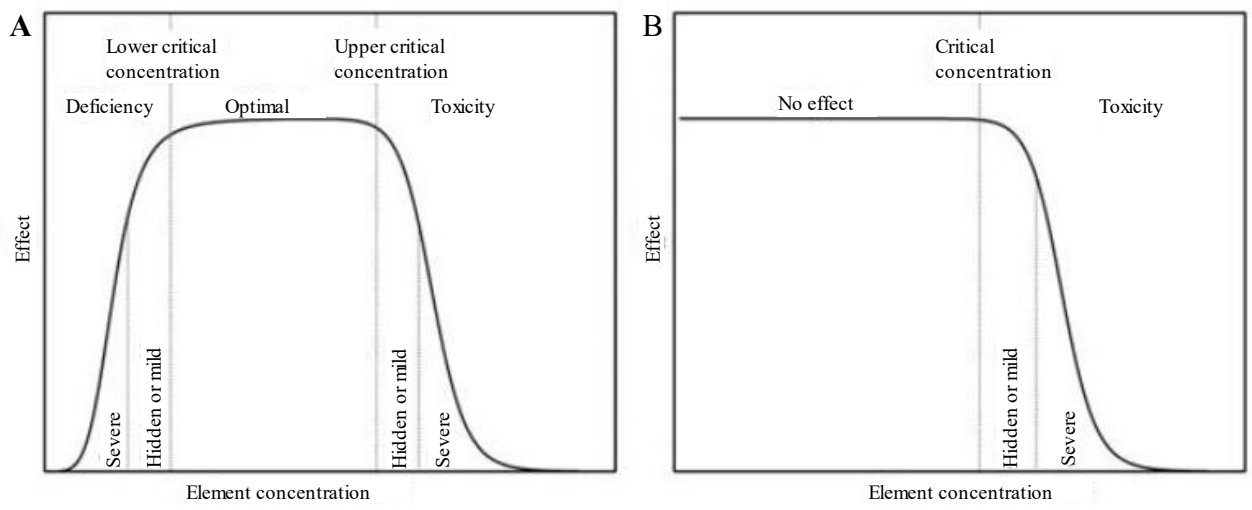

Figure I.4 Dose-effect curves for (A) an essential and (B) a non-essential element. [Adapted from Frunzo et al.,2019].

When growing at the higher end of the optimal concentration range of essential elements, some organisms can take up more than their current needs, a tendency called luxury uptake (Chapin et al. 1990). This behaviour can not only benefit the organism itself in case of posterior nutrient deficiency or provide a competitive and evolutionary advantage (de Mazancourt & Schwartz, 2012; Lemaire & Gastal, 2019; Merchant et al., 2020), but also lead to a nutrient imbalance (Römheld, 2011).

In the case of non-essential elements, their absence or low concentration does not cause deficiency, and there are no effects as long their concentrations remain below the critical concentration, after which they are toxic (**Figure I.4-B**).

The study of nutrient homeostasis in photosynthetic organisms dates several decades (Scott & Hayward, 1953), yet the big expansion of the subject started in the early 2000's. In the past 20 years, advances were made in elemental profiling (Huang & Salt, 2016), in understanding nutrient interactions (Huang et al., 2021; Malasarn et al., 2013), but also in our knowledge of the response to abiotic stress such as metal deficiency or excess (e.g., Clemens, 2001, 2006; Thiriet-Rupert et al., 2021), salinity, drought or the intersection of these subjects (e.g., Barzana et al., 2021), providing valuable information on transporters, transcription factors, and metal-binding proteins associated with those processes.

A key element of this progress has been the development of tools designed to characterize the *ionome*. The term *ionome* was coined almost two decades ago, as a way to describe "all the mineral nutrient and trace elements found in an organism - extending the metallome to include metals, metalloids and non-metals" of biological importance (Lahner et al., 2003a). The study of the ionome, *ionomics*, relies on (Salt et al., (2008), **Figure I.5**):

- Elemental analysis: done using the electronic properties of the atom (absorption, emission, and fluorescence spectroscopy) or the nuclear properties (radioactivity or atomic number). The technique choice depends on the elements to detect and desired sensitivity, sample preparation, analysis time and cost per sample;
- Genetic tools: the use of genomic or transcriptomic data from natural or artificially induced variation can be used to identify alleles or genes involved in ionome regulation;
- Bioinformatics: applied in the management of large datasets, metadata and workflow (from experiment setup to data analysis and presentation), and association studies for population mapping.

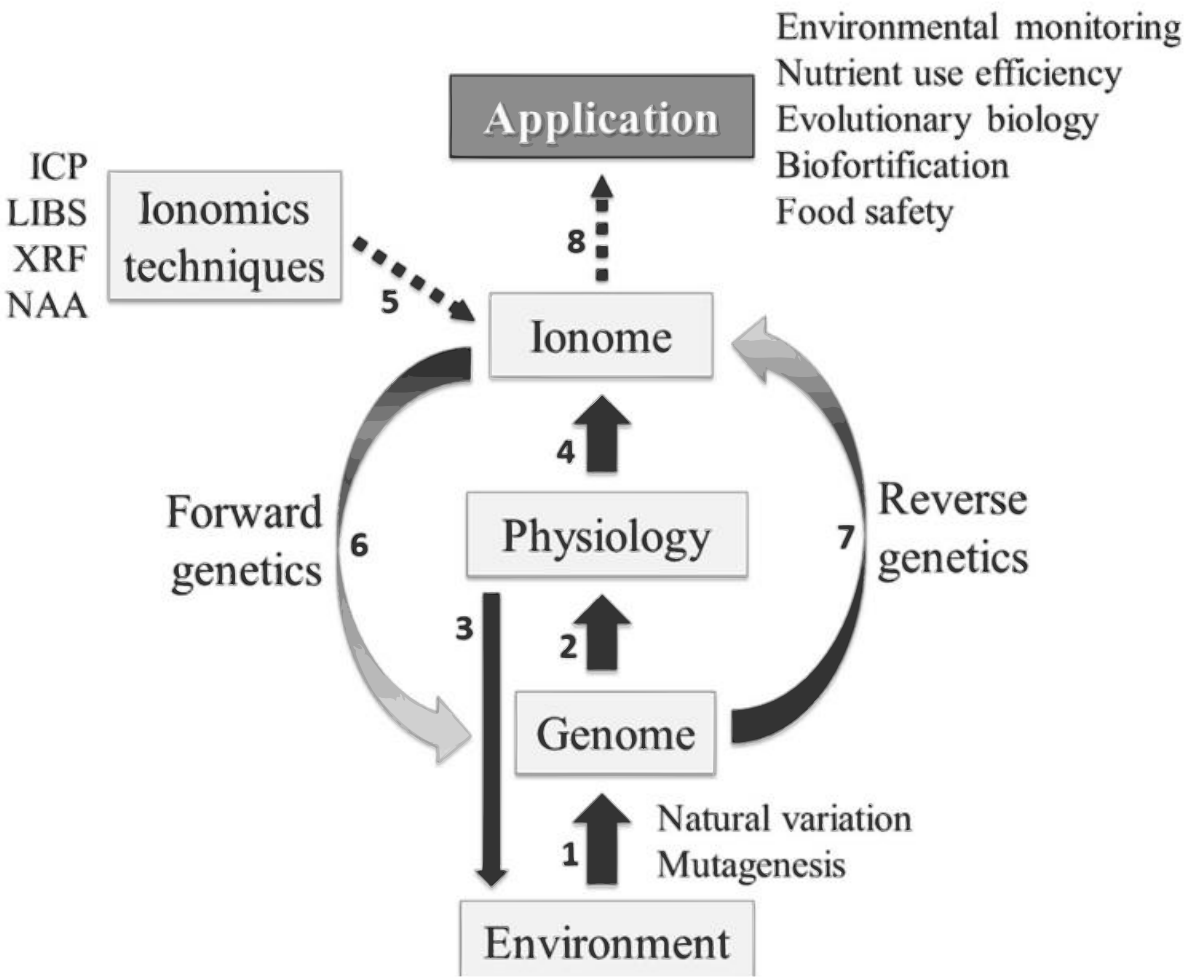

Figure I.5 Processes affecting the plant ionome and main steps for ionomic studies. (1) Selective pressure from the environment; (2) alterations in absorption and distribution; (3) plants can affect element bioavailability in the surrounding environment; (4) ionome results of the physiology, determined by the genome and the environment; (5) techniques used to study the ionome: ICP- Inductively Coupled Plasma, LIBS- Laser-Induced Breakdown Spectroscopy, XRF- X-Ray Fluorescence, NAA- Neutron Activation Analysis; (6) identification of regulatory genes using mutants or natural variation; (7) a gene is mutated/ has its expression changed before ionome characterization; (8) knowledge obtained can then be used in multiple domains. [Retrieved from Pita-Barbosa et al. 2019]

These tools are used in an effort to not only quantify the elements present in an organism, but also account for developmental changes and/or in response to the environment and genetic modifications, combining several other "*omics*" (Salt, Baxter, and Lahner 2008; Pita-Barbosa et al. 2019). Thanks to them, several actors involved in nutrient homeostasis have been identified, such as (**Figure I.6**):

- Transporters, with different specificities and selectivities, participate in the mobilisation of ions to and from the cytoplasm, but also to transport ions in and out of intracellular compartments, across membranes (e.g., Blaby-Haas & Merchant, 2012; Hanikenne et al., 2020; Sasaki et al., 2016);

- Assimilation enzymes, which incorporate nutrients (e.g., nitrogen, sulphur, zinc) into carbon macromolecules required for growth (e.g., Fernandez & Galvan, 2008; Kopriva et al., 2009);
- Chelators that bind cations, making them available for uptake (e.g., Khan et al., 2018) or reducing the bioavailability of cations with high reactivity (e.g., Balzano et al., 2020);
- Sensors, such as protein phosphorylation (e.g., Tan et al., 2020) or metal responsive domains (e.g., Sommer et al., 2010), which help the cell monitor the extra- and intracellular nutrient levels and adjust other homeostasis processes (see Podar & Maathuis, (2022) for a review on plants);
- Transcription factors, which can also be involved in nutrient sensing, control the transcriptional response to nutritional stress, and are often involved in an intricate regulatory network (e.g., Gao et al., 2019; Sommer et al., 2010).

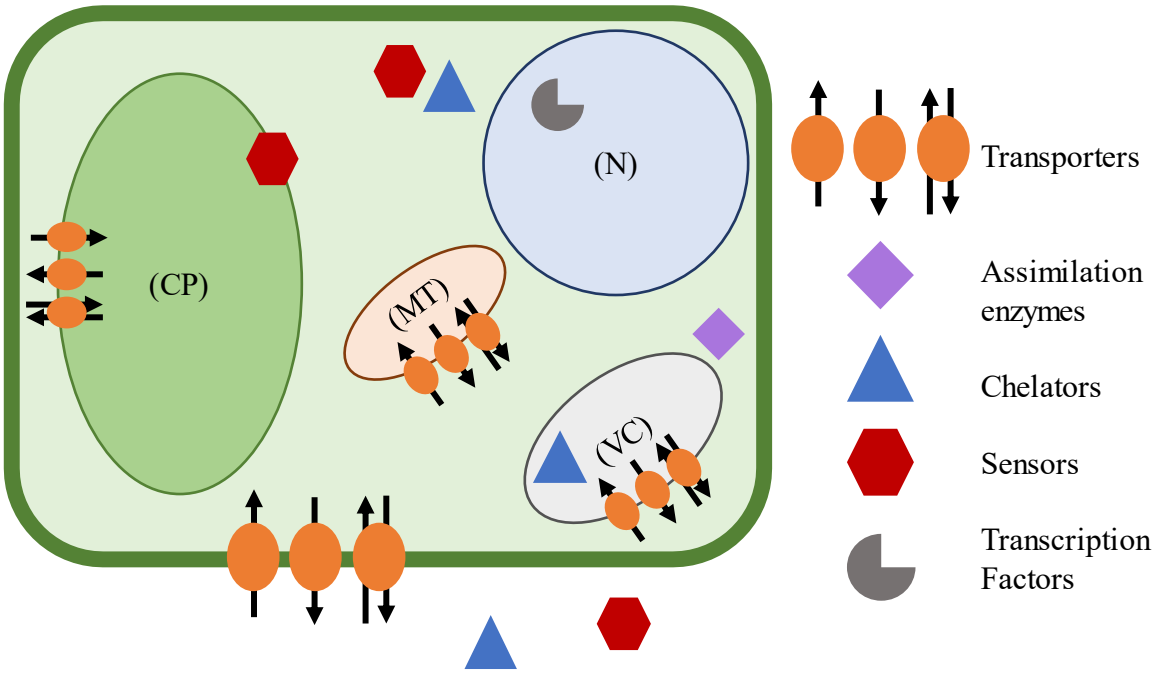

Figure I.6 Simplified scheme of key actors involved in nutrient homeostasis in a photosynthetic cell, with emphasis on the nucleus (N) and its response to nutrient stress, mitochondria (MT), chloroplast (CP), and vacuole (VC). Represented are: transporters which facilitate in/out transport of ions; assimilation enzymes involved in macronutrient import; chelators located extracellularly, in the cytosol and organelles; sensors involved in assessing the nutritional status of the environment/cell/organelle; transcription factors involved in gene regulation.

a) Nutrient homeostasis under nutrient deficiency

Nutrient deficiency can limit primary production across terrestrial (Ågren et al., 2012; Fisher et al., 2012) and aquatic (Bergström, 2010; Carstensen et al., 2011; Moore et al., 2013) ecosystems. As such, organisms have developed several strategies to manage nutrient concentrations below optimal.

When dealing with a single-element deficiency, it may occur that the limiting element is included in a very specialized network to maintain its homeostasis. Nonetheless changes in the accumulation of a single element most of the time impact other elements due to the overlap of homeostasis networks, their chemical properties and interactions with each other, as well as similar interactions with biological molecules (Baxter, 2009). Baxter (2015) proposed that analysing the whole ionome instead of independent element responses could provide better and more sensitive insight of phenotypical changes occurring upon stressing conditions. Indeed, some interactions among macronutrients (e.g., N and P), micronutrients (e.g., Cu and Fe), as well as macro and micronutrients (e.g., P and Fe) are known and have been subject to several studies (Ågren, et al. 2012; reviewed in Fan et al. 2021; and Hanikenne et al. 2020). Some examples of these interactions are:

- Cation competition, which results from a nutrient imbalance in the medium. For instance, Ca supplementation increases Mg uptake but after a threshold Mg uptake is negatively impacted by high availability of Ca, as well as K and Mn (reviewed in Gransee & Führs, 2013). This competition can also be antagonistic, in which a nutrient can alleviate the effects of metal toxicity. Ca, as well as Mg, can relieve aluminium toxicity by competing for the same membrane transporters (Lazarević et al., 2014);
- Accompanying anions, such as Cl^-, SO_4^{2-}, NO_3^-, $H_2PO_4^-$, can alter low affinity transport (Britto & Kronzucker, 2008). While SO_4^{2-}, $NO_3^-$and $H_2PO_4^-$ can be metabolized and/or stored in the cell, Cl^- temporarily increases the electrochemical gradient which, in turn, increases uptake rates;
- Uptake modulation. Deficiency/excess of one nutrient leads to the regulation of another nutrient uptake. Nitrogen supplementation increases P uptake during P-starvation, while N-starvation supresses P-starvation responses (reviewed in Kumar et al., 2021);
- Some metals are required co-factors in pathways related to another element. For example, multicopper oxidases (MCO) take part in high affinity Fe uptake (Maldonado et al., 2006), and Fe is required for N_2 fixation in diazotrophic cyanobacteria (Schoffman et al., 2016);
- Nutrient storage, such as the main P-reservoir in seeds, phytate (White & Veneklaas, 2012) or the conserved vacuole-like acidocalcisomes (Docampo et al., 2005), are also a source of K, Mg, Ca, Mn, Fe and Zn.

b) Natural variation in the study of nutrient homeostasis

Experimental designs allowed the identification of natural variants associated with variation in nutrient homeostasis in species such as rice (Chaiwong et al., 2018), *A. thaliana* (Baxter et al., 2010), Chlamydomonas (Siaut et al., 2011). The use of natural variation also allowed the identification of QTLs that correlate with nutrient accumulation (Buescher et al., 2010a) and tolerance to metal toxicity (Induri et al., 2012), as well as of genes responsible for nutrient transport and

accumulation (Loudet et al. 2007; Huang and Salt 2016). It has also been shown that a single polymorphism can affect the accumulation of several elements (Baxter, 2015).

Some examples of how the use of natural variation contributed the study of nutrient homeostasis are:

- In rice, QTLs were mapped related to K^+ and Na^+ accumulation in seedling roots and shoots, using a high salt-tolerance *indica* variety and a salt-susceptible elite *japonica* variety (Lin et al., 2004). Five QTLs were found associated with 4 salt-tolerance traits in the roots, and 3 QTLs were found for 3 traits in the shoots. These QTLs did not overlap, suggesting different transport strategies, despite the negative correlation between shoot Na^+ and K^+ content.
- In *Arabidopsis halleri*, the study of 2 non-metallicolous and 2 metallicolous populations allowed for a better understanding of how Zn, Fe, P, K, Ca, Mn are distributed in the different seed structures (Babst-Kostecka et al., 2020).

The ionome of an individual depends both on its genetic background, the surrounding environment and the interaction between those (Genotype x Environment interaction, GxE) (reviewed in Des Marais et al. 2013). For this type of traits, investigating only a few populations may not be enough to fully describe observations or predict the behaviour of the species, as alleles, only present in certain populations, that affect the phenotype may be overlooked (Baxter & Dilkes, 2012). Studying the genetic variation of the ionome can shed light on the mechanisms of how and why populations adapt to certain environments, such as nutrient limitation.

C. The model eukaryotic microalga *Chlamydomonas reinhardtii*

1. Morphology and physiology

Chlamydomonas is a unicellular green microalga found in temperate soils (Sasso et al., 2018), first described in 1888 by Dangeard (Harris, 2009b). Chlamydomonas cells are usually 5-10 µm in diameter and have a characteristic cup-shaped chloroplast at the base of the cell, which encases the pyrenoid (where Rubisco is concentrated), and a light sensing eyespot near the inner envelope membrane. The haploid nucleus, containing a GC-rich genome of approximately 112 Mb (Craig et al., 2022; Merchant et al., 2007), is located at the centre of the cell, while the contractile vacuoles and the flagella basal bodies are in the anterior region. In addition, each cell houses multiple mitochondria, Golgi bodies and starch granules, and is enveloped in a hydroxyproline-rich glycoprotein and carbohydrate cell wall (Harris, 2001; Salomé & Merchant, 2019; Sasso et al., 2018) (**Figure I.7**). Due to the presence of traits associated with both plants (chloroplast) and animals (flagella/cilia), Chlamydomonas is often referred to as "half plant-half beast" (Merchant et al., 2006) or "planimal" (Redding & Cole, 2008).

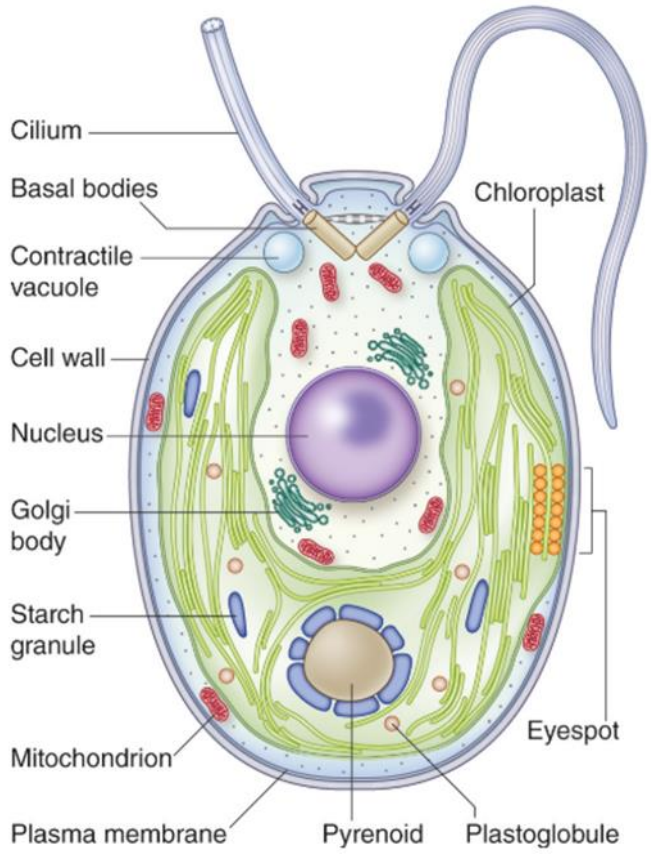

Kingdom
Plantae
Subkingdom
Viridiplantae
Phylum
Chlorophyta
Class
Chlorophyceae
Order
Chlamydomonadales
Family
Chlamydomonadaceae
Genus
Chlamydomonas
Species
Chlamydomonas reinhardtii

Figure I.7 Chlamydomonas vegetative cell structure (left) and taxonomy (right). [Retrieved from Sasso et al. (2018)]

Interestingly, despite having a chloroplast that occupies roughly half the cell, photosynthesis in Chlamydomonas is not essential. Chlamydomonas can grow using several sources of carbon and energy: (i) given light and CO_2 as sole carbon source (photoautotrophy), (ii) given light and an alternative carbon source such as acetate (mixotrophy), or (iii) in the dark with a reduced carbon

source (heterotrophy), which earnt it the green/photosynthetic yeast alias (Goodenough, 1992; Rochaix, 1995). Besides alternative carbon sources, most wild-type strains can metabolise ammonium and nitrate as nitrogen supplies (Harris, 2009a).

Chlamydomonas can be cultured in different liquid or solid media (see Harris 2009a for a comparison of the most often used media). Nonetheless, TAP (Tris-Acetate-Phosphate) (Gorman & Levine, 1965) is the most frequently used medium. In minimal media (without acetate), wild-type strains can divide 3-4 times a day, when grown at 25°C and with a light intensity of 200-400 µmol photons.m^{-2}.sec^{-1} (Harris, 2001). In a more general manner, depending on the strain, the light intensity, temperature and composition of the medium, strains can double 3-5 times a day (Harris, 2009a).

2. Chlamydomonas as a model organism

Several traits such as oxygenic photosynthesis and flagellar assembly have been studied in Chlamydomonas as a model since more than half a century before the sequencing of its whole genome (Dutcher, 2000; Grossman et al., 2003; Harris, 2001). Several characteristics contributed to the use of Chlamydomonas in genetic, biochemical, cytological, and molecular approaches(Salomé & Merchant, 2019), namely:

i. ease of culture in laboratory, on both solid and liquid media;
ii. fast doubling rate under sufficient nutrients;
iii. facultative autotrophy and metabolic plasticity;
iv. haploid genome, suitable for classical genetics;
v. high recombination rate during the sexual cycle.

Chlamydomonas is an outgroup of the volvocine group, which comprises closely related uni- and multicellular algae, making it a suitable candidate to investigate the evolution of multicellularity, sex determination and anisogamy evolution (Herron & Michod, 2008; Ratcliff et al., 2013; Umen & Coelho, 2019; Umen & Olson, 2012). Additionally, Chlamydomonas is also used to study the cell cycle, thanks to its position close to the animal/plant crossroad (Fang et al. 2006; Pérez-Pérez et al. 2017; Ma et al. 2021). Another domain in which Chlamydomonas is a fit model is the study of abiotic stress response, with research made to investigate how it reacts to osmotic stress (Colina et al., 2020; Tietel et al., 2020), heat shock (reviewed in Schroda et al. 2015), as well as metal toxicity and remediation (Cheng et al., 2019; Elbaz et al., 2010; Hanikenne, 2003; Jamers et al., 2009; Thiriet-Rupert et al., 2021a) and nutrient limitation (Allen et al., 2007b; Devadasu et al., 2016; Malasarn et al., 2013).

3. Life cycle

The Chlamydomonas life cycle can be divided in two parts: vegetative growth and sexual reproduction.

a) Vegetative growth

During the vegetative phase of the life cycle, Chlamydomonas divides mitotically. Chlamydomonas can be grown under different light regimes (continuous light, different photoperiods, darkness), nonetheless the presence of a light/dark cycle allows for the synchronization of cultures, as it happens in other algae species (Otero & Goto, 2005; Tamiya, 1963). While the knowledge on the exact synchronisation mechanism is still incomplete, and recent efforts have been made into perfecting the picture (e.g., Shelton et al., 2017), it is widely accepted that light works as a secondary checkpoint after they pass commitment phase, beyond which cells undergo at least one full cell cycle (Harris, 2001) (**Figure I.8**). Heldt et al. (2020) proposed a new model of commitment phase, which uses a single light-dependent sizer, named size-oscillator, to connect the three previously considered independent mechanisms (reviewed in Cross et al., 2015):

(i) Size-dependent passage to the commitment phase, in which the mother cell must pass a minimum size in order to divide;

(ii) Time-dependent control of the commitment phase, which is dependent of light quality;

(iii) Mitotic sizer, which ensures the right number of divisions occurs in order to ensure a determined daughter size.

The Chlamydomonas division occurs in two phases: during the daylight hours, it increases volume, reaching a size ~8-fold its birth size; in the dark, it undergoes several rounds of mitotic divisions, proportional to the growth attained (Cross et al., 2015; Harris, 2001). Opting for a multiple fission strategy (**Figure I.8 B**) allows Chlamydomonas to maximise growth during the time it can photosynthesise. This decoupling and rhythmicity of growth phase and division phase is still preserved in cells cultured in continuous light, despite the absence of a dark phase (Heldt et al., 2020; Ma et al., 2021). In situations of stress, these divisions occur without degradation of the cell wall, and 4-16 daughter cells can be found inside the same cell wall, in a palmelloid structure (reviewed in de Carpentier et al., 2019).

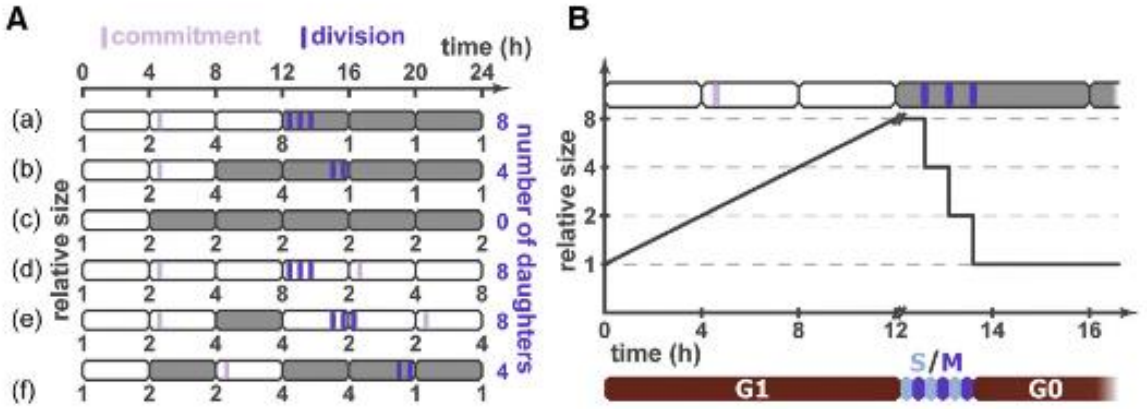

Figure I.8 Multiple fission in Chlamydomonas. (A) Scheme of growth-interruption experiment results. Each rectangle represents a 4h interval in light (white) or dark (grey) periods. Cell size relative to birth is marked under each row (black) and the number of daughter cells on the right side (purple). (B) Relative cell size during a 12h light/ 12h dark photoperiod. The cell cycle phase is indicated below. [Adapted from Heldt et 2020].

b) Sexual reproduction

Chlamydomonas is an isogamous heterothallic microalga: in the absence of nitrogen, cells differentiate into identical-looking gametes, of either mating type *plus* (*mt+*) or *minus* (*mt-*) (Harris, 2001; Sager & Granick, 1954). The mating type is determined by the *MID* (MInus Dominant) gene presence (*mt-*) or absence (*mt+*) in the MT locus, which contains key genes for differentiation, including the mt+-specific gene *FUS1* (adhesion protein FUS1) (Ferris et al., 1997, 1996).

There are four major steps in the Chlamydomonas sexual cycle (**Figure I.9**), studied and summarized by Nishimura et al. (2010, 2017; 2002, 2012):

1. Gametogenesis: after acclimating to N starvation, cells begin the "differentiation program", which includes the production of *mt*-specific agglutinins in the flagella, responsible for recognition and cellular adhesion to an opposing *mt* partner.
2. Zygote formation: agglutinin interaction starts a cascade of signalling pathways, leading to the shedding of the cell wall, activation of the apical mating structures and cell fusion.
3. Zygote maturation: flagella loose adhesion, are reduced and absorbed, the chloroplastidal and mitochondrial DNAs are degraded in *mt-* and *mt+* cells, respectively; chloroplasts fuse together before chloroplast and chlorophyll degradation, lipids are accumulated, and a thick cell wall is developed. After a period of darkness, zygotes develop into zygospores (dormant stage).
4. Germination: when exposed to favourable conditions, the zygospore undergoes meiosis, forming a tetrad of 2 *mt+* and 2 *mt-* daughter cells, which live independently after leaving the tetrad membrane.

Due to zygospore stickiness, mating type can be determined not only by PCR (Werner & Mergenhagen, 1998), but also by crossing a strain of unknown mating type to wild-types of known

mating-type: a zygospore pellicle layer, with thickness related to mating efficiency, can be seen at the surface of the media or sticking to the test tube/ well wall (Harris, 2009a).

Chlamydomonas mating is remarkable for its relatively high recombination rate, estimated to be ~10 cM/Mb on average (Merchant et al., 2007), compared with the 1.9 cM/Mb on average for plants and 2.5 cM/Mb on average for animals (reviewed in Stapley et al., 2017). This high recombination rate is characterised by the presence of recombination hotspots, as well as the high frequency of sexual reproduction in a laboratory setting and may be overestimated for natural strains (Hasan & Ness, 2020). In addition, a positive correlation, but no bias, between the genome GC-content and the occurrence of crossover or non-crossover events during meiosis was found, similarly to what has been described for other species (Liu et al., 2018).

Another key point is the uniparental inheritance of mitochondria and the chloroplast. Although this non-Mendelian inheritance has received much attention for decades, the mechanism is still not fully uncovered, namely how the non-target DNA is "protected" (Nishimura, 2017). It is known, however, that the degradation of the *mt*- chloroplast DNA occurs shortly after zygote formation (Nishimura et al., 1999) while the *mt*+ mitochondrial DNA stays active for a few more hours (Nakamura et al. 2003). Despite being encased by the chloroplast, the pyrenoid of both parents is still visible after chloroplast fusion under phase-contrast imagery (Nishimura et al., 2002).

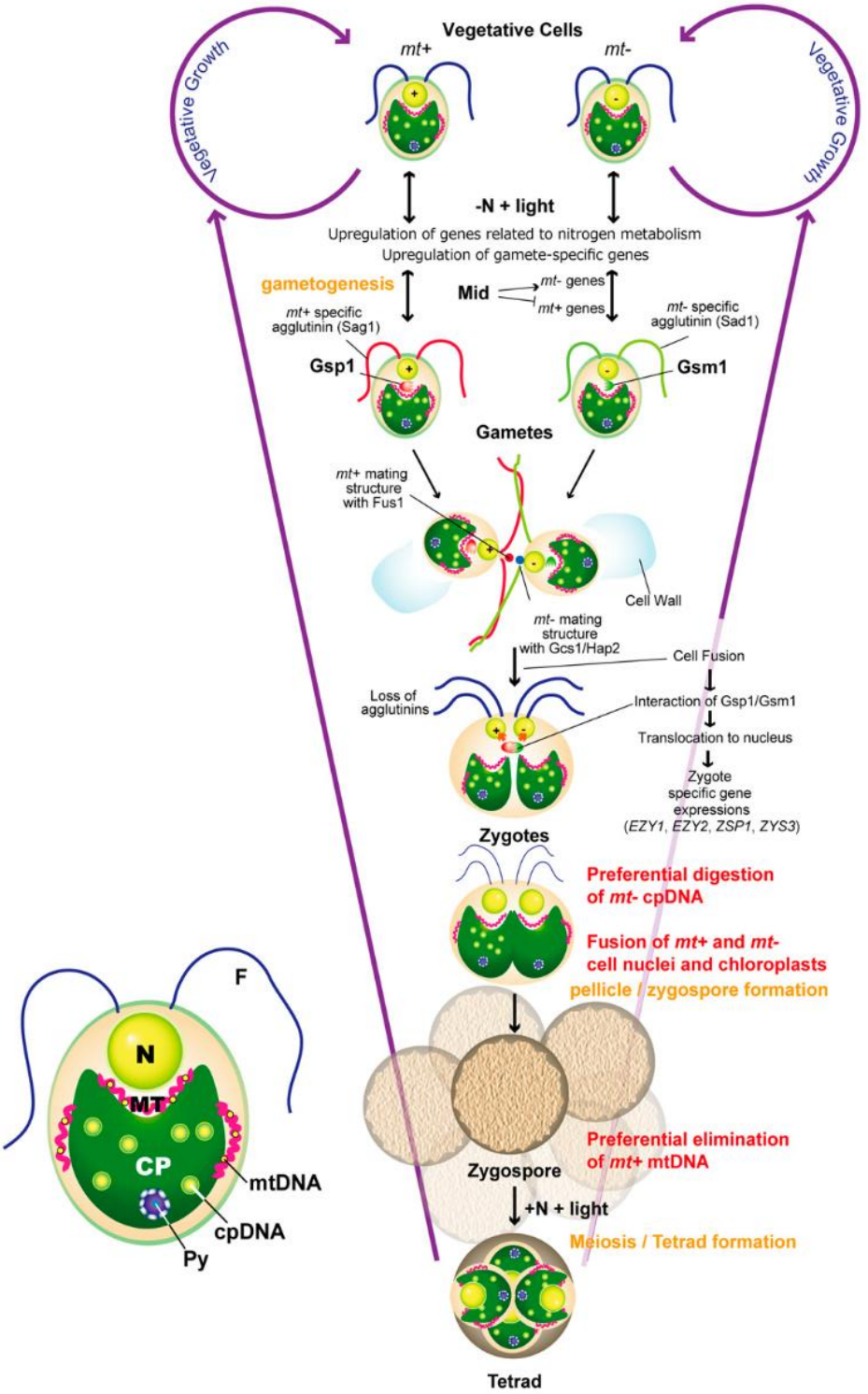

Figure I.9 The life cycle of Chlamydomonas, with emphasis on the sexual cycle. Highlight of key structures for Chlamydomonas mating (bottom left panel): flagella (F), nucleus (N), and a cup-shaped chloroplast (CP), pyrenoid (Py), mitochondria (MT). The cpDNA and mtDNA are complexed with proteins to form nucleoids. [Retrieved from Nishimura et al., **(**2012)].

MID-Transcription factor to switch on mt- program and switch off mt+ program; **FUS1**-Encodes mt+ fringe glycoprotein for mating structure adhesion; **Sag1**/**Sad1**-Agglutinins with complementary adhesion to the opposite mt; **Gsp1**/**Gsm1**-Regulator involved in the activation of the zygotic program; **Gcs1**/**Hap2**-Protein essential for membrane fusion; **EZY1**/ **EZY2**-Polypeptide involved in uniparental inheritance (chloroplast); **ZSP1**-Zygote-specific wall protein; **ZYS3**-Zygote-specific protein controlling endoplasmic reticulum systems

4. Chlamydomonas as a model organism

a) Chlamydomonas as a model for nutrient homeostasis

Despite being a model for the study of several traits, several decades passed before Chlamydomonas was introduced as model for nutrient homeostasis (Hanikenne 2003), despite earlier studies from Merchant (1992; 1986a, 1986b, 1987; 1995). Indeed, its flexibility for carbon and nitrogen sources, combined with the ease of nutrient supply tuning in the growth media, allowed to unveil information regarding timing of assimilation, intracellular location and transport of nutrients (reviewed in Merchant et al., 2006). Several studies have been made, characterising the Chlamydomonas nutritional profile in TAP media (Merchant, 2010), the Cu, Fe and N nutrition (reviewed in Glaesener et al. 2013; Merchant et al. 2020; Fernandez and Galvan 2007), Mn storage (Tsednee et al., 2019), sulphur sensing and response (Sawyer et al. 2015; González-Ballester et al. 2010), as well as N and P interaction (Kamalanathan et al., 2016), among others. Some noteworthy discoveries regarding Chlamydomonas nutrient homeostasis:

- Cu-regulated plastocyanin/cytochrome c_6 balance (Merchant & Bogorad, 1986a). This study showed that under Cu deficiency, plastocyanin is replaced by cytochrome c_6, allowing a reduction of Cu demand and direction of available Cu to processes that depend exclusively on Cu. It was also showed that cytochrome c_6 accumulation is dependent of Cu concentration in the media, but independent of photosynthesis.
- Characterization of S transport (Yildiz et al., 1994). By comparing S starved and unstarved cells, the authors remarked the existence of a high-affinity S uptake in S starved cultures, which preceded the increase of arylsulfatase activity. Through inhibition tests, it was shown that cytoplasmatic protein synthesis is required for this high-affinity uptake to occur and that S uptake can be powered by oxidative phosphorylation or photophosphorylation.
- Timing of the early N starvation response preceding gametogenesis (Merchán et al., 2001). Using differential display technique, 10 new genes (nitrogen-controlled genes, NCG1-10) were identified in response to N starvation, none of which is *mt*-specific: NCG1 was detected after 15 minutes, NCG25 after 30 minutes, NCG6 after 1-2h, NCG7-9 after 5h and NCG10 after 10h. The swiftness of the first response, suggested that NH_4^+ in the media may actually repress the response of the detected genes.
- Modelling of the Cu-dependent Fe assimilation pathway (Allen et al., 2007a). By surveying the genome, a ferrireductase, *FRE1*, and two ZIP family proteins, *IRT1* and *IRT2* were identified. A proteomic approach allowed the identification of the extracellular Fe assimilation proteins *FEA1* and *FEA2*, expressed coordinatively with *FOX1*, a multi-Cu Fe-oxidase, and *FTR1*, a ferric permease. Two models, differing on *FEA1/2* function, were

proposed: in one, *FEA* binds ferrous Fe, increasing its availability for the ferroxidase/ferric transporter complex; in the other, *FEA* binds ferric Fe and functions upstream *FRE1*.

- Mono- and divalent cation exchanger CrCAX1 role in cation homeostasis and mild Co^{2+} tolerance (Pittman et al., 2009a). Functional characterization of the first cation/H^+ in Chlamydomonas. Cr*CAX1* is a H^+-coupled Ca^{2+} and Na^+ transporter, homologous to *CAX* genes of *A. thaliana* and *S. cerevisiae*. Cr*CAX1* expressed in *A. thaliana* and *S. cerevisiae* induced NaCl tolerance in both species, thanks to its Na^+/H^+ exchange ability. The expression of Cr*CAX1* in yeast also led to a mild Co^{2+} tolerance, hinting at the possibility of this transporter to transport Co^{2+} and Cd^{2+}.
- Impact of Zn-deficiency on Cu homeostasis and CO_2 assimilation (Malasarn et al., 2013). Zn deficiency induced the expression of several carbonic anhydrases; however proteins were barely detected in immunoblots, leading to a disruption of the carbon concentration mechanism. The Zn-dependent transcription factor *CRR1* (copper response regulator) was also impacted, being regulated similarly as in Cu deficiency, to which authors concluded that intracellular Cu must be unavailable (e.g., in plastocyanin) to avoid mismetallation.
- Cu allocation during Cu deficiency in photosynthesis and respiration (Kropat et al., 2015). As plastocyanin can be replaced by cytochrome c_6 as an electron carrier, plastocyanin is degraded by *CRR1*-dependent proteolysis during Cu deficiency. The authors hypothesise that plastocyanin works as a Cu reservoir for proteins which are more dependent on Cu, such as cytochrome *c* oxidase and ferroxidase, and studied the prioritization of Cu-using pathways (photosynthesis with plastocyanin, iron assimilation with ferroxidase, and respiration with cytochrome oxidase) in function of Cu availability (from deficiency to excess). Under Fe-limited photoheterotrophic condition (maximal Cu demand), priority is given to cytochrome oxidase over ferroxidase, followed by plastocyanin. despite acetate increasing respiration rate, this priority is maintained in phototrophy, as well as cytochrome oxidase and intracellular Cu increase by 2-3-fold.

b) Genetic diversity in laboratory and natural strain of Chlamydomonas

The Chlamydomonas strains mainly used in molecular studies could be grouped into three sublineages believed to have been isolated from a single zygospore by Smith in 1945, until the early 2000s (Harris, 2009b). Gallaher et al. (2015) proposed, instead, the occurrence of an ancestral cross between strains with 2% relative divergence, and the progeny of this cross was then crossed 2 times more with the parent containing Haplotype 1, accounting for 74.8% of the laboratory Chlamydomonas genome (**Figure I.10 A**). By identifying the genome blocks where the 2% variation was, it was possible to examine the relatedness of 39 laboratory strains, identify strain histories as well as mislabelled strains (**Figure I.10 B**), and conclude that in place of three sublineages there might have actually been five (**Figure I.10 C**). This alternative Haplotype 2 is believed to be responsible for the phenotypical variation observed in many of the strains commonly used in the laboratory such as: diameter, ability to metabolize nitrogen, response to light, cell wall production and nutrient utilization (Gallaher et al., 2015).

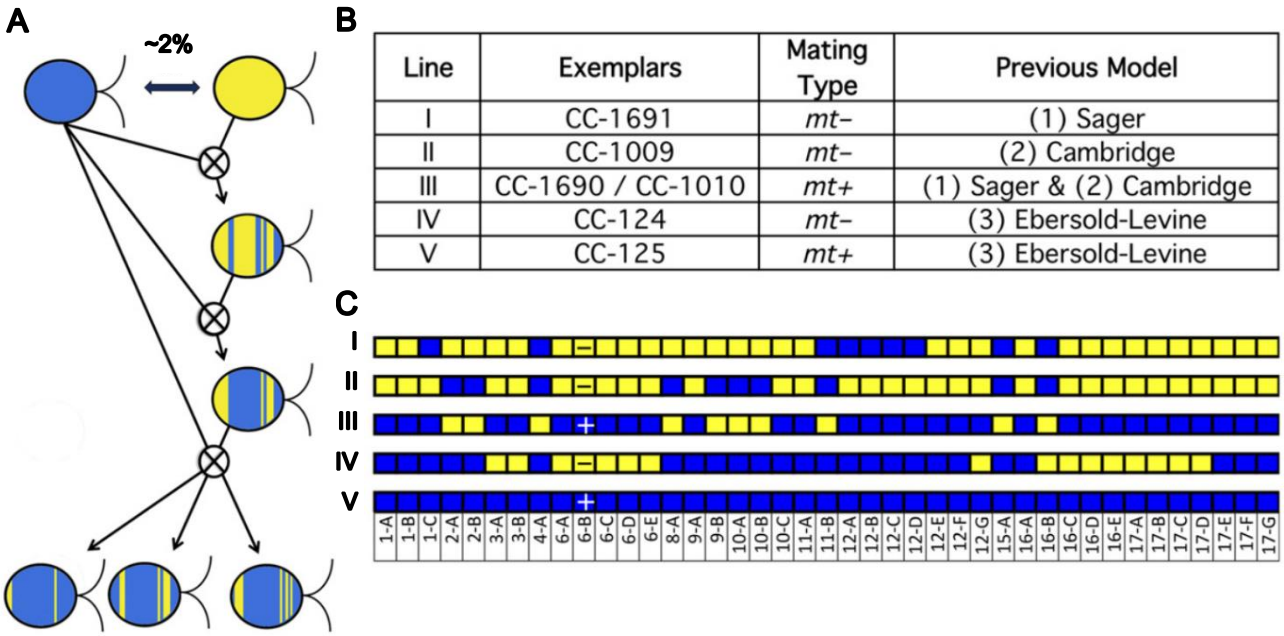

Line	Exemplars	Mating Type	Previous Model
I	CC-1691	*mt−*	(1) Sager
II	CC-1009	*mt−*	(2) Cambridge
III	CC-1690 / CC-1010	*mt+*	(1) Sager & (2) Cambridge
IV	CC-124	*mt−*	(3) Ebersold-Levine
V	CC-125	*mt+*	(3) Ebersold-Levine

Figure I.10 Distribution of the 2 haplotypes among laboratory strains. (A) Initial cross between two strains with 2% sequence divergence, haplotype 1 (blue) and haplotype 2 (yellow). In subsequent crosses, the contribution of the haplotype 2 parent was reduced to 25.2%. (B) New model for the strains initially distributed by Smith, dividing them in 5 lines. Whole-Genome Sequencing revealed that the strains from lineage III, CC-1690 and CC-1010, are actually the same strain despite being previously included in different lineages. (C) Haplotype pattern of the 5 lineages in the new proposed model. The + or – signs in block 6-B represent the mating type. [Adapted from Gallaher et al., (2015)].

Concomitantly, Flowers et al. (2015) found evidence that support (**Figure I.11**):(i) the existence of geographically structured populations in North American field strains, which will differ at ~3% of the sites and (ii) population size is among the highest known for eukaryotes (2 orders higher than Arabidopsis), implying a more efficient elimination of low fitness alleles, (iii) deletions and nonsense mutations in laboratory strains are older than their lab introduction, making copy number gains of chromosomal segments due to adaptative overexpression of genes the most likely source of

polymorphism, (iv) phenotypic differences reflecting the extensive genotypic diversity, as observed by differences in cell size and culture growth of synchronized cultures with normalized cell concentration. In the same study, the authors also suggest that this variation should be considered (i.e. inclusion of strains from different populations) when conducting all sorts of studies.

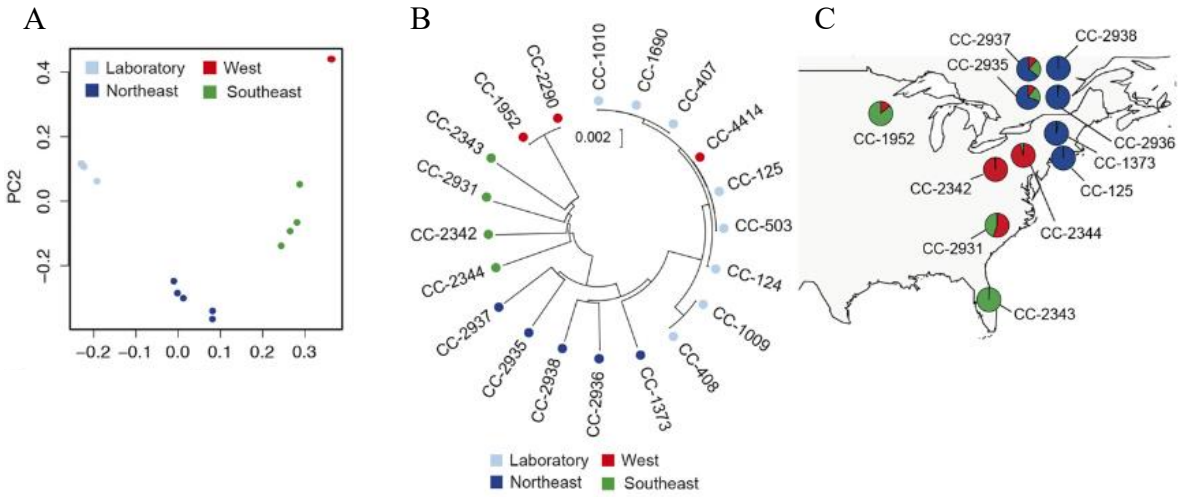

Figure I.11 Population structure in Chlamydomonas. (A) PCA of the genotypes showing a geographic clustering of the strains. (B) Neighbour-joint tree for 20 strains, colour coded according to the geographic grouping. (C) Admixture proportions in each strain by sampling location. [Adapted from Flowers et al., (2015)]

The influence of variation has been previously documented:

- In addition to cell size and cell cycle, phototactic behaviour and fitness can be affected (Malcom et al., 2015). The genetic diversity of the strains used in this study is in line with the one described in Jang & Ehrenreich (2012), but lower than the one described by Flowers et al. (2015). Among 18 lines tested, some were completely asynchronous while others had strong synchronisation, and there was a magnitude >74-fold variation despite some lines being cultured in a laboratory for decades. The fitness variation observed among different lines and culture media was the result of both plasticity (the ability of a phenotype to generate an adaptive response to environmental challenges) and canalization (the process in which phenotypes take relatively constant forms regardless of environmental and genetic perturbations), suggesting that interactions between genetics and environment may not be linear.
- Hyperoxia tolerance, pyrenoid morphologies and H_2O_2 signalling can differ between natural strains (Neofotis et al., 2021). The progeny of the crossing between a hyperoxia-tolerant strain and a sensitive one displayed a 2:2 segregation pattern of the pyrenoid morphology: 2 of the tetrad strains had completely sealed and robust rings, like the tolerant parent while the other 2 had fragmented, porous structures like the sensitive parent. Progeny growth under hyperoxia resembled that of the parent whose pyrenoid they inherited, although more extreme, suggesting the influence of additional factors controlling biomass production in hyperoxic condition. H_2O_2 effect on pyrenoid biosynthesis was confirmed in a laboratory

strain, but when testing the natural strains, only the tolerant strain increased its production under hyperoxia. In addition, ROS staining revealed a concentration in the peroxisome in the tolerant strain while the sensitive strain's ROS were dispersed in the cell.

More recently, Lucker et al., (2022) identified loci relevant for fitness increase by crossing two phenotypically distinct parents (CC-1009 and CC-2343), and then pooling and competing the progeny (polyculture) under industry-relevant conditions. This setting allowed the selection of strains which outcompeted segregants with lower fitness in various conditions (e.g., high oxygen, salt or temperature). The authors then proceeded to identify regions contributing to the increase of fitness using an approach that accounts for modifications induced by selection: Selection-Enriched Genomic Loci (SEGL). This approach allowed the identification of regions encoding 10 to over 2000 genes, limiting conclusions about how many loci actually contribute to traits related to domestication. Nonetheless, the trade-offs observed in some traits did not significantly impact productivity, even improving productivity in other conditions.

D. Purpose of this thesis

The structured variation found by Flowers et al. (2015), as well as the variation described in that study and in Gallaher et al. (2015), provide a foundation for the design of QTL mapping experiments including strains from diverse backgrounds. By selecting strains from different locations with different phenotypes and creating a mapping population, a large amount of phenotypic and genetic diversity will be generated, which will allow the dissection of the genetic architecture of nutrient homeostasis.

For this thesis, after phenotyping an initial panel of candidates in order to select the parental strains, a MAGIC design using Chlamydomonas was made to create a multiparent recombinant population encompassing both natural and laboratory variation.

The aims of this thesis are the:

(i) Description of the natural variation in the Chlamydomonas ionome via the characterization of the ionomic variation among 24 Chlamydomonas strains, from both laboratory and natural backgrounds, in 10 different single deficiency media;

(ii) Creation and establishment of a MAGIC design protocol using Chlamydomonas;

(iii) Characterization of the MAGIC population, including the quantification of the variation in the MAGIC population at the genotypic and phenotypic levels;

(iv) Identification of a mineral nutrition QTLome and documenting loci influencing nutrient homeostasis under nutrient deficiency in Chlamydomonas.

II. Natural variation of nutrient homeostasis mechanisms in *Chlamydomonas reinhardtii*

The following chapter was submitted for publication.

Natural variation of nutrient homeostasis mechanisms among laboratory and field strains in *Chlamydomonas reinhardtii*

Sara M. Esteves[1], Alice Jadoul[1], Fabrizio Iacono[2], Marie Schloesser[1], Bernard Bosman[3], Monique Carnol[3], Tom Druet[4], Pierre Cardol[2], Marc Hanikenne[1]

[1] InBioS-PhytoSystems, Translational Plant Biology, University of Liège, Belgium;
[2] InBioS-PhytoSystems, Genetics and Physiology of Microalgae, University of Liège, Belgium;
[3] InBioS-PhytoSystems, Laboratory of Plant and Microbial Ecology, University of Liège, Belgium
[4] Medical Genomics-Unit of Animal Genomics (GIGA), University of Liège, Belgium

Corresponding author
Marc Hanikenne, marc.hanikenne@uliege.be
University of Liège
InBioS - PhytoSystems
Quartier de la Vallée, 1
Chemin de la Vallée, 4 - Bât B22
B4000 Liège
Belgium
Tel: +32-4-3663844

A. Highlights

Extensive genetic variation has been identified within the model microalga *Chlamydomonas reinhardtii*. We describe how this variation influences the response to nutrient deficiency, highlighting differences between natural and lab strains.

B. Abstract

Natural variation among individuals and populations exists in all species, playing key roles in response to environmental stress and adaptation. Micro- and macro-nutrients have a wide range of functions in photosynthetic organisms and mineral nutrition thus plays a sizable role in biomass production. To maintain nutrient concentrations inside the cell within physiological limits and prevent the detrimental effects of deficiency or excess, complex homeostatic networks have evolved in photosynthetic cells. The microalga *Chlamydomonas reinhardtii* (Chlamydomonas) is a unicellular eukaryotic model for studying such mechanisms. In this work, twenty-four Chlamydomonas strains, comprising field isolates and laboratory strains, were examined for intraspecific differences in nutrient homeostasis. Growth and mineral content were quantified in mixotrophy (TAP), as full nutrition control, and compared to autotrophy (TMP, -acetate) and 9 deficiency conditions for macronutrients (-Ca, -Mg, -N, -P, -S) and micronutrients (-Cu, -Fe, -Mn, -Zn). Growth differences among strains were relatively limited. However, similar growth was accompanied by highly divergent mineral accumulation among strains. The expression of nutrient status marker genes and photosynthesis were scored in pairs of contrasting field strains, revealing distinct transcriptional regulation and nutrient requirements. Leveraging this natural variation should enable a better understanding of nutrient homeostasis mechanisms in Chlamydomonas.

Keywords

Chlamydomonas reinhardtii, ionome, natural variation, nutrient deficiency, nutrient homeostasis, photosynthesis, iron, manganese

C. Introduction

Photosynthetic organisms require both macro- and micro-nutrients in sufficient amount to sustain growth and complete their life cycle. Outside an adequate supply range, they cannot maintain homeostasis, leading to nutrient deficiency or toxicity (Römheld, 2011). Nevertheless, photosynthetic organisms have colonized very diverse environments, both in soil and water, characterized by extreme variations of nutrient supply, and therefore present a high diversity of nutrient homeostatic networks (Huang & Salt, 2016). For instance, four distinct iron (Fe) uptake machineries, of diverse evolutionary origins, are found, and in many cases co-exist, in algae (Blaby-Haas et al. 2017). Complex and tightly regulated mechanisms evolved to deal with inadequate nutrient availability, such as exclusion or hyperaccumulation to manage metal excess (Hanikenne & Nouet, 2011; Krämer, 2010), or inducible high affinity uptake, sparing and recycling systems to cope with nutrient deficiencies (Gutu et al., 2011; Marschner, 2011; Miramar et al., 2003; Saito et al., 2011).

Species display more or less wide ecological ranges with variation among and within their populations allowing colonization and subsistence in diverse environments, thanks to phenotypic plasticity or local adaptation (VanWallendael et al., 2022). Hence, different strategies to maintain nutrient homeostasis are reflected in the ionome (defined by Lahner et al., 2003b; and Salt et al., 2008 as the mineral nutrient and trace element composition), which can be used to distinguish strains/accessions thanks to characteristic ionomic profiles (Atwell et al., 2010; Baxter et al., 2012; Buescher et al., 2010b). Considering natural variation within species not only provides a broader picture of a species behaviour but is instrumental for the identification of new genes and ecologically relevant alleles as it allows the study of quantitative (continuous) traits while the use of mutants is more suited for qualitative (discrete) trait analysis (Alonso-Blanco & Koornneef, 2000; Weigel, 2012), increasing the power of model organisms (Gasch et al., 2016). Examining natural variation of the ionome in *Arabidopsis thaliana* (Arabidopsis) (Huang & Salt, 2016; Pita-Barbosa et al., 2019) has for instance allowed identifying key genes involved in mineral nutrition or metal tolerance (Atwell et al., 2010; Baxter et al., 2008; Chao et al., 2012). In that respect selecting crop varieties with high nutrient-use efficiency is an important goal for breeders (Bhatt et al., 2020; Thiébaut & Hanikenne, 2022).

Chlamydomonas reinhardtii (Chlamydomonas) is a single-cell biflagellate green microalga used as a model to dissect fundamental biological processes (Harris, 2001; Salomé & Merchant, 2019; Sasso et al., 2018). Chlamydomonas is a reference in the study of photosynthesis (e.g., Dent et al., 2001; Wakao et al., 2021a), and related processes such as light perception (e.g., Choudhary et al., 2019; Hart & Gardner, 2021), CO_2 concentration (e.g., Fei et al., 2022; Moroney & Ynalvez, 2007) or biofuel production (e.g., Fakhimi & Tavakoli, 2019; Rupprecht, 2009), but also of the cell cycle (e.g., Ma et al., 2021), mobility (Shih et al., 2013) or multicellularity (e.g., Bernardes et al., 2021). It

also serves as model for nutrition-related studies, including, nitrogen, sulfur, phosphate (Calatrava et al., 2017; Plouviez et al., 2022; Saroussi et al., 2017) as well metal homeostasis (Blaby-Haas & Merchant, 2017a; Hanikenne, 2003; Merchant et al., 2006).

So far, research into the Chlamydomonas biology has so far mostly relied on a limited set of strains, related to the strains isolated by Smith (Harris, 2009b; Smith, 1946; Smith & Regnery, 1950), hereafter referred to as laboratory strains. Nonetheless, 39 of these strains display high genotypic variation (up to 2%) in large regions of their genomes, corresponding to two distinct haplotypes, as well as phenotypic diversity (Gallaher et al., 2015). Field isolates hereafter referred as natural strains, display even higher (up to 3%) randomly distributed genetic variation in their genomes (Flowers et al., 2015).

Intraspecific variation in cellular zinc (Zn), copper (Cu), manganese (Mn) and Fe contents for 4 Chlamydomonas laboratory strains grown mixotrophically in TAP medium was reported (Kropat et al., 2011), whereas variation of growth, cell size and chlorophyll content in a partially overlapping set of 5 laboratory strains upon varying Fe supply was also described (Gallaher et al., 2015). Nonetheless, nutrient homeostasis research in Chlamydomonas mostly relied on the study of a handful of strains and mutants (Hui et al., 2022; Ibuot et al., 2017; Kochoni et al., 2022; Pittman et al., 2009b). Here, we aimed to uncover the extent of intraspecific variation in nutrient homeostasis in Chlamydomonas and to assess how the use of a few selected strains may provide an incomplete picture of homeostasis mechanisms. In particular, we: (i) explored the variation of growth and ionome profile within a panel of 14 natural and 10 laboratory Chlamydomonas strains grown mixotrophically in TAP, photoautotrophically in TMP as well as in 9 TAP media deficient for single nutrients (calcium, magnesium, nitrogen, phosphorus, sulphur, copper, iron, manganese and zinc), (ii) assessed the partitioning of this variation among laboratory and natural strains, and (iii) scored as phenotypic traits the expression of nutrient deficiency marker genes, examined the distinct molecular strategies deployed to manage nutrient deficiency in selected pairs of contrasting natural strains.

D. Results and discussion

1. Growth and ionome variation in mixotrophy and autotrophy

The 24 laboratory (L) and natural (N) strains (**Table S.II.1**) were initially grown in liquid medium in mixotrophy (TAP) and photoautotrophy (TMP). Cell density was recorded (OD_{750}, as a proxy to estimate biomass) from day 3 to 7 of culture, with an intermediary sampling point at day 4 for element profiling (**Figure S.II.1**). Final cell density (at day 7) in TAP medium was overall 4 times higher than in TMP (**Figure S.II.2, Dataset S.II.1 and S.II.2**). Cell density of the least growing strain in TAP [(N) CC-1374] was approximately 5x higher than growth of the least growing strain in TMP [(L) CC-5325]. Three laboratory strains (CC-5325, CC-125 and CC-3348) were among the 3 least

growing strains in TMP medium while the 3 least growing strains in TAP were natural strains (CC-1374, CC-2343, CC-2935) (**Figure II.1A**). In contrast, a laboratory strain (CC-1418) was one of the most growing strains in both TAP and TMP. Overall, the range of cell density variation at day 4, i.e., the range between the least and the most growing strains, among laboratory strains was larger in TMP (3.3x) than in TAP (1.5x), whereas the opposite was observed for natural strains, with a 1.64x range in TMP and a 2.7x range in TAP (**Dataset S.II.1**).

In TAP, copper (Cu) accumulation was the most variable trait, with a 12x range between the most and the least accumulating strains, whereas iron (Fe) accumulation was the least variable trait (2x) among micronutrients (**Figure II.2A**, **Dataset S.II.3**). Among macronutrients, calcium (Ca) accumulation displayed the widest variation (9x) upon growth in TAP, whereas phosphorus (P) accumulation was the least variable (2x). (**Figure II.2A**). Variation of Cu and Fe accumulation was larger in natural strains whereas Ca and P accumulation varied more in laboratory strains (**Dataset S.II.3**).

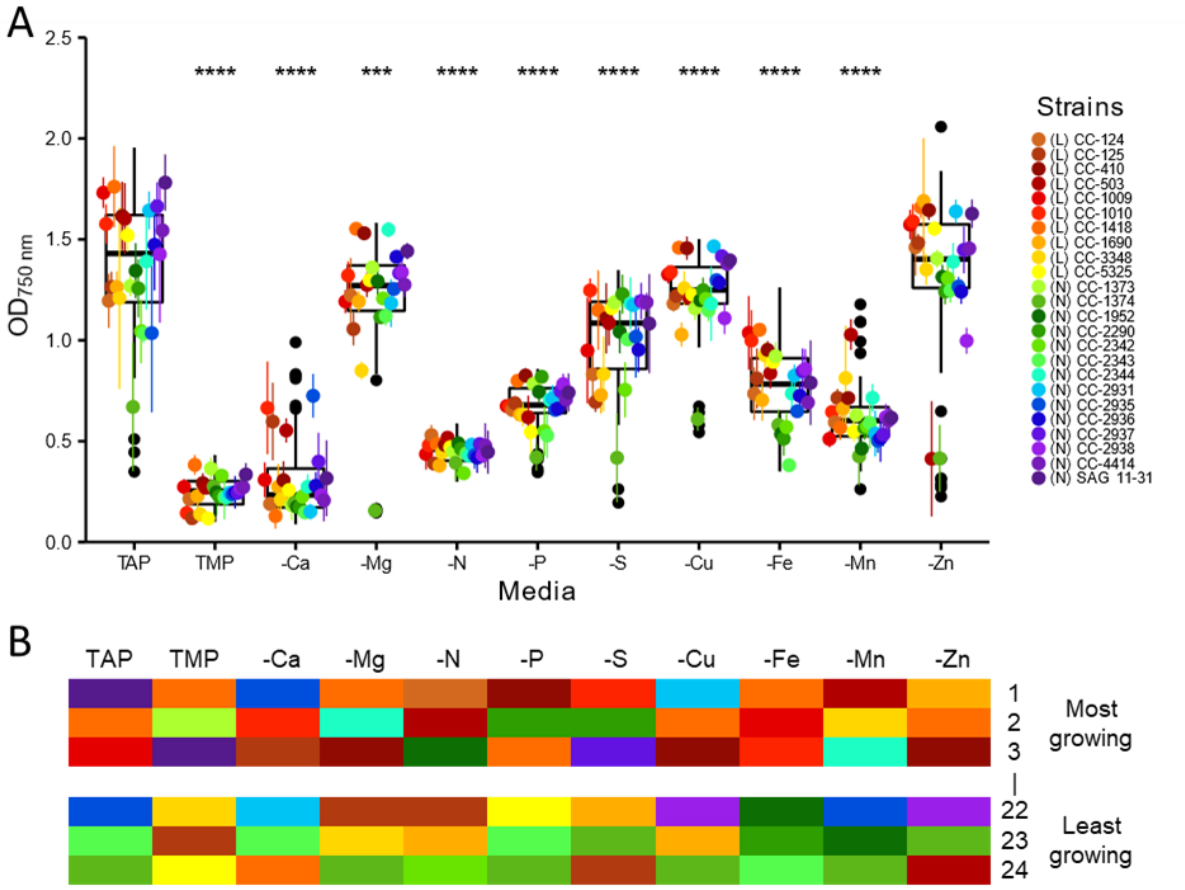

Figure II.1 Variation of the impact of nutrient deficiencies on growth of 24 Chlamydomonas strains. (A) Growth, measured as optical density at 750 nm (OD750nm), at day 4 of culture on TAP (mixotrophy, control), TMP and TAP with single deficiencies for 5 macroelements (-Ca, -Mg, -N, -P, -S) or 4 microelements (-Cu, -Fe, -Mn, -Zn). The boxes represent the 1st quartile, median and 3rd quartile of the raw data, and the whiskers extend from the median ± 1.5 interquartile range whereas outliers are represented by black dots. Each coloured dot represents the mean ± SD for each strain. Values are from 2 independent experiments, with 2 replicates each (n=4). The laboratory strains (L) are coloured in a yellow-dark red scale and the natural strains (N) are coloured in green-violet. The strains are ordered according to the colour key. OD750nm average values for each treatment were compared with the values of the TAP control condition using the Wilcoxon test, and significant differences are indicated with *: p <= 0.05, **: p <= 0.01, ***: p <= 0.001 and ****: p <= 0.0001. (B) Ranking of the strain growth from the most (1) to the least (24) performing. Rectangles are color-coded as in (A).

In TMP, the accumulation of all elements, with the stark exception of Cu, was higher than in TAP (**Figure II.2B**), with average Ca accumulation being the most increased (2.5x). The reduction in Cu content might result from decreased cellular Cu requirement, as respiration is decreased during photoautotrophic growth (Kropat et al., 2015). Similar to TAP, Cu accumulation was the most variable trait (11x), together with Ca accumulation (9x), and Fe accumulation varied the least (3x).

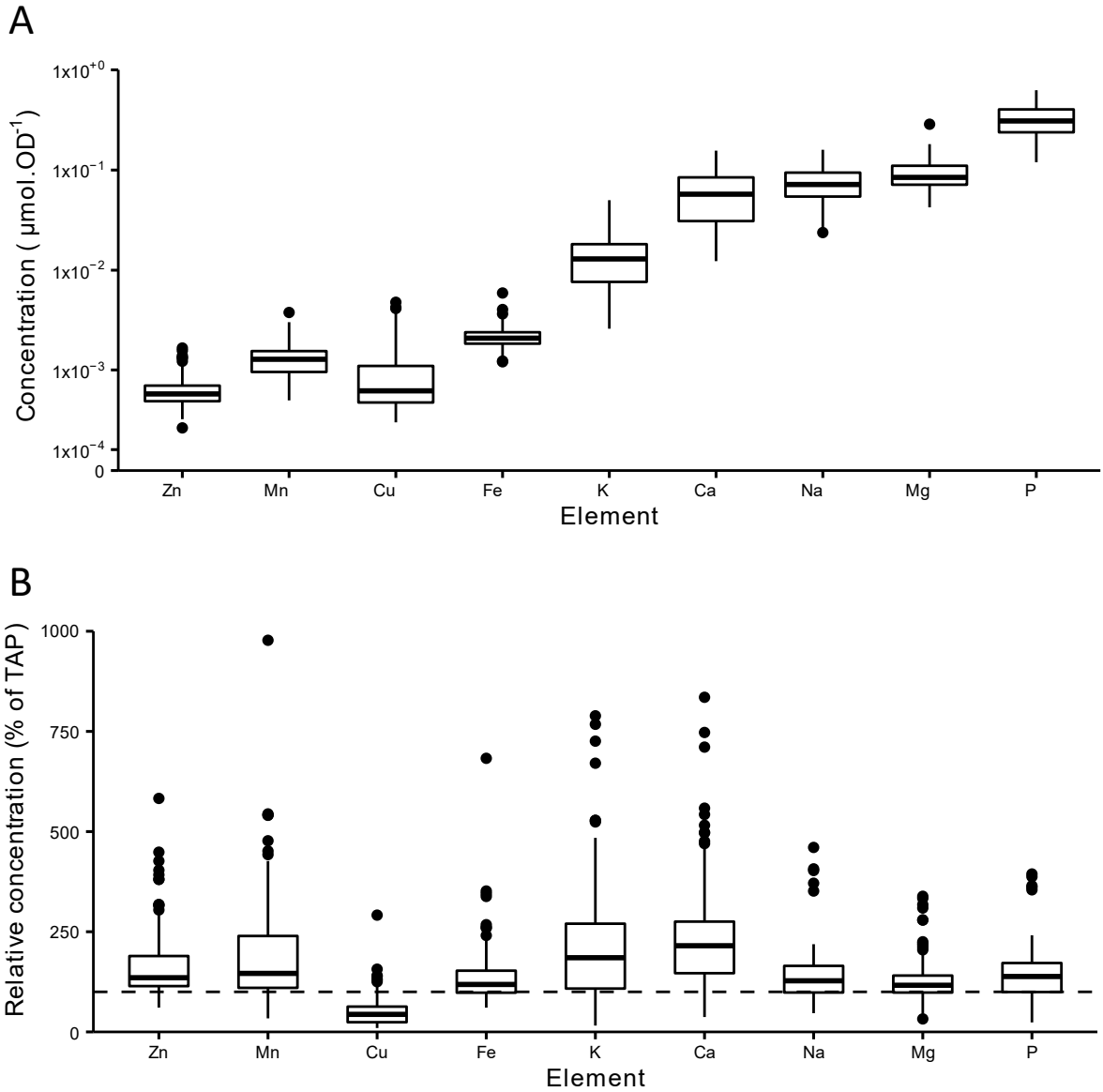

Figure II.2 Ionome profiling (ICP-AES) of the 24 strains cultured in TAP (A) and TMP (B) media. Elements are ordered from left to right by growing concentrations in cells (µmol. OD-1). In TMP, the values are relative to TAP (100%, noted with a dashed line). Values are from 2 independent experiments, with 2 replicates each (n=4).

The relative abundance of the micro- and macroelements reported here agrees with previous observations in 5 wild-type and 2 mutant strains in varied growth conditions (Merchant et al., 2006). However, the range of accumulation variation among strains in a single medium exceeds by far what has been previously reported in Chlamydomonas (Merchant et al., 2006). It is also much larger than ionome variation reported in roots or leaves of Arabidopsis accessions grown in hydroponics or on soil (Baxter et al., 2012). For instance, the range of Cu accumulation in roots of Arabidopsis

accessions was reported to be ~3x (Baxter et al., 2012), whereas it is ~12x in Chlamydomonas (**Figure II.2A**). The extent of variation observed among Chlamydomonas strains is comparable to variation observed between mutant and wild-type yeast strains (Yu et al., 2012).

2. Growth and ionome variation under nutrient deficiency

The strains were next grown for 7 days in TAP liquid medium either fully (-Ca, -Mn, -Zn) or partially (-Cu, -Fe, -Mg, -S, -P and -N) deprived of a mineral nutrient (**Table S.II.2**). Depending on the element, using partial or full depletion allowed finding a balance between inducing a deficiency response while at the same time maintaining growth. These differences in treatments determined different intensities of nutrient deficiency and, for the most part, may explain the differences in growth observed among deficiency conditions (**Figure II.2A**).

All nutrient deficiency treatments negatively impacted median growth of the strain panel at day 4, with the exception of -Zn (**Figure II.1A**). However, after 7 days of culture, all treatments resulted in lower average cell density comparatively to the TAP full nutrition control: this reduction ranged from 0.9x for -Zn to 0.3x for -Mn (**Figure S.II.3**). The absence or very weak effect of Zn deficiency (no Zn added in the medium, **Table S.II.2**) on growth was striking. Indeed, Chlamydomonas cells contain similar concentrations of micronutrients (Merchant et al., 2006 and **Figure II.2B**), but Mn deficiency (no Mn added in the medium as well, **Table S.II.2**) had a much stronger impact on growth than Zn deficiency, for instance. Both treatments also had a very different effects on residual Zn or Mn accumulation in the cells, with 0.2x and 0.02x reductions, respectively (**Figure II.3, Dataset S.II.4**). TAP medium was suggested to contain Zn in excess (Merchant et al. 2006), and Zn may be carried over in cells from the pre-culture. Alternatively, Chlamydomonas might be able to take up trace Zn contaminants present in the chemicals and acid-washed vessels used to prepare the TAP medium (Merchant & Helmann, 2012).

Laboratory strains overall tolerated nutrient deficiencies better than natural strains, representing ~70% of the top 3 most growing strains across all conditions. In contrast, natural strains represented ~63% of the bottom 3 least growing strains (**Figure II.1B, Dataset S.II.5**). The most growing laboratory strain in TAP [(L) CC-1418] was also among the 3 most growing strains under -Cu, -Fe, -Mg, -P and -Zn, whereas in contrast it was the strain the most impacted by -Ca. Two other laboratory strains were among the 3 most growing strains for multiple deficiency treatments: (L) CC-410 (-Cu, -Mg, -P and -Zn), and (L) CC-1010 (-Ca, -Fe and -S). On the other hand, the strains most often among the least growing strains were from both backgrounds: (N) CC-1374 (-Cu, -Mg, -Mn, -P, -S, -Zn), (L) CC-125 (-Mg, -N, -S), (L) CC-1690 (-Cu, -N, -S) and (N) CC-2343 (-Ca, -Fe, -P). However, while (N) CC-1374 and (N) CC-2343 were already among the least growing strains in TAP, the (L) CC-125 and (L) CC-1690 strains were in the top 3 most growing strains in -Ca and -Zn, respectively.

Overall, significant growth differences between natural (N) and laboratory (L) strains were observed in 6 out of 11 media, including TAP and TMP **(Figure S.II.4)**.

Average mineral accumulation levels in the strain panel were either increased (31% of all observations) or decreased (69% of all observations) by nutrient deficiencies, indicative of the tight

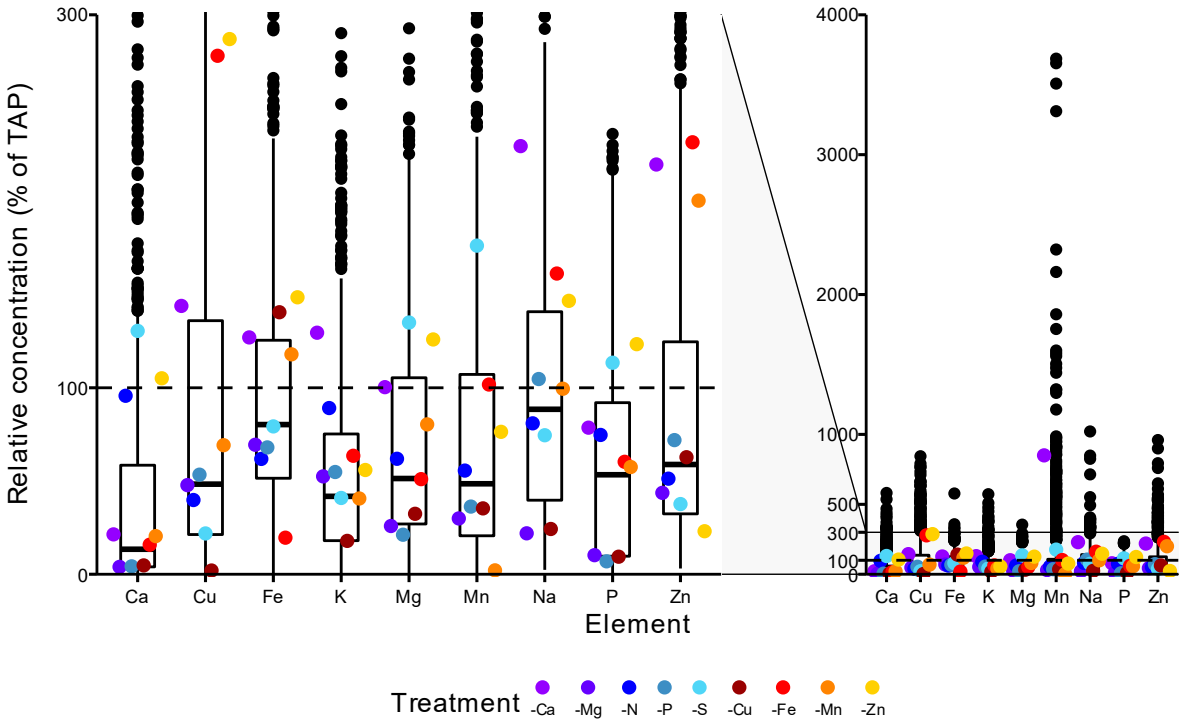

Figure II.3 Variation of the impact of mineral deficiencies on the ionome profile of 24 Chlamydomonas strains. Samples were analysed by ICP-AES at day 4 of culture on TAP (mixotrophy, control) and on TAP with single deficiencies of 5 macroelements (-Ca, -Mg, -N, -P, -S) or 4 microelements (-Cu, -Fe, -Mn, -Zn). The concentrations of the 9 quantified elements (Ca, Cu, Fe, K, Mg, Mn, Na, P, Zn) are represented relatively to their concentrations in TAP (100%, noted with a dashed line). The boxes represent the 1st quartile, median and 3rd quartile of the raw data, and the whiskers extend from the median ± 1.5 interquartile range whereas outliers are represented by black dots. Coloured dots represent the relative average element concentrations per treatment: macronutrient deficiencies (-Ca, -Mg, -N, -P, -S) in blue scale and micronutrient deficiencies (-Cu, -Fe, -Mn, -Zn) in red scale. The entire dataset is presented in the right panel, and a focus on the relative concentrations ranging 0%-300% relative to the control is shown in the left panel.

interconnections among nutrient homeostasis networks (**Figure II.3, Dataset S.II.5**). In particular, the elements whose supply was limited in the medium all displayed on average a strongly reduced accumulation in the strains, ranging from a 0.3x reduction for Mg to a 0.02x for Cu, indicating that the deficiency treatments were effective. Whereas average growth reduction ranged between 1x and 0.2x, the impact of nutrient deficiencies on element accumulation was massive ranging from 0.3x to 1.3x for Mg to 0.02x to 8.5x for Mn compared to TAP. Across all conditions and strains, Fe accumulation again appeared the most tightly regulated, as in TAP, whereas the most variable elements were other micronutrients, Cu, Mn and Zn.

Most striking was the global effect of Ca deficiency on Mn accumulation which on average increased by 8.5x across the 24-strain panel compared to TAP. Ca-Mn interactions have been described previously, as both elements co-localise in acidocalcisomes, lysosome-derived structures storing metals in excess for future use, in Chlamydomonas (Tsednee et al., 2019). Several

transmembrane transporters [e.g., CAX (Cation Exchanger) or BICAT (bivalent cation transporter)] involved in the transport of both Ca and Mn have been identified in plants, including for the import of these elements into the chloroplast, as well as other compartments, where Mn may also replace Ca at Ca-binding-sites (reviewed in He et al., 2021). Mn levels also raised in S deficiency (1.8x), and the element was likely stored in acidocalcisomes, which seem to play a role in trace element homeostasis in S deficiency (Schmollinger et al., 2021).

Cu was strongly accumulated upon Ca (1.4x), Fe (2.8x) and Zn (2.9x) deficiencies. Zn displayed higher accumulation upon Mn (2x), Ca (2.2x) and Fe (2.3x) deficiencies, and conversely Fe accumulated more in cells upon Cu (1.4x) and Zn (1.5x) deficiencies. The interplay between these nutrients has been observed previously and is at least in part due to shared or interacting uptake pathways (Allen et al., 2007b; la Fontaine et al., 2002; Malasarn et al., 2013) or in the case of Ca and micronutrients to co-localization in the acidocalcisomes (Schmollinger et al., 2021).

Compared to TAP, Ca accumulation was negatively affected in a similar fashion by Ca, but also Fe and Mn deficiencies (~0.2x), and even more so by Cu, Mg and P deficiencies (<0.05x) (**Figure II.3**). P was the second most negatively affected element, with strong accumulation reduction upon Cu and Mg deficiencies (~0.1x). This interaction between P and Mg homeostasis was expected, as Mg is chelated by rRNA and ATP, the largest cytoplasmic reservoirs of Pi and Mg. Co-regulation mechanisms have been described, such as ATP reduction via Pi uptake inhibition during Mg starvation (Bruna et al., 2021) or translocation of P from mature to young leaves during Mg deficiency in *Arabidopsis* (Ogura et al., 2020).

A number of nutrient interactions observed in this study were reported before in individual strains, such as an increased Cu and Fe accumulation upon Zn deficiency described for CC-4532 (Malasarn et al., 2013) or reduced P accumulation in Mn deficiency reported for strain CC-425 (Allen et al., 2007b) suggesting that, although subjected to important variation, the direction of these interactions is conserved among strains. In contrast, on average across the 24 strains, Mn concentrations decreased upon Zn deficiency and Fe concentrations increased upon Mn deficiency while opposite trends were observed in individual strains by Malasarn et al. (2013) and Allen et al. (2007b), respectively, suggesting that nutrient interactions can also occur in opposite directions among strains.

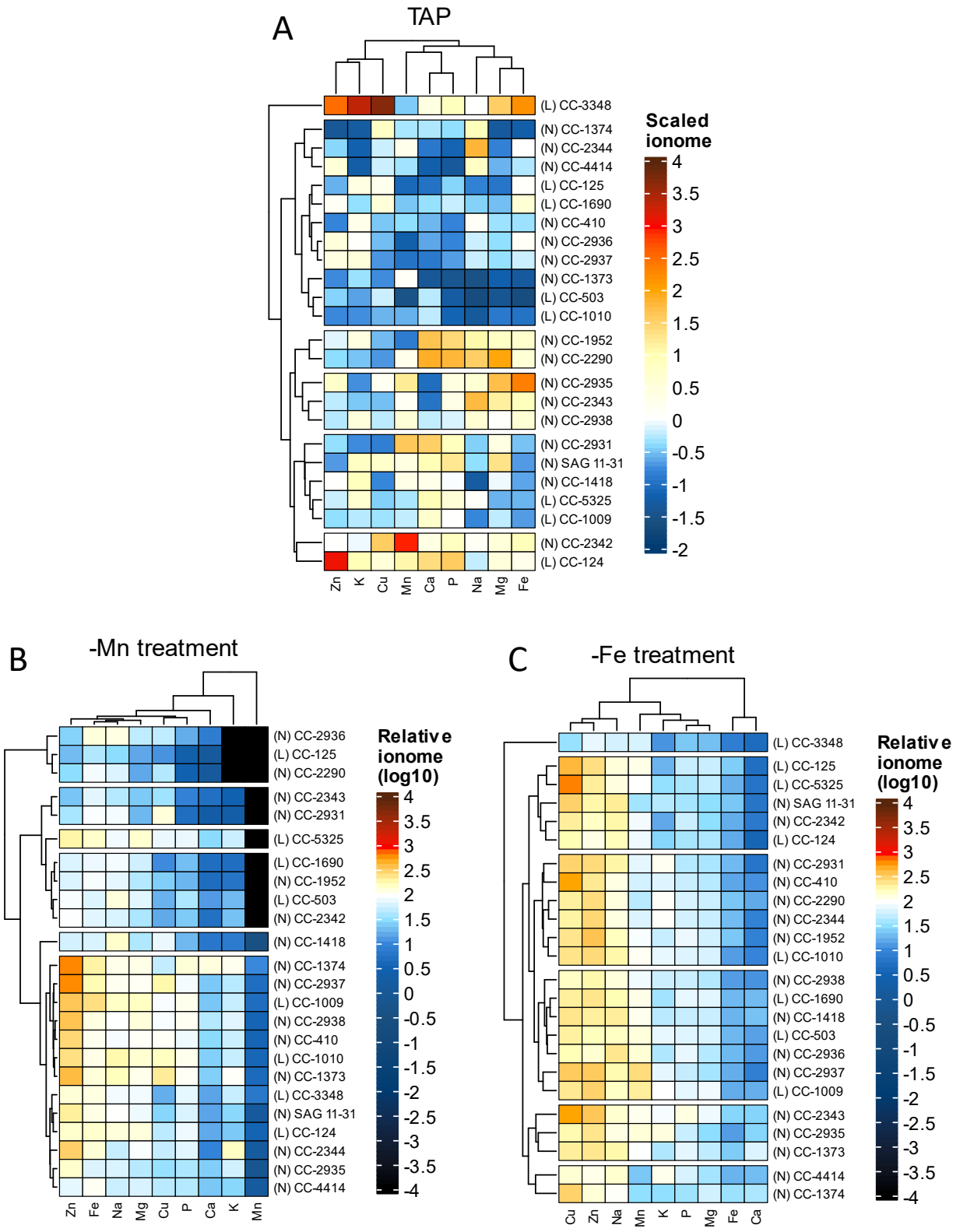

Figure II.4 Clustering of 24 Chlamydomonas strains based on their ionome profiles. The concentrations of 9 elements (Ca, Cu, Fe, K, Mg, Mn, Na, P, Zn) were measured by ICP-AES in samples collected at day 4 of culture in TAP (mixotrophy, control) (A) or in TAP with Mn (B) or Fe (C) deficiencies. Concentration values are provided as mean values from 2 independent experiments, with 2 replicates each (n=4). (A) TAP. The average values per strain were centred on the average values across the 24 strains and scaled around this average, per column (values are provided in Dataset S9). Central values are in white. (B-C) Mn and Fe deficiencies, respectively. The average concentrations are relative to the TAP condition. For easier representation, null values were replaced by 10[-4]. The data was scaled using a log10 transformation and the control value, represented as 2 (100% = 10[2] %), is coloured in white. Dendrograms represent the Euclidean distance clustered by complete linkage. Strain origin [natural (N) or laboratory (L)] is shown between brackets. Boxed strains were used for detailed pairwise comparisons

3. Ionome variation at the strain level under nutrient deficiency

Hierarchical clustering of the element profiling data was next conducted to further assess the determinants of the ionomic variation in Chlamydomonas (**Figure S.II.5, Dataset S.II.6**). It is remarkable that the growth conditions had a bigger impact on the clustering than the strain origin, lab or natural. This for instance contrasts with (i) the footprint of local adaptation in the metal hyperaccumulator *Arabidopsis halleri*, where geographic origin has more impact on the ionome and transcriptome than the exposure to Zn or cadmium (Cd) excess (Corso et al., 2021, 2018; Schvartzman et al., 2018) or (ii) a number of ionomic traits in Arabidopsis (Campos et al. 2021). In Chlamydomonas, the treatment clusters seldom contained strains grown in other conditions. Mn deficiency was a noticeable exception, with strains distributing in two distant clusters, independently of their lab or natural origin, whereas strains exposed to N deficiency were the most dispersed among clusters (**Figure S.II.5**).

A more detailed analysis of data clustering was then conducted for individual growth conditions. It showed that, even in TAP, very distinct element accumulation patterns were observed among strains **(Figure II.4A)**. Most clusters grouped both lab and natural strains, suggesting again that strain origin was not the most discriminating factor. The (L) CC3348 strain displayed the most divergent ionome profile, marked by high Fe, Zn, K and Cu, but low Mn, accumulation **(Figure II.4A)**.

Upon Mn deficiency **(Figure II.4B)**, 10 strains, 4 of which laboratory strains, accumulated Mn below detection levels and, for 3 of those, K could not be detected either. The effect of Fe deficiency on the strain ionomes displayed a general trend: an overaccumulation of Cu, Zn and Na coupled with an under accumulation of Mg, Fe and Ca **(Figure II.4 C)**, with the exception of strain (L) CC-3348, which under accumulated all elements.

Clustering in the other deficiency media showed the same blend of natural and laboratory strains, and how the accumulation of some elements was key for clustering **(Figure S.II.6)**. Briefly, in TMP, two laboratory strains (CC-5325 and CC-1010) were an exception with increased Cu accumulation opposite to the lower accumulation observed in all other strains (**Figure II.1G**). Although it varied in amplitude (40x), Mn accumulation in -Ca condition was a conserved trait in all strains, with the exception of strain CC-2342 **(Figure S.II.6 E)**. Overall the -N, -Zn and -S conditions had the lowest impact on the ionomes **(Figure S.II.6 B, H, D)**, whereas the -P, -Mg and -Cu conditions had a strong negative effect on the accumulation of most elements in cells **(Figure S.II.6 C, F, G)**.

At the end of this analysis, pairs of divergent natural strains were selected for a deeper exploration of the variation of the Mn and Fe deficiency responses (by scoring expression of nutrient status marker genes and photosynthetic parameters), as these conditions had a strong impact in the ionome phenotypes (**Figure II.4B-C**).

a) Manganese deficiency response in two natural strains

Two natural strains with contrasting ionome phenotypes upon Mn deficiency were selected: (N) CC-2290, which accumulated Mn and K below detection levels, and (N) CC-1373, which accumulated those two elements **(Figure II.4B)**. In this condition, the strains also differed in their accumulation of Fe (1.5x), Cu (5.1x), Mg (7.3x), Zn (13x) and P (33x), all those elements being more accumulated in CC-1373 (**Figure S.II.7, Dataset S.II.7**).

NRAMP1 (*Natural Resistance-Associated Macrophage Protein 1*), a gene strongly induced by Mn deficiency (Allen et al., 2007b) whose product was suggested to transport Mn in yeast (Rosakis & Köster, 2005) and to be a Mn assimilation transporter in Chlamydomonas (Allen et al., 2007b), was constitutively lower expressed (4x) in TAP in strain CC-2290 (**Figure II.5A**). *NRAMP1* moreover failed to be induced by Mn deficiency in strain CC-2290, which resulted in a 125x lower expression than in strain CC-1373 **(Figure II.5A)**. Similarly, the expression of *MTP4* (*Metal Tolerance Protein 4*) was lower in CC-2290 in TAP and was not induced by Mn deficiency, compared to CC-1373 (8x induction) (**Figure II.5A**). *MTP4* was previously shown to be Mn-deficiency inducible in a laboratory strain and encodes an Mn-transporting MTP, possibly involved in Mn internal storage (Allen et al. 2007b; Ibuot et al., 2020).

Allen et al. (2007b) showed that Mn deficiency in the CC-425 lab strain resulted in reduced Fe accumulation, and in the transcriptional induction of genes encoding the Fe uptake machinery in Chlamydomonas (for review, see Blaby-Haas & Merchant, 2012, 2017a; Hanikenne et al., 2009). In the natural strain CC-1373, two components of this machinery [*FRE1* (*Ferric Reductase 1*) and *FOX1* (*Ferroxidase 1*)], used as Fe deficiency marker genes) were upregulated by Mn deficiency. As for *NRAMP1* and *MTP4*, the Mn-responsiveness of these genes was abolished in strain CC-2290 **(Figure II.5A)**. Albeit less marked, a similar expression profile was observed for the *IRT1* (*Iron-Regulated Transporter 1*) gene, involved in an alternative Fe^{2+} uptake pathway than *FOX1* (Hanikenne et al. 2009; Blaby-Haas & Merchant, 2012, 2017), among the two strains **(Figure II.5A)**, resulting in a ~20x lower expression of the gene in strain CC-2290 compared to CC-1373 upon Mn deficiency.

Chlamydomonas possesses two superoxide dismutase (SOD) isozymes: a Mn containing (MnSOD) in the mitochondria, and a Fe containing (FeSOD) in the chloroplast (Kitayama et al., 1999). The MnSOD is encoded by 5 genes (*MSD1-5*). *MSD3* is the isoform most induced transcriptionally by both Mn and Fe deficiency and MnSOD activity was reported to be reduced under Mn deficiency (Allen et al., 2007b). This loss in activity is not compensated by an increased expression or activity of the plastid FeSOD (FSD1) in the CC-425 laboratory strain (Allen et al., 2007b). In strain CC-1373, the expression of both *MSD3* and *FSD1* was strongly induced by Mn deficiency **(Figure II.5A)**, suggesting a compensation mechanism replacing MnSOD by FeSOD, in contrast to CC-425. *MSD3* was constitutively highly expressed in both TAP and -Mn conditions and *FSD1* was down-regulated by -Mn in strain CC-2290.

The two natural strains further differed in their Cu and Zn accumulation levels upon Mn deficiency (**Figure II.4B**), and marker genes for the Cu and Zn nutritional status were investigated. The *CTR2* gene, encoding a high affinity Cu transporter located at the plasma membrane and responsive to Cu (Castruita et al., 2011; Page et al., 2009), was significantly induced in strain CC-1373 by Mn deficiency, unlike in strain CC-2290. In contrast, the expression of *ZRT1* and *ZRT3*, two Zn-nutrition responsive transporters (Malasarn et al., 2013), was unaltered by Mn deficiency, although *ZRT1* was significantly overexpressed in CC-1373 compared to CC-2290 **(Figure II.5A)**.

The contrasted expression patterns of Mn-, Fe-, Cu- and Zn-responsive genes, encoding metal transporters, in the two strains are likely to account for the contrasted Mn (*NRAMP1, MTP4*), as well as Fe (*FRE1*, *FOX1*), Cu (*CTR2*) and Zn (*ZRT1*) accumulation levels in the two strains in control and/or in Mn deficiency conditions (**Figure II.4B**). Differential expression between the two strains does not only concern genes encoding functions in metal uptake at the plasma membrane, but also reflects different intracellular storage (*MTP4*) and metal usage (*FSD1*/*MSD3*) strategies. Some of the transporters may influence the accumulation of several elements. Hence, *NRAMP1* has been reported to also transport Zn (Chang et al., 2020). Given the low selectivity for metal cations, including Mn and Zn, of the IRT1 homolog in Arabidopsis (Dubeaux et al., 2018; Vert et al., 2001), it may directly contribute to Mn and Zn uptake. The reduced Cd accumulation in an *irt1* Chlamydomonas mutant (Thiriet-Rupert et al., 2021a) indeed suggests that IRT1 may also transport divalent metal cations other than Fe. Noticeably, despite some major differences of *NRAMP1*, *FRE1* or *FOX1* gene expression in TAP, there was only relatively minor variation of Fe (1.5x), Mn (1.04x, not significant), and Zn (1.2x, not significant) accumulation between strains CC-2290 and CC-1373 (**Figure S.II.7**).

Interactions between Mn and Fe, Zn or Cu homeostasis have been extensively documented in both flowering plants (Hanikenne et al., 2020; Ricachenevsky et al., 2018; Socha & Guerinot, 2014) and Chlamydomonas (Allen et al., 2007b; Blaby-Haas & Merchant, 2017a; Castruita et al., 2011; Hanikenne et al., 2009, 2005b; Urzica et al., 2012) mainly because these nutrients share transporters and chelators. In Chlamydomonas, Fe-deficiency response elements are for instance found in the promoter of genes encoding Mn transporters (e.g., MTP4, Fei et al., 2009). The diversity of the molecular response to Mn deficiency among two natural strains highlights that these interactions can take different forms within the species, suggesting possible divergence in Mn sensing and regulatory mechanisms.

Mn deficiency is known to lead to secondary P deficiency and to the up-regulation of a number of P transporters in the CC-425 laboratory strain (Allen et al., 2007b). This transcriptional regulation was however suggested to be independent of the P deprivation regulatory network (Allen et al., 2007b). Natural strains CC-1373 and CC-2290 displayed opposite P accumulation profiles: in strain CC-1373, P accumulation was low on TAP and slightly increased (1.1x) upon Mn deficiency (**Figure II.4A-B**) whereas it was high on TAP and decreased (0.03x) upon Mn deficiency in strain CC-2290

(**Figure II.4A-B**). The P accumulation profiles were essentially mirrored by the expression of *PTB2*, a P-nutrition responsive phosphate transporter-encoding gene (Grossman & Aksoy, 2018; Moseley et al., 2006), whose expression was induced by Mn deficiency in CC-1373 and was constitutively high in CC-2290 (**Figure II.5A**).

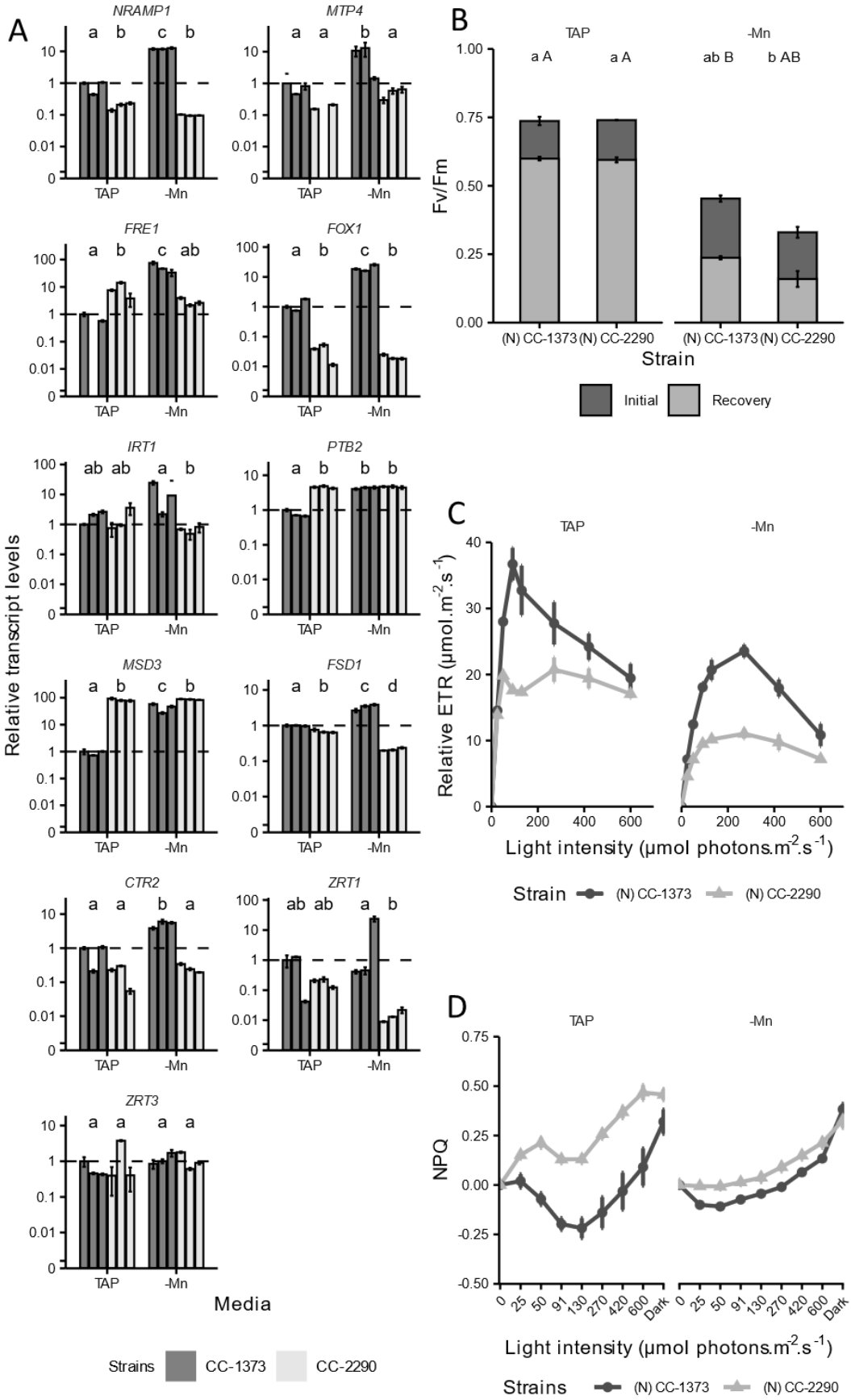

Figure II.5 Variation of the nutrient marker gene and photosynthetic responses to Mn deficiency between the CC-1373 and CC-2290 Chlamydomonas natural strains. Samples were collected at day 4 of culture in TAP and in TAP -Mn media.

Figure II.5 (cont) (A) Relative transcript levels of the *NRAMP1*, *MTP4*, *FRE1*, *FOX1*, *IRT1*, *PTB2*, *MSD3*, *FSD1*, *CTR2*, *ZRT1* and *ZRT3* genes in the strains CC-1373 and CC-2290. Values are means ± SE of 3 technical PCR replicates performed on samples from 2 to 3 biological replicates for each strain and condition. The expression levels are relative the CbLp and RPL13 housekeeping genes and to the average of the 3 technical replicates of the first biological replicate of strain CC-1373 in TAP medium (1 unit, noted with a dashed line). The Y-axis is transformed using a pseudo-logarithmic scale, starting at 0.001 (unlabelled tick mark). Statistically different (Dunn test, $p<0.05$) expression levels are represented with different letters. **(B)** Maximum quantum yield of photosystem II (Fv/Fm) of dark-adapted samples before (initial, dark grey) and 23 minutes after (recovery, light grey) the saturation curve measurement. **(C)** Relative electron transport (rETR) upon exposure to increasing light intensity (0-600 µmol photons.m^{-2}.s^{-1}). **(D)** Non-photochemical quenching (NPQ) upon exposure to increasing light intensity (0-600 µmol photons.m^{-2}.s^{-1}) followed by darkness (Dark). (B-D) Values are means ± SD (n=3). Non-parametric pairwise multiple comparisons were performed using Dunn's test and the different grouping letter were attributed when statistical differences were found. Small letters in **(B)** refer to the initial Fv/Fm while the capital letters refer to the recovery. Statistics for rETR and NPQ data can be found in **Dataset S.II.7**.

Mn is essential for photosynthesis: it is a key component of the oxygen-evolving complex (OEC– Mn_4CaO_5), thanks to its multiple oxidation states, which allow the catalysis of water deprotonation and electron transfer through the photosynthetic chain (Merchant & Sawaya, 2005; Shen, 2015). Mn-deficiency is known to impact photosynthesis at the photosystem II (PSII) level (Allen et al., 2007b; Teichler-Zallen, 1969). Therefore, some photosynthetic parameters were evaluated in the two strains: (i) the maximum quantum yield of photosystem II (PSII) photochemistry (Fv/Fm), (ii) the relative electron transfer rate of photosystem II (rETR) at different light intensities, (iii) non photochemical quenching (NPQ) at different light intensities, and (iv) photoinhibition measured from Fv/Fm recovery in the dark after the exposure to actinic light (reviewed in Murchie & Lawson, 2013). In TAP, both strains exhibited similar Fv/Fm and rETR upon low light exposure (**Figure II.5B-C, Dataset S.II.8)**. This was reflected by similar OD_{750nm} for CC-2290 and CC-1373 achieved at day 4 (Figure 1A). In contrast, upon high light exposure in TAP, rETR values were lower and NPQ values higher in CC-2290 (**Figures II.5C-D**). Under Mn deficiency at all light intensities, CC-2290 was more impacted than CC-1373 (**Figures II.5C**), with lower rETR values, which is consistent with the stronger growth reduction observed for CC-2290 in these conditions. Altogether, these observations point to a donor-side PSII limitation at the level of the OEC because of low intracellular [Mn] in CC-2290. In addition, a lower chla:b ratio was observed in CC-2290 under Mn deficiency, which suggested a higher PSII:PSI stoichiometry, as previously observed in pea (Chow et al., 1990), or a larger chlb-rich PSII antenna size in CC-2290 (**Figure S8C**).

b) Iron deficiency response in two natural strains

Fe deficiency resulted in variation of Fe accumulation among natural strains (**Figure II.4C, Dataset S.II.6**) but had even more impact on the accumulation of other elements (**Figure II.4C**) and on cell density (**Figure S.II.3**). Two natural strains, CC-2343 and CC-4414, differing for P (1.9x), Zn (2.6x), Mn (3.3x) and Cu (4x) accumulation (**Figure S.II.9, Dataset S.II.9)**, as well as growth (1.8x), upon Fe deficiency were further characterized.

Components of the Fe uptake machinery were differentially expressed in the two natural strains (**Figure II.6A**). *FOX1* was less expressed in TAP and displayed lower induction by Fe deficiency in strain CC-2343, having a higher Fe accumulation in both conditions (**Figure II.4A, C**), compared to strain CC-4414. *FRE1* and *IRT1* were in contrast expressed at similar levels and strongly

induced by Fe deficiency in both strains (**Figure II.6A**). All 3 genes were previously reported to be strongly induced by Fe deficiency in the CC-425 and CC-4532 laboratory strains (Allen et al., 2007a, 2007b; Glaesener et al., 2013; Urzica et al., 2013).

Similarly, the *CTR2* and *CYC6* (*Cytochrome c_6*) genes were up-regulated by Fe deficiency in strain CC-4414 only (**Figure II.6A**). As mentioned above, CTR2 is involved in Cu uptake, whereas *CYC6* encodes an heme-containing cytochrome, which substitutes for plastocyanin under Cu deficiency enabling maintenance of photosynthesis in these conditions (Kropat et al., 2015; Merchant, 1998; Merchant & Bogorad, 1986). The *CTR2* and *CYC6* induction by Fe deficiency in strain CC-4414 suggests a higher Cu requirement and Cu sparing, through plastocyanin replacement, in the strain, possibly to support the strong induction of the FOX1 multicopper oxidase (Kropat et al., 2015). It however did not fully compensate this increased Cu demand, as the CC-4414 strain accumulated less Cu (0.25x) than strain CC-2373 upon Fe deficiency (**Figure II.4C**).

NRAMP1 expression was similar between the two strains in TAP (**Figure II.6A**), consistent with their similar Mn accumulation (**Figure II.4A**). *NRAMP1* was previously shown to respond to Mn but not Fe deficiency in Chlamydomonas laboratory strains (Allen et al., 2007b; Urzica et al., 2012). This does not exclude that NRAMP1 can transport other metal cations than Mn (Chang et al., 2020), including Fe, as its distantly related NRAMP1 plant homologs (Blaby-Haas & Merchant, 2012; Hanikenne et al., 2005b), which are involved in both Mn and Fe homeostasis (Cailliatte et al., 2010; Castaings et al., 2016; Chen et al., 2019). In our conditions, Fe-deficiency led to reduced (0.2x) Mn accumulation in strain CC-4414, which was not compensated by increased expression of *NRAMP1*, in agreement with previous reports in lab strains (Allen et al., 2007b). In contrast, in strain CC-2343, Fe deficiency had a positive effect on Mn nutrition, with higher Mn accumulation (1.1x) accompanied by decreased *NRAMP1* expression. Fe deficiency induces the *IRT1* and *IRT2* genes (Figure 6A, Blaby-Haas & Merchant, 2012; Urzica et al., 2012), whose products might be responsible for increased Mn uptake (Dubeaux et al., 2018).

Chlamydomonas cells experiencing Fe deficiency are more susceptible to oxidative damage (Naumann et al., 2007) and the transcriptional response to Fe deficiency involves a large set of oxidative stress response genes (Urzica et al., 2012). In laboratory strains, strong induction of *MSD3* (encoding a chloroplast and mitochondria localized MnSOD), at the transcript, protein and activity levels, has been reported upon Fe deficiency (Allen et al., 2007b; Page et al., 2012; Urzica et al., 2012). FeSOD, also chloroplast-localized, encoded by *FSD1*, has a more complex fate. It is not transcriptionally regulated by Fe deficiency. However, in these conditions, the FSD1 protein is initially degraded, before *de novo* synthesis and Fe re-acquirement enabled by an Fe sparing machinery triggered at the expense of other Fe-containing proteins (Allen et al., 2007b; Page et al., 2012; Urzica et al., 2012). The CC-2343 and CC-4414 natural strains deployed distinct strategies to

deal with the Fe deficiency-induced oxidative stress: CC-2343 induced *FSD1* expression whereas CC-4414 induced *MSD3* as described in laboratory strains (**Figure II.6A**).

Fv/Fm and rETR were reduced upon Fe deficiency in both CC-2343 and CC-4414 natural strains **(Figure II.6B-C, Dataset S.II.10)**, indicating impaired photosynthesis. However, the photosynthetic apparatus of strain CC-4414 was more impacted upon Fe deficiency as indicated by lower maximum rETR, lower NPQ at most light intensities, and a lower Fv/Fm recovery. In Chlamydomonas laboratory strains, a major target of Fe deficiency is the Fe-rich PSI complex, which is subject to reduction and remodelling, as well as other Fe-requiring photosystem proteins, with the purpose of sparing Fe and prioritizing respiration (Moseley et al., 2002; Page et al., 2012; Yadavalli et al., 2012). Despite these preventive measures, electron flow between PSII and PSI was shown to be disturbed, leading to ROS generation, which primarily targets PSII (Naumann et al., 2007). Here, strain CC-4414 displayed an increased chla:b ratio upon Fe deficiency, indicative of an increased PSI:PSII ratio (Chow et al., 1990), which may suggest either (i) a lower capacity to recycle and remodel PSI in these conditions and/or (ii) a higher sensitivity of PSII to ROS. The higher NPQ observed in CC-4414 upon Fe deficiency, at least at some light intensities (**Figure II.6D, Dataset S.II.10**), may support the latter hypothesis. Chlorosis was reported to be not visible at early Fe-deficiency stages (Moseley et al., 2002; Terauchi et al., 2010; Urzica et al., 2012). At day 4, both CC-2273 and CC-4414 cell culture appeared lighter green **(Figure S.II.10A)**, which may be linked to the decrease in chlorophyll:carotenoid ratio in Fe-deficiency **(Figure S.II.10D)**.

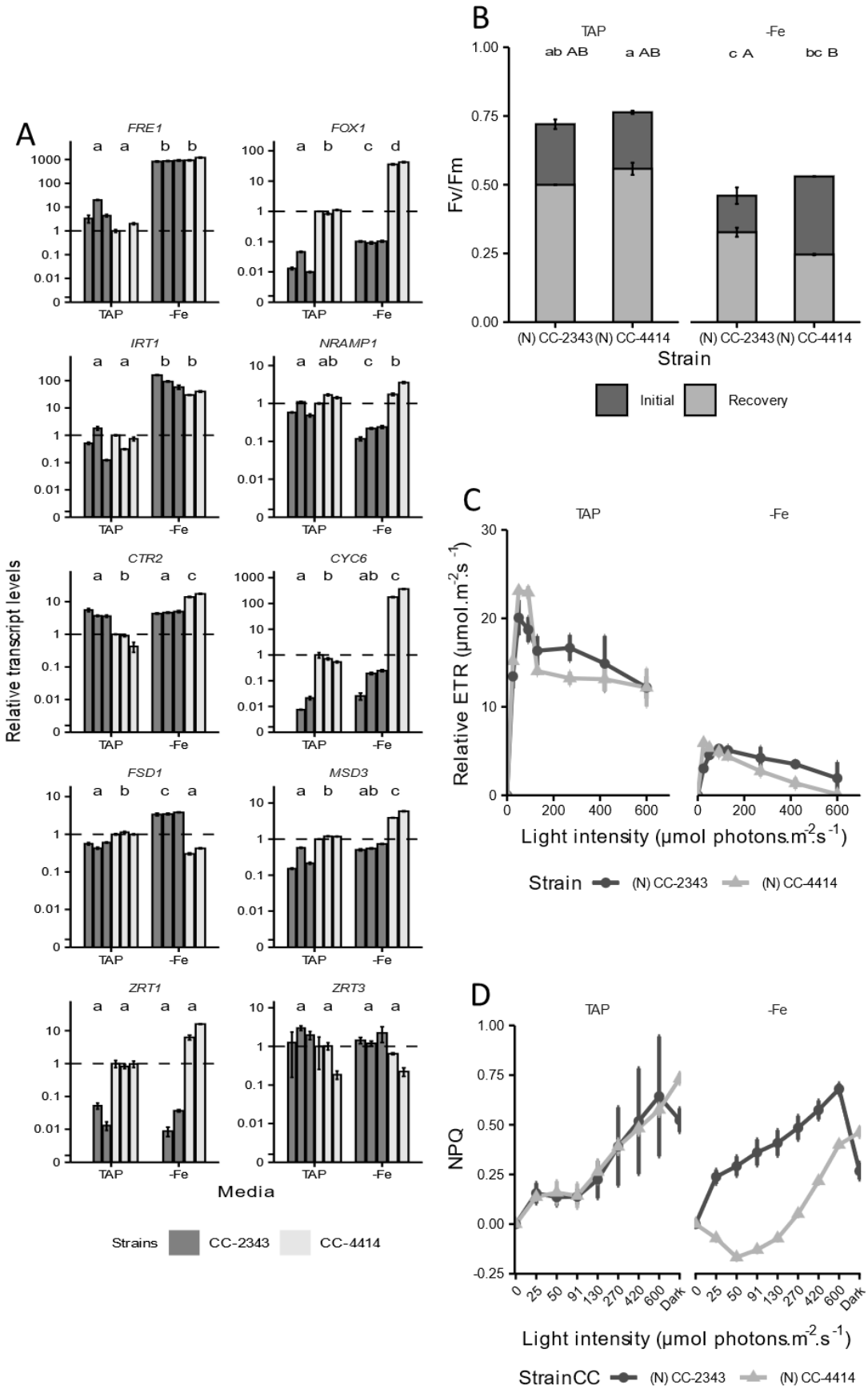

Figure II.6 Variation of the nutrient marker gene and photosynthetic responses to Fe deficiency among the CC-2343 and CC-4414 Chlamydomonas natural strains. Samples were collected at day 4 of culture in TAP and in TAP -Fe media.

Figure II.6 (cont) (A) Relative transcript levels of the *FRE1*, *FOX1*, *IRT1*, *NRAMP1*, *CTR2*, *CYC6*, *FSD1*, *MSD3*, *ZRT1* and *ZRT3* genes in strains CC-2343 and CC-4414. Values are means ± SE of 3 technical PCR replicates performed on samples from 2 to 3 biological replicates for each strain and condition. The expression levels are relative the CbLp and RPL13 housekeeping genes and to the average of the 3 technical replicates of the first biological replicate of the strain CC-4414 in TAP medium (1, noted with a dashed line). The Y-axis is scaled using a pseudo-logarithmic scale, starting at 0.001 (unlabelled tick mark). Statistically different (Dunn test, $p<0.05$) expression levels are represented with different letters. **(B)** Maximum quantum yield of photosystem II (Fv/Fm) of dark- (initial, dark grey) and light-adapted cells (recovery, light grey). **(C)** Relative electron transport (rETR) of the strains exposed to an increasing light intensity (0-600 µmol photons.m-2.s-1). **(D)** Non-photochemical quenching (NPQ) upon exposure to increasing light intensity (0-600 µmol photons.m-2.s-1) followed by darkness (Dark). (B-D) Values are means ± SD (n=3). Non-parametric pairwise multiple comparisons were performed using Dunn's test and the different grouping letter were attributed when statistical differences were found. Small letters in (B) refer to the initial Fv/Fm while the capital letters refer to the recovery. Statistics for rETR and NPQ can be found in **Dataset S.II.9**.

The response of Chlamydomonas laboratory strains to reduced Fe supply in the medium has been characterized in details, distinguishing two stages: (i) a deficiency response, when Fe supply is reduced but is more or less sufficient to sustain growth essentially thanks to the induction of the Fe uptake pathways (*FOX1*/*FTR1* on one side and *IRT1*/*IRT2* on the other side); and (ii) a limitation response, when Fe supply is so low that cells are strongly affected and trigger massive reorganisation of the photosynthetic apparatus to spare Fe (Allen et al., 2007a; la Fontaine et al., 2002; Merchant et al., 2006; Moseley et al., 2002; Naumann et al., 2007; Page et al., 2012; Urzica et al., 2012). Here, we reduced Fe supply to 1.8 µM Fe, corresponding to the deficiency stage described above (**Table S.II.2**). However, Fe accumulation and Fe-responsive gene expression patterns, together with oxidative stress management and photosynthetic responses, altogether suggest that the two natural strains handle Fe homeostasis distinctly, with strain CC-4414 experiencing a stronger Fe deficiency possibly stemming from less efficient Fe uptake, reduced Fe sparing capacity and/or higher Fe requirements, even on TAP, which in turn impacts the accumulation and use of other metals, such as Cu, Mn and Zn. That such variation of Fe homeostasis existed in Chlamydomonas was previously shown (Gallaher et al., 2015). We provide here some molecular understanding of the mechanisms underlying such variation.

E. Conclusions

In this study, we describe the large extent of phenotypic variation that exists in a panel of 24 Chlamydomonas strains, in line with the important genetic variation previously reported among laboratory and natural strains (Flowers et al., 2015; Gallaher et al., 2015). This variation was evident in both mixo- and photoautotrophy, as well as upon deficiency of essential macro- and microelements. Growth variation was observed in all tested conditions, with in several cases partitioning of this variation among natural and laboratory strains. Strikingly, much larger variation was observed at the ionome level, including for observed interactions between elements. This variation was quite extensive in comparison to other model organisms such as yeast or Arabidopsis (e.g., Atwell et al., 2010; Baxter et al., 2012; Yu et al., 2012). Higher impact of growth conditions on the ionome vs biomass production suggests that, among strains, distinct ionome equilibrium (i.e. distinct homeostatic networks) are able to support growth. Dissecting the molecular mechanisms underlying these differences in selected pairs of natural strains exposed to Mn or Fe deficiency, respectively, revealed the contrasted strategies of the strains to manage nutrient deficiency. These analyses highlighted differences in metal requirements as well as major differences in the transcriptional regulation of metal homeostasis genes, suggesting that distinct metal sensing and signalling may also take place among strains. In conclusion, our study underlines the extent of phenotypic variation within the Chlamydomonas species and leveraging this natural variation should enable a better understanding of nutrient homeostasis mechanisms in Chlamydomonas and in photosynthetic organisms.

F. Methods

1. Chlamydomonas strains

Twenty-four *Chlamydomonas reinhardtii* strains were acquired from the Chlamydomonas Resource Center and SAG Culture Collection of Algae as described in **Table S.II.1**. Strains were maintained on 1.5% plant agar (Duchefa Biochemie B.V.) Tris-Acetate-Phosphate (TAP) medium (Gorman & Levine, 1965) under 100 $\mu E.m^{-2}.s^{-1}$ continuous light.

2. Culture conditions

TAP medium was used as control and base for all mineral deficiency media. All TAP media contained 1 $mL.L^{-1}$ of glacial acetate and the final solution was titrated to pH 7.0 with HCl. TMP medium was prepared as described by Gorman & Levine (1965). The nine single deficiency media were prepared as described in **Table S.II.2**. N, P, S and Fe deficiency conditions were based on previous work by Figueroa-Torres et al. (2017), Barreiro et al. (2013), Laurinavichene et al. (2002) and Glaesener et al. (2013), respectively; and the other deficiency conditions were determined in preliminary experiments.

For each experiment, freshly growing cells on TAP agar plates were used to initiate pre-cultures in TAP liquid medium. After two-days, the cell density was quantified by measuring the optical density at 750 nm (OD_{750nm}) using a spectrophotometer (GENESYS™ 20 Visible Spectrophotometer, Thermo Scientific™). These pre-cultures were then used to inoculate 35 mL of media (TAP, TMP or TAP with a single mineral deficiency), to a final concentration of approximately 10^4 $cells.mL^{-1}$. The OD_{750nm} was then measured from day 3 until day 7 to follow growth (**Figure S.II.1**) (Thiriet-Rupert et al., 2021a).

To minimize contamination by trace amounts of micronutrients (Cu, Fe, Mn, Zn), all glassware was rinsed with HCl, plasticware was preferred and, if not possible, the material was rinsed with 1M EDTA. All assays including all 24 Chlamydomonas strains were conducted in two independent experiments, with two biological replicates each (n=4).

3. ICP-AES analysis

At day 4 of the cultures, samples for ICP-AES were prepared based on the protocol by Thiriet-Rupert et al.(2021a). Briefly, 10 mL of culture were harvested in metal-free tubes and centrifuged at 2000 x *g* for 5 min to remove the media. Cells were resuspended with 5 mL of 5 mM EDTA (pH 7.0) and centrifuged at 2000 x *g* for 5 min, this step was repeated twice. The pellet was then washed with 5 mL distilled water. After centrifugation at 2000 x *g* for 5 min, 3 mL of >65% (v/v) nitric acid were added to the pellet, then stored at 4°C for 2 days for digestion. Before analysis, distilled water was used to bring the final volume to 10 mL and 200 µL of >65% (v/v) nitric were added to each sample.

The elements Ca, Cu, Fe, potassium (K), sodium (Na), Mg, Mn, P and Zn were quantified using Inductively Coupled Plasma Atomic Emission Spectroscopy (ICP-AES) (Vista AX CCD Simultaneous ICP-AES, Varian). The results were normalized using the OD_{750nm}.

4. RNA extraction and qRT-PCR

Total RNA was extracted using an adapted genomic DNA extraction protocol followed by selective RNA precipitation with LiCl (Loppes & Radoux, 2001; Newman et al., 1990).

At day 4 of the cultures, 10^7 cells were harvested and centrifuged at 2000 x *g* for 5 min. The pellet was frozen with liquid N_2 and kept at -80°C until extraction. Extraction was initiated by resuspending the cells in lysis buffer [2% SDS (w/v), 400 mM NaCl, 40 mM EDTA, 100mM Tris HCl pH 8.0], adding phenol/chloroform/isoamyl alcohol (25:24:1) and incubating 5 minutes with agitation. The aqueous phase was separated by 5 min centrifugation at 15000 x *g* and re-extracted with chloroform/isoamyl alcohol (24:1). Total RNAs were precipitated overnight at 4 °C in 8 M LiCl and collected by a 5 min centrifugation at 15000 x *g*. Pelleted total RNAs were then washed with 70% ethanol, centrifuged, and diluted in RNase free H_2O. DNA contaminations were removed using the DNase Max kit (Qiagen) following the manufacturer's instructions. Total RNA concentration was determined spectrophotometrically using a NanoDrop 2000 (Thermo Scientific) and the RNA quality was confirmed using agarose gel electrophoresis. Complementary DNA (cDNA) synthesis was performed from 1 µg of total RNAs using the RevertAid RT Reverse Transcription Kit (Thermo Fisher Scientific). Quantitative reverse transcription-PCR (qRT-PCR) was performed using the QuantStudio™ 5 system (Thermo Fisher Scientific) and the Takyon™ Low ROX Probe 2X MasterMix dTTP blue (Eurogentec). Each reaction contained the master mix, 125 nM of each primer (**Table S.II.3**) and 4 µl of 50x-diluted cDNA and was performed in triplicate. The reaction conditions were as follows: (i) pre-PCR at 50 °C for 2 min, then 95 °C for 10 min, (ii) 40 cycles of PCR at 95 °C for 15 s and 60 °C for 15 s, (iii) melting curve at 95 °C for 15 s, 60 °C for 15 s and 95 °C for 15 s. Primers were designed ensuring that they annealed in non-polymorphic sequences between strains to be compared and are described in **Table S.II.3.**

Gene expression was calculated using the qbase+ software, version 3.2 (Biogazelle, Zwijnaarde, Belgium) (Hellemans et al., 2008), by the $2^{-\Delta\Delta CT}$ method using *CBLP* and *RPL13* as reference genes and normalized to one of the replicates (Livak & Schmittgen, 2001; Nouet et al., 2015; Thiriet-Rupert et al., 2021a). The stability of the reference genes in our experimental conditions was confirmed during the normalization step embedded in qBase (M = 0.212, CV = 0.074). Statistical analysis using one-way ANOVA was performed using the software's statistics wizard.

5. Photosynthesis and pigment analysis

100 µL of 4-day old cultures were transferred to a white 96-well plate and dark adapted for 10 min (Kalaji et al., 2014). Time-resolved chlorophyll fluorescence was then measured using a

SpeedZen 200 fluorescence imaging system (Johnson et al., 2009) equipped with red LEDs (650-670nm) for actinic and saturating lighting, and blue LEDs (450-470 nm) as fluorescence detection lights. PSII variable fluorescence was monitored through a saturation curve composed of 7 light-steps (25, 50, 91, 130, 270, 420, 600 µmol of quanta m^{-2} s^{-1}) of 4 minutes each (one saturating pulse of 220ms every minute). Fv/Fm was calculated on dark-adapted samples as "Fm-Fs/Fm", while rETR was calculated as "(Fm'-Fs'/Fm')*light intensity" and non-photochemical quenching (NPQ) was calculated was calculated as "Fm-Fm'/Fm' " the last two pulses at each light-step were averaged. The saturation curve was followed by 23 minutes of dark and a final pulse was used to monitor the photoinhibitory effect of the actinic light on the Fv/Fm (Fv/Fm recovery).

For pigment quantification, 1 mL of 4-day old culture was centrifuged at 2000 x *g* for 5 min and the lipophilic pigments were extracted using 1 mL of methanol. The supernatant was recovered after centrifuging the samples at 2000 x *g* for 5 min and the absorbance was measured at 470 nm, 652 nm and 665 nm. Chlorophyll *a* and *b*, carotenoid and concentrations were calculated as described in Wellburn (1994).

6. Data analysis and representation

Unless otherwise stated, data treatment was performed using RStudio IDE for R (R Core Team, 2022; RStudio Team, 2021). Data was organized using tidyverse *v1.3.1* (Wickham et al., 2019), reshape2 *v1.4.4* (Wickham, 2007), summarized using Rmisc *v1.5* (Hope, 2013) and statistical analyses (Kruskal-Wallis and pairwise Dunn tests) were performed using the FSA *v0.6.1* (Ogle et al., 2021) and rcompanion *v2.4.1* (Mangiafico, 2021) packages.

Data was then plotted using the packages ggpubr *v0.4.0* (Kassambara, 2020) or ComplexHeatmap *v2.8.0* (Gu et al., 2016) with custom-made colour scales using circlize *v0.4.13* (Gu et al., 2014). Plots were exported in vector image format using the svglite *v2.0.0* (Wickham et al., 2021) package.

G. Acknowledgements

We thank A. Degueldre, R. Houet, and S. Banneux for technical support, as well as F. Bouché, A. Caccamo and F. Vega de Luna for helpful discussions. Funding was provided by the University of Liège (ARC GreenMagic to M.H., P.C. and T.D.) and by the "Fonds de la Recherche Scientifique-FNRS" (MIS-F.4511.16, PDR-T0120.18, PDR-T.0104.22 to M.H.). F.I. was supported by the FRIA. P.C and T.D. are Senior Research Associate and Research Director of the F.R.S.-FNRS, respectively.

H. Author contributions

M.H., P.C. and T.D. conceived and directed the research. M.H., S.M.E., A.J., F.I. and P.C. designed experiments. S.M.E, A.J., B.B., M.S., F.I., P.C., B.B. and M.C. performed experiments. S.M.E., M.H., F.I. and P.C. analysed and interpreted the data. S.M.E. and M.H. generated all Figures and Supporting Information material. S.M.E. and M.H. wrote the manuscript, with comments of all authors.

III. A MAGIC population to study mineral nutrition

The work presented in this chapter stems from the contribution of Sara M. Esteves (SME), Marc Hanikenne (MH), Tom Druet (TD), Pierre Cardol (PC), Fabrizio Iaconno (FI), Alice Jadoul (AJ), Stéphanie Banneux (SB), Rebecca Houet (RH) and Agnieszka Misztak (AM). Under the supervision of MH, TD and PC, SME, FI and AJ created the crossing scheme and performed the MAGIC design (point A). SE, AJ and SB phenotyped the progeny in nutrient deficiency, SME analysed the results under MH supervision (point B). AJ and RH prepared the samples for sequencing, TD and AM mapped and curated the QTLs (point C). SME analysed the results under the supervision of MH and TD (point D).

A. The MAGIC design

In order to map QTLs related to nutrient homeostasis in Chlamydomonas, a multiparent population has been generated. The first step consisted in a selection of founder strains among the 24 Chlamydomonas strains in the initial panel (Chapter II), followed by the creation of the resource and, the selection of the progeny strains.

1. Founder strain selection

The founder strains for the MAGIC design were chosen based on three criteria: (i) mating type (4 *mt*+, 4 *mt*-), mating ability and efficiency, (ii) variation of nutrient homeostasis (summarized below) and photosynthetic phenotypes (F. Iacono, PhD thesis, 2023) and (iii) strain origin, population structure and genetic diversity (Flowers et al., 2015; Gallaher et al., 2015) (*cf.* **Table V.1**).

a) Mating ability and efficiency

All *mt*+ strains (13) were crossed with all the *mt*- strains (11) to assess the mating efficiency among the initial panel of 24 strains (**Figure III.1**). The *mt*+ strains CC-125, CC-503, CC-1690, CC-4414, CC-1374 and SAG 11-31 were excluded due to their low mating efficiency. CC-3348 had good mating efficiency but displayed a long lag phase compared to the other strains and was also excluded. *mt*- strains CC-5325, CC-2290, CC-2342, CC-2938, CC-1009 and CC-124 were also excluded due to their reduced mating efficiency.

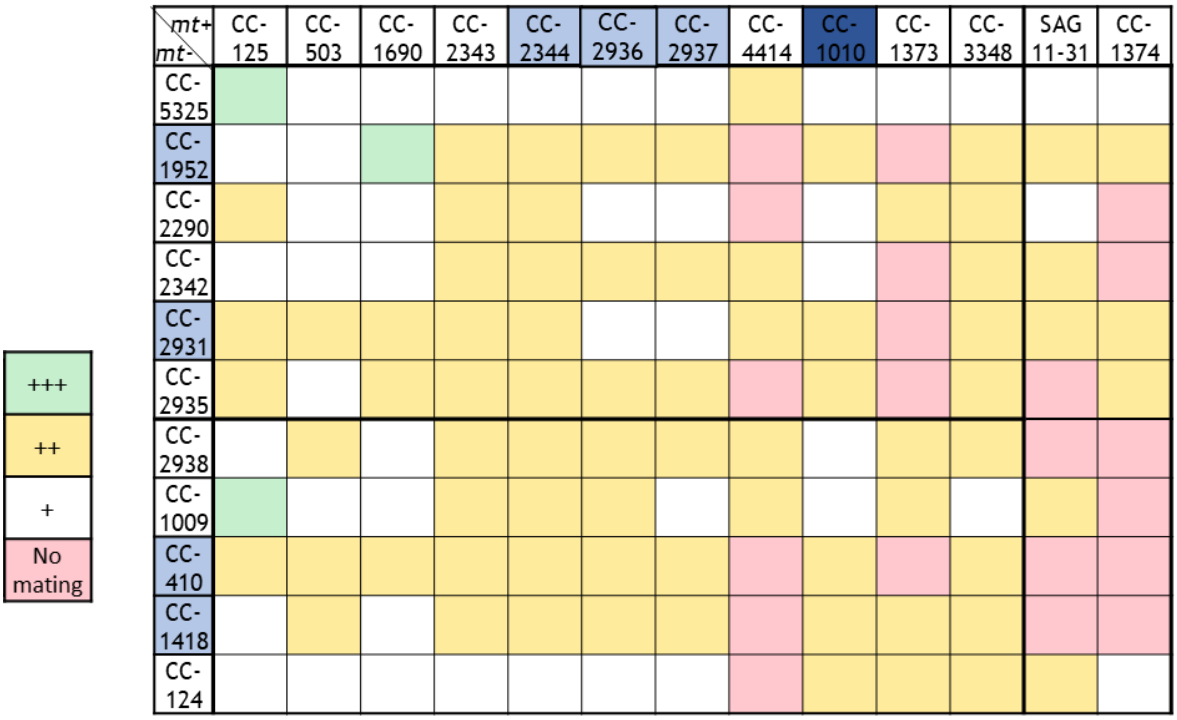

Figure III.1 Qualitative assessment of mating efficiency. All *mt*+ strains were crossed with all the *mt*- strains and the crosses were classed in 4 categories according to the obtained number of zygotes: *no mating*, if no zygotes were found (pink); + if less than 10 were found (white); ++, for more than 10 (yellow) and +++ if the 20 µL inoculated droplet was saturated with zygotes (>100, green). Selected strains are highlighted in light blue (natural strains) and dark blue (laboratory strains).

b) Nutrient homeostasis

A principal component analysis (PCA) was performed on the ionome data recorded under nutrient deficiency obtained in Chapter II (**Figure S.III.1**), restricting the analysis to the strains with a good mating efficiency (in white, yellow and green in **Figure III.1**). The first 2 dimensions explained more than half of the observed variation (54.4%) and separated the strains into 2 distinct clusters along dimension 1, grouping strains whose phenotype correlated positively with the treatments (positive half) and those which correlated negatively (negative half), but failed to separate natural and laboratory strains (**Figure III.2**). Indeed, laboratory strains CC-410 and CC-1418 clustered with natural strains CC-2936 and CC-2937 along the positive dimension 1. In the same way, laboratory strain CC-124 clustered with natural strain CC-2344 on the top left. Natural strains CC-2935, CC-2931 and CC-1952 clustered on bottom left, while natural strains CC-1373 and CC-2344, as well as laboratory strain CC-1010 clustered alone on the top right, top left and top right, respectively.

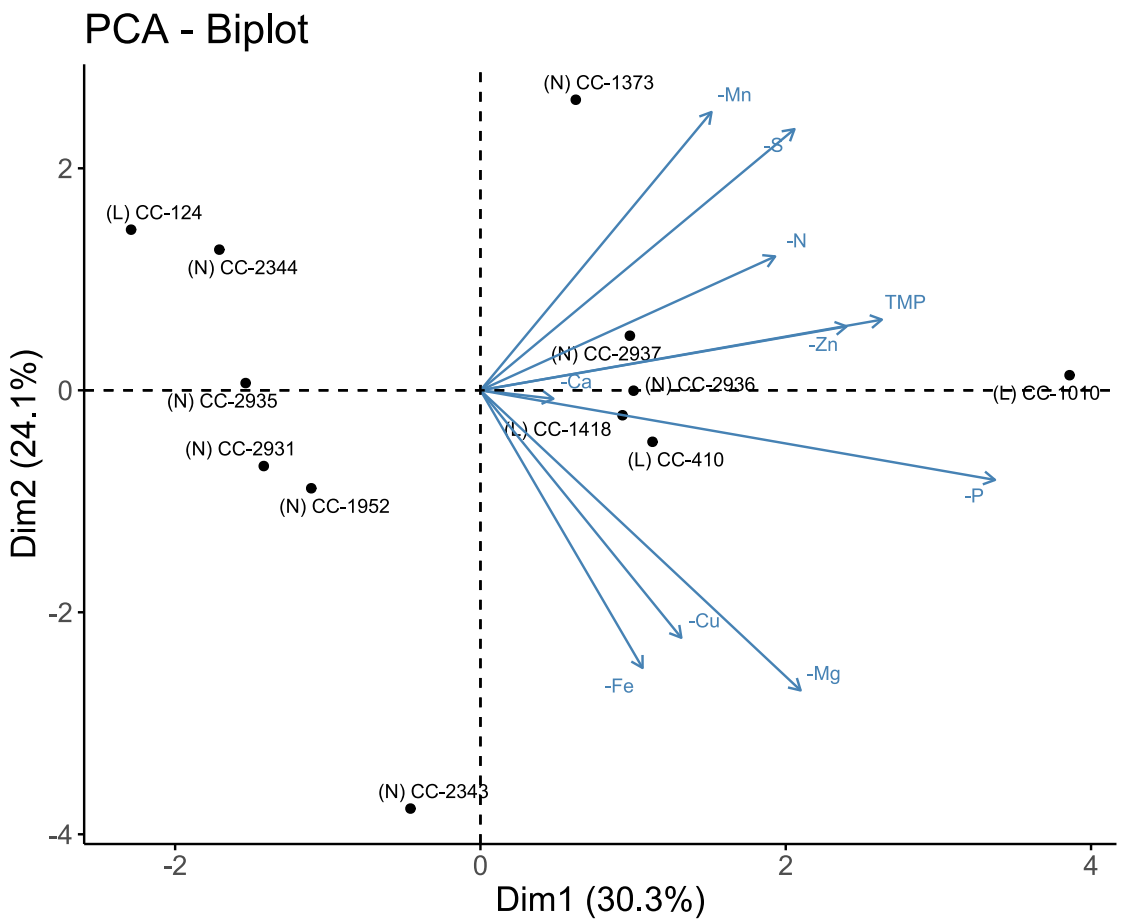

Figure III.2 Principal component analysis of the candidate strain ionome data in response to nutrient deficiency. µM acetate (TMP), 0 µM Ca, 5.4 µM Mg, 2748 µM N, 56.6 µM S, 100 µM P, 1.8 µM Fe, 0.006 µM Cu, 0 µM Mn or 0 µM Zn. The 2 first dimensions explained 54.4% of the variation observed, and separated -Mn, -S, -N, TMP and -Zn treatments (top right) from -Ca, -P, -Mg, -Cu and -Fe (bottom right).

c) Strain origin, population structure and genetic diversity

Strains CC-410 and CC-1418 were whole-genome sequenced during the course of this project and their files was added to the data of Flowers et al., (2015), which already included the remaining strains with good mating efficiency. Variant calling identified 8,313,680 variants on the 17 linkage groups of the *Chlamydomonas* genome, 5,673,187 of them were kept for analysis after filtering. The proportion of distinct genotypes between each pairs of strains was counted and used as a measure of genetic distance to produce a neighbour-joining tree (**Figure III.3**). The structure of this tree was similar to the one obtained by Flowers et al., (2015). The two newly sequenced strains, CC-410 and CC-1418, clustered together with the laboratory strains CC-408 and CC-1009 and were genetically close.

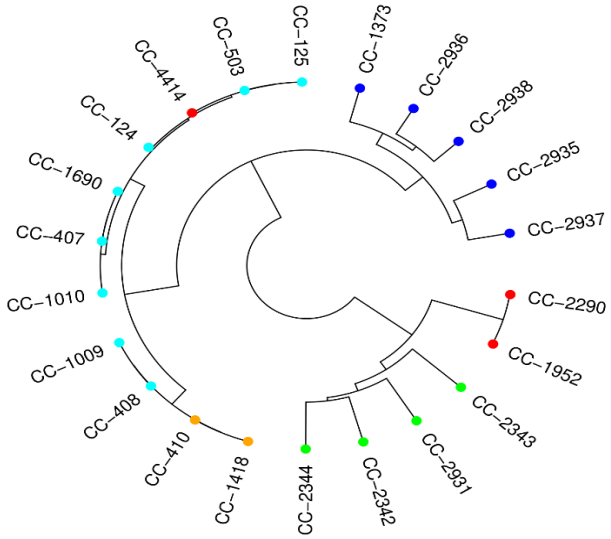

Figure III.3 Neighbor-joining tree of the relationship among the candidate strains and the strains used by Flowers et al. (2015). Strains are coloured according to their origin (natural strains are coded in green (Southeast of North America), red (West of North America) and dark blue (Northeast of North America), laboratory strains are coded in light blue –, and the newly sequenced strains in orange –). The tree was obtained based on the Jukes-Cantor distances and data consisting of 5,673,187 high quality SNPs.

d) Selected strains

The 8 selected strains were CC-2344, CC-2936, CC-2937 and CC-1010 for *mt+*; and CC-1952, CC-2931, CC-410 and CC-1418 for *mt-*.

Exclusion criteria are summarized in **Table III.1**. Despite being extremely similar at the sequence level, strains CC-410 and CC-1418 were expected to have different origins (**Table S.II.1**) and their photosynthetic phenotype (ETR) differed between each other and from strain CC-1010 (F. Iacono, PhD thesis, 2023), and were included in the design. The selection of these strains resulted in less genetic diversity among the founders, as laboratory strains present less diversity than natural strains. However, the number of natural strains available as founders was limited and they did not all match the selection criteria. Note also that founder strains were chosen for the MAGIC design based

on their phenotypes and mating abilities before the whole-genome sequence results for strains CC-410 and CC-1418 were available. Nonetheless, the selected field strains (CC-1952, CC-2344, CC-2931, CC-2936 and CC-2937) captured well the different sub-populations previously described (**Figure III.3**).

Table III.1 Criteria by which strains were excluded (X) from de MAGIC design. Selected strains are highlighted in green. Strains noted with (*) were selected based on their photosynthetic phenotype and before the sequencing results were available.

Strain	Mating type	Origin	Mating	Genotype	Phenotype
CC-124	-	Lab	X	X	
CC-125	+	Lab	X	X	
CC-410	-	Field*		X*	X*
CC-503	+	Lab	X	X	
CC-1009	-	Lab	X	X	
CC-1010	+	Lab			
CC-1373	+	Field	X	X	
CC-1374	+	Field	X	X	X
CC-1418	-	Field*		X*	X*
CC-1690	+	Lab	X	X	
CC-1952	-	Field			
CC-2290	-	Field	X	X	
CC-2342	-	Field	X	X	
CC-2343	+	Field		X	
CC-2344	+	Field			
CC-2931	-	Field			
CC-2935	-	Field		X	
CC-2936	+	Field			
CC-2937	+	Field			
CC-2938	-	Field	X	X	
CC-3348	+	Lab		X	X
CC-4414	+	Field	X	X	
CC-5325	-	Lab	X	X	
SAG 31-11	+	Field	X	X	

2. Crossing scheme

For simplification purposes, the selected eight strains were coded in the following text and figures as letters (*mt+*) and numbers (*mt-*) as described in **Table III.2**.

Table III.2 MAGIC design strain code

mt+	(A) CC-2344	(B) CC-2936	(C) CC-2937	(D) CC-1010
mt-	(1) CC-1952	(2) CC-2931	(3) CC-410	(4) CC-1418

The progeny was named by merging the parental codes, e.g., the cross Ax1 had a progeny called *A1*, with the *mt+* parent code always written first. This coding became very helpful through the generations, as it was possible to track the crossings leading to a certain progeny by checking its code, e.g., strain *A1B2C3D4+* resulted of the crossing of the strain *A1B2+* and the strain *C3D4-*, which themselves were the result of the crossing of *A1+* and *B2-*, and *C3+* and *D4-*, respectively.

In short, the strains were crossed 2-by-2 in a diallel-like design, in eight independent batches. At each generation, 1 progeny of each *mt* was selected to serve as parent for the next generation. At generations 3 and 6, when all founders were expected to contribute equally to each progeny, 1 strain from each batch was assigned to a new batch and the crossing process was continued until F8 (**Figure III.4**).

a) First generation (F1)

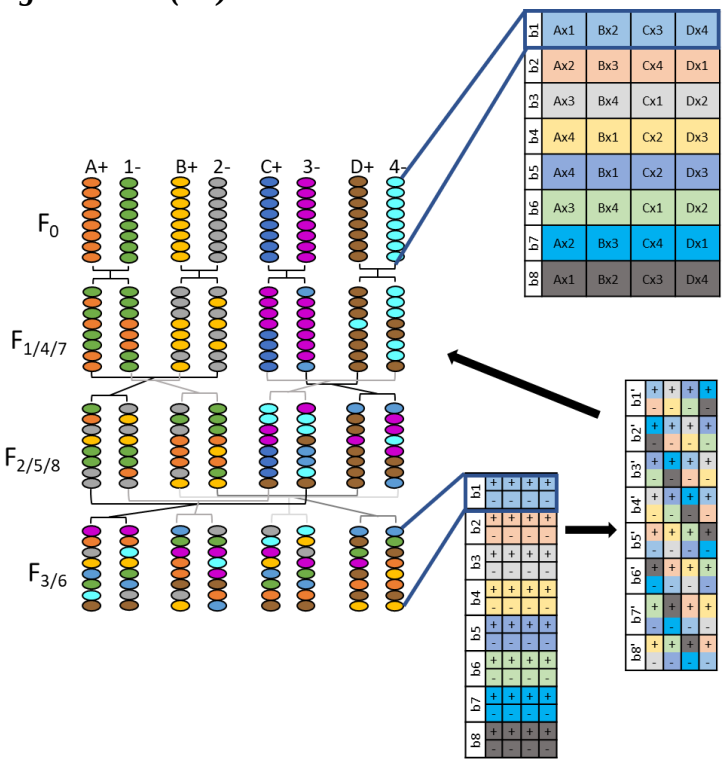

Figure III.4 Building a MAGIC design using Chlamydomonas. The crossing scheme is shown for one batch (b) (left). At each generation strains were crossed in such a way that all founders were expected to contribute only once in F3 strains (twice at F6). A full design was made of 8 independent batches (b1-b8) which differed in the initial crossing of the founders (top right). At F3 (and F6), batches were mixed and assigned to 8 new batches (b1'-b8') before the start of F4 (or F7) generations (bottom left).

The first generation (F1) was obtained by crossing all 4 *mt+* strains with all 4 *mt-* strains (**Figure III.2**). For each cross, four progenies of each *mt* were then selected and sorted to one of four

designs, named Alpha (α), Beta (β), Gamma (γ), Delta (δ). From here on, both text and tables, information about the crossing scheme will be provided for design *α* only as example.

All vs All

	A	B	C	D
1	A1	B1	C1	D1
2	A2	B2	C2	D2
3	A3	B3	C3	D3
4	A4	B4	C4	D4

F1							
α		β		γ		δ	
A1α +	A1α -	A1β +	A1β -	A1γ +	A1γ -	A1δ +	A1δ -
A2α +	A2α -	A2β +	A2β -	A2γ +	A2γ -	A2δ +	A2δ -
A3α +	A3α -	A3β +	A3β -	A3γ +	A3γ -	A3δ +	A3δ -
A4α +	A4α -	A4β +	A4β -	A4γ +	A4γ -	A4δ +	A4δ -
B1α +	B1α -	B1β +	B1β -	B1γ +	B1γ -	B1δ +	B1δ -
B2α +	B2α -	B2β +	B2β -	B2γ +	B2γ -	B2δ +	B2δ -
B3α +	B3α -	B3β +	B3β -	B3γ +	B3γ -	B3δ +	B3δ -
B4α +	B4α -	B4β +	B4β -	B4γ +	B4γ -	B4δ +	B4δ -
C1α +	C1α -	C1β +	C1β -	C1γ +	C1γ -	C1δ +	C1δ -
C2α +	C2α -	C2β +	C2β -	C2γ +	C2γ -	C2δ +	C2δ -
C3α +	C3α -	C3β +	C3β -	C3γ +	C3γ -	C3δ +	C3δ -
C4α +	C4α -	C4β +	C4β -	C4γ +	C4γ -	C4δ +	C4δ -
D1α +	D1α -	D1β +	D1β -	D1γ +	D1γ -	D1δ +	D1δ -
D2α +	D2α -	D2β +	D2β -	D2γ +	D2γ -	D2δ +	D2δ -
D3α +	D3α -	D3β +	D3β -	D3γ +	D3γ -	D3δ +	D3δ -
D4α +	D4α -	D4β +	D4β -	D4γ +	D4γ -	D4δ +	D4δ -

Figure III.5 All versus all crossing scheme of the 8 founder parents (left). F1 progeny sorting in the 4 MAGIC designs, each design included a *mt+* and *mt-* strain from each cross (right).

b) Crossing scheme α: second and third generations (F2 and F3)

Practically, gametogenesis was induced in two 24-well plates per *mating type* (plates 1 and 2 *mt+*, plates 3 and 4 *mt-*), organized as described below (**Figure III.7**, left panel). After 1 day in M-N medium, cultures of plates 3 and 4 were transferred to plates 1 and 2, respectively, generating 32 crosses. After 1h, 3h and 6h of mating, zygotes were plated. After zygote maturation and germination, the *mt* of 12-26 colonies per cross was determined by colony PCR and one colony of each *mt* was randomly selected for each cross (64 progenies in total) (**Figure III.6**, right panel).

Plate 1					
	b1	A1+	B2+	C3+	D4+
	b2	A2+	B3+	C4+	D1+
	b3	A3+	B4+	C1+	D2+
	b4	A4+	B1+	C2+	D3+

Plate 3					
	b1	B2-	A1-	D4-	C3-
	b2	B3-	A2-	D1-	C4-
	b3	B4-	A3-	D2-	C1-
	b4	B1-	A4-	D3-	C2-

Plate 2					
	b5	A4+	B1+	C2+	D3+
	b6	A3+	B4+	C1+	D2+
	b7	A2+	B3+	C4+	D1+
	b8	A1+	B2+	C3+	D4+

Plate 4					
	b5	B1-	A4-	D3-	C2-
	b6	B4-	A3-	D2-	C1-
	b7	B3-	A2-	D1-	C4-
	b8	B2-	A1-	D4-	C3-

b1	A1B2+	B2A1+	C3D4+	D4C3+
	A1B2-	B2A1-	C3D4-	D4C3-
b2	A2B3+	B3A2+	C4D1+	D1C4+
	A2B3-	B3A2-	C4D1-	D1C4-
b3	A3B4+	B4A3+	C1D2+	D2C1+
	A3B4-	B4A3-	C1D2-	D2C1-
b4	A4B1+	B1A4+	C2D3+	D3C2+
	A4B1-	B1A4-	C2D3-	D3C2-
b5	A4B1+	B1A4+	C2D3+	D3C2+
	A4B1-	B1A4-	C2D3-	D3C2-
b6	A3B4+	B4A3+	C1D2+	D2C1+
	A3B4-	B4A3-	C1D2-	D2C1-
b7	A2B3+	B3A2+	C4D1+	D1C4+
	A2B3-	B3A2-	C4D1-	D1C4-
b8	A1B2+	B2A1+	C3D4+	D4C3+
	A1B2-	B2A1-	C3D4-	D4C3-

Figure III.6 Plate organization for gametogenesis induction of the F1 population, batches are noted with the letter *b* (left). *Mt+* strains were differentiated in plates 1 and 2, *mt-* strains in plates 3 and 4. The genetic backgrounds of the strains obtained at F2 for design α are shown in the right panel.

The same process was then repeated to generate the F3 generation, ensuring that F2 parents had different parents themselves (**Figure III.7**). At this point, the F3 strain names were composed of all 4 letters and 4 numbers used as founder codes, evidencing the fact that the genomes of these strains theoretically contained an equal contribution of all 8 founder lines. At this stage, the design γ was lagging behind and was abandoned (see D. General discussion).

Plate 1	b1	A1B2+	C3D4+	B2A1+	D4C3+
	b2	A2B3+	C4D1+	B3A2+	D1C4+
	b3	A3B4+	C1D2+	B4A3+	D2C1+
	b4	A4B1+	C2D3+	B1A4+	D3C2+

Plate 2	b5	A4B1+	C2D3+	B1A4+	D3C2+
	b6	A3B4+	C1D2+	B4A3+	D2C1+
	b7	A2B3+	C4D1+	B3A2+	D1C4+
	b8	A1B2+	C3D4+	B2A1+	D4C3+

Plate 3	b1	A1B2-	C3D4-	B2A1-	D4C3-
	b2	A2B3-	C4D1-	B3A2-	D1C4-
	b3	A3B4-	C1D2-	B4A3-	D2C1-
	b4	A4B1-	C2D3-	B1A4-	D3C2-

Plate 4	b5	A4B1-	C2D3-	B1A4-	D3C2-
	b6	A3B4-	C1D2-	B4A3-	D2C1-
	b7	A2B3-	C4D1-	B3A2-	D1C4-
	b8	A1B2-	C3D4-	B2A1-	D4C3-

b1	A1B2|C3D4+	C3D4|A1B2+	B2A1|D4C3+	D4C3|B2A1+
	A1B2|C3D4-	C3D4|A1B2-	B2A1|D4C3-	D4C3|B2A1-
b2	A2B3|C4D1+	C4D1|A2B3+	B3A2|D1C4+	D1C4|B3A2+
	A2B3|C4D1-	C4D1|A2B3-	B3A2|D1C4-	D1C4|B3A2-
b3	A3B4|C1D2+	C1D2|A3B4+	B4A3|D2C1+	D2C1|B4A3+
	A3B4|C1D2-	C1D2|A3B4-	B4A3|D2C1-	D2C1|B4A3-
b4	A4B1|C2D3+	C2D3|A4B1+	B1A4|D3C2+	D3C2|B1A4+
	A4B1|C2D3-	C2D3|A4B1-	B1A4|D3C2-	D3C2|B1A4-
b5	A4B1|C2D3+	C2D3|A4B1+	B1A4|D3C2+	D3C2|B1A4+
	A4B1|C2D3-	C2D3|A4B1-	B1A4|D3C2-	D3C2|B1A4-
b6	A3B4|C1D2+	C1D2|A3B4+	B4A3|D2C1+	D2C1|B4A3+
	A3B4|C1D2-	C1D2|A3B4-	B4A3|D2C1-	D2C1|B4A3-
b7	A2B3|C4D1+	C4D1|A2B3+	B3A2|D1C4+	D1C4|B3A2+
	A2B3|C4D1-	C4D1|A2B3-	B3A2|D1C4-	D1C4|B3A2-
b8	A1B2|C3D4+	C3D4|A1B2+	B2A1|D4C3+	D4C3|B2A1+
	A1B2|C3D4-	C3D4|A1B2-	B2A1|D4C3-	D4C3|B2A1-

Figure III.7 Plate organization for gametogenesis induction of the F2 population (left). *Mt+* strains were differentiated in plates 1 and 2, *mt-* strains in plates 3 and 4. The genetic backgrounds of the strains obtained at F3 for design α are shown in the right panel.

c) Crossing scheme α: fourth to eighth generations (F4 to F8)

Considering that all founder lines were expected to have contributed equally to the F3 strains and that the 8 batches were kept independent (except in case of failed crosses), each strain from the original batches (*b*) were sorted into one of the secondary batches (*b'*). The 8 strains (4 *mt+* and 4 *mt-*) of 1 batch *b* end up in 8 different secondary batches *b'*. The new secondary batches *b'* were composed of 1 strain from each of the original batches, whose only common ancestors are the founders, as described in **Figure III.8**.

b1	A1B2| C3D4+	C3D4| A1B2+	B2A1| D4C3+	D4C3| B2A1+
	A1B2| C3D4-	C3D4| A1B2-	B2A1| D4C3-	D4C3| B2A1-
b2	A2B3| C4D1+	C4D1| A2B3+	B3A2| D1C4+	D1C4| B3A2+
	A2B3| C4D1-	C4D1| A2B3-	B3A2| D1C4-	D1C4| B3A2-
b3	A3B4| C1D2+	C1D2| A3B4+	B4A3| D2C1+	D2C1| B4A3+
	A3B4| C1D2-	C1D2| A3B4-	B4A3| D2C1-	D2C1| B4A3-
b4	A4B1| C2D3+	C2D3| A4B1+	B1A4| D3C2+	D3C2| B1A4+
	A4B1| C2D3-	C2D3| A4B1-	B1A4| D3C2-	D3C2| B1A4-
b5	A4B1| C2D3+	C2D3| A4B1+	B1A4| D3C2+	D3C2| B1A4+
	A4B1| C2D3-	C2D3| A4B1-	B1A4| D3C2-	D3C2| B1A4-
b6	A3B4| C1D2+	C1D2| A3B4+	B4A3| D2C1+	D2C1| B4A3+
	A3B4| C1D2-	C1D2| A3B4-	B4A3| D2C1-	D2C1| B4A3-
b7	A2B3| C4D1+	C4D1| A2B3+	B3A2| D1C4+	D1C4| B3A2+
	A2B3| C4D1-	C4D1| A2B3-	B3A2| D1C4-	D1C4| B3A2-
b8	A1B2| C3D4+	C3D4| A1B2+	B2A1| D4C3+	D4C3| B2A1+
	A1B2| C3D4-	C3D4| A1B2-	B2A1| D4C3-	D4C3| B2A1-

SORTING →

b1'	A1B2| C3D4+	C3D4| A1B2+	B2A1| D4C3+	D4C3| B2A1+
	A1B2| C3D4-	C3D4| A1B2-	B2A1| D4C3-	D4C3| B2A1-
b2'	A2B3| C4D1+	C4D1| A2B3+	B3A2| D1C4+	D1C4| B3A2+
	A2B3| C4D1-	C4D1| A2B3-	B3A2| D1C4-	D1C4| B3A2-
b3'	A3B4| C1D2+	C1D2| A3B4+	B4A3| D2C1+	D2C1| B4A3+
	A3B4| C1D2-	C1D2| A3B4-	B4A3| D2C1-	D2C1| B4A3-
b4'	A4B1| C2D3+	C2D3| A4B1+	B1A4| D3C2+	D3C2| B1A4+
	A4B1| C2D3-	C2D3| A4B1-	B1A4| D3C2-	D3C2| B1A4-
b5'	A4B1| C2D3+	C2D3| A4B1+	B1A4| D3C2+	D3C2| B1A4+
	A4B1| C2D3-	C2D3| A4B1-	B1A4| D3C2-	D3C2| B1A4-
b6'	A3B4| C1D2+	C1D2| A3B4+	B4A3| D2C1+	D2C1| B4A3+
	A3B4| C1D2-	C1D2| A3B4-	B4A3| D2C1-	D2C1| B4A3-
b7'	A2B3| C4D1+	C4D1| A2B3+	B3A2| D1C4+	D1C4| B3A2+
	A2B3| C4D1-	C4D1| A2B3-	B3A2| D1C4-	D1C4| B3A2-
b8'	A1B2| C3D4+	C3D4| A1B2+	B2A1| D4C3+	D4C3| B2A1+
	A1B2| C3D4-	C3D4| A1B2-	B2A1| D4C3-	D4C3| B2A1-

Figure III.8 F3 strain shuffling into new batches for design α. For better visualization, each original batch (*b*) was assigned a colour (left panel). During the sorting, strains from each original batch were distributed into one of the 8 new batches (*b'*). The new batches (*b'*) thus contained strains of all the 8 original batches (8 different colours) (right panel).

New codes were also attributed to the strains for simplification purposes (**Figure III.9**), *mt+* strains were labelled from A to F' and *mt-* strains were numbered 1 to 4 within each batch (too maintain them in the single digits), with the correspondent batch as superscript (e.g., 1^3 for a strain of *b3'*). F3 strains were then used as a new set of founders. Strains were differentiated and crossed as described in **Figure III.10**. After this, F5 and F6 generations followed the same crossing scheme as described above in **Figure III.4** and **Figure III.5**, respectively.

b1’	A1B2| C3D4 +	C4D1| A2B3 +	B4A3| D2C1 +	D3C2| B1A4 +
	A4B1| C2D3 -	C1D2| A3B4 -	B3A2| D1C4 -	D4C3| B2A1 -
b2’	A4B1| C2D3 +	C1D2| A3B4 +	B3A2| D1C4 +	D4C3| B2A1 +
	A1B2| C3D4 -	C4D1| A2B3 -	B4A3| D2C1 -	D3C2| B1A4 -
b3’	A4B1| C2D3 +	C3D4| A1B2 +	B3A2| D1C4 +	D2C1| B4A3 +
	A1B2| C3D4 -	C2D3| A4B1 -	B4A3| D2C1 -	D1C4| B3A2 -
b4’	A1B2| C3D4 +	C2D3| A4B1 +	B4A3| D2C1 +	D1C4| B3A2 +
	A4B1| C2D3 -	C3D4| A1B2 -	B3A2| D1C4 -	D2C1| B4A3 -
b5’	A3B4| C1D2 +	C2D3| A4B1 +	B2A1| D4C3 +	D1C4| B3A2 +
	A2B3| C4D1 -	C3D4| A1B2 -	B1A4| D3C2 -	D2C1| B4A3 -
b6’	A2B3| C4D1 +	C3D4| A1B2 +	B1A4| D3C2 +	D2C1| B4A3 +
	A3B4| C1D2 -	C2D3| A4B1 -	B2A1| D4C3 -	D1C4| B3A2 -
b7’	A2B3| C4D1 +	C1D2| A3B4 +	B1A4| D3C2 +	D4C3| B2A1 +
	A3B4| C1D2 -	C4D1| A2B3 -	B2A1| D4C3 -	D3C2| B1A4 -
b8’	A3B4| C1D2 +	C4D1| A2B3 +	B2A1| D4C3 +	D3C2| B1A4 +
	A2B3| C4D1 -	C1D2| A3B4 -	B1A4| D3C2 -	D4C3| B2A1 -

NEW LABELS →

b1’	A+	B+	C+	D+
	1^{1}-	2^{1}-	3^{1}-	4^{1}-
b2’	E+	F+	G+	H+
	1^{2}-	2^{2}-	3^{2}-	4^{2}-
b3’	I+	J+	K+	L+
	1^{3}-	2^{3}-	3^{3}-	4^{3}-
b4’	M+	N+	O+	P+
	1^{4}-	2^{4}-	3^{4}-	4^{4}-
b5’	Q+	R+	S+	T+
	1^{5}-	2^{5}-	3^{5}-	4^{5}-
b6’	U+	V+	W+	X+
	1^{6}-	2^{6}-	3^{6}-	4^{6}-
b7’	Y+	Z+	A’+	B’+
	1^{7}-	2^{7}-	3^{7}-	4^{7}-
b8’	C’+	D’+	E’+	F’+
	1^{8}-	2^{8}-	3^{8}-	4^{8}-

Figure III.9 New name codes of the F3 strains for design α. *Mt*+ strains were coded from A to F’ and *mt*- strains from each batch were coded from 1 to 4, with the batch number in superscript.

Plate 1				
b1	A+	B+	C+	D+
b2	E+	F+	G+	H+
b3	I+	J+	K+	L+
b4	M+	N+	O+	P+

Plate 2				
b5	Q+	R+	S+	T+
b6	U+	V+	W+	X+
b7	Y+	Z+	A’+	B’+
b8	C’+	D’+	E’+	F’+

Plate 3				
b1	1^{1}-	2^{1}-	3^{1}-	4^{1}-
b2	1^{2}-	2^{2}-	3^{2}-	4^{2}-
b3	1^{3}-	2^{3}-	3^{3}-	4^{3}-
b4	1^{4}-	2^{4}-	3^{4}-	4^{4}-

Plate 4				
b5	1^{5}-	2^{5}-	3^{5}-	4^{5}-
b6	1^{6}-	2^{6}-	3^{6}-	4^{6}-
b7	1^{7}-	2^{7}-	3^{7}-	4^{7}-
b8	1^{8}-	2^{8}-	3^{8}-	4^{8}-

b1’	$A1^{1}$+	$B2^{1}$+	$C3^{1}$+	$D4^{1}$+
	$A1^{1}$-	$B2^{1}$-	$C3^{1}$-	$D4^{1}$-
b2’	$E1^{2}$+	$F2^{2}$+	$G3^{2}$+	$H4^{2}$+
	$E1^{2}$-	$F2^{2}$-	$G3^{2}$-	$H4^{2}$-
b3’	$I1^{3}$+	$J2^{3}$+	$K3^{3}$+	$L4^{3}$+
	$I1^{3}$-	$J2^{3}$-	$K3^{3}$-	$L4^{3}$-
b4’	$M1^{4}$+	$N2^{4}$+	$O3^{4}$+	$P4^{4}$+
	$M1^{4}$-	$N2^{4}$-	$O3^{4}$-	$P4^{4}$-
b5’	$Q1^{5}$+	$R2^{5}$+	$S3^{5}$+	$T4^{5}$+
	$Q1^{5}$-	$R2^{5}$-	$S3^{5}$-	$T4^{5}$-
b6’	$U1^{6}$+	$V2^{6}$+	$W3^{6}$+	$X4^{6}$+
	$U1^{6}$-	$V2^{6}$-	$W3^{6}$-	$X4^{6}$-
b7’	$Y1^{7}$+	$Z2^{7}$+	$A’3^{7}$+	$B’4^{7}$+
	$Y1^{7}$-	$Z2^{7}$-	$A’3^{7}$-	$B’4^{7}$-
b8’	$C’1^{8}$+	$D’2^{8}$+	$E’3^{8}$+	$F’4^{8}$+
	$C’1^{8}$-	$D’2^{8}$-	$E’3^{8}$-	$F’4^{8}$-

Figure III.10 Plate organization for gametogenesis induction of the F3 population differentiated in plates 1 and 2, *mt*- strains in plates 3 and 4. The genetic backgrounds of the strains obtained at F4 for design α are shown in the right panel.

Alike F3, F6 strains were assumed to have received an equal contribution of all the founders. As for the F4 generation, the same of sorting F6 strains before generating the F7 generation was repeated (**Figure III.11**). Similarly, new names were given to the F6 strains ahead of the F7 generation (**Figure III.12**), *mt*+ strains were labelled from a to f' and *mt*- strains were numbered 1 to 4 within each batch, with the correspondent batch as superscript.

Two more rounds of crossing were performed, as described above, in order to generate an F8 generation.

B1'	$A1^{1}B2^{1}\|$ $C3^{1}D4^{1}+$	$C3^{1}D4^{1}\|$ $A1^{1}B2^{1}+$	$B2^{1}A1^{1}\|$ $D4^{1}C3^{1}+$	$D4^{1}C3^{1}\|$ $B2^{1}A1^{1}+$
	$A1^{1}B2^{1}\|$ $C3^{1}D4^{1}-$	$C3^{1}D4^{1}\|$ $A1^{1}B2^{1}-$	$B2^{1}A1^{1}\|$ $D4^{1}C3^{1}-$	$D4^{1}C3^{1}\|$ $B2^{1}A1^{1}-$
b2'	$E1^{2}F2^{2}\|$ $G3^{2}H4^{2}+$	$G3^{2}H4^{2}\|$ $E1^{2}F2^{2}+$	$F2^{2}E1^{2}\|$ $H4^{2}G3^{2}+$	$H4^{2}G3^{2}\|$ $F2^{2}E1^{2}+$
	$E1^{2}F2^{2}\|$ $G3^{2}H4^{2}-$	$G3^{2}H4^{2}\|$ $E1^{2}F2^{2}-$	$F2^{2}E1^{2}\|$ $H4^{2}G3^{2}-$	$H4^{2}G3^{2}\|$ $F2^{2}E1^{2}-$
b3'	$I1^{3}J2^{3}\|$ $K3^{3}L4^{3}+$	$K3^{3}L4^{3}\|$ $I1^{3}J2^{3}+$	$J2^{3}I1^{3}\|$ $L4^{3}K3^{3}+$	$L4^{3}K3^{3}\|$ $J2^{3}I1^{3}+$
	$I1^{3}J2^{3}\|$ $K3^{3}L4^{3}-$	$K3^{3}L4^{3}\|$ $I1^{3}J2^{3}-$	$J2^{3}I1^{3}\|$ $L4^{3}K3^{3}-$	$L4^{3}K3^{3}\|$ $J2^{3}I1^{3}-$
b4'	$M1^{4}N2^{4}\|$ $O3^{4}P4^{4}+$	$O3^{4}P4^{4}\|$ $M1^{4}N2^{4}+$	$N2^{4}M1^{4}\|$ $P4^{4}O3^{4}+$	$P4^{4}O3^{4}\|$ $N2^{4}M1^{4}+$
	$M1^{4}N2^{4}\|$ $O3^{4}P4^{4}-$	$O3^{4}P4^{4}\|$ $M1^{4}N2^{4}-$	$N2^{4}M1^{4}\|$ $P4^{4}O3^{4}-$	$P4^{4}O3^{4}\|$ $N2^{4}M1^{4}-$
b5'	$Q1^{5}R2^{5}\|$ $S3^{5}T4^{5}+$	$S3^{5}T4^{5}\|$ $Q1^{5}R2^{5}+$	$R2^{5}Q1^{5}\|$ $T4^{5}S3^{5}+$	$T4^{5}S3^{5}\|$ $R2^{5}Q1^{5}+$
	$Q1^{5}R2^{5}\|$ $S3^{5}T4^{5}-$	$S3^{5}T4^{5}\|$ $Q1^{5}R2^{5}-$	$R2^{5}Q1^{5}\|$ $T4^{5}S3^{5}-$	$T4^{5}S3^{5}\|$ $R2^{5}Q1^{5}-$
b6'	$U1^{6}V2^{6}\|$ $W3^{6}X4^{6}+$	$W3^{6}X4^{6}\|$ $U1^{6}V2^{6}+$	$V2^{6}U1^{6}\|$ $X4^{6}W3^{6}+$	$X4^{6}W3^{6}\|$ $V2^{6}U1^{6}+$
	$U1^{6}V2^{6}\|$ $W3^{6}X4^{6}-$	$W3^{6}X4^{6}\|$ $U1^{6}V2^{6}-$	$V2^{6}U1^{6}\|$ $X4^{6}W3^{6}-$	$X4^{6}W3^{6}\|$ $V2^{6}U1^{6}-$
b7'	$Y1^{7}Z2^{7}\|$ $A'3^{7}B'4^{7}+$	$A'3^{7}B'4^{7}\|$ $Y1^{7}Z2^{7}+$	$Z2^{7}Y1^{7}\|$ $B'4^{7}A'3^{7}+$	$B'4^{7}A'3^{7}\|$ $Z2^{7}Y1^{7}+$
	$Y1^{7}Z2^{7}\|$ $A'3^{7}B'4^{7}-$	$A'3^{7}B'4^{7}\|$ $Y1^{7}Z2^{7}-$	$Z2^{7}Y1^{7}\|$ $B'4^{7}A'3^{7}-$	$B'4^{7}A'3^{7}\|$ $Z2^{7}Y1^{7}-$
b8'	$C'1^{8}D'2^{8}\|$ $E'3^{8}F'4^{8}+$	$E'3^{8}F'4^{8}\|$ $C'1^{8}D'2^{8}+$	$D'2^{8}C'1^{8}\|$ $F'4^{8}E'3^{8}+$	$F'4^{8}E'3^{8}\|$ $D'2^{8}C'1^{8}+$
	$C'1^{8}D'2^{8}\|$ $E'3^{8}F'4^{8}-$	$E'3^{8}F'4^{8}\|$ $C'1^{8}D'2^{8}-$	$D'2^{8}C'1^{8}\|$ $F'4^{8}E'3^{8}-$	$F'4^{8}E'3^{8}\|$ $D'2^{8}C'1^{8}-$

SORTING →

b1''	$A1^{1}B2^{1}\|$ $C3^{1}D4^{1}+$	$C3^{1}D4^{1}\|$ $A1^{1}B2^{1}+$	$B2^{1}A1^{1}\|$ $D4^{1}C3^{1}+$	$D4^{1}C3^{1}\|$ $B2^{1}A1^{1}+$
	$A1^{1}B2^{1}\|$ $C3^{1}D4^{1}-$	$C3^{1}D4^{1}\|$ $A1^{1}B2^{1}-$	$B2^{1}A1^{1}\|$ $D4^{1}C3^{1}-$	$D4^{1}C3^{1}\|$ $B2^{1}A1^{1}-$
b2''	$E1^{2}F2^{2}\|$ $G3^{2}H4^{2}+$	$G3^{2}H4^{2}\|$ $E1^{2}F2^{2}+$	$F2^{2}E1^{2}\|$ $H4^{2}G3^{2}+$	$H4^{2}G3^{2}\|$ $F2^{2}E1^{2}+$
	$E1^{2}F2^{2}\|$ $G3^{2}H4^{2}-$	$G3^{2}H4^{2}\|$ $E1^{2}F2^{2}-$	$F2^{2}E1^{2}\|$ $H4^{2}G3^{2}-$	$H4^{2}G3^{2}\|$ $F2^{2}E1^{2}-$
b3''	$I1^{3}J2^{3}\|$ $K3^{3}L4^{3}+$	$K3^{3}L4^{3}\|$ $I1^{3}J2^{3}+$	$J2^{3}I1^{3}\|$ $L4^{3}K3^{3}+$	$L4^{3}K3^{3}\|$ $J2^{3}I1^{3}+$
	$I1^{3}J2^{3}\|$ $K3^{3}L4^{3}-$	$K3^{3}L4^{3}\|$ $I1^{3}J2^{3}-$	$J2^{3}I1^{3}\|$ $L4^{3}K3^{3}-$	$L4^{3}K3^{3}\|$ $J2^{3}I1^{3}-$
b4''	$M1^{4}N2^{4}\|$ $O3^{4}P4^{4}+$	$O3^{4}P4^{4}\|$ $M1^{4}N2^{4}+$	$N2^{4}M1^{4}\|$ $P4^{4}O3^{4}+$	$P4^{4}O3^{4}\|$ $N2^{4}M1^{4}+$
	$M1^{4}N2^{4}\|$ $O3^{4}P4^{4}-$	$O3^{4}P4^{4}\|$ $M1^{4}N2^{4}-$	$N2^{4}M1^{4}\|$ $P4^{4}O3^{4}-$	$P4^{4}O3^{4}\|$ $N2^{4}M1^{4}-$
b5''	$Q1^{5}R2^{5}\|$ $S3^{5}T4^{5}+$	$S3^{5}T4^{5}\|$ $Q1^{5}R2^{5}+$	$R2^{5}Q1^{5}\|$ $T4^{5}S3^{5}+$	$T4^{5}S3^{5}\|$ $R2^{5}Q1^{5}+$
	$Q1^{5}R2^{5}\|$ $S3^{5}T4^{5}-$	$S3^{5}T4^{5}\|$ $Q1^{5}R2^{5}-$	$R2^{5}Q1^{5}\|$ $T4^{5}S3^{5}-$	$T4^{5}S3^{5}\|$ $R2^{5}Q1^{5}-$
b6''	$U1^{6}V2^{6}\|$ $W3^{6}X4^{6}+$	$W3^{6}X4^{6}\|$ $U1^{6}V2^{6}+$	$V2^{6}U1^{6}\|$ $X4^{6}W3^{6}+$	$X4^{6}W3^{6}\|$ $V2^{6}U1^{6}+$
	$U1^{6}V2^{6}\|$ $W3^{6}X4^{6}-$	$W3^{6}X4^{6}\|$ $U1^{6}V2^{6}-$	$V2^{6}U1^{6}\|$ $X4^{6}W3^{6}-$	$X4^{6}W3^{6}\|$ $V2^{6}U1^{6}-$
b7''	$Y1^{7}Z2^{7}\|$ $A'3^{7}B'4^{7}+$	$A'3^{7}B'4^{7}\|$ $Y1^{7}Z2^{7}+$	$Z2^{7}Y1^{7}\|$ $B'4^{7}A'3^{7}+$	$B'4^{7}A'3^{7}\|$ $Z2^{7}Y1^{7}+$
	$Y1^{7}Z2^{7}\|$ $A'3^{7}B'4^{7}-$	$A'3^{7}B'4^{7}\|$ $Y1^{7}Z2^{7}-$	$Z2^{7}Y1^{7}\|$ $B'4^{7}A'3^{7}-$	$B'4^{7}A'3^{7}\|$ $Z2^{7}Y1^{7}-$
b8''	$C'1^{8}D'2^{8}\|$ $E'3^{8}F'4^{8}+$	$E'3^{8}F'4^{8}\|$ $C'1^{8}D'2^{8}+$	$D'2^{8}C'1^{8}\|$ $F'4^{8}E'3^{8}+$	$F'4^{8}E'3^{8}\|$ $D'2^{8}C'1^{8}+$
	$C'1^{8}D'2^{8}\|$ $E'3^{8}F'4^{8}-$	$E'3^{8}F'4^{8}\|$ $C'1^{8}D'2^{8}-$	$D'2^{8}C'1^{8}\|$ $F'4^{8}E'3^{8}-$	$F'4^{8}E'3^{8}\|$ $D'2^{8}C'1^{8}-$

Figure III.11 F6 strain shuffling into new batches for design α. For better visualization, each secondary batch (*b'*) was assigned a colour (left panel). During the sorting, strains from each secondary batch were distributed into one of the 8 tertiary (*b''*). The new batches (*b''*) thus contained strains of all the 8 secondary batches (8 different colours) (right panel).

b1”	A1¹B2¹| C3¹D4¹ +	G3²H4²| E1²F2² +	J2³I1³| L4³K3³ +	P4⁴O3⁴| N2⁴M1⁴ +
	Q1⁵R2⁵| S3⁵T4⁵ -	W3⁶X4⁶| U1⁶V2⁶ -	Z2⁷Y1⁷| B’4⁷A’3⁷ -	F’4⁸E’3⁸| D’2⁸C’1⁸ -
b2”	Q1⁵R2⁵| S3⁵T4⁵ +	W3⁶X4⁶| U1⁶V2⁶ +	Z2⁷Y1⁷| B’4⁷A’3⁷ +	F’4⁸E’3⁸| D’2⁸C’1⁸ +
	A1¹B2¹| C3¹D4¹ -	G3²H4²| E1²F2² -	J2³I1³| L4³K3³ -	P4⁴O3⁴| N2⁴M1⁴ -
b3”	C3¹D4¹| A1¹B2¹ +	F2²E1²| H4²G3² +	L4³K3³| J2³I1³ +	M1⁴N2⁴| O3⁴P4⁴ +
	S3⁵T4⁵| Q1⁵R2⁵ -	V2⁶U1⁶| X4⁶W3⁶ -	B’4⁷A’3⁷| Z2⁷Y1⁷ -	C’1⁸D’2⁸| E’3⁸F’4⁸ -
b4”	S3⁵T4⁵| Q1⁵R2⁵ +	V2⁶U1⁶| X4⁶W3⁶ +	B’4⁷A’3⁷| Z2⁷Y1⁷ +	C’1⁸D’2⁸| E’3⁸F’4⁸ +
	C3¹D4¹| A1¹B2¹ -	F2²E1²| H4²G3² -	L4³K3³| J2³I1³ -	M1⁴N2⁴| O3⁴P4⁴ -
b5”	B2¹A1¹| D4¹C3¹ +	H4²G3²| F2²E1² +	I1³J2³| K3³L4³ +	O3⁴P4⁴| M1⁴N2⁴ +
	R2⁵Q1⁵| T4⁵S3⁵ -	X4⁶W3⁶| V2⁶U1⁶ -	Y1⁷Z2⁷| A’3⁷B’4⁷ -	E’3⁸F’4⁸| C’1⁸D’2⁸ -
b6”	R2⁵Q1⁵| T4⁵S3⁵ +	X4⁶W3⁶| V2⁶U1⁶ +	Y1⁷Z2⁷| A’3⁷B’4⁷ +	E’3⁸F’4⁸| C’1⁸D’2⁸ +
	B2¹A1¹| D4¹C3¹ -	H4²G3²| F2²E1² -	I1³J2³| K3³L4³ -	O3⁴P4⁴| M1⁴N2⁴ -
b7”	D4¹C3¹| B2¹A1¹ +	E1²F2²| G3²H4² +	K3³L4³| I1³J2³ +	N2⁴M1⁴| P4⁴O3⁴ +
	T4⁵S3⁵| R2⁵Q1⁵ -	U1⁶V2⁶| W3⁶X4⁶ -	A’3⁷B’4⁷| Y1⁷Z2⁷ -	D’2⁸C’1⁸| F’4⁸E’3⁸ -
b8”	T4⁵S3⁵| R2⁵Q1⁵ +	U1⁶V2⁶| W3⁶X4⁶ +	A’3⁷B’4⁷| Y1⁷Z2⁷ +	D’2⁸C’1⁸| F’4⁸E’3⁸ +
	D4¹C3¹| B2¹A1¹ -	E1²F2²| G3²H4² -	K3³L4³| I1³J2³ -	N2⁴M1⁴| P4⁴O3⁴ +

NEW NAMES →

b1”	a+	b+	c+	d+
	1¹-	2¹-	3¹-	4¹-
b2”	e+	f+	g+	h+
	1²-	2²-	3²-	4²-
b3”	i+	j+	k+	l+
	1³-	2³-	3³-	4³-
b4”	m+	n+	o+	p+
	1⁴-	2⁴-	3⁴-	4⁴-
b5”	q+	r+	s+	t+
	1⁵-	2⁵-	3⁵-	4⁵-
b6”	u+	v+	w+	x+
	1⁶-	2⁶-	3⁶-	4⁶-
b7”	y+	z+	a’+	b’+
	1⁷-	2⁷-	3⁷-	4⁷-
b8”	c’+	d’+	e’+	f’+
	1⁸-	2⁸-	3⁸-	4⁸-

Figure III.12 New name codes of the F6 strains for design α. *Mt*+ strains were coded from a to f’ and *mt*- strains from each batch were coded from 1 to 4, with the batch number in superscript.

d) Progeny selection

The multiparent population was selected at F8 (**Figure III.13**). As in the previous crossings, several colonies were picked for *mt* determination. However, after *mt* determination, 8 colonies were selected per crossing (4 *mt*+ and 4 *mt*-), forming a *family*. At this point, the design α was constituted of 32 families of 8 strains each (256 strains).

b1”	a1¹b2¹	c3¹d4¹	b2¹a1¹	d4¹c3¹
b2”	e1²f2²	g3²h4²	f2²e1²	h4²g3²
b3”	i1³j2³	k3³l4³	j2³i1³	l4³k3³
b4”	m1⁴n2⁴	o3⁴p4⁴	n2⁴m1⁴	p4⁴o3⁴
b5”	q1⁵r2⁵	s3⁵t4⁵	r2⁵q1⁵	t4⁵s3⁵
b6”	u1⁶v2⁶	w3⁶x4⁶	v2⁶u1⁶	x4⁶w3⁶
b7”	y1⁷z2⁷	a’3⁷b’4⁷	z2⁷y1⁷	b’4⁷a’3⁷
b8”	c’1⁸d’2⁸	e’3⁸f’4⁸	d’2⁸c’1⁸	f’4⁸e’3⁸

Figure III.13 Genotypes of the F8 families for design α. *Mt*+ strains were coded from a to f’ and *mt*- strains from each batch were coded from 1 to 4, with the batch number in superscript.

e) Crossing schemes ß, γ and δ

The production of the 4 designs was conducted in parallel and α was described here in separate section only for the clarity of the presentation.

In order to maximize the variability between designs, the order of the *mt+* strains differed in each design (**Figure III.14**):

- *A* was crossed with *B*, *C* was crossed with *D* for the *α* design,
- *A* was crossed with *C*, *B* was crossed with *D* for *β*,
- *A* was crossed with *D*, *B* was crossed with C for *γ*,
- Design *δ* was similar to design *α*.

Additionally, to avoid the crossing of strains with the same founders, the 4 strains with founders in common were assigned to 4 different batches to generate the F2. In addition to the 4 batches created to separate the F1 with common founders, 4 more were made, in a mirrored structure (i.e., batches 1/8, 2/7, 3/6, 4/5 are similar). Besides increasing the variability generated, the 4 extra batches served as a backup: in the eventuality of an unsuccessful crossing, colonies were picked from the same cross in another batch.

α	A	B	C	D
1	A1	B1	C1	D1
2	A2	B2	C2	D2
3	A3	B3	C3	D3
4	A4	B4	C4	D4

β	A	C	B	D
1	A1	C1	B1	D1
2	A2	C2	B2	D2
3	A3	C3	B3	D3
4	A4	C4	B4	D4

γ	A	D	B	C
1	A1	D1	B1	C1
2	A2	D2	B2	C2
3	A3	D3	B3	C3
4	A4	D4	B4	C4

δ	A	B	C	D
1	A1	B1	C1	D1
2	A2	B2	C2	D2
3	A3	B3	C3	D3
4	A4	B4	C4	D4

Figure III.14 Crossing order of the four MAGIC designs. The different colours represent the batches (blue for batch 1, yellow for batch 2, grey for batch 3 and orange for batch 4) in which the strains were crossed in F2, to avoid crossing strains with the same founders.

In addition to design α, the designs β and δ were obtained. Design γ was abandoned as it was lagging several generations behind the other three designs due to the low progeny output.

f) Summary of the crossing scheme

In summary, the 3 designs that progressed to the F8 allowed to generate a total of 96 families of 8 strains each (768 F8 strains in total). At this point, each F8 progeny strain was assigned a number from 1 to 768. Numbers 1-256 were assigned to design α, 257-512 to design δ and 513-768 to design β. The first 4 strains of each *family* (e.g., 1-4, 9-12, etc.) corresponded to the *mt+* strains while the last 4 (e.g., 5-9, 13-16, etc.) corresponded to the *mt-* strains.

B. Phenotyping of the GreenMAGIC population

The 768 progeny and the 8 founder strains were phenotyped in 6 out of the 11 conditions used in Chapter II to study intraspecific variation of nutrient homeostasis in Chlamydomonas: TAP, as control; 2 macronutrient deficiencies: 0 µM calcium (-Ca), 56.6 µM sulphate (-S); and 3 micronutrient deficiencies: 0.006 µM copper (-Cu), 1.8 µM iron (-Fe) and 0 µM manganese (-Mn). A total of 15 parameters were measured for each condition:

- Three parameters calculated using the OD_{750nm}: cell density after 4 days of culture, fold-change of cell density (between day 0 and day 4 of culture) and sedimentation after 10 minutes (as a proxy for motility, sedimentation was measured as an increase of OD over time),
- The accumulation in cells of 9 elements of the ionome (Ca, Cu, Fe, K, Mg, Mn, Na, P and Zn), quantified by ICP-AES;
- Three photosynthetic parameters: maximum potential quantum efficiency of Photosystem II (Fv/Fm), efficiency of Photosystem II (ΦPSII) and nonphotochemical quenching (NPQ), using a SpeedZen camera.

In order to phenotype such a number of strains and conditions, the experimental setup described in Chapter II was adapted: (i) Erlenmeyer flasks were replaced by 24-well plates and (ii) the progeny was divided into 8 batches of 96 strains (one strain per family) that were phenotyped in duplicate during 8 weeks (1 batch in duplicate per week). The 8 founders were phenotyped along with each batch, to measure batch effects.

1. Bias sources

Given the amount and diversity of data generated, as well as the organisation of the MAGIC design and phenotyping of the progeny, 4 sources of bias were possible:

- the normality of the dataset,
- the 3 different designs in which the F8 strains were generated;
- the 8 batches in which the progeny was divided for phenotyping;
- the 2 biological replicates made during phenotyping.

For this reason, before the mapping of QTLs, the impact of each of these factors on the phenotypes were evaluated.

a) Normality of the data

All the 15 measured parameters followed a non-normal distribution in the 6 conditions tested (Shapiro-Wilk test, $p < 10^{-9}$) (**Figure III.15, Figure S.III.2-7**). Extreme values (average ± 4*SD) were excluded from the analysis, as well as values where the OD was negative or null, which

corresponded to ~0.2% out of the ~0.33% of the datapoints removed. For concentration measures, the data was normalised with a logarithm transformation.

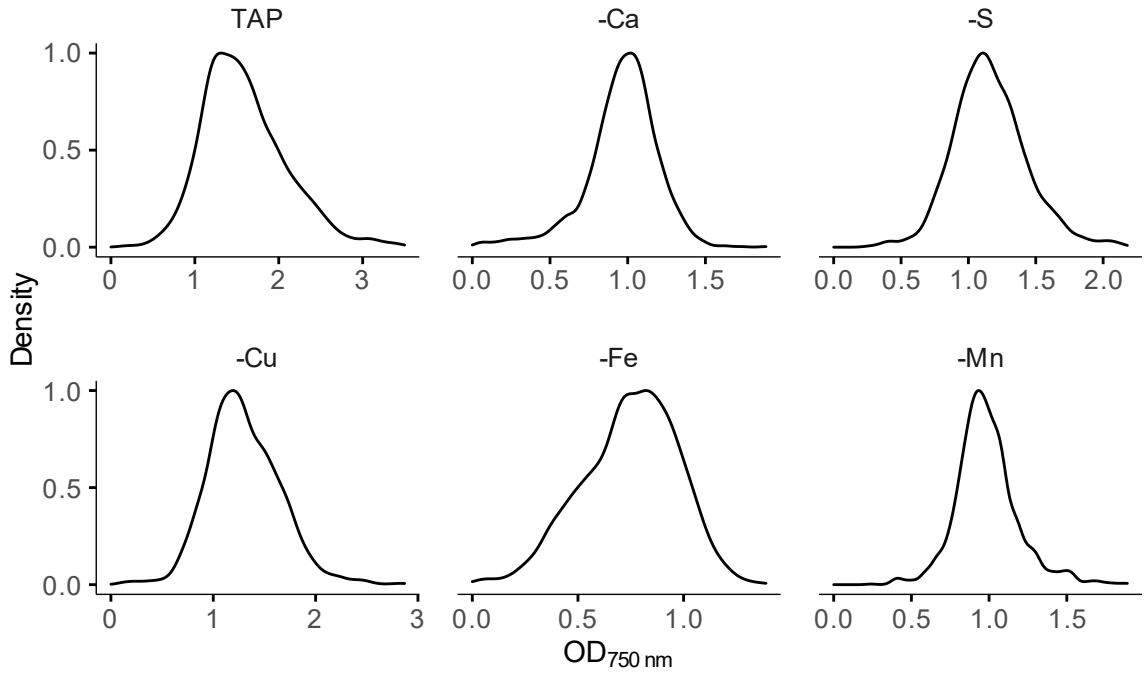

Figure III.15 Examples of the phenotyping data distribution. The density plots represent the distribution of the OD_{750nm} measured for each treatment across the 768 samples, scaled to a maximum of 1.

b) Batch and replicate effect

Due to the elevated number of strains to phenotype, the phenotyping was divided in 8 batches of 96 progeny strains, in duplicate, plus the 8 parents added as controls to each batch.

The correlation among the different batches was studied to assess the degree of variation introduced by phenotyping the progeny at different times (**Table III.3, Figures S.III.9-11**). Excluding the Sedimentation parameter, all traits measured had a significant correlation among batches. Indeed, the sedimentation observations for batch 1 were weakly correlated to the ones of other batches ($-0.043 \leq r^2 \leq 0.065$), and only significantly correlated with batches 4 and 8. Among the other traits, the strongest correlations between batches were found for biomass produced (cell density), Ca and Mn concentrations, as well as the photosynthetic parameters Fv/Fm and ΦPSII. On the other hand, OD fold-change and sedimentation, Cu, Fe and K concentrations, and NPQ also had strong correlations, but over a wider range (moderately weak to moderately strong).

As for the 2 replicates, overall, the correlations were very strong ($r \geq 0.774$) for all traits except sedimentation and Mg concentration (**Table III.3**). However, this correlation was also affected by the batch effect (**Figure S.III.12**), with low correlation between the 2 replicates in the batch 1 for the sedimentation trait. Additionally, batch 2 contained outlier datapoints for Cu and K concentrations,

as well as batch 1 and 7 for the OD fold-change trait and batch 5 for Zn concentration. The photosynthetic parameters, with the exception of NPQ, had the strongest correlation between replicates ($r^2 \geq 0.970$) in all batches. This effect was incorporated in the QTL model, which used both replicates and included batch effect in the fixed effects.

Table III.3 Pearson correlation among the 8 batches used to phenotype the progeny, and between the 2 replicates within each batch.

Effect	Trait	Correlation	Significance (p-value)
Batch	Biomass	0.569 – 0.726	< 0.001
	OD fold-change	0.163 – 0.726	< 0.001
	Sedimentation	-0.048 – 0.726	Batch 1: >0.05, except pairs Batch1/Batch4 and Batch1/Batch8 Batches 2-8: < 0.001
	Ca	0.655 – 0.811	< 0.001
	Cu	0.147 – 0.705	< 0.001
	Fe	0.377 – 0.829	< 0.001
	K	0.153 – 0.544	< 0.001
	Mg	0.413 – 0.672	< 0.001
	Mn	0.560 – 0.753	< 0.001
	Na	0.457 – 0.761	< 0.001
	P	0.394 – 0.644	< 0.001
	Zn	0.488 – 0.720	< 0.001
	Fv/Fm	0.798 – 0.858	< 0.001
	ΦPSII	0.893 – 0.925	< 0.001
	NPQ	0.179 – 0.487	< 0.001
Replicate	Biomass	0.879	All traits $< 2.2x10^{-16}$
	OD fold-change	0.938	
	Sedimentation	0.437	
	Ca	0.932	
	Cu	0.687	
	Fe	0.643	
	K	0.798	
	Mg	0.630	
	Mn	0.821	
	Na	0.821	
	P	0.860	
	Zn	0.847	
	Fv/Fm	0.970	
	ΦPSII	0.981	
	NPQ	0.774	

c) Design effect and treatment effect

Another factor potentially influencing the phenotypes observed was the crossing design from which the progeny strains were selected. The 15 phenotypes observed in the 6 media tested were dissected using PCA (**Figure III.16**). Despite the first 2 components explaining 65% of the observed variation, they failed to separate the 3 designs. The phenotype of the strains originating from different designs overlapped considerably, indicating that the different designs did not introduce a strong bias.

The founders were also included in this analysis, which allowed not only to compare the variation among them in the new experimental setup, but also to compare the initial variation among founders with the variation generated by the MAGIC design. The progeny strains dispersed around the founder strains, inside the ellipses, suggesting an increase in phenotypic variation among the GreenMAGIC progeny.

One more deduction can be made regarding the dispersion of the data: the treatments -Ca, -Mn and -Fe had a strong positive correlation, similarly to -Cu and TAP, and these 2 groups were positively correlated with each other. TAP and -Cu are also positively correlated with -S, which in turn had a weak negative correlation with -Fe, -Mn and -Ca. Similarly to batch effect, the impact of the design was also included in the QTL model fixed effects.

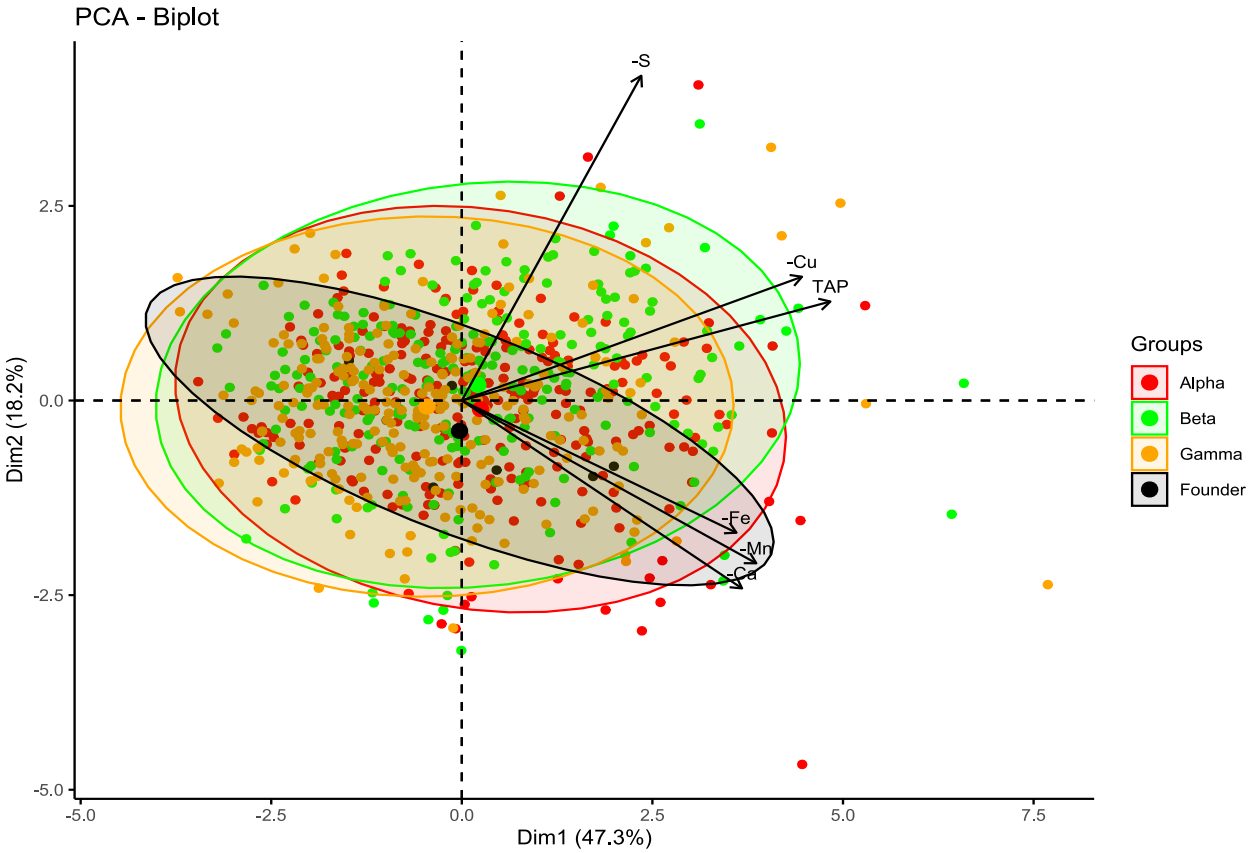

Figure III.16 PCA of the MAGIC design progeny and 8 founder strain phenotypes upon growth in the 6 conditions (TAP, -Ca, -S, -Cu, -Fe, -Mn). Strains were coloured according to the design from which they were selected (red for Alpha, green for Beta, orange for Gamma, black for the founders) and ellipses comprise 95% of each design's individuals. The 2 first dimensions (dim1 and dim2) explained 65.4% of the observed variation, and separated -S, -Cu and TAP treatments (top right) from -Fe, -Mn and -Ca (bottom right). Founders can be found in top left (2), bottom left (3, 2 superposed) and bottom right (3). Note that only 766 progeny were included in the analysis as strains 443 and 448 (Gamma design) were excluded due to the presence of missing values.

2. Founder vs Progeny phenotypic variation

Globally, the phenotypic variation observed for the terminal lines exceeded that of the founders (**Figure III.16**). Looking in more detail, variation in the GreenMAGIC progeny increased for OD-related traits, ranging from 1.34x to 7.38x the variation observed in the founder lines (**Tables III.4-5**), while it ranged from 0.84x to 4.54x for photosynthesis-related traits (**Tables III.4-5**), and from 0.62x to 15.71 for ionome-related traits (**Tables III.6-8**). Strikingly, for many of the biomass-related phenotypes observed in the terminal lines, the minimum values were up to 73x lower than those obtained for the founders (e.g., minimum biomass recorded in -Ca is 0.01 for progeny while it is 0.73 for the founders).

Regarding total biomass after 4 days of culture, the smallest increase of variation within the progeny compared to the founders was observed in -Fe (1.34x), in contrast with the highest increase in variation observed in -Ca (2.85x). This differed from the variation observed for OD fold-change over the same period, where the lowest increase of variation was observed in -Ca (3.27x) and the highest was observed in -Cu (7.38x). Overall, increase of variation in OD fold-change was larger than the increase in variation in total biomass. Progeny sedimentation variation had its highest and lowest increases in variation in micronutrient deficiencies, -Cu (3.63x) and -Fe (1.42x), respectively.

Photosynthetic traits Fv/Fm and Φ PSII displayed the highest increase in variation compared with the founder lines in -Cu treatment (4.54x and 2.71x, respectively), while -S led to the least increase in variation in both cases (1.50x and 0.84x, respectively). Contrastingly, the highest increase in variation in NPQ was observed in control media, TAP (3.01x), while the lowest was in -Mn (1.08x).

The increase of variation observed in the progeny nutrient accumulation versus the founders was unevenly distributed between macro- and micro-nutrients: macronutrient variation ranged from 0.62x to 4.62x the variation observed for the founders, while micronutrient variation ranged from almost the same as in the founders (0.98x) to an almost 16-fold difference (15.71x). The multiparent progeny had a higher variation than the founder lines for 50 out of 56 combinations of nutrient cellular concentrations and treatments, with the variation for [Fe] in TAP and -Ca, and [Cu] in -Fe being more than 10x that of the founders. On the other hand, decreases in phenotypic variation (6 out of 56 combinations) occurred mostly in -Fe treatment [Ca], [Fe], [Mg] and [P] traits which varied 0.77x to 0.98x compared to founders. The 2 remaining nutrient/treatment combination were [Ca] in -Mn and [K] in -S, with 0.82x and 0.62x decreases in variation, respectively.

Table III.4 Summary statistics of the GreenMAGIC progeny phenotyping of OD-related and photosynthetic traits in TAP, -Ca and -S. OD-related traits were biomass (OD after 4 days), OD fold change (FC) and Sedimentation. Variation in the GreenMAGIC population – MAGIC variation (MV) – was calculated using the ratio between the phenotypic range (maximum – minimum) measured in the progeny and the founders (>1, increase in variation; <1 decrease in variation).

			Biomass	OD FC	Sedimentation	Fv/Fm	Φ PSII	NPQ
TAP	Min.	Founders	0.98	65.17	-0.56	0.64	0.20	-0.08
		MAGIC	0.18	34.96	-1.89	0.26	0.07	-0.43
	1st Qu.	Founders	1.30	85.36	0.19	0.69	0.28	0.06
		MAGIC	1.23	109.53	-0.38	0.68	0.27	0.11
	Median	Founders	1.52	99.51	0.30	0.71	0.32	0.15
		MAGIC	1.52	144.67	-0.12	0.71	0.31	0.24
	Mean	Founders	1.53	127.53	0.23	0.71	0.32	0.16
		MAGIC	1.59	180.29	-0.17	0.70	0.31	0.27
	3rd Qu.	Founders	1.66	134.71	0.36	0.73	0.35	0.23
		MAGIC	1.90	195.89	0.11	0.73	0.35	0.41
	Max.	Founders	2.68	399.48	0.78	0.77	0.47	0.54
		MAGIC	3.50	1792.00	0.83	0.79	0.61	1.44
	MAGIC variation (MV)		1.95	5.26	2.03	4.08	2.00	3.01
-Ca	Min.	Founders	0.73	35.10	0.05	0.58	0.17	-0.11
		MAGIC	0.01	3.88	-0.18	0.18	0.03	-0.39
	1st Qu.	Founders	0.91	57.69	0.18	0.68	0.27	0.02
		MAGIC	0.85	69.56	0.10	0.67	0.29	0.06
	Median	Founders	1.00	67.19	0.21	0.70	0.32	0.10
		MAGIC	0.98	88.50	0.14	0.70	0.33	0.16
	Mean	Founders	1.03	89.06	0.21	0.70	0.33	0.12
		MAGIC	0.96	108.31	0.14	0.69	0.32	0.16
	3rd Qu.	Founders	1.15	89.77	0.24	0.72	0.38	0.21
		MAGIC	1.10	118.50	0.17	0.72	0.36	0.26
	Max.	Founders	1.39	300.65	0.35	0.78	0.47	0.43
		MAGIC	1.89	872.00	0.36	0.77	0.48	1.16
	MAGIC variation (MV)		2.85	3.27	1.80	2.95	1.50	2.88
-S	Min.	Founders	0.45	21.21	-0.33	0.12	0.02	-0.26
		MAGIC	0.26	16.97	-0.64	-0.05	0.00	0.00
	1st Qu.	Founders	0.97	53.40	0.01	0.27	0.04	-0.01
		MAGIC	0.98	72.37	-0.11	0.17	0.03	0.00
	Median	Founders	1.11	63.29	0.15	0.46	0.06	0.08
		MAGIC	1.14	87.61	0.02	0.28	0.04	0.09
	Mean	Founders	1.11	68.42	0.13	0.41	0.11	0.10
		MAGIC	1.16	101.53	0.03	0.29	0.05	0.11
	3rd Qu.	Founders	1.22	75.30	0.29	0.55	0.17	0.16
		MAGIC	1.32	111.59	0.16	0.40	0.06	0.20
	Max.	Founders	1.62	163.13	0.45	0.64	0.34	0.68
		MAGIC	2.18	581.05	1.14	0.73	0.27	1.07
	MAGIC variation (MV)		1.64	3.97	2.28	1.50	0.84	1.14

Table III.5 Summary statistics of the MAGIC phenotyping OD-related and photosynthetic traits in -Cu, -Fe and -Mn. OD-related traits were biomass (OD after 4 days), OD fold change (FC) and Sedimentation. Variation in the GreenMAGIC population – MAGIC variation (MV) – was calculated using the ratio between the phenotypic range (maximum – minimum) measured in the progeny and the founders (>1, increase in variation; <1 decrease in variation).

			Biomass	FC	Sedimentation	Fv/Fm	Φ PSII	NPQ
-Cu	Min.	Founders	1.00	54.76	-0.60	0.62	0.33	-0.25
		MAGIC	0.11	20.26	-0.70	0.22	0.06	-0.45
	1st Qu.	Founders	1.33	82.43	-0.15	0.68	0.41	-0.01
		MAGIC	1.05	91.19	-0.16	0.67	0.38	0.05
	Median	Founders	1.50	98.39	0.06	0.70	0.44	0.12
		MAGIC	1.26	119.98	-0.06	0.71	0.43	0.20
	Mean	Founders	1.48	117.66	0.02	0.69	0.44	0.14
		MAGIC	1.29	156.35	0.03	0.69	0.42	0.18
	3rd Qu.	Founders	1.63	117.77	0.18	0.72	0.47	0.31
		MAGIC	1.51	157.54	0.06	0.73	0.47	0.31
	Max.	Founders	1.98	356.09	0.36	0.75	0.54	0.46
		MAGIC	2.87	2244.32	2.78	0.80	0.63	0.90
	MAGIC variation (MV)		2.82	7.38	3.63	4.54	2.71	1.90
-Fe	Min.	Founders	0.28	20.73	-0.19	0.19	-0.02	-0.07
		MAGIC	0.01	0.73	-0.40	-0.04	-0.03	-0.18
	1st Qu.	Founders	0.51	36.72	0.11	0.36	0.00	0.06
		MAGIC	0.60	52.16	0.01	0.32	-0.01	0.03
	Median	Founders	0.65	46.38	0.17	0.50	0.01	0.09
		MAGIC	0.77	70.07	0.08	0.42	0.00	0.07
	Mean	Founders	0.67	55.19	0.15	0.46	0.01	0.09
		MAGIC	0.75	84.87	0.07	0.41	0.01	0.07
	3rd Qu.	Founders	0.82	59.37	0.24	0.54	0.02	0.14
		MAGIC	0.91	92.53	0.14	0.51	0.02	0.10
	Max.	Founders	1.31	174.64	0.34	0.65	0.07	0.22
		MAGIC	1.39	528.00	0.35	0.68	0.17	0.55
	MAGIC variation (MV)		1.34	3.43	1.42	1.57	2.23	2.54
-Mn	Min.	Founders	0.24	11.66	-0.20	0.19	0.02	-0.36
		MAGIC	0.38	22.86	-0.65	0.08	0.09	-0.46
	1st Qu.	Founders	0.70	40.05	0.12	0.48	0.17	-0.06
		MAGIC	0.87	62.74	-0.02	0.49	0.22	-0.04
	Median	Founders	0.88	51.02	0.19	0.53	0.25	0.06
		MAGIC	0.97	75.32	0.15	0.53	0.26	0.06
	Mean	Founders	0.85	52.35	0.19	0.49	0.21	0.06
		MAGIC	0.99	89.22	0.08	0.52	0.26	0.05
	3rd Qu.	Founders	1.00	56.34	0.28	0.56	0.29	0.17
		MAGIC	1.08	93.86	0.19	0.56	0.29	0.14
	Max.	Founders	1.35	125.84	0.40	0.60	0.36	0.69
		MAGIC	1.89	567.53	0.34	0.72	0.50	0.67
	MAGIC variation (MV)		1.36	4.77	1.65	1.56	1.21	1.08

Table III.6 Summary statistics of the MAGIC phenotyping of ionome traits in TAP and -Ca. Ionome concentrations are expressed in nmol/OD. Variation in the GreenMAGIC population Variation in the GreenMAGIC population – MAGIC variation (MV) – was calculated using the ratio between the phenotypic range (maximum – minimum) measured in the progeny and the founders (>1, increase in variation; <1 decrease in variation).

			[Ca]	[Cu]	[Fe]	[K]	[Mg]	[Mn]	[Na]	[P]	[Zn]
TAP	Min.	Founders	3.31	0.16	0.93	12.37	54.39	0.47	0.00	165.00	0.41
		MAGIC	4.11	0.00	0.38	1.35	15.00	0.08	0.00	41.91	0.09
	1st Qu.	Founders	42.97	0.34	1.87	34.76	78.40	0.67	10.63	283.60	0.57
		MAGIC	40.26	0.35	1.62	12.52	73.98	0.90	11.16	277.74	0.60
	Median	Founders	61.27	0.53	2.11	43.41	89.86	1.11	21.99	345.40	0.78
		MAGIC	64.82	0.53	2.05	23.40	97.69	1.57	17.70	362.88	0.75
	Mean	Founders	68.04	0.58	2.23	43.11	101.50	1.39	30.35	378.80	0.80
		MAGIC	68.86	0.64	2.19	27.34	104.53	1.80	20.08	385.66	0.80
	3rd Qu.	Founders	103.90	0.68	2.42	53.00	125.27	1.84	52.78	461.40	0.93
		MAGIC	90.86	0.75	2.57	37.32	126.32	2.40	26.05	476.44	0.94
	Max.	Founders	142.46	1.45	6.40	85.79	168.74	5.05	82.28	684.50	1.98
		MAGIC	245.75	3.86	59.13	105.86	389.32	9.19	131.99	1267.78	4.46
	MAGIC variation (MV)		1.74	2.99	10.74	1.42	3.27	1.99	1.60	2.36	2.78
-Ca	Min.	Founders	1.52	0.00	1.15	17.95	42.84	0.66	10.19	127.30	0.42
		MAGIC	0.00	0.00	0.07	0.00	0.00	0.00	0.00	0.00	0.00
	1st Qu.	Founders	2.01	0.46	2.08	41.59	120.83	3.72	45.76	298.90	0.70
		MAGIC	1.70	0.62	1.76	22.30	102.00	4.98	60.49	275.30	0.56
	Median	Founders	2.32	0.72	2.31	51.36	136.20	5.32	68.68	374.30	0.83
		MAGIC	2.21	0.85	2.01	38.14	121.20	6.56	73.63	323.50	0.68
	Mean	Founders	14.69	0.77	2.42	53.30	138.06	5.19	70.56	378.00	1.03
		MAGIC	3.18	0.87	2.11	38.32	126.40	6.80	77.53	336.30	0.73
	3rd Qu.	Founders	3.25	1.04	2.55	62.32	160.50	6.64	96.09	422.70	1.01
		MAGIC	2.99	1.07	2.27	52.27	146.20	8.27	89.17	386.00	0.82
	Max.	Founders	194.35	2.37	4.11	116.80	249.30	10.54	165.35	922.20	5.38
		MAGIC	529.22	10.93	46.58	217.39	528.20	27.09	640.81	1590.40	10.62
	MAGIC variation (MV)		2.74	4.61	15.71	2.20	2.56	2.74	4.13	2.00	2.14

Table III.7 Summary statistics of the MAGIC phenotyping of ionome traits in -S and -Cu. Ionome concentrations are expressed in nmol/OD. Variation in the GreenMAGIC population Variation in the GreenMAGIC population – MAGIC variation (MV) – was calculated using the ratio between the phenotypic range (maximum – minimum) measured in the progeny and the founders (>1, increase in variation; <1 decrease in variation).

			[Ca]	[Cu]	[Fe]	[K]	[Mg]	[Mn]	[Na]	[P]	[Zn]
-S	Min.	Founders	37.01	0.00	0.94	5.89	105.40	0.96	0.00	307.60	0.13
		MAGIC	5.25	0.00	0.00	0.00	3.96	0.19	0.00	25.49	0.00
	1st Qu.	Founders	107.44	0.00	1.56	21.39	166.00	2.43	2.71	555.40	0.27
		MAGIC	117.33	0.12	1.33	10.09	158.34	2.92	7.63	488.24	0.25
	Median	Founders	163.03	0.00	1.94	27.19	204.50	3.52	7.04	625.60	0.33
		MAGIC	157.60	0.18	1.67	17.64	194.00	4.23	11.73	599.12	0.31
	Mean	Founders	153.04	0.07	2.03	28.88	204.80	3.79	10.05	645.10	0.36
		MAGIC	157.93	0.23	1.78	19.92	197.77	4.53	12.77	610.40	0.33
	3rd Qu.	Founders	190.04	0.08	2.48	33.34	233.60	4.94	14.27	744.00	0.40
		MAGIC	196.31	0.28	2.05	27.40	233.88	5.87	16.76	721.62	0.38
	Max.	Founders	301.41	0.51	5.19	122.81	564.90	11.48	51.15	1736.90	1.34
		MAGIC	600.47	3.33	33.63	72.94	651.39	20.63	79.23	2068.27	8.47
	MAGIC variation (MV)		2.25	6.53	7.91	0.62	1.41	1.94	1.55	1.43	7.00
-Cu	Min.	Founders	4.78	0.00	0.09	7.72	7.37	0.24	6.30	26.99	0.64
		MAGIC	1.44	0.00	0.18	0.00	1.11	0.00	0.00	2.42	0.04
	1st Qu.	Founders	60.39	0.00	3.54	33.68	90.60	1.17	10.33	357.73	0.91
		MAGIC	57.63	0.00	3.99	19.27	109.66	1.77	15.15	383.84	0.94
	Median	Founders	99.89	0.00	4.48	47.18	108.22	1.65	17.64	424.31	1.05
		MAGIC	96.47	0.00	5.10	35.00	139.86	2.59	21.66	502.35	1.21
	Mean	Founders	95.05	0.08	4.34	46.62	114.58	1.79	23.53	431.42	1.17
		MAGIC	99.51	0.03	5.46	38.10	148.01	2.94	23.77	518.67	1.28
	3rd Qu.	Founders	130.00	0.00	5.63	56.70	144.74	2.42	30.57	532.25	1.27
		MAGIC	133.64	0.04	6.35	52.07	177.90	3.69	29.72	631.11	1.52
	Max.	Founders	182.13	1.98	11.81	94.91	229.96	3.38	69.72	782.83	4.30
		MAGIC	324.71	7.29	53.25	237.00	681.57	23.26	293.28	2052.94	9.94
	MAGIC variation (MV)		1.82	3.68	4.53	2.72	3.06	7.41	4.62	2.71	2.70

Table III.8 Summary statistics of the MAGIC phenotyping of ionome traits in -Fe and -Mn. Ionome concentrations are expressed in nmol/OD. Variation in the GreenMAGIC population Variation in the GreenMAGIC population – MAGIC variation (MV) – was calculated using the ratio between the phenotypic range (maximum – minimum) measured in the progeny and the founders (>1, increase in variation; <1 decrease in variation).

			[Ca]	[Cu]	[Fe]	[K]	[Mg]	[Mn]	[Na]	[P]	[Zn]
-Fe	Min.	Founders	1.62	0.00	0.00	6.56	23.46	0.42	9.90	78.78	0.70
		MAGIC	0.85	0.00	0.00	0.00	9.08	0.00	0.00	34.21	0.00
	1st Qu.	Founders	4.55	0.00	0.00	21.45	37.92	1.30	22.82	162.67	2.01
		MAGIC	4.63	0.38	0.23	13.29	39.06	1.50	26.59	158.06	2.10
	Median	Founders	6.85	0.23	0.10	34.94	55.91	2.20	33.35	202.10	2.44
		MAGIC	7.15	0.52	0.30	21.81	52.83	3.28	38.34	206.00	2.88
	Mean	Founders	32.90	0.25	1.37	44.21	78.05	2.39	43.20	301.72	2.61
		MAGIC	9.90	0.51	0.38	28.79	60.82	4.01	43.74	229.03	3.21
	3rd Qu.	Founders	12.90	0.40	0.26	52.98	82.15	3.32	55.98	303.19	3.16
		MAGIC	11.26	0.64	0.39	37.18	74.48	5.58	53.46	269.50	3.84
	Max.	Founders	340.89	0.91	16.55	217.95	370.45	5.30	150.25	1639.55	5.31
		MAGIC	262.56	13.12	16.25	378.30	343.85	23.65	362.48	1359.72	18.12
	MAGIC variation (FC)		0.77	14.42	0.98	1.79	0.96	4.85	2.58	0.85	3.93
-Mn	Min.	Founders	13.03	0.00	2.61	23.16	60.85	0.07	2.50	192.00	1.16
		MAGIC	1.26	0.00	0.00	1.70	2.64	0.00	0.00	9.91	0.04
	1st Qu.	Founders	37.64	0.26	3.99	37.99	111.61	0.11	7.33	366.40	1.54
		MAGIC	42.52	0.48	3.62	21.72	119.81	0.12	13.97	390.96	1.46
	Median	Founders	60.92	0.37	4.57	48.95	133.38	0.14	14.10	467.50	1.80
		MAGIC	63.13	0.60	4.48	34.55	142.94	0.15	21.27	483.41	1.85
	Mean	Founders	71.37	0.40	4.74	51.01	144.09	0.14	19.28	488.40	2.10
		MAGIC	71.89	0.66	4.59	37.58	150.36	0.14	22.52	498.76	2.28
	3rd Qu.	Founders	91.75	0.48	5.11	61.65	168.52	0.16	21.19	584.80	2.16
		MAGIC	95.16	0.75	5.37	52.09	173.24	0.17	29.18	583.35	2.53
	Max.	Founders	339.48	1.44	12.54	115.07	307.47	0.32	69.27	1219.60	5.76
		MAGIC	269.81	5.80	17.84	99.28	398.71	0.53	79.29	1152.79	18.84
	MAGIC variation (FC)		0.82	4.03	1.80	1.06	1.61	2.12	1.19	1.11	4.09

C. Quantitative trait mapping

1. Genetic characterization of the terminal lines

The 768 progeny lines were sequenced using the Illumina technology at an average coverage depth of 9.2x. A total of 3,121,994 of high-quality variants distributed in the 17 linkage groups were selected after quality filtering and used to infer the mosaic structure of the progeny (i.e. to infer from which founders the different segments of the progeny's genomes were inherited).

Considering the founder lines were selected based on their phenotype, before the sequences of two of these strains were available (see Section A.1 above), unmistakable distinction between 3 of the founder strains contribution was challenging. Indeed, strains CC-410 and CC-1418 were almost genetically identical and shared a high degree of sequence similarity with the laboratory strain CC-1010, and the three of them will be referred as the laboratory strains hereafter. Globally, founder strains shared identical-by-descent (IBD) DNA segments ranging from 1.42 to 6552.93 kb in average, with a proportion ranging from 0.796 to 1 for the laboratory strains and 0.007 to 0.358 for the natural strains (**Table S.III.1).**

a) Mosaic structure

To build the mosaic structure of each progeny, chromosome segments inherited without interruption from one founder, referred to as a tract, were identified using a hidden Markov model. Two examples of mosaic structure can be found below: one where all founders contribute relatively long tracts to a progeny strain (**Figure III.17**) and another with an elevated number of short tracts, which might result from the sequencing of more than one colony (admixture pattern). **Figure III.18** represents an extreme case of this pattern.

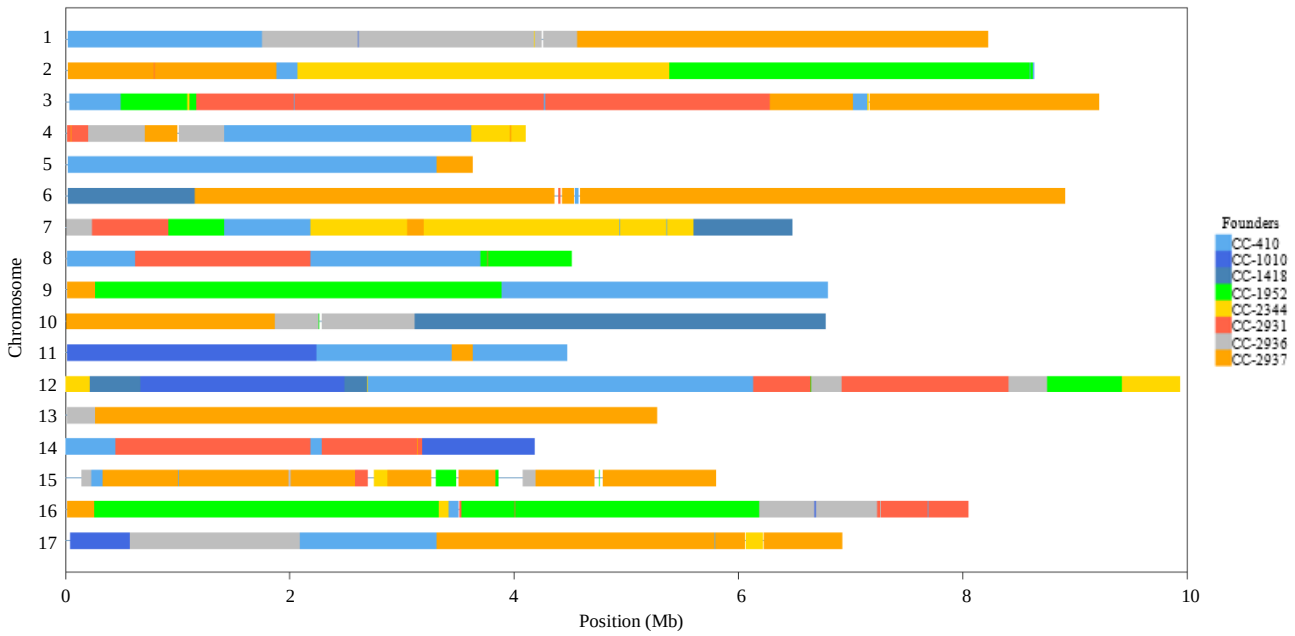

Figure III.17 Example of mosaic structure of a progeny strain. Each chromosome is represented as a bar and the colour indicates which founder contributed to that segment.

This admixture pattern, which might also result from the presence of two or several copies of the same chromosomal fragment within the genome of the strain, was relatively frequent: 18 strains had an elevated degree of admixture, 11 had a minor degree and, from the remaining 739 strains, 124 displayed this pattern in at least one chromosome.

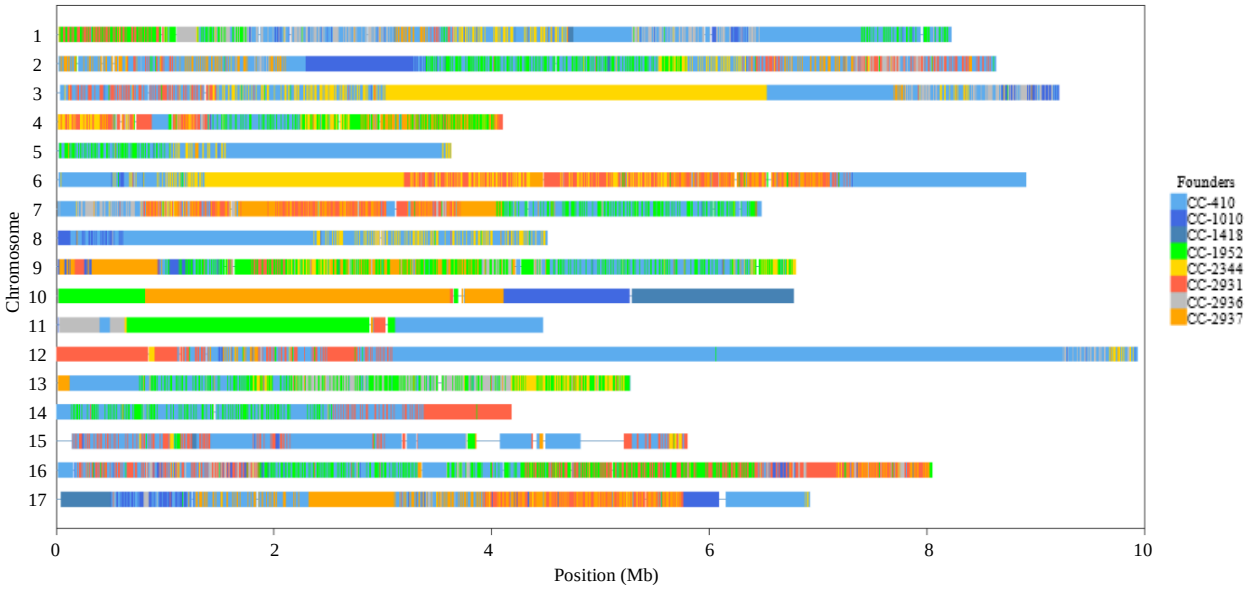

Figure III.18 Example of mosaic structure of a progeny strain with an admixture pattern. Each chromosome is represented as a bar and the colour indicates which founder contributed to that segment.

As extremely short tracts are unlikely and probably due to errors in the estimating of the founder probabilities (for instance due to problems in the sequencing data), the founder probabilities were smoothed by selecting the most frequent contributing founder in an ~1000 variants window centred around each SNP. Following this smoothing procedure, the average number of tracts per strain was estimated to be 76.4, with an average tract length of 1,457 kb. Tract length is expected to decrease with the number of generations, their length in Morgans being exponentially distributed with a rate equal to the number of generations G (the mean length being equal to 1/G Morgans). The distribution of the tract length observed in the progeny matches with expectations for 6 to7 generations of crossing with a recombination rate of 10 cM/Mb. The proportion of each founder's contribution was close to the expected 0.125 proportion for an F8 progeny (**Table III.9**). Laboratory founder strains had an average contribution ranging from 0.076 to 0.171, though distinction between the strains was hard due to their sequence similarity. The 3 laboratory strains contributed, overall, 0.403 of the whole genome of F8 lines, close to the expected theoretical value of 0.375. On the other hand, natural strain contribution had a smaller range (0.109 to 0.146) than the laboratory strains. It was also observed that some of the progeny lines were missing the contribution of at least one founder.

Table III.9 Distribution of average contribution of each founder to the genomes of the GreenMAGIC progeny. Laboratory strains are highlighted in blue.

Strain	Average contribution	
	Per progeny line	Per genomic position (10 kb windows)
CC-410	0.156	0.157
CC-1418	0.076	0.075
CC-1010	0.171	0.171
CC-1952	0.113	0.111
CC-2344	0.110	0.109
CC-2931	0.118	0.118
CC-2936	0.146	0.148
CC-2937	0.113	0.110
Sum laboratory	0.403	0.403
Sum natural	0.600	0.596
Sum	1.003	0.999

A closer look at founder contribution to the progeny genomes, in 10 kb windows, revealed that this contribution varied along chromosomes, reaching high values for certain segments. Besides the absent contribution of some founders, certain founder lines contributed considerably more for some genomic windows (**Figure III.19**): for example, strain CC-1952 contributed more than 70% of a segment near the end of chromosome 16 and strain CC-2937 was responsible for approximately half of the founder contribution at the end of chromosome 4.

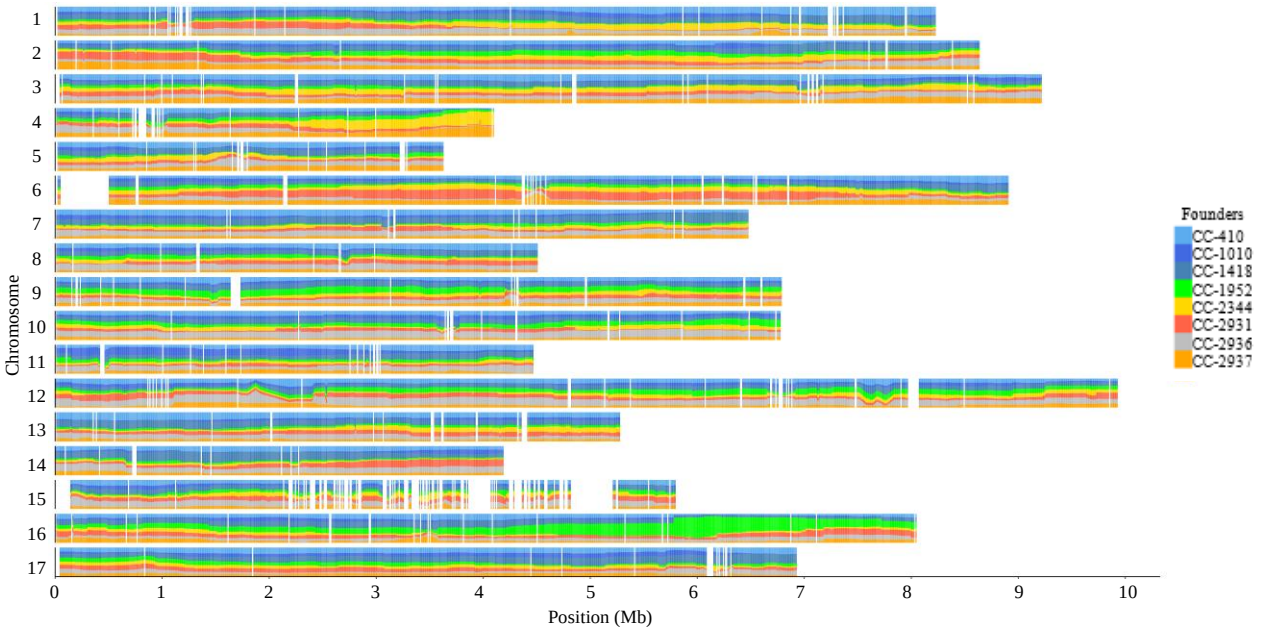

Figure III.19 Founder contribution to the F8 lines along the genome. The contributions are averaged over the 768 F8 lines.

To evaluate the impact of our crossing design on the linkage disequilibrium (LD) structure, determining the mapping resolution, the LD among 10 kb windows was calculated as the correlation between IBD probabilities between pairs of windows. If it is assumed that windows containing causative variants (causal windows) present a high correlation LD (r^2>0.9) with the windows having the most significant associations (lead window), the number of windows in high LD and their distance would be indicative of the mapping resolution in this study. Therefore, the number of windows with a r2>0.9 with each window was counted. Based on these observations, it was estimated that for 50% and 95% of the windows in the genome, less than 37 and 68 additional windows were in high LD, respectively, corresponding to confidence intervals lower 370 kb and 680 kb. In the same way, the distance to the most remote window in high LD for 50% and 95% of the 10kb windows was 240 kb and 540 kb. If QTLs are randomly distributed, these values are indicative of the mapping resolution expected in the design.

b) Population structure and relatedness

From the 3,121,994 variants retained after quality filtering, 2,712,214 bi-allelic variants were selected to perform principal component analysis (**Figure III.20**). The first 2 components accounted for only 6.7% of the total variation. Indeed, the variance explained by the different components individual eigenvectors was so small that 235 of them were needed to explain 90% of the variation. Despite this, the first two components separated the three crossing designs (**Figure III.20 A**), which is no longer true for the subsequent components (**Figure III.20 B**), supporting low levels of population structure within the GreenMAGIC progeny.

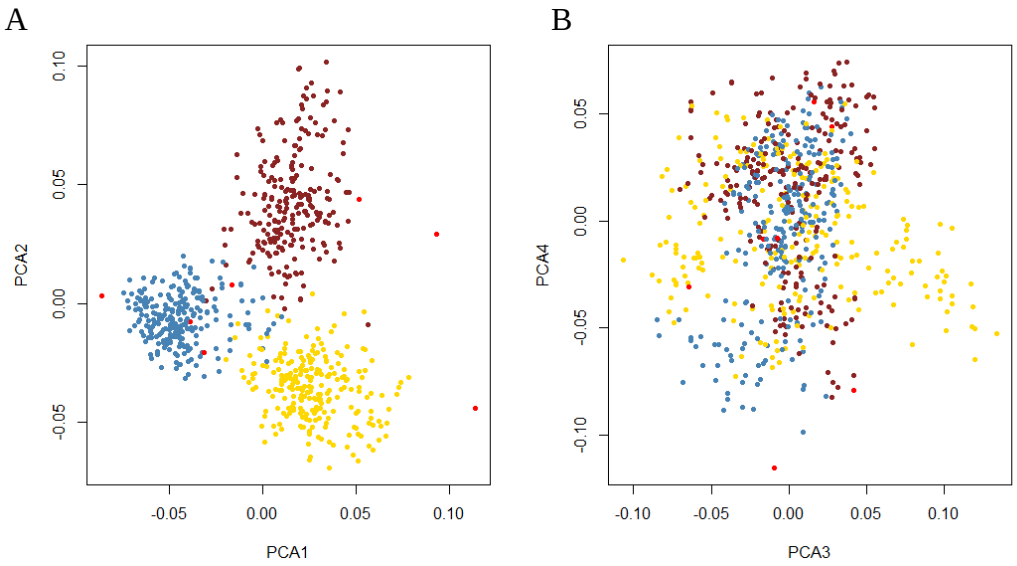

Figure III.20 Population structure of the GreenMAGIC progeny obtained through PCA of 2,712,214 bi-allelic variants. Strains are coloured according to the crossing design of origin (blue – alpha, brown – beta, yellow – delta, red - founders). (A) The first 2 components only explained 6.7% (PC1 – 3.8%, PC2 – 2.9%), but allowed the separation of F8 according to the different crossing designs. (B) Components 3 (2.3%) and 4 (2.1%) no longer separated the strains according to the different crossing designs.

Similarity among the progeny was then measured as the proportion of identical genotypes, which may or may not be inherited from a common ancestor (identical-by-state, IBS), among pairs of progeny strains. These similarity indices (S) ranged from 0.563 to 0.999, with an average of 0.680 and a median of 0.675. Ninety-two pairs of strains were further found to have less than 5% genotypic differences (S >0.95) and 126 progeny strains had at least one "clone".

We then estimated the relatedness between strains based on the segments they inherited from the founders (if at one position, two strains inherited their genetic material from the same founder, they were considered to be identical-by-descent (IBD) at that position). The pairwise relatedness of strains was lower than the IBS similarity, ranging from 0.023 to 0.893. The average relatedness was 0.159 on average, higher than the theoretical 0.125. However this theoretical value does not take into account the family structure (expected relatedness of 0.5 within family). Relatedness among strains also highlighted the different aspects of population structure (**Figure III.21**): relatedness is higher among strains issued from the same crossing design (three main blocks in the figure), and even more so among the 8 strains from each family. Indeed, the average relatedness of strains from the same or different families was 0.491 and 0.155, respectively, in agreement with the expectations (**Figure III.22 A**).

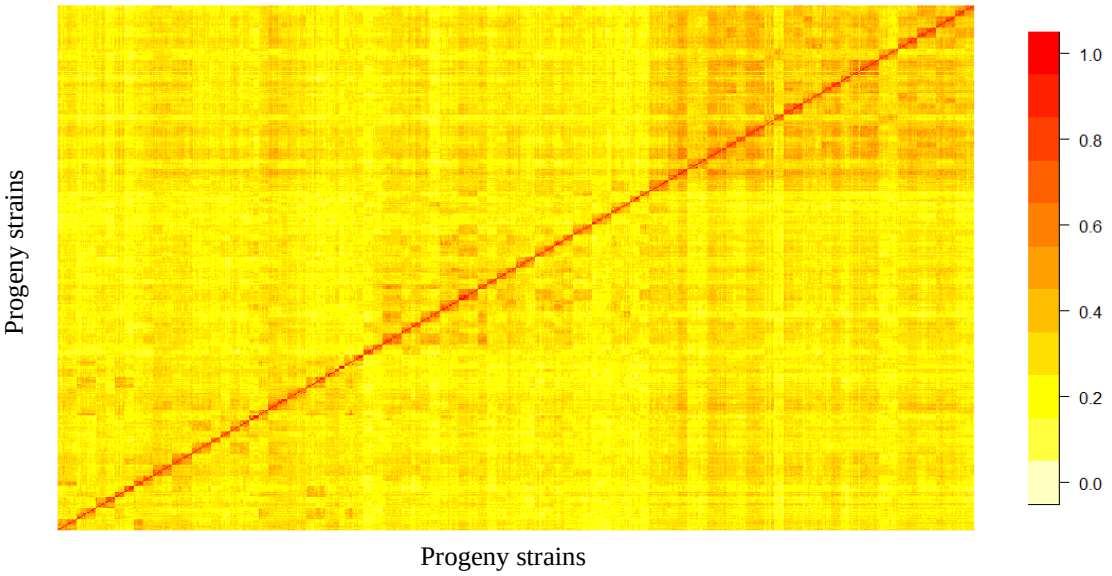

Figure III.21 Estimated relatedness among the progeny lines. The figure represents a heatmap of the relationship matrix. Each cell represents a pair of F8 lines. Lines are sorted by family and crossing design. The intensity of the colour indicates the level of relatedness.

Once again, the relatedness between families was higher than the theoretical 0.125, possibly due to residual cryptic structure, such as the relatedness between neighbouring families. However, these estimates were made assuming the founder lines were unrelated while two of the founders are identical and close to a third one. Correcting the model to include information on IBD segments shared by founder lines increased the average relatedness to 0.648 and 0.286 within and between

families, respectively (**Figure III.22 B**). In downstream analyses, lines of strains found to be identical (clones) were considered as a single individual with multiple records, resulting in 700 unique GreenMAGIC strains which were used for the association study.

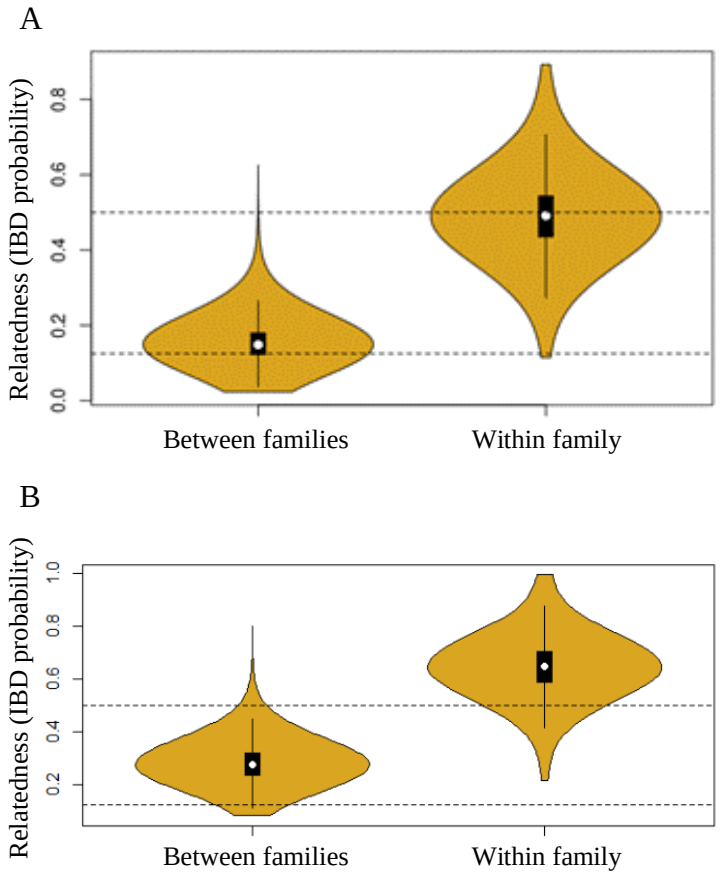

Figure III.22 Distribution of the estimated relatedness between and within progeny families. (A) Estimation assuming unrelatedness among founders. (B) Estimation considering the IBD segments among the founders.

c) Heritability

As mentioned above, variation within the progeny was, in most cases, higher than in the founder strains. This variation could be due to genetics or variation in the experimental setup, nonetheless, the correlation among biological replicates was elevated (**Tables III.3-8**). This is compatible with a high heritability. In agreement, heritability (h^2) estimated with a linear mixed model (LMM) was moderately weak to high for most traits (0.10-0.86), with the lowest values observed for the biomass-related traits, followed by ionome- and photosynthesis-related traits (**Table III.10, Figure III.23**): the trait with overall the lowest heritability was OD FC (0.29-0.40) and the highest for Fv/Fm (0.69-0.86). Note that heritability for the [Cu] trait could not be calculated because of the unknown nature of the null values (16% of the data, 11% in -Cu), which could be due to a real absence of Cu in the biomass or [Cu] below the limit of detection of the ICP-AES equipment.

Table III.10 Average heritability (h^2) of 14 phenotypic traits measured upon growth of the GreenMAGIC progeny in the 6 media.

	TAP	-Ca	-S	-Cu	-Fe	-Mn	Mean
Biomass	0.66	0.50	0.63	0.65	0.59	0.53	0.59
OD FC	0.40	0.36	0.31	0.29	0.34	0.33	0.34
Sedimentation	0.42	0.31	0.50	0.35	0.60	0.71	0.48
Fv/Fm	0.83	0.84	0.81	0.69	0.86	0.77	0.80
Φ PSII	0.64	0.59	0.66	0.49	0.64	0.66	0.61
NPQ	0.68	0.51	0.68	0.56	0.45	0.58	0.58
[Ca]	0.79	0.26	0.68	0.64	0.70	0.77	0.64
[Fe]	0.63	0.48	0.52	0.52	0.10	0.56	0.47
[K]	0.78	0.51	0.64	0.58	0.60	0.61	0.62
[Mg]	0.69	0.72	0.59	0.43	0.71	0.62	0.63
[Mn]	0.83	0.62	0.80	0.76	0.77	0.21	0.66
[Na]	0.59	0.51	0.25	0.45	0.41	0.56	0.46
[P]	0.72	0.73	0.64	0.41	0.66	0.62	0.63
[Zn]	0.61	0.72	0.55	0.48	0.56	0.85	0.63
Mean	0.66	0.55	0.59	0.52	0.57	0.60	

Nutrient deficiency resulted in lower heritability, as the highest heritability were almost systematically found for traits measured in TAP ($\bar{x}$ h^2 =0.66). The main exceptions are the Sedimentation and [Zn] traits, for which maximum heritability was observed in -Mn. Deficiency in one nutrient strongly reduced the heritability of that nutrient accumulation trait (e.g., [Ca] in -Ca (0.26), [Fe] in -Fe (0.10), [Mn] in -Mn (0.21)) and, despite the inability to estimate heritability for [Cu], traits measured in -Cu were the ones which presented the lowest average heritability.

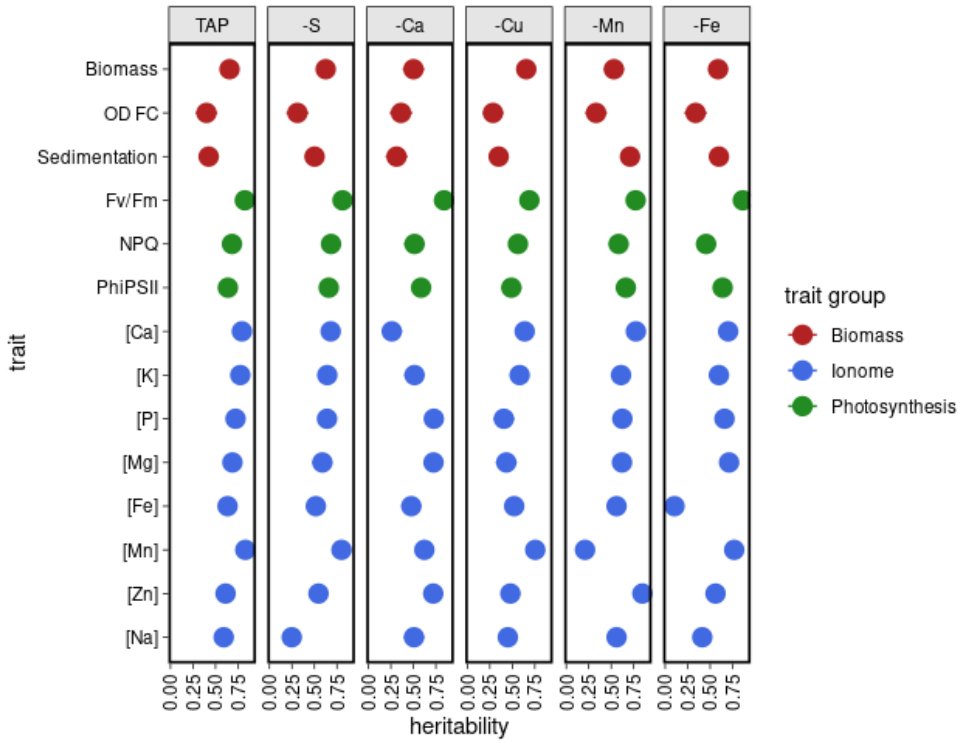

Figure III.23 Heritability estimated for 14 mineral nutrition traits measured upon growth of the GreenMAGIC progeny in the 6 culture conditions (TAP, -Ca, -Cu, -Fe, -Mn, -S). Dots represent mean heritability ± SD and are coloured according to the trait group: red for biomass-related traits, blue for ionome and green for photosynthesis.

d) Genetic correlations

The genetic correlation among phenotypes measured in different pairs of conditions (**Table III.11)**, as well as between traits in each condition (**Figure S.III.16-17**) was next examined. In this analysis, the [Cu] trait was also excluded due to missing data.

The mean genetic correlations for phenotypic traits among pairs of growth conditions were moderate, with only 3 pairs (TAP/-Cu, TAP/-Mn and -Cu/-Mn) displaying a mean genetic correlation higher than 0.5, highlighting the major impact of the environmental variable 'culture condition' (**Table III.11**). The highest mean genetic correlation for those traits was observed for the pair TAP/-Cu, which curiously had the lowest heritability, possibly due to the low impact of the deficiency. The TAP and -Cu conditions were also included in other high genetic correlation ($r_g^2 \geq 0.45$) pairs: -Cu/-Mn **(**0.60), TAP/-Mn (0.58), -S/-Cu (0.50) and TAP/-S (0.45). This contrasts with the conditions -Ca and -Fe, whose correlations with other conditions remained below 0.4, suggesting more extreme conditions or more impactful elements. Overall, the growth media were different enough to make genotype-by-environment interactions the strongest interactions, as reflected by the low estimated genetic correlations between conditions. The lowest correlations ($r_G^2 < |0.20|$) were observed for the pairs -Ca/-S (for 8 out 14 traits), -Ca/-Mn (5/14 traits), and 4 other condition pairs had weak genetic correlations for 4 phenotypes. Globally, changes in growth condition had a distinct impact on the genetic correlation within the phenotypic traits (**Table III.11**). The highest average genetic correlation was found for Fv/Fm (0.61), followed by OD FC (0.57) and [K] (0.506), suggesting these traits to be more stable and less influenced by environmental factors. Three other traits presented moderately high genetic correlation across conditions, sedimentation (0.49), [Mg] (0.45) and [P] (0.45), while the remaining trait correlations were below 0.40. For 10 traits, the genetic correlation was above 0.90, systematically for TAP/-Cu comparisons, indicating that the involved genetic variants were almost identical for these phenotypes (**Figure S.III.15)**.

Genetic correlations among traits upon growth in TAP control medium (**Figure S.III.16 A**) divided the traits in three main groups: (i) the growth-related traits biomass and OD FC (0.43), (ii) photosynthesis-related traits (>0.50) and (iii) nutrient related traits (-0.04 – 0.91). Surprisingly, the sedimentation trait was clustered with the last group, displaying a strong correlation with [Na] (0.68), [K] (0.63) and [Fe] (0.55). High genetic correlations were observed among some mineral traits: [Fe] was strongly correlated with both [K] and [Na] (0.78), [Zn] as wells as [Mg] and [P] (0.55 – 0.60), whereas [P] had strong correlations with [Mg] (0.91) and [Ca] (0.79). Inversely, [Mn] had a low genetic correlation with the other elements. Nutrient concentrations presented negative genetic relationships with growth measurements (-0.81 to -0.04), with Ca presenting the weakest (closer to 0) and Fe the strongest (-0.81) negative genetic correlations, respectively. Weak genetic correlations were found between nutrient concentrations and the photosynthetic traits (-0.31 to 0.26), as well as between growth and photosynthesis (-0.31 – 0.18).

The analysis of genetic correlations among traits in the different deficiency media (**Figure S.III.16 B-C** and **Figure S.III.17**) revealed a loss in the "cluster-by-trait-type" structure which was observed in TAP, with growth- and photosynthesis-related traits clustering together (-Ca, -S, -Cu) or dispersed among ionome-related traits (-Fe and -Mn). Genetic correlations between biomass and FC ranged from 0.26 (-Cu) to 0.60 (-Fe), centred around the value obtained in TAP. Similarly, to control, correlations between these traits and the ionome traits was mainly negative (-0.76 – 0.23). On the other hand, genetic correlations among ionome traits in deficiency media were mainly positive (-0.36 – 0.86). The strong positive correlation between [P] and [Mg] observed in TAP was also observed under all deficiencies (0.84 – 0.96). The same was not true for the [Fe] and [Na]/[K]/[Zn] correlations, which were impacted by all treatments, in particular -Ca and -Fe (-0.06 – 0.32 and -0.07 – 0.32, respectively). The genetic correlations between photosynthetic traits were also impacted by the treatment, with the Fv/Fm/NPQ genetic correlations being reduced in -S, -Fe and -Mn, while the Fv/Fm/Φ PSII correlation increased in -Ca, -S and -Cu. The correlation strength among photosynthesis- and ionome-related traits increased with nutrient deficiency (-0.48 – 0.46), as did the correlation with growth-related parameters (-0.39 – 0.41).

Table III.11 Genetic correlations for the 14 phenotypic traits measured in 15 pairwise combinations of the 6 different growth conditions.

	TAP/ -Ca	TAP/ -S	TAP/ -Cu	TAP/ -Fe	TAP/ -Mn	-Ca/ -S	-Ca/ -Cu	-Ca/ -Fe	-Ca/ -Mn	-S/ -Cu	-S/ -Fe	-S/ -Mn	-Cu/ -Fe	-Cu/ -Mn	-Fe/ -Mn	Average
Biomass	0.36	0.59	0.92	0.21	0.55	0.51	0.36	0.27	0.08	0.46	0.27	0.05	0.20	0.59	0.20	0.38
OD FC	0.56	0.37	0.95	0.48	0.57	0.57	0.63	0.62	0.68	0.38	0.36	0.44	0.57	0.69	0.67	0.57
Sedimentation	0.43	0.64	0.82	0.56	0.50	0.19	0.33	0.35	0.25	0.72	0.49	0.59	0.40	0.32	0.70	0.49
Fv/Fm	0.83	0.35	0.93	0.62	0.76	0.29	0.79	0.57	0.66	0.47	0.50	0.48	0.56	0.75	0.63	0.61
Φ PSII	0.53	0.13	0.90	0.02	0.71	0.05	0.57	-0.13	0.71	0.14	0.54	0.28	0.09	0.74	0.19	0.36
NPQ	0.63	0.28	0.65	0.11	0.56	0.36	0.62	-0.17	0.63	0.25	0.20	0.30	0.18	0.76	0.15	0.37
[Ca]	-0.06	0.35	0.95	0.33	0.83	-0.08	-0.06	0.32	0.13	0.48	0.16	0.25	0.30	0.78	0.46	0.34
[Fe]	0.05	0.52	0.76	0.47	0.40	-0.02	-0.06	0.18	-0.08	0.70	0.54	0.61	0.15	0.79	-0.03	0.33
[K]	0.33	0.79	0.97	0.32	0.73	0.28	0.33	-0.05	0.43	0.81	0.36	0.69	0.36	0.71	0.53	0.51
[Mg]	0.40	0.45	0.95	0.24	0.72	0.03	0.48	0.57	0.64	0.53	0.05	0.19	0.35	0.71	0.50	0.45
[Mn]	0.33	0.09	0.92	0.42	0.33	0.22	0.42	0.26	0.09	0.31	0.23	0.10	0.44	0.28	0.07	0.30
[Na]	0.35	0.60	0.92	0.23	0.36	0.18	0.27	0.40	0.14	0.60	0.59	0.38	0.17	0.31	0.38	0.39
[P]	0.39	0.50	0.96	0.21	0.67	-0.05	0.34	0.52	0.63	0.60	0.17	0.12	0.26	0.59	0.49	0.43
[Zn]	0.19	0.63	0.71	0.29	0.37	0.04	0.26	0.38	0.54	0.50	0.27	0.24	0.33	0.41	0.26	0.36
Average	0.38	0.45	0.88	0.32	0.58	0.18	0.38	0.29	0.40	0.50	0.34	0.34	0.31	0.60	0.37	

2. QTL mapping

A total of 67 QTLs for 84 phenotypic trait/growth condition pairs ([Cu] was excluded from the analysis) were identified, corresponding to less than one QTL per trait (**Figure III.24**). No QTLs were mapped for the OD FC trait, which had the lowest heritability.

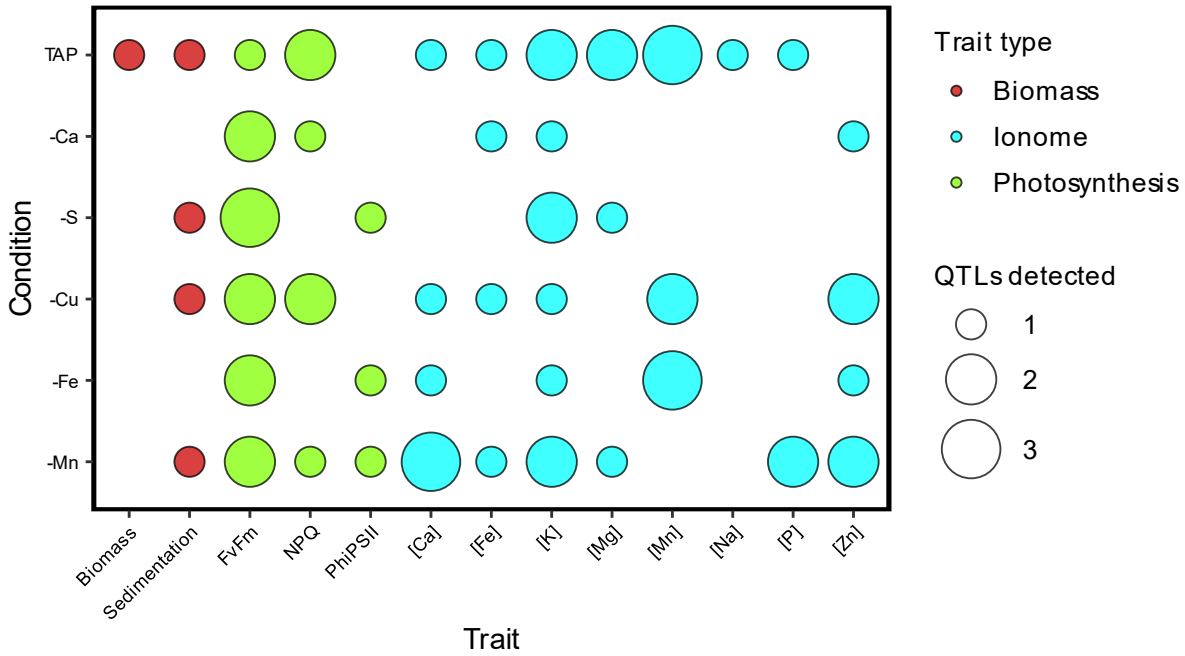

Figure III.24 Summary of the QTLs detected for nutrient deficiency-related traits. The numbers of QTLs detected for each phenotypic trait (x-axis) / growth condition (y-axis) pair represented with a circle colour-coded according to the trait type (red: biomass, blue: ionome, green: photosynthesis) and size according to the number of QTLs (small: 1, medium: 2, big: 3).

Among these 67 QTLs, 5 QTLs were related to growth traits (biomass and sedimentation), 21 were related to photosynthesis traits and 41 were related to ionome traits. A single QTL was identified for each biomass and [Na] traits, respectively. Three QTLs were detected for the [P] and Φ PSII traits. In contrast, the Fv/Fm, [K] and [Mn] traits were associated with 12, 9 and 8 QTLs, respectively.

Despite the relatively small cohort of F8 lines, some QTLs were highly significant: 29 of the mapped QTLs have a maximum LOD score above 10 (**Table III.12**), pointing towards the segregation of genetic variants with large effects in the terminal lines. The remaining 38 QTLs had a LOD score between 10 and 6.625, the Bonferroni corrected threshold (**Table III.13**). The complete list of genes in these intervals can be found in **Supplemental dataset S.III.1**.

The variance associated with the QTL effects was first estimated using the variance among the founder haplotype effects (the effects transmitted by each of the eight founders at a specific genomic position). Alternatively, this variance can be approximated as the reduction of polygenic variance in models without and with the QTL. As both approaches gave similar results, the ones obtained with the second approach are reported here. The proportion of genetic variance associated with single QTL ranged from 2.6% to 51.3%. Among the QTLs identified, 41 captured more than 10% of the genetic variance, 6 of which capture more than 30% of the genetic variance. The most significant QTLs, QTL1and 2, a pleiotropic QTL on chromosome 10 affecting [Zn] in -Mn and -Ca, captured respectively 51.3% and 46.6% of the genetic variance.

Table III.12 List of the significant nutrition-related QTLs mapped with a Max $\log_{10}$(p-val) >10. QTLs are ordered by descending order of significance. Chromosome number, positions on the chromosome, size (in Mb) and number of genes of the interval are relative to the v6 of the Chlamydomonas genome. Ionome-related QTLs are highlighted in grey, photosynthesis-related QTLs are highlighted in green, and biomass-related in white.

QTL n.er	Media	Trait	Chromosome	Start (Mb)	Stop (Mb)	Gene n.er	Max $\log_{10}$ (p-val)	Size (Mb)	Genetic variance explained (%)
1	-Mn	[Zn]	10	5.63	5.71	15	87.80	0.08	46.4
2	-Ca	[Zn]	10	5.63	5.71	15	43.36	0.08	51.3
3	-Fe	[Mn]	16	5.13	5.77	108	20.22	0.64	14.9
4	-Mn	Fv/Fm	3	4.55	4.9	59	18.79	0.35	14.7
5	TAP	[Mn]	3	2.49	2.71	36	17.69	0.22	11.5
6	TAP	Fv/Fm	9	2.02	2.33	46	17.68	0.31	15.9
7	-Mn	[Mg]	16	6.32	6.45	18	17.61	0.13	25.8
8	-Cu	[Mn]	3	2.49	2.71	36	17.43	0.22	16
9	-S	Phi PSII	2	7.21	7.59	61	17.21	0.38	26
10	-Ca	Fv/Fm	9	2.01	2.33	47	17.20	0.32	16.8
11	-Fe	[Mn]	9	3.46	3.69	31	16.74	0.23	12.2
12	-Mn	NPQ	1	8.05	8.2	27	16.54	0.15	15.8
13	-Mn	[Fe]	1	7.34	7.85	74	15.39	0.51	24
14	-Mn	[Zn]	1	8	8.21	36	15.32	0.21	7.9
15	-Cu	NPQ	1	8.09	8.2	16	14.12	0.11	22.2
16	TAP	[K]	2	7.21	7.58	59	13.94	0.37	12.6
17	-Mn	Sed.	1	7.42	8.22	119	13.61	0.8	12.8
18	TAP	[Mg]	16	6.32	6.56	38	13.42	0.24	15.6
19	-S	Sed.	2	7.21	7.35	22	12.37	0.14	15
20	-Mn	[P]	16	6.32	6.6	44	12.34	0.28	20.4
21	-S	Fv/Fm	2	7.21	7.63	66	12.13	0.42	12.6
22	-S	[K]	2	7.2	7.58	60	11.62	0.38	16.1
23	-Fe	Fv/Fm	9	2.01	2.34	49	11.32	0.33	6.4
24	-Ca	NPQ	1	8.08	8.2	18	11.31	0.12	3
25	-Mn	[Ca]	7	1.58	2.34	117	11.16	0.76	9.5
26	-Cu	Sed.	2	7.21	7.73	84	10.48	0.52	33.1
27	-Fe	Phi PSII	2	7.2	7.74	88	10.43	0.54	21.2
28	-Mn	[K]	1	7.1	7.87	100	10.32	0.77	17.2
29	-Fe	[Mn]	3	2.59	2.94	56	10.04	0.35	7

Table III.13 List of the significant nutrition-related QTLs mapped with a Max $\log_{10}$(p-val) <10. QTLs are ordered by descending order of significance. Chromosome number, positions on the chromosome, size (in Mb) and number of genes of the interval are relative to the v6 of the Chlamydomonas genome. Ionome-related QTLs are highlighted in grey, photosynthesis-related QTLs are highlighted in green and biomass-related in white.

QTL n.er	Media	Trait	Chromosome	Start (Mb)	Stop (Mb)	Gene n.er	Max $\log_{10}$ (p-val)	Size (Mb)	Genetic variance explained (%)
30	-Cu	[Mn]	10	2.21	2.5	43	9.68	0.29	7.2
31	TAP	NPQ	8	1.49	2.57	180	9.46	1.08	11.6
32	-Fe	[Ca]	16	4.82	5.15	48	9.39	0.33	13.4
33	-S	Fv/Fm	15	2.82	3.24	24	9.23	0.42	2.6
34	TAP	NPQ	16	7.45	7.86	71	9.20	0.41	6.6
35	TAP	[Mn]	1	7.51	7.82	46	9.12	0.31	8.1
36	TAP	[Mn]	10	2.21	2.51	44	9.09	0.3	7
37	TAP	[P]	16	6.22	6.57	57	8.91	0.35	7.1
38	TAP	[K]	1	7.21	7.92	94	8.74	0.71	7.9
39	-Fe	[K]	1	7.39	7.83	64	8.56	0.44	10.3
40	TAP	[Na]	2	7.21	7.59	61	8.41	0.38	17.4
41	-Mn	[K]	2	7.2	7.69	79	8.31	0.49	13
42	-Mn	[Ca]	16	6.32	6.83	80	8.20	0.51	8.3
43	TAP	[Ca]	7	1.58	2.73	183	8.12	1.15	8.3
44	TAP	Biomass	10	2.48	4.08	245	8.12	1.6	5.8
45	-Cu	[Fe]	1	4.63	6.41	286	8.11	1.78	15.3
46	TAP	Sed.	2	7.21	7.74	87	7.97	0.53	13.6
47	-S	[K]	1	6.91	8.09	163	7.92	1.18	5.9
48	-Mn	[P]	7	1.58	2.76	186	7.84	1.18	6.3
49	TAP	[Mg]	10	2.21	2.73	86	7.73	0.52	6.9
50	-Cu	[Ca]	7	1.42	2.13	118	7.70	0.71	7.7
51	-Cu	[K]	2	7.2	7.62	64	7.64	0.42	11.7
52	-Cu	Fv/Fm	1	8.06	8.21	25	7.42	0.15	5.4
53	-Mn	Fv/Fm	9	0.44	0.59	24	7.41	0.15	5.2
54	-S	Fv/Fm	3	4.31	6.26	371	7.40	1.95	5.8
55	-Mn	Phi PSII	1	7.46	7.92	70	7.38	0.46	6.9
56	-Cu	NPQ	16	7.45	7.99	94	7.36	0.54	9.5
57	-Ca	Fv/Fm	1	8.07	8.21	21	7.35	0.14	2.8
58	-Ca	[Fe]	1	7.2	8.21	138	7.29	1.01	22.1
59	-Cu	Fv/Fm	9	2.01	2.34	49	7.12	0.33	8.9
60	-S	[Mg]	15	2.59	3.02	20	7.10	0.43	20.4
61	-Mn	[Ca]	4	2.48	2.77	29	6.96	0.29	4.7
62	-Fe	[Zn]	12	5.4	5.86	84	6.93	0.46	15.6
63	TAP	[Fe]	10	2.51	4.18	262	6.89	1.67	7.8
64	-Ca	[K]	2	7.18	7.33	26	6.85	0.15	16.7
65	-Fe	Fv/Fm	3	3.96	4.4	83	6.77	0.44	4.3
66	-Cu	[Zn]	12	5.4	5.71	58	6.74	0.31	12.4
67	-Cu	[Zn]	1	5.49	6.15	106	6.71	0.66	13.2

a) Pleiotropy and genotype-by-environment interactions

Several chromosomal regions contained more than one QTL based on overlapping confidence intervals (**Figure III.25**). It is remarkable that while no QTLs were mapped on 6 chromosomes (5, 6, 11, 13, 14, 17) and a single QTL was mapped on chromosomes 8 and 4, chromosomes 1 and 2 harboured more than 10 QTLs each, approximately in the same region. The remaining chromosomes also harboured pleiotropic regions although to a smaller extent.

Some QTLs were found to either (i) affect different phenotypes in the same growth condition, (ii) the same phenotype in different growth conditions or (iii) both, representing 5, 2 and 8 QTLs, respectively (**Table III.15**).

"Condition-specific QTLs" were only few, occurring twice, in TAP (for both biomass and [Fe] traits) and in -Cu (for both [Fe] and [Zn] traits). In contrast, most of the QTLs affecting different traits were also significant in more than one growth condition. Two outstanding QTLs, affecting a large number of phenotypic trait / growth condition combinations, were located on chromosomes 1 (Cre01_7400000, 12 photosynthesis and nutrient accumulation traits) and 2 (Cre02_7400000, 13 sedimentation, photosynthesis and nutrient accumulation traits). Additionally, the QTL on chromosome 8 (Cre08_2000000) was associated to 10 photosynthesis-related traits.

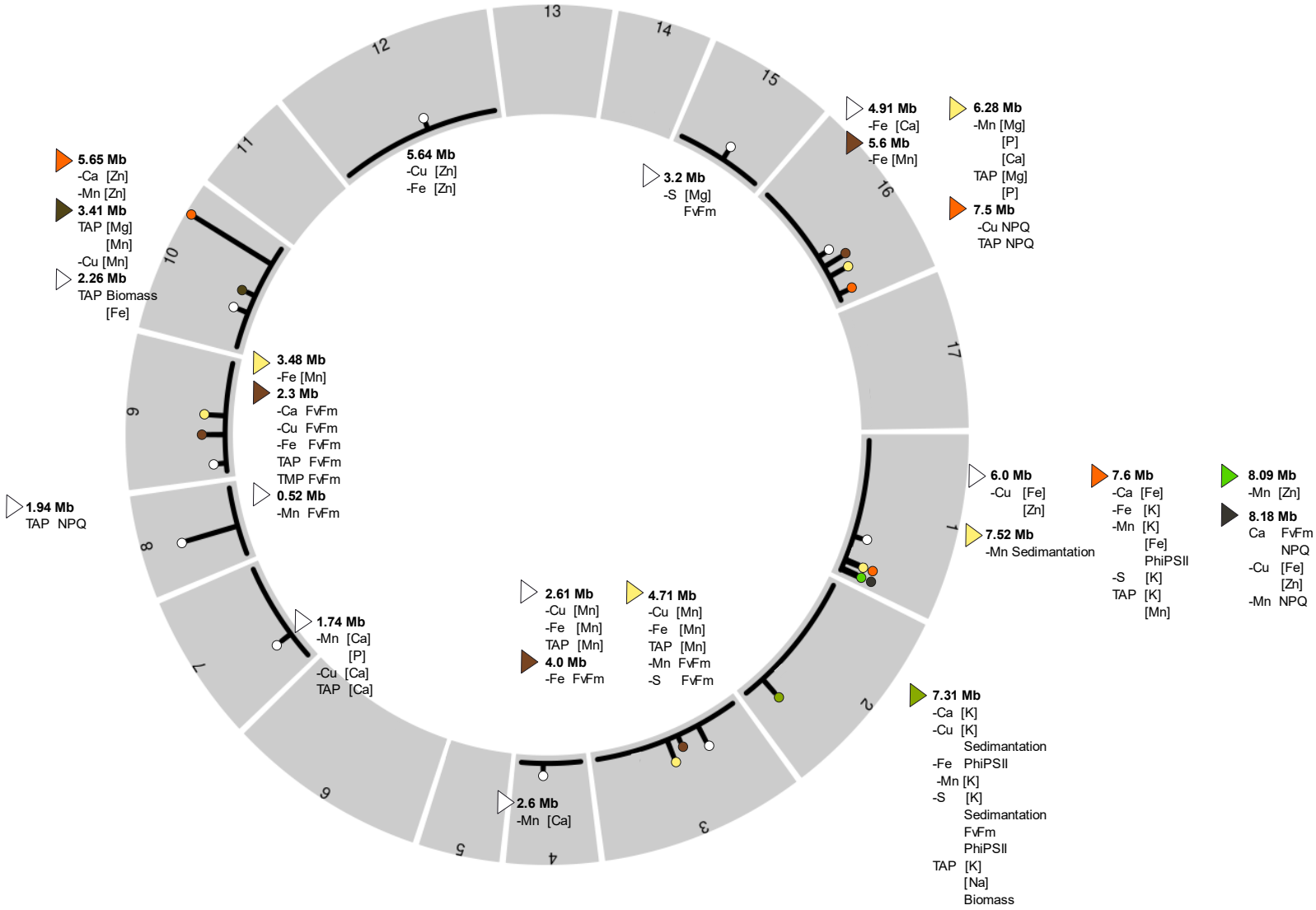

Figure III.25 Visual representation of the mineral nutrition QTLs. The circle represents the Chlamydomonas genome, and each section represents one of the 17 chromosomes, with size proportional to the chromosome size. QTL are presented as a lollipop chart with peaks at the centre of the confidence interval and size proportional to the QTL signal.

Table III.14 Summary of QTL regions harbouring multiple QTLs related to mineral nutrition. QTLs affecting single phenotypes in multiple conditions are classified as SP, and QTLs associated to multiple phenotypes in one condition as MP. QTL positions are indicative, in the centre of confidence interval and are based on the v6 Chlamydomonas genome. Traits between parenthesis were measured as part of the thesis of Iacono (2023) and were added as an indication (NPQ_n: non-photochemical quenching measured at *n* µmol of quanta m^{-2} s^{-1}, ST_ETR_n: state transition electron transfer rate at *n* µmol of quanta m^{-2} s^{-1}, ST_qI: state transition photoinhibition, FmDR_*n* m: maximum fluorescence after *n* min of dark relaxation, ST_FmDR: state transition FmDR).

Position	QTLs	Phenotypes observed	N.^{er} of conditions	Traits	Classification
Cre01 _ 5700000	2	2	1	[Fe] and [Zn] in -Cu	MP
Cre01 _ 7400000	12	7	7	[K] in TAP, -Fe, -Mn, -S; [Fe] in -Ca, -Mn; (ST_ETR_{270} in TMP, TAP); [Mn] in TAP; (NPQ_{130} in TMP); ΦPSII in -Mn; (ST_qI in TMP)	SP MP
Cre01 _ 8100000	5	2	2	NPQ in -Ca, -Cu, Mn; Fv/Fm in -Ca, -Cu	SP MP
Cre02 _ 7400000	13	6	7	[K] in TAP, -Ca, -Cu, -Mn, -S; Sedimentation in TAP, -Cu, -S; ΦPSII in -S, -Fe; [Na] in TAP; Fv/Fm in -S; (NPQ_{130} in TMP)	SP MP
Cre03 _ 2600000	3	1	3	[Mn] in TAP, -Cu, -Fe	SP
Cre07 _ 1800000	4	2	3	[Ca] in TAP, -Cu, -Mn; [P] in -Mn	SP MP
Cre08 _ 2000000	10	7	3	(FmDR_11m in TAP and TMP); (FmDR_1m in TAP and TMP); (NPQ_{420} in TAP and TMP); (Fv/FM in TMP); NPQ in TAP; (NPQ_{130} in TMP); (ST_FmDR in TMP)	SP MP
Cre09 _ 2150000	5	1	5	Fv/Fm in TAP, -Ca, -Cu, -Fe, (TMP)	SP
Cre10 _ 2400000	3	2	2	[Mn] in TAP, -Cu; [Mg] in TAP	SP MP
Cre10 _ 3200000	2	2	1	Biomass and [Fe] in TAP	MP
Cre10 _ 5650000	2	1	2	[Zn] in -Ca, -Mn	SP
Cre12 _ 5600000	2	1	2	[Zn] in -Cu and -Fe	SP
Cre16 _ 6400000	5	3	2	[Mg] in TAP, -Mn; [P] in TAP, -Mn; [Ca] in -Mn	SP MP
Cre16 _ 7600000	2	1	2	NPQ in TAP, Cu	SP
Cre17 _ 4800000	5	3	3	Fv/Fm in -Mn, -S, (TMP); (FmDR_11m and ST_FmDR in TMP)	SP MP

Among the QTLs associated with one trait in multiple conditions, two QTLs related to [K] were significant in 4 and 5 conditions out of 6 (on chromosome 2 and chromosome 1, respectively), and a QTL related to Fv/Fm was detected in 4 different growth conditions (on chromosome 9). The genome-wide association studies for that specific traits in the 6 conditions are represented in **Figure III.26 A** and is used to illustrate pleiotropy. The number of QTLs per condition ranged from 1 (e.g.,

TAP) to 3 (e.g., -S), on chromosomes 1, 3 and 9 (**Figure III.26A**). Even if these QTLs influenced the phenotype in different conditions (from 2 to 5), they were never genome-wide significant in all conditions. This might result from a lack of power to detect the QTL in some conditions. For instance, the QTL on chromosome 9 affecting Fv/Fm presented an analogous likelihood ratio (LR) curve for -Mn, close to genome-wide significance and there is also some signal in -S, despite them not being significant (**Figure III.26 B**).

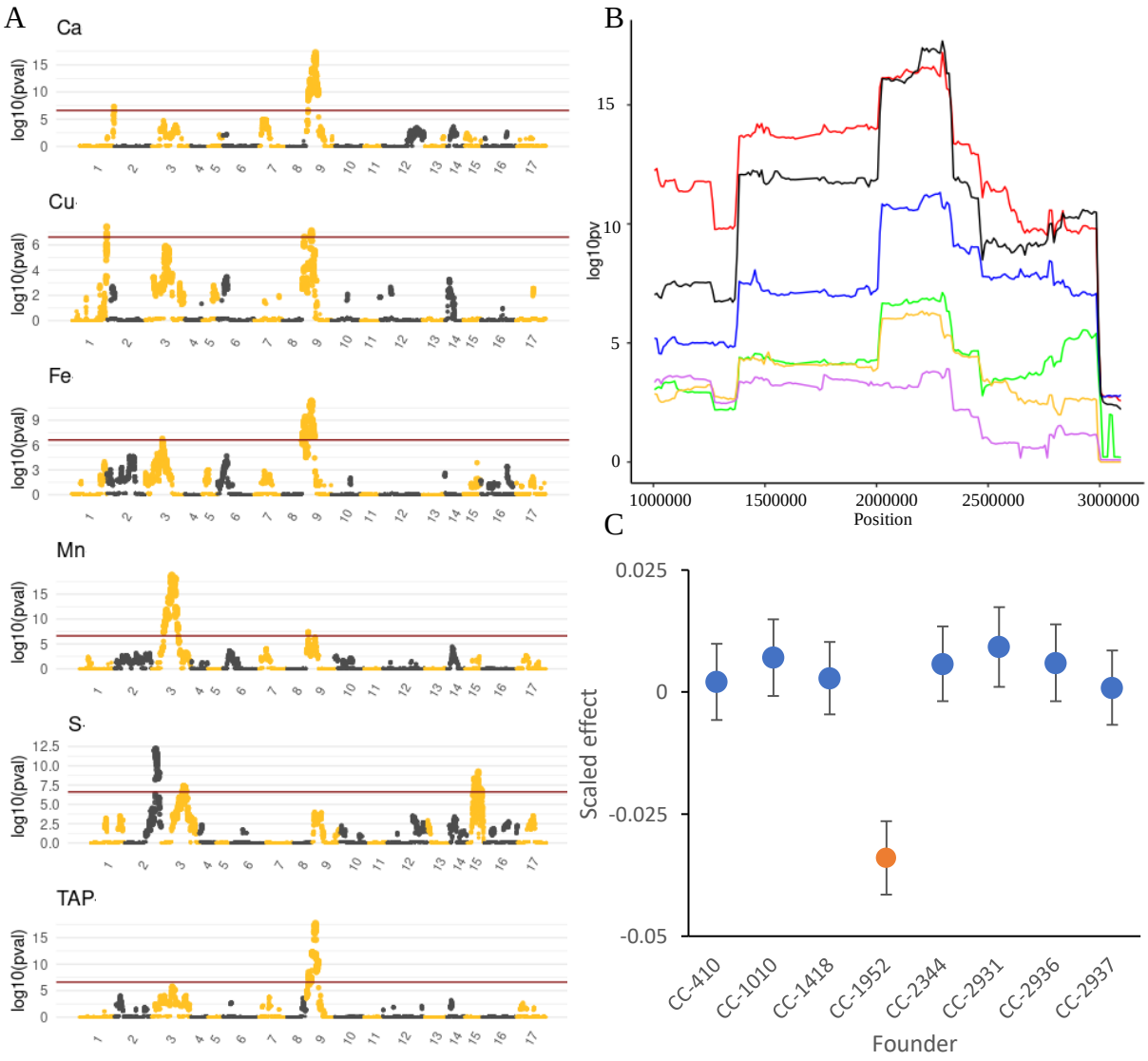

Figure III.26 Example of pleiotropic QTLs detected thanks to the GreenMAGIC population. (A) Manhattan plot of QTLs affecting Fv/Fm (t4) in the six different growth conditions. (B) Focus on the genetic neighbourhood of the QTL on chromosome 9 and its confidence interval for each media tested (from the bottom up: -S in violet, -Mn in yellow, -Cu in green, -Fe in blue, -Ca in red, TAP in black). (C) Scaled average ± se of the effect of each founder. Founders with a positive and negative contribution are coloured in blue and in orange, respectively.

3. Fine mapping and remarkable QTLs

A multiple-trait QTL association analysis within the QTL regions is currently being performed in order to reduce the size of the confidence intervals by taking advantage, whenever possible, of the observed pleiotropy. Indeed, multiple-trait QTL mapping first results point towards a higher LR test compared to the single-trait approach in most cases and confidence intervals were either reduced or remained unchanged. The same results also show that final confidence intervals ranged from 0.07 to 1.48 Mb, a 25% reduction compared to the initial estimate (0.08-1.95 Mb) and contained at most 225 genes. These are still preliminary results and will not be explored in much detail.

From the dozens of QTLs mapped, 4 were chosen to be analysed in more detail due to their significance level or the presence of interesting genes in the interval:

a) A [Zn] QTL in -Mn and -Ca conditions

For the QTL located on chromosome 10 and associated with [Zn] in both -Mn and -Ca conditions (QTLs 1 and 2 in **Table III.12**), more than 240 bi-allelic variants were in high linkage disequilibrium with the lead bi-allelic variant and thus present the same statistical evidence for causality (**Figure III.27A**). Analysis of the founder haplotype effect showed that the alleles specific to strain CC-2937 had a distinct effect from those of the other founders (**Figure III.27B**).

The variants in high linkage disequilibrium were distributed among the 15 genes within the QTL confidence interval, indicating that all of them should be considered as candidate genes. Among the 15 genes, 6 were annotated (encoding 3 Scavenger receptor cysteine rich (SRCR) proteins, a proton P-type ATPase, a cytosolic 80S ribosomal protein and an OctotricoPeptide Repeat protein), 3 non-annotated genes encoded proteins with enzymatic activity (2 peptidases and 1 transferase), and no information regarding their gene ontology (GO) was available for the remaining 6 genes (**Table III.15**).

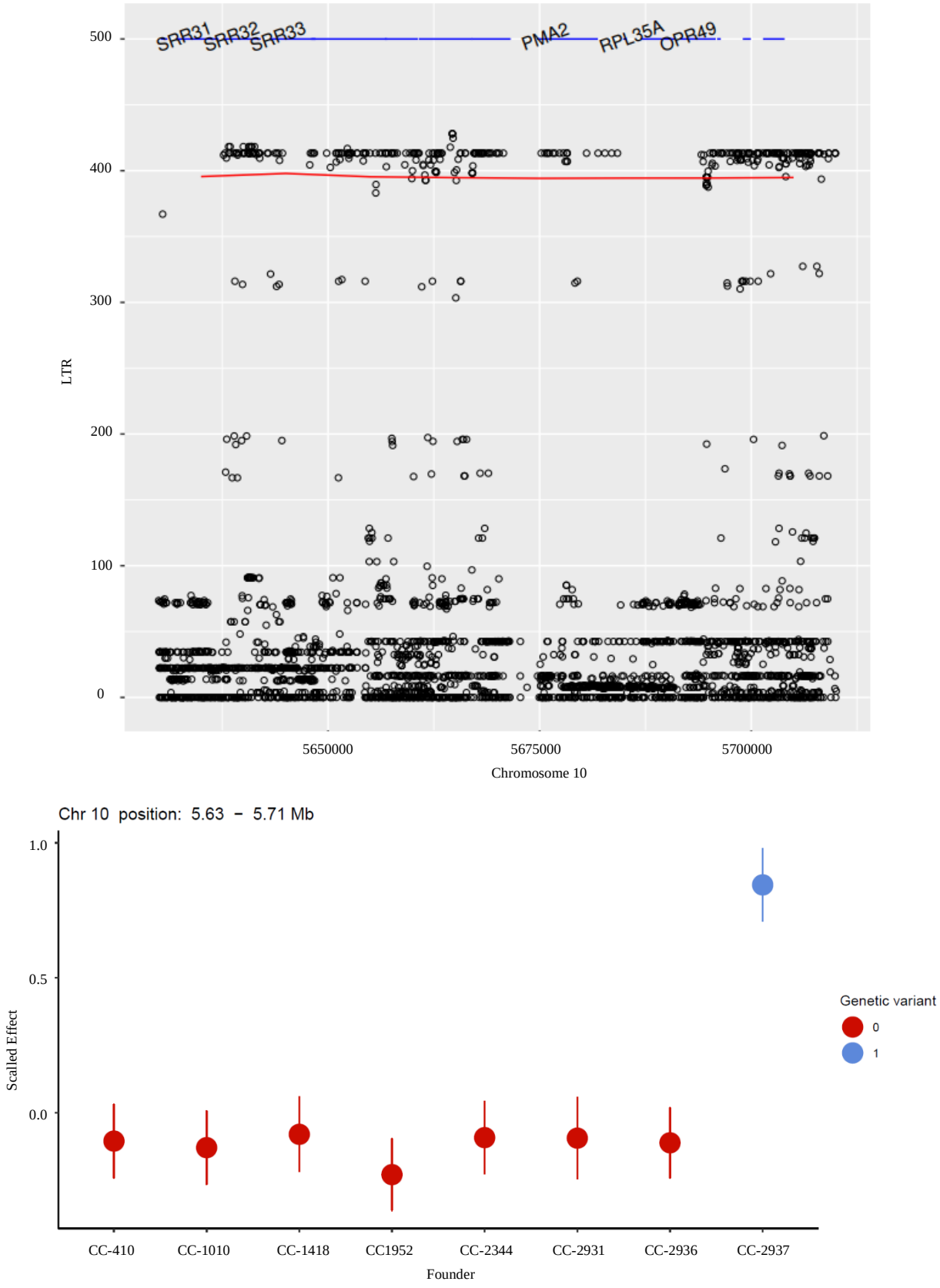

Figure III.27 Overview of the [Zn] QTL on chromosome 10. (A) Manhattan plot showing the likelihood ratio test (LRT) scores for variant association. Each dot represents one SNP and its relationship with the LTR of 10 kb windows (non-consecutive), denoted as a red line. Genes are denoted with a blue line above their position, and annotated genes are identified. (B) Founder haplotype effect, scaled. Reference allele is coloured in red, variants are coloured in blue and green.

Table III.15 List of genes present in the confidence interval of the [Zn] in -Mn and -Ca (QTLs 1 and 2). NA: not applicable

Locus ID (v6)	Locus ID (v5)	Start bp (v6)	Stop bp (v6)	Description	Gene Symbol	GO term	GO description
Cr_10_ 49624	Cre10. g801190	5630255	5631039			NA	NA
Cr_10_ 49628	Cre10. g458800	5632001	5637092	Scavenger receptor cysteine rich (SRCR) protein	*SRR31*	NA	NA
Cr_10_ 49632	Cre10. g458850	5637588	5642051	Scavenger receptor cysteine rich (SRCR) protein	*SRR32*	NA	NA
Cr_10_ 49636	Cre10. g458900	5643084	5648514	Scavenger receptor cysteine rich (SRCR) protein	*SRR33*	NA	NA
Cr_10_ 49641	Cre10. g458950	5648031	5656920			0016757	Transferase activity, transferring glycosyl groups
Cr_10_ 49645	Cre10. g459000	5656750	5660621			NA	NA
Cr_10_ 49650	Cre10. g459050	5660713	5667007			0006508; 0070008; 0004252; 0008236	Proteolysis;Serine-type (endo-,exo-) peptidase activity
Cr_10_ 49655	Cre10. g459100	5666950	5671577			NA	NA
Cr_10_ 49659	Cre10. g459200	5674660	5681886	P-type ATPase/cation transporter, plasma membrane	*PMA2*		
Cr_10_ 49663	Cre10. g459250	5684855	5685330	Cytosolic 80S ribosomal protein L35a	*RPL35A*	0005622; 0003735; 0006412; 0005840	Intracellular; Structural constituent of ribosome; Translation; Ribosome
Cr_10_ 49667	Cre10. g459300	5686915	5691073			NA	NA
Cr_10_ 49671	Cre10. g459350	5691549	5695809	OctotricoPeptide Repeat protein 49	*OPR49*		
Cr_10_ 49675	Cre10. g801191	5695963	5696397			NA	NA
Cr_10_ 49680	Cre10. g459400	5699003	5699947			NA	NA
Cr_10_ 49685	Cre10. g801192	5701385	5703938			0006508;0004252	Proteolysis; Serine-type endopeptidase activity

b) [Mn] QTL in TAP condition

For the QTL associated to [Mn] in TAP condition located on chromosome 10 (QTL 36 in **Table III.13**), a single variant in a single gene was significantly associated with the QTL (**Figure III.28 A**). This variant was linked to founder CC-1010 (**Figure III.28 B**), in a region where it is identical to CC-410 and CC-1418 at all other positions. This variant, which was a missense variant with moderate effect as predicted by the SnpEff tool (Cingolani, 2022), occurred in a -gene not fully characterized, encoding a protein with a predicted ubiquitin ligase activity (**Table III.16**).

Table III.16 Gene significantly contributing to [Mn] QTL in TAP condition on chromosome 10.

Locus ID (v6)	Locus ID (v5)	Start bp (v6)	Stop bp (v6)	Description	Gene Symbol	GO term	GO description
Cr_10_47088	Cre10.g433900	224603	2258741	NA	NA	0005515; 0004842	Protein binding; ubiquitin-protein ligase activity

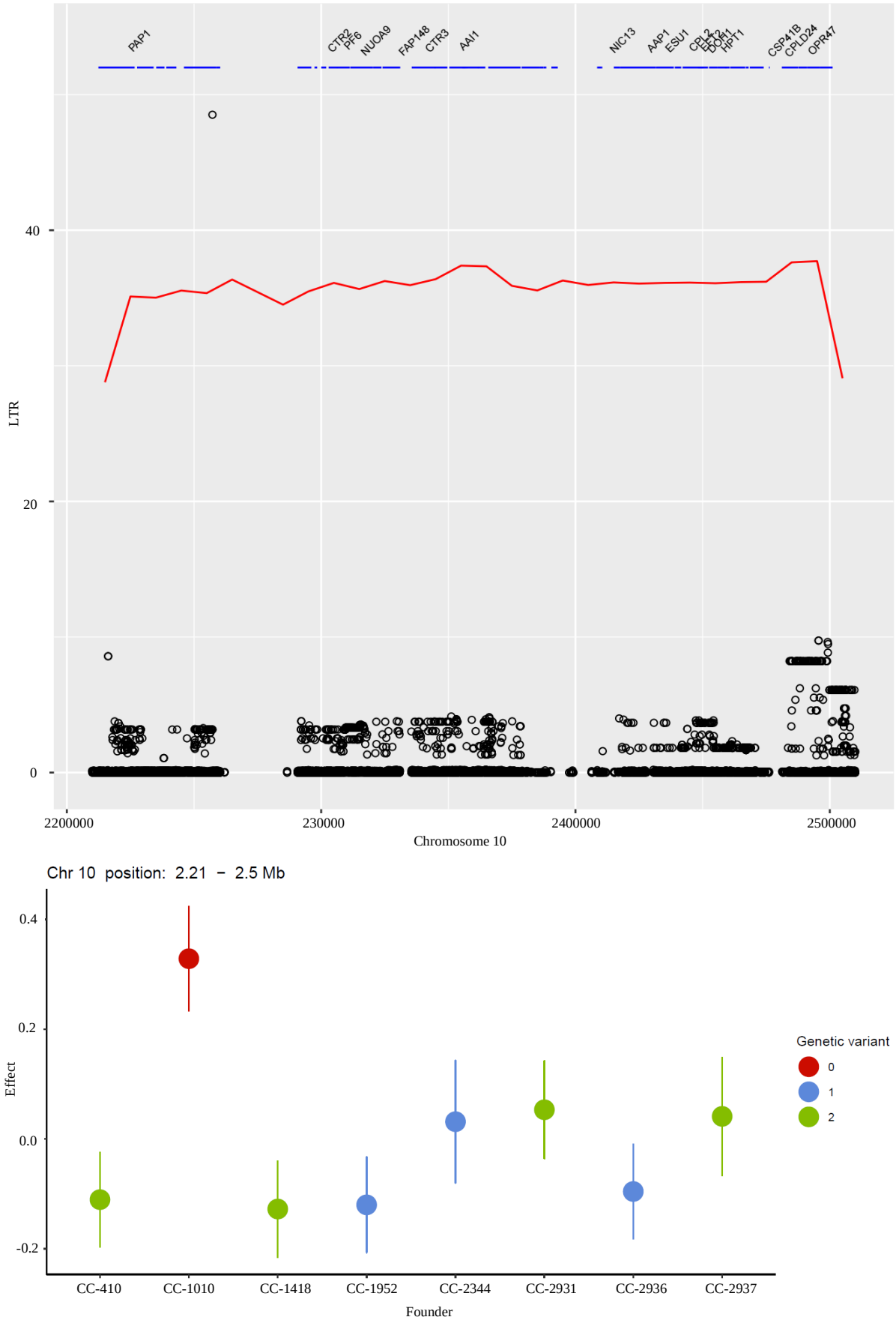

Figure III.28 Fine mapping of [Mn] QTL in TAP condition on chromosome 10 (QTL 36). (A) Manhattan plot showing the likelihood ratio test (LRT) scores for variant association. Each dot represents one SNP and its relationship with the LTR of 10 kb windows (non-consecutive), denoted as a red line. Genes are denoted with a blue line above their position, and annotated genes are identified. Only one SNP, at the position 2257252 and inside a gene, was above the significance threshold. (B) Founder haplotype effect, scaled. Reference allele is coloured in red, variants are coloured in blue and green

c) [Mn] QTL in TAP, -Cu and -Fe conditions

[Mn] in TAP, -Cu and -Fe (QTL 8, 8, 29 in **Table III.12**) conditions was significantly correlated with a region of chromosome 3, which contained 3 genes encoding metal transporter proteins (MTP2-4, which form a clade of Mn-transporting MTPs) in close proximity among the ~40 genes in the QTL confidence interval (**Table III.17**). Between MTP3 and MTP4, 3 genes are not characterized in detail: 1 of which has no information available, while the other 2 are described as Zn binding.

Table III.17 Metal transporter genes in the QTL related to [Mn] in TAP, -Cu and -Fe on chromosome 3 (QTL 8, 8, 29).

Locus ID (v6)	Locus ID (v5)	Start bp (v6)	Stop bp (v6)	Description	Gene Symbol	GO term	GO description
Cr_03_14846	Cre03.g160550	2632329	2636779	Metal Transport Protein 4	MTP4	0016021; 0006812; 0008324; 0055085	Integral to membrane; cation transport; cation transmembrane transporter activity; transmembrane transport
Cr_03_14850	Cre03.g160600	2638395	2642324			0008270; 0003700; 0043565; 0006355	Zn ion binding; sequence-specific DNA binding transcription factor activity; sequence-specific DNA binding; regulation of transcription, DNA-dependent
Cr_03_14854	Cre03.g160650	2644631	2654574			NA	NA
Cr_03_14859	Cre03.g160700	2657570	2661856			0008270; 0003700; 0043565; 0006355	Zn ion binding; sequence-specific DNA binding transcription factor activity; sequence-specific DNA binding; regulation of transcription, DNA-dependent
Cr_03_14863	Cre03.g160750	2662177	2666973	Metal Transport Protein 3	MTP3	0055085; 0008324; 0006812; 0016021	Transmembrane transport; cation transmembrane transporter activity; cation transport; integral to membrane
Cr_03_14867	Cre03.g160800	2667167	2671871	Metal Transport Protein 2	MTP2	0008324; 0006812; 0016021; 0055085	Cation transmembrane transporter activity; cation transport; integral to membrane; transmembrane transport

d) [K] QTLs in TAP, -Ca, -S, -Cu and -Mn conditions

Accumulation of K in 5 out of the 6 tested media (TAP, -Ca, -S, -Cu and -Mn, QTLs 65, 16, 22, 51 and 41 in **Tables III.12-13**, respectively) was significantly correlated with a region of chromosome 2. Three-quarters of the genes in the QTL confidence interval were not fully characterized, and among the ones with a description, there was an autophagy-related gene (**Table III.18**).

Table III.18 Autophagy-related gene in the confidence interval of QTLs related to [K] in TAP, -Ca, -S, -Cu and -Mn on chromosome 2. (QTLs 65, 16, 22, 51 and 41)

Locus ID (v6)	Locus ID (v5)	Start (v6)	Stop (v6)	Description	Gene Symbol	GO term	GO description
Cr_02_11863	Cre09.g391245	7258392	7263965	Autophagy related	ATG1	0006468; 0004672; 0005524	protein phosphorylation; protein kinase activity; ATP binding

D. General discussion

In this chapter, a Multi-parent Advanced Generation Inter-Cross (MAGIC) population was generated to dissect the genetic architecture of complex traits in Chlamydomonas using natural variation. Compared to the analysis of mutants, the study of natural variation has the advantage of allowing the identification of genes and alleles in different genetic backgrounds, as well as providing insight on the generation and maintenance of variation, and the adaptive response of the founder lines (Chietera & Chardon, 2014).

To create this MAGIC population, eight founder lines were selected to generate 768 F8 terminal lines, which were then exposed to nutrient deficiency and their growth, ionome and photosynthetic ability were measured and correlated to their genetic variation.

1. Establishment of the MAGIC design

MAGIC designs have been used in crops for a couple of decades to study traits of interest (reviewed in Arrones et al., 2020). Nonetheless, such a design had not yet been applied to model microalga Chlamydomonas despite the important genetic variation reported within the genomes of laboratory strains (Gallaher et al., 2015) as well as natural strains (Flowers et al., 2015), their mitochondria and chloroplast genomes (Gallaher et al., 2018), and the evolutionary capacity (Lucker et al., 2022; Thiriet-Rupert et al., 2021a) as well as phenotypic variation of the species (Bajhaiya et al., 2016; Gallaher et al., 2015; Zhang et al., 2022b). For this reason, a crucial objective of this project was the establishment of the 8-way diallel-like design itself.

First, founder lines were selected mainly due to their mating ability (**Figure III.1**) and phenotypic diversity (both at nutritional (**Figure III.2**) and photosynthetic levels) (**Table III.1**). However, two of the strains included in the design had not been sequenced at the start of the project and, despite being described as natural strains in strain collections, CC-410 and CC-1418 clustered with reference laboratory strains upon whole genome sequencing and were genetically almost identical (**Figure III.3**). The inclusion of these two identical strains, closely related to a third strain, effectively reduced the genetic variability ingenerated by the MAGIC design as this is directly linked to the variability observed in the founder lines. In reality, given the three laboratory strains are very closely related, despite having 8 founder lines, the design is in fact closer to a 6-way design. A diallel-like design was used in this work due to the nature of Chlamydomonas sexual reproduction cycle, which generates 2 daughter cells of each mating type (**Figure I.7**), instead of a funnel-type design. Opting for a diallel-like design has the advantage of covering all possible crossing combinations in multiple funnels and generating a higher diversity of allele combinations (Arrones et al., 2020), which might help compensate the unintentional choice of 3 close related founders.

Second, in order to increase the germination rate of the zygotes and streamline the experimental procedure, adaptations to the traditional tetrad dissection protocol (Jiang & Stern, 2009) were made (*cf.* Mating conditions and progeny selection in chapter V). Briefly, instead of selecting one zygote and dissecting each of the 4 daughter cells to obtain 4 isolated colonies, several zygotes were germinated at the same time and spread on a Petri dish to generate multiple isolated colonies. This approach, while timesaving, caused two issues: (i) the possible transfer of parental cells to the next generation, (ii) a possible absence of separation between colonies of the same and different tetrads, resulting in colonies with mixed genotypes, both points could have had strong impacts in the progeny and their effects will be discussed further ahead.

At each step of the process, more than one cross had a small number of zygotes forming and/or germinating. In the case where few zygotes were obtained, this was often solved by harvesting zygotes in one of the plates made after a longer mating period, indicating that 1h (and, less often 3h) was not enough time for some strains to mate. In the case of diminished germination, it is possible that (i) the zygotes were also killed during the chloroforming step meant to kill unmated parental cells, due to the presence of chloroform-sensitive zygospores or cell wall expansion from premature germination; this is the least likely cause (Harris, 2009a); (ii) the zygotes were unable to switch from dormancy to active metabolism (Aoyama et al., 2014). Less often, no zygotes were obtained at all (in the alternative batch (i.e., batches 1/8, 2/7, 3/6, 4/5 are similar) or the plates prepared after a longer mating period) suggesting a mating failure, which might be due to several issues: (i) a too short/long gametogenesis period , (ii) an absence of flagella/ paralyzed strains or (iii) the presence of palmelloid structures which impeded cell's free swimming and may require overnight mating (Harris, 2009). Aggregates and palmelloid structures differ in the way that aggregates are made of tens to thousands of cells held together by an extracellular matrix and are dependent on cell size and mobility, while palmelloids are composed of 4-16 cells surrounded by a membrane and are stress regulated (de Carpentier et al., 2019; Sathe & Durand, 2016). This difference and their impact on mating should have been considered more carefully.

In spite of these rare occurrences where crosses failed, after 8 rounds of crosses, 8 strains were isolated from each of the 32 crosses in each of the 3 MAGIC designs, producing 96 families of 8 strains each.

2. Characterization of the GreenMAGIC population

Once the 768 progeny strains were obtained, quantifying the extent of the phenotypic variation in response to nutrient deficiency and the level of shuffling of the founder chromosomes obtained at the end of the MAGIC design were the next objectives.

a) Phenotypic variation

In addition to the biomass (measured as $OD_{750\ nm}$) and the 9 ionome elements measured for the 24-strain panel (see Chapter II), new phenotypes were also scored: OD fold-change (FC, $OD_{750\ nm}$ variation between day 0 and day 4 of culture), sedimentation ($OD_{750\ nm}$ variation after 10 minutes) and 3 photosynthetic parameters (Fv/Fm, ΦPSII and NPQ). These 15 traits were measured in 6 different growth conditions (TAP, -Ca, -S, -Fe, -Cu and -Mn), for a total of 90 traits for which QTLs could be mapped.

A first inspection of the data revealed a skewed data distribution with the presence of outliers in each condition (**Figure III.15**, **Figure S.III.2-6**). Due to the large number of samples, the phenotyping was divided in 8 96-strain batches. Overall, batches were significantly correlated with each other, indicating that no major batch effects were created, with exception of the sedimentation trait (**Table III.3**, **Figure S.III.7-11**). Chlamydomonas sedimentation and swimming are a result from multiple signals influencing its positioning, mainly photo-, chemo-, thermo-and gravitaxis (Feinleib & Curry, 1971; Govorunova & Sineshchekov, 2005; Sekiguchi et al., 2018; Yoshimura et al., 2003, respectively), as well as the presence and motility of the flagella (Marshall, 2009).

The phenotypes of the GreenMAGIC progeny in the different growth conditions were dispersed around the founders' phenotypes and the 3 crossing designs used to generate the GreenMAGIC population were not a main component of the observed variation (**Figure III.16**). Among growth conditions, a strong positive correlation between the phenotypes measured in TAP and -Cu conditions was detected despite the strong deprivation ($^1/_{1000}$ of the control Cu concentration). Chlamydomonas however possesses an efficient Cu sparing mechanism (Merchant & Bogorad, 1986b, Chapter II), which ensures Cu allocation to processes where it cannot be replaced, and which delays visible Cu starvation symptoms. It is also possible that there were traces of Cu in the system, despite the effort done to reduce this occurrence (see Chapter V). The other growth conditions were also positively correlated with TAP, but more moderately, hinting at the negative impact of the deficiency treatments. Surprisingly, the phenotypes measured in -S condition had a weak negative correlation with those measured in -Ca, -Fe and -Mn conditions, possibly due to the type of the deficiency applied: while Ca, Fe and Mn were omitted from the media, SO_4^{2-} is the accompanying anion of many of the salts used in TAP media (Hutner et al., 1950; Sueoka, 1960) and was replaced by the Cl^-, which can globally influence nutrient transport (Britto & Kronzucker, 2008).

Globally, there was an increase in the phenotypic variation observed among the GreenMAGIC strains compared to the founders for 92% of the traits, ranging from 1.08x (NPQ in -Mn) to 15.71x ([Fe] in -Ca) the variation among the founder strains, and the remaining 8% ranged from 0.62x ([K] in -S) to 0.98x ([Fe] in -Fe) (**Table III.4-8**). While an increase in phenotypic variation is expected when generating a recombinant population (Pierre et al., 2022), a reduction of variation of some traits in the progeny lines has also been reported in maize by Liu et al., (2020), who used a crossing scheme derived from the traditional MAGIC (Complete-diallel plus Unbalanced Breeding-derived Inter-Cross (CUBIC) design) to generate the mapping population.

b) Genetic variability

(1) Mosaic structure

Once the GreenMAGIC population was sequenced, SNPs were used to infer most probable ancestry (reviewed in Scott et al., 2020). For most progeny strains, founders contributed long tracts of their genome (**Figure III.17**). However, for about 4% of the GreenMAGIC strains, an elevated number of small founder genome tracts could be observed in their genome (**Figure III.18**). This apparent larger segmentation of the genome inheritance may be the result of the selection and sequencing of multiple colonies with the same *mt* which were not visually distinguishable at the selection (*cf* point D.III.1. Establishment of the MAGIC design point above). Despite the combination of the data from hundreds of GreenMAGIC progeny allowing the inference of complete chromosomal mosaics regarding the haplotype even with founder information missing (Davies et al., 2016), the ancestry of some regions could not be identified. This could be due to the exclusion of poor-quality SNPs or, in the particular case of chromosome 15, its high degree of fragmentation and repeat content (Craig et al., 2022). By using multiple SNPs to better understand the overall contribution of all founders towards the entirety of the progeny, and the probability of each founder to contribute to a variant as well as the surrounding variants, ancestry determination and the distinction between opposing traits occurring in the same marker allele (Mott et al., 2000a) was improved (**Figure III.19**). Using this approach, the average contribution of each founder (**Table III.19**) is closer to what would be expected after 6-7 generations rather than the 8 performed. This fact, in addition to some of the MAGIC progeny strains missing the contribution of some founders, implies the selection of unmated strains at initial stages of the design (intermediate genotyping at F3, data not shown). Indeed, as meiosis occurs after mating, nitrogen re-supply leads to gamete dedifferentiation into vegetative cells (Matsuda et al., 1992). Nonetheless, the founder contributions, individual and by origin, are close to the expected theoretical contributions of 12.5%.

(2) Population structure

Despite having a low levels of population structure in GreenMAGIC populations (and other synthetic) populations, it remains an important factor to account for as population structure can have

a negative influence on QTL mapping, by generating false-positives and reducing the statistical power of the mapping (Kang et al., 2008; Kover et al., 2009; Mackay & Powell, 2007). The first aspect investigated related to population structure was the effect of using 3 crossing designs on the genetic diversity (**Figure III.20**), which showed that the 3 designs accounted for only a small portion of the observed genetic variation. Then, similarity among strains was also considered, while considering that the same allele could derive from different founders (**Figure III.21**). As expected, the 8 strains selected from the same F8 cross (a family) had a higher degree of similarity among each other, neighbouring families (which shared the same grandparents) and strains from the same design, than with strains issued from one of the other designs. In fact, average relatedness within families was close to the expected 0.5 for strains with the same parents but the average relatedness between families was higher than the expected 0.125 (**Figure III.22A**), and higher values were obtained when correcting for the fact that founders were related (**Figure III.22B**). This high relatedness among strains is not entirely unexpected, as strains issued from one crossing design were expected to be more closely related to each other than to strains from different crossing designs, as observed by Scott et al., (2020). Indeed, while each of the 24 batches (8 batches x 3 independent designs) represented a diallel-like design, the mixing at the F3 and F6 effectively reduced the number of independent designs to 3 (*cf* **Figure III.4**), which impacted the overall relatedness between strains. Nonetheless, 700 unique strains were kept for analysis, a value above the 200-500 non-redundant progeny lines suggested by Valdar et al., (2006b) in order to map QTLs explaining 5% of the observed phenotypic variance. Accounting for this similarity among strains in the QTL models allows for a better control of population structure effects on QTL mapping, as it is an effective way of compensating strains relatedness, reducing the number of false positives, by including the similarity matrix in the model used (Kang et al., 2008; Pereira et al., 2018; Sul et al., 2018).

(3) Heritability

The phenotypic variation observed in the progeny had a high degree of repeatability (*cf* 2(a) point above). Repeatability gives an indication of the upper bound for heritability, high levels are thus compatible with heritable traits. High repeatability is linked to high heritability in cases where environmental variation is low, as repeatability is a result of both environmental and genetic variation (Boake, 1989; Dohm, 2002). Narrow-sense heritability (h^2), which refers to the portion of phenotypic variance explained by additive genetic variance (Xu, 2013), tends to be higher in plants (e.g., Stadlmeier et al., (2018): wheat seedling resistance to powdery mildew, 0.93) than in animals (e.g., Sutera et al., (2021): milk yield and composition in dairy sheep, 0.06-0.15) due to the existence of multiple individuals (lines/ strains) sharing the same genotype (Schmidt et al., 2019). In this study, aside from [Cu], for which h^2 was not calculated due to the high number of null values of uncertain origin, heritability ranged from 0.10 to 0.86 (**Table III.10**, **Figure III.23**). The lowest heritability

values (0.10 – 0.26) were observed for the accumulation of the nutrient removed from the media ([Ca] in -Ca, [Fe] in -Fe, [Mn] in -Mn), as well as [Na] in -S in response to the increase in [Cl] in the medium, highlighting the strength of the environmental stress in these cases. Additionally, moderate heritability was documented for sedimentation in -Ca (0.31) and -Cu (0.35), as well as OD FC after 4 days (>0.40). A moderate heritability in these conditions was not unexpected, given the role of Ca in flagellar movement (Schmidt & Eckert, 1976) and the fact that Cu deficiency impacts oxygen-sensing (del Campo et al., 2004), which might influence chemotaxis. Additionally, as cells were diluted by the same factor and not to the same concentration, the number of cell divisions until reaching stationary phase may have differed depending on the initial cell concentration, which may have impacted the heritability of OD FC across all treatments.

(4) Genetic correlations

Cross-trait genetic correlations to evaluate the shared contribution of genetic variation were investigated from a general point-of-view (i.e. for all traits in all growth condition pairwise combinations **Table III.11**), as well as between traits in each condition (**Figure S.III.16-17**). Despite the fact that such analyses provide valuable information on the relation between two traits, determining the causality of such genetic correlation is less straight forward: one trait can cause the other, both traits can be controlled by a factor under genetic control, or traits can be controlled by factors with same (positive correlation) or opposing (negative correlation) effect direction (Kraft et al., 2020). Additionally, regardless of the importance of the genetic correlation (over environmental correlation) in traits with high heritability, the strength of the correlation can be diminished through recombination in cases where it is caused by linkage (Falconer, 1960). Genetic correlations can not only be caused by one or more loci impacting the different traits (pleiotropy), but also by separate loci in linkage disequilibrium each affecting one trait (see review by Gardner & Latta, 2007).

Overall, the average genetic correlations showed a higher variation between conditions (0.18 - 0.88) than within traits (0.30 - 0.61) (**Table III.11**). Following the trend observed previously, where the traits in TAP and -Cu had a strong positive correlation (**Figure III.16**), a strong correlation between TAP and -Cu was also found at the genetic level for the different traits (0.65 - 0.97), highlighting the elevated level of common genetic influence or the weak effect of the treatment. While most of the genetic correlations were moderate to high, 20% were weak ($r_G^2 < |0.20|$), suggesting that these traits are influenced by a different set of genes. However, as the genetic correlation is the "net effect" of all genes affecting the trait and pleiotropy does not always result in detectable correlations (Falconer, 1960), it is not unreasonable that these traits are influenced by the same set of genes but with opposing effects. Given the nature of genetic correlations and the values observed in the GreenMAGIC population, the mapping of different QTLs associated with the same trait was very likely.

3. Mapped QTLs

The identification of QTL related to biomass production, photosynthesis and nutrient accumulation in response to nutrient deficiency is important not only in the context of algae biotechnology, but also in crop improvement and biofortification. Nonetheless, QTL mapping in microalgae in general, and in Chlamydomonas in particularly, is lagging in comparison to crop plants (Lucker et al., 2022; Zhang et al., 2022b). The study performed here in order to map QTLs associated to nutrient deficiency was successful for half of the traits: 67 QTLs were mapped for 45 out of the 90 traits measured, with 18 traits having more than 1 QTL related to it (**Figure III.24**). In addition to the [Cu] trait, which was excluded from previous analyses and QTL mapping (*cf* results above), no QTLs were mapped for the OD FC trait and only a handful were mapped for biomass and sedimentation. Indeed, in addition to being the product of several genes and their interaction, biomass production, OD fold-change and sedimentation are also expected to be the result of multiple cellular processes (such as nutrient homeostasis and photosynthesis) and their interactions, which reduces the effect of each polymorphism on a single trait (Goddard et al., 2016). For this reason, it was unsurprising than most of the QTLs mapped under different nutrition regimens were related to photosynthesis and nutrient accumulation. Photosynthesis biochemistry is highly conserved among plants, despite being highly polygenic, and several photosynthesis QTLs have been mapped (e.g., cold response in A. thaliana Prinzenberg et al., 2020; reviewed in Theeuwen et al., 2022). The highest number of photosynthesis-related QTLs mapped in this study (12) was associated with maximum potential photosynthetic performance (Fv/Fm), explaining 2.6%-16.8% of the phenotypic variance observed (**Table III.12-13**, list of genes in **Dataset S.III.I**), and was detected across all 6 tested conditions. A recent study in *A. thaliana* by Nam et al., (2021) has detected 38 QTLs related to a P-dependent regulation of chlorosis under -Fe and photosynthesis regulation, highlighting the necessity of further studies on photosynthesis adaptation in response to nutrient availability. Two other traits were associated to a high number of QTLs: [K] (5%-17.2% of the variance) and [Mn] (7%-16% of the variance). QTLs were previously mapped for both traits in plants: (i) K accumulation in response to abiotic stress, as K homeostasis is key for wheat tolerance to salt (Asif et al., 2018) and possibly nutrient deficiency (discussed below); (ii) Mn accumulation in lentil, in an effort to study Mn biofortification (Ates et al., 2018). QTLs regarding the accumulation of other nutrients (such as Ca, Fe, Mg, P, and Zn) have also been identified in other crops, such as rice (Du et al., 2013), (Jin et al., 2013), common bean (Blair et al., 2016) or tomato (Asins et al., 2020).

The maximum confidence interval size of the QTLs mapped here (1.95 Mb) was a third of that obtained by Kover et al (2009) when establishing a MAGIC design using *A. thaliana,* and about a quarter fall within the 300 kb window around the QTL midpoint, where authors suggest is the true location of a QTL explaining 10% of the phenotypic variation. More recently, Liu et al., (2020)

mapped a QTL explaining 13% in a 334 kb confidence interval, using a MAGIC-like design to map QTLs in maize. These values are more in line with values obtained here (**Table III.12-13**).

a) Pleiotropy

QTL distribution across the whole genome appeared to be non-homogeneous, with a concentration of QTLs on chromosomes 1 and 2, contrasting with chromosomes 4 and 8 (**Figure III.25**). Interestingly, 11 of the QTLs identified in another branch of the project focusing solely on photosynthesis and using a different experimental protocol (Iacono, PhD thesis, 2023) were located within the confidence intervals of 4 nutrition-related QTLs (**Table III.14**). QTL co-location can be due to the pleiotropic effect of one gene or specific traits being influenced by multiple genes in close linkage and, while tempting to assume co-location as evidence of causality, further analysis are needed to confirm that relationship (Kazmi et al., 2012; Pelgas et al., 2011).

In most cases (52%), the association was highly divergent between conditions indicating strong genotype-by-environment association. A striking example is the major QTL association with Zn concentration that has the most significant association in -Ca and -Mn (**Table III.12**) but is not significant in the four other conditions. Another example are the multiple QTLs related to Fv/Fm can be found on chromosome 9 around 2.1 Mb (**Figure III.26**). A signal was detected in all conditions tested, although it remains below the significance threshold for -Mn and -S, highlighting the strength of the environmental stress (**Figure III.26 B**). Upon analysis of the progeny phenotype considering the founder from which the fragment in that regions were inherited from, it became clear that the contribution of strain CC-1952 to the Fv/Fm trait was different from the remaining founders (**Figure III.26 C**). Analysis of the founder haplotype effect guides the belief that the selective pressures over the natural strain CC-1952, and the remaining natural strains and laboratory strains (CC-410, CC-1418 and CC-1010) were different and resulted in distinct phenotypes.

b) Fine mapping and remarkable QTLs

A total of 7704 non-unique genes were comprised within the confidence intervals of the QTLs mapped relating to mineral nutrition (**Supplemental data II**), nonetheless, more than half (64%) were not characterized in detail. A selection of 4 loci relating to nutrient concentrations will be discussed in more detail below: (1) the locus with the highest $\log_{10}$(p-val) in 2 conditions, (2) a QTL with a single SNP above the significance threshold, (3) a QTL with 3 nutrient-specific transporter genes in the interval, and (4) a locus related to nutrient accumulation in 5 out of the 6 conditions tested. These loci were selected as their intervals are simple enough to make them good candidates for a first analysis.

(1) [Zn] QTLs in -Mn and -Ca conditions

The two QTLs with the strongest significance levels were located in the same interval on chromosome 10 and relate to the [Zn] traits in 2 growth conditions (**Table III.12**). The identification

of candidate genes was simplified by (i) the relatively small confidence interval (80 kb), counting less than 300 bi-allelic variants, (ii) the fact that founder haplotype effect pointed towards the contribution of only one founder line (**Figure III.27 A**). More than half the genes in the interval are annotated or have available information regarding their ontology (**Table III.15**). Among those for which information is available, the focus was directed to 6 characterised types of genes:

(i) genes involved in the apoptotic processes. 3 Scavenger receptor cysteine rich (*SRCR*) protein (*SRCR31-33*: Cr_10_49628, Cr_10_49632, Cr_10_49636). SRCR proteins are one of the most studied pattern recognition molecules due to their self/non-self-recognition role, and the importance of this process in the establishment of multicellularity in eukaryotes (Casella et al., 2014). The SRCR superfamily is highly conserved in eukaryotes, despite being absent in some plant and diatom lineages, hinting that their origin precedes the separation between plants and animals (reviewed in Martínez et al., 2011). In Chlamydomonas, SRCR protein domains are required in the formation of protein intradomain disulphide bridges possibly involved in ligand binding and endocytosis (Wheeler et al., 2008). A recent study showed a SRCR protein (*SSR3*) to be differentially up-regulated in the secretome of a salinity-tolerant Chlamydomonas (Ves-urai et al., 2021), however the study of SRCR function in response to stress in plants lags behind in comparison to animals. Nonetheless, Scavenger receptors are known to be involved in phagocytosis of apoptotic cells, in addition to the previously mentioned roles (Platt & Gordon, 1998). Zn is known to be a key element in eukaryotic apoptosis, and to be as tightly regulated as Ca due to their complementarity (Colvin et al., 2010). Furthermore, as discussed above (discussion of the previous Chapter and Allen et al., 2007b), Mn deficiency can impact the antioxidant response leading to oxidative stress, which can also be part of the apoptotic signalling cascade depending on the duration and intensity (Franco et al., 2009). On the other hand, the Chlamydomonas cytosolic 80S ribosomal protein L35a (*RPL35A*, Cr_10_ 49663) is a gene without introns, studied within the biotechnological scope as a candidate for heterologous gene expression (López-Paz et al., 2017). Chlamydomonas RPL35A is an ortholog of human *RPL35A*, whose overexpression inhibited apoptosis in immortalized Jukart cells exposed to UV and serum starvation (OMA Orthology database; Altenhoff et al., 2021). In our growth conditions, it was evident that some strains were beyond exponential phase at day 4 of culture and that growth was more limited in 24-well plate than in flask, making it possible that some of the strains were already undergoing apoptosis in -Ca and -Mn conditions.

(ii) A H^+ P-type ATPase (*PMA2*, Cr_10_ 49655). PMA2 contributes to the regulation of intracellular pH and its expression can increase Chlamydomonas survival in acidic environments (Choi et al., 2021). Chlamydomonas *PMA2* is an ortholog to *A. thaliana* AHA7 and shares high similarity to AHA2 (Urzica et al., 2012). AHA7 is part of the P_{3A} ATPase subfamily, which participates in the creation of H^+ electrochemical gradients used by secondary transporters (Axelsen

& Palmgren, 2001; Pedersen et al., 2012). It is likely that at the time of sampling in -Ca and -Mn, cellular electrochemical gradient was disrupted due to the absence of Ca or oxidative stress due to the absence of Mn, which could impact secondary Zn transport.

(iii) OctotricoPeptide Repeat protein 49 (*OPR49*, Cr_10_ 49671). OPRs are characterized by a set of approximately 38 degenerate consensus motifs in tandem arrays of 2-24 motifs, forming an α-solenoid structure with predicted location in the organelles for almost all proteins of the family (Hammani et al., 2014) They are not as common in land plants as they are in algae and their detailed characterization is still trailing (reviewed in Macedo-Osorio et al., 2021) but they are known to be involved in mRNA maturation/stability and translation (Cavaiuolo et al., 2017; Wang et al., 2015). While OPRs have a post-transcriptional role, Zn participates in the regulation of gene expression (Blaby-Haas & Merchant, 2017b; Daniel & tom Dieck, 2004).

Three other genes were identified, 1 coding for a protein with transferase activity and 2 coding for a protein with peptidase activity:

(iv) Transferase activity, transferring glycosyl groups (Cr_10_ 49641). This gene is a candidate xylosyltransferase (XylT) involved in protein N-glycosylation, with only 10% shared identity with plant xylosyltransferases, despite the presence of a common C-terminal glycosyltransferase motif in both (Lucas et al., 2020). Protein glycolysation is one of the key process in the maintenance of adhesiveness during the formation of aggregates, which can occur due to stress (de Carpentier et al., 2019; Snell, 1985), and was more evident in the -Ca and -Mn treatments than in the other conditions tested (not shown). As this gene product is not fully characterized, its relationship with Zn is unclear and, for this reason, the existence of Zn-binding domains in its structure was investigated. Zn-binding domains are commonly made from cysteine, histidine, glutamate, and aspartate (CHED) which account for 96% of all Zn-binding sites (Chen et al., 2013). Several bioinformatic tools have been developed to calculate the probability of an amino acid (aa) in a protein to bind catalytic Zn (bound to 3 aa, Zn3) and structural Zn (bound to 4 aa, Zn4), such ZincBinder (Srivastava & Kumar, 2018), which does not depend on protein structure. The prediction made by ZincBinder using the sequence available at UniProt resulted in 20 Zn-binding aa, 10 of which were histidines and 9 were cysteines, despite no additional information regarding the nature of the Zn bound was supplied. In any case, this prediction hints at the possibility of differential gene expression in response to alterations in Zn homeostasis.

(v) 2 Serine-type enzymes with peptidase activity (Cr_10_49650, Cr_10_49685). No studies were found relative to both genes, but a 1396 aa protein coded by Cr_10_49650 was inferred from homology with *C. incerta* and *C. schloesseri* (50% identity with both) in the UniProt database (Craig et al., 2021) and while most regions were disordered, a peptidase S9 catalytic domain was identified between the 933 and the 1006 residues. A serine protease has been previously identified in

Chlamydomonas during gamete activation, where it was involved in cell wall degradation (Snell et al., 1989). Serine protease role in cell wall degradation, in addition to the 24 Zn-binding residues predicted by ZincBinder, lead us to a similar conclusion as the ones drawn before: the Zn-status of the cell may influence gene expression and that cells might have started the degradation of cell components.

From these genes, the 4 genes related to the apoptotic process and the ATPase seem to be the best candidates, as they might directly impact Zn recycling and transport, respectively. The characterisation of mutants for those genes can help elucidate their role in Zn homeostasis.

(2) [Mn] in TAP condition

The QTL on chromosome 10 determining cellular [Mn] in TAP contained a single SNP above the significance threshold, located on the Cr_10_47088 locus. This locus contains an E2 ubiquitin conjugating enzyme (Phytozome resource, Goodstein et al., 2012), or an E3 ubiquitin-protein ligase *HUWE1* coding gene possibly related to photosynthesis, photoprotection or associated processes (Wakao et al., 2021b) and osmotic stress pathways (Vilarrasa-Blasi et al., n.d., preprint). E3 ligases are thought to be involved in metal sensing and are involved in nutrient stress regulation in plants: for instance, increasing concentrations of Mn (and other non-iron metals) leads to the ubiquitination of the Fe (Zn, Mn and Co) transporter *IRT1* and its subsequent degradation in Arabidopsis (reviewed in Mackinnon & Stone, 2022). It is possible that a similar role is played by this ubiquitin-related gene in Chlamydomonas. This gene is a good candidate for functional analysis as there is only one significative SNP.

(3) [Mn] in TAP, -Cu and -Fe conditions

Three QTLs were found on chromosome 3 relative to [Mn]: one upon growth in TAP and two in deficiency media (-Cu and -Fe). These 3 QTL confidence intervals superposed in a region of about 180 kb (**Table III.12**), where 3 MTP encoding genes (*MTP2-4*) can be found in proximity (**Table III.17**). The Chlamydomonas genome contains 5 MTPs (Hanikenne et al., 2005a), which are involved in Mn tolerance and deficiency response (Allen et al., 2007b, Chapter II). Several of the transporters overexpressed to deal with micronutrient deficiency have low selectivity and can transport more than one metal cation (Krämer et al., 2007, Chapter II), which might explain why median [Mn] is 1.6x and 2.1x higher in -Cu and -Fe than in TAP, respectively (**Table III.6-8**). The MTPs found in this interval are good candidate genes as they might help mitigate the potential secondary Mn-toxicity derived from Cu or Fe deficiency, and the potential Mn deficiency of cells in TAP as they arrive to stationary phase.

(4) [K] in TAP, -Ca, -S, -Cu and -Mn conditions

QTLs associated with [K] on chromosome 2 were identified for 5 out of the 6 tested growth conditions, intersecting between 7.21 Mb and 7.33 Mb (**Table III.12-13**). The absence of a QTL

significantly associated with [K] in the -Fe condition might be related to the data quality: while [K] in -Fe is not statistically different from [K] in TAP ($p = 0.73$, **Table III.6-8**), a strong QTL was detected for the latter (**Table III.12**). Among the few annotated genes in this region, the presence of autophagy related *ATG1* was noticeable, due its role in autophagy induction upon nutrient starvation (reviewed in Noda & Fujioka, 2015). The role of autophagy during nutrient deficiency in algae has been previously described in the context of carbon metabolism under N-, P- and S-deficiency (reviewed in Kajikawa & Fukuzawa, 2020), as well as its activation by Ni^{2+}, Cu^{2+} and Co^{2+} (Pérez-Martín et al., 2015), and its regulation by the Target of Rapamycin (TOR) kinase (Pérez-Pérez & Crespo, 2010). *ATG1*, in particular, has been studied in yeast, where it has been showed that the formation of *ATG1* complexes is nutrient-dependent unlike in mammals (Mizushima et al., 2011) and that it responds to K nutrition, being essential for adequate cell growth and autophagy (Rangarajan et al., 2020). It is possible that the formation of *ATG1* complexes is also regulated by nutrient availability in Chlamydomonas, similar to what happens in yeast, and participates in other nutrient metabolism in addition to carbon.

E. Conclusion

In this chapter, the previously described extensive phenotypic and genotypic variation (Chapter I and references therein) was used to map QTLs in Chlamydomonas. A set of 8 founder lines from both natural and laboratory backgrounds was used to build a multiparent recombinant population using a MAGIC design, from which 768 strains were selected and phenotyped in mixotrophy and nutrient deficiency for traits related to the ionome, photosynthesis and growth.

The phenotypic variation observed in the progeny strains was higher than that of the founder lines for the majority of traits and conditions, and there was a high degree of shuffling in the progeny lines, despite having 5 founder lines instead of the initial 8, and a smaller effective number of generations than expected. The correlation between traits and conditions was moderate to high as did heritability, with the exception of the elements quantified in the respective element deficiency, where the environment played a more important role, hinting at a high probability of mapping QTLs for the traits phenotyped.

A total of 67 nutrition-related QTLs were mapped for half the traits quantified, with multiple QTLs associated with the same trait in multiple conditions, multiple traits in one condition or both. From the QTLs mapped, several contained a small enough number of genes and/or plausible candidate genes worth investigating in further studies.

IV. General conclusion and perspectives

A. General conclusion

The objectives of this thesis were fourfold: starting by the description of Chlamydomonas ionome variation in response to nutrient deficiency, passing by the creation and characterization of a MAGIC population, and ending with the mapping of a QTLome related to nutrient deficiency.

First, the description of the natural variation in the Chlamydomonas ionome under nutrient deficiency allowed for further analysis of the previously described genomic variation among Chlamydomonas strains, and it was reflected in the growth variation observed for the 24 Chlamydomonas strains studied and, more importantly, at the ionome level. These differences were not only evident among strains individually, but also between the group of strains commonly used for research studies (laboratory strains) and the group of field isolate strains (natural strains), sustaining the claims of an "untapped reservoir of variation" worth being explored. Furthermore, a deeper comparison of pairs of natural strains exposed to nutrient deficiency revealed differences in nutrient requirements and homeostasis, as well as in photosynthesis.

Secondly, while MAGIC designs have been long implemented as a resource to study trait variation in crops, they had yet to be adapted to Chlamydomonas. The establishment of a MAGIC design protocol for Chlamydomonas required the adaptation of the standard mating protocol in order to produce zygotes in bulk, increase chances of germination and ensure the attainability of several generations in a short amount of time. The selected progeny consisted of more than 700 strains selected from 3 different crossing designs made with a set of 8 founder strains mated for 8 generations.

Furthermore, the characterization of the terminal lines by phenotyping it under nutrient deficiency for traits related to its growth, photosynthesis and ionome and it revealed that the shuffling of alleles through sexual recombination generated, for the vast majority of the traits, more variation within the progeny than among founders. Genotypic characterisation revealed that the effective number of generations was slightly inferior to 8, but the extent of the fragmentation of the genome hinted at the prospect of mapping QTLs with a good resolution.

Lastly, the identification of a nutrition related QTLome lead to the mapping of more than 60 QTLs for the different traits measured under nutrient deficiency, 2/3 of which related to nutrient accumulation and 1/3 to photosynthesis and biomass production. Among the identified QTL, some were related to more than one trait/condition, comprised a small number of genes and some contained good candidate genes as well.

Overall, this thesis emphasised the natural variation in Chlamydomonas nutrient interactions and homeostasis, exposing a variety of mechanisms to manage nutritional deficiencies. Furthermore, it explored that variation to create a GreenMAGIC population, a hypothesis generating tool that will be made available to the Chlamydomonas community through the Chlamydomonas Resource Center (University of Minnesota, USA) in order to pursue further studies.

B. Perspectives

Several lines of investigation are possible considering the results obtained during this thesis and the availability of the resource, namely:

(i) Further characterization of the phenome under nutrient deficiency: changes in cell morphology and the formation of aggregates/palmelloids, and relation between the ionome and photosynthesis;

(ii) Exploration of the fine mapping dataset: the use of a multi-locus mapping approach can reduce the confidence intervals and genes comprised, increasing the mapping precision;

(iii) Survey of the candidate genes: phenotyping of available mutants for the genes in the QTLs identified and complementation assays, in parallel with measurements of gene expression in founder lines with opposing effects;

(iv) Mapping of eQTLs: as some of the differences in nutrient homeostasis could be traced back to differences in gene expression, mapping of genomic regions involved in the quantitative regulation of gene expression may provide valuable information;

(v) Inclusion of GreenMAGIC strains in other studies: as the population was made available at the Chlamydomonas Resource Center, strains with interesting phenotypes and diverse genotypes may be included as the sample for studies from other laboratories. Furthermore, this population can be used to explore different sets of traits, such as mobility, cell cycle/multicellularity or drought response related traits.

Additionally, studies using the GreenMAGIC population for fine mapping may reduce the phenotyping effort, as suggested by Huang et al., (2013), by performing selective phenotyping in lines that maximize genetic diversity.

V. Material and methods

A. Culture media

All media used in this thesis are described and summarised below. Tris-Acetate-Phosphate (TAP, Gorman & Levine, 1965) was used as control media for the different treatments, and as base for the gametogenesis inducing media.

1. Macronutrient solutions

Solution A, source of N, Mg, S and Ca, was used as macronutrient source for TAP. For each macronutrient deficiency, the solution was modified accordingly (**Table V.1**).

Table V.1 Composition of each macronutrient solution

	Solution A	Solution A -N	Solution A 1/10N	Solution A - Mg	Solution A -Ca	Solution A -S
NH_4Cl	16g		1.6g	16g	16g	16g
$MgSO_4.7H_2O$	4g	4g	4g		4g	
$CaCl_2$	1.51g	1.51g	1.51g	1.51g		1.51g
$MgCl_2$						3.3g

2. Micronutrient solution

The oligo solution, source of B, Co, Mo, Zn, Mn, Fe, Cu and S, was used as source of micronutrients for TAP media. For each micronutrient deficiency tested (-Cu, -Fe, -Mn and -Zn), as well as -S, the solution was modified accordingly (**Table V.2**). All salts, except EDTA, were dissolved in 550 mL water. EDTA was dissolved separately in 250 mL water with heating. The first solution was heated at 100°C then EDTA was added, and the mix was heated at 100°C. The temperature was then reduced to 90-80°C and pH was adjusted with 1 M KOH to 6.5-6.8. The volume was brought to 1 L with distilled water and let to stand in a flask closed with cotton wool. Once turned red, the solution was filtered, divided into 250 mL bottles and stored at 4°C until use.

Table V.2 Composition of each micronutrient solution., for a volume of 1L of distilled water.

	Oligo Solution	Oligo Solution-Cu / -Fe	Oligo Solution -Mn / -Zn	Oligo Solution -S
EDTA	50g			
H_3BO_3:	11.4g			
$CoCl_2.6\ H_2O$	1.61g			
$(NH4)_6Mo_7O_{24}.\ H_2O$	1.1 g			
$ZnSO_4.7H_2O$	22g	22g	-	-
$MnCl_2.4\ H_2O$	5.06g	5.06g	-	-
$FeSO_4.7\ H_2O$:	4.99g	-	4.99g	-
$CuSO_4.5\ H_2O$	1.57g	-	1.57g	-
$ZnCl_2$	-	-	-	10.43g
$FeCl_2$	-	-	-	2.28g
$CuCl_2$	-	-	-	0.85g

3. Buffers and other solutions

The following buffers and solutions were needed to prepare the different growth media used in the thesis.

Buffer II:~ 100ml (pH = 7.0)

1M $K_2HPO_4.3H_2O$: 228.22 g. L^{-1}

1M KH_2PO_4: 136.09 g.L^{-1}

This buffer was prepared by adjusting the pH of 70 mL of 1M $K_2HPO_4.3H_2O$ pH=7 with 1M KH_2PO_4 (~30 mL).

Solution B

$K_2HPO_4.3H_2O$: 18.78 g. L^{-1}

KH_2PO_4: 7.26 g. L^{-1}

0.6 M KCl: 45.04 g.L^{-1}

1 M $MgSO_4.7H_2O$: 246.5 g. L^{-1}

100 mM $ZnSO_4.7H_2O$: 28.8 g. L^{-1}

100 mM $MnCl_2.4\ H_2O$: 19.8 g. L^{-1}

100 mM $FeSO_4.7\ H_2O$: 27.8 g. L^{-1}

100 mM $CuSO_4.5\ H_2O$: 24.9 g. L^{-1}

4. Media composition

The difference in media composition between TAP, TMP and nutrient deficiency (-Ca, -Cu, -Fe, -Mg, -Mn, -N, -P, -S, -Zn) media is summarised in **Table V.3**. The media used for gametogenesis (M-N) induction is also described in this table. The pH was adjusted with smoking HCl (37%) and brought the volume to 1L, then autoclaved at 121°C for 20 minutes.

Table V.3 Summary table of the composition of all the media used.: TAP control media (mixotrophy), TMP (autotrophy), M-N (used to induce gametogenesis), macronutrient deficiency (-Ca, -N, -Mg, -P, -S) and micronutrient deficiency (-Cu, -Fe, -Mn and -Zn).

	TAP	**TMP**	**M-N**	**TAP -Ca**	**TAP 1/10 N**	**TAP 1/75 Mg**	**TAP 1/10 P**	**TAP -S**	**TAP -Cu**	**TAP -Fe**	**TAP -Mn**	**TAP -Zn**
Solution A	25 mL	25 mL	-	-	-	0.333 mL	25 mL	-	25 mL	25 mL	25 mL	25 mL
Solution A -N	-	-	25 mL	-	-	-	-	-	-	-	-	-
Solution A 1/10 N	-	-	-	-	25 mL	-	-	-	-	-	-	-
Solution A - Mg	-	-	-	-	-	0.667 mL	-	-	-	-	-	-
Solution A -Ca	-	-	-	25 mL	-	-	-	-	-	-	-	-
Solution A -S	-	-	-	-	-	-	-	25 mL	-	-	-	-
Solution B	-	-	50 mL*	-	-	-	-	-	-	-	-	-
1 M Tris	20 mL	20 mL	-	20 mL	20 mL	20 mL	20 mL	20 mL	20 mL	20 mL	20 mL	20 mL
Buffer II	1 mL	1 mL	-	1 mL	1 mL	1 mL	0.100 mL	1 mL	1 mL	1 mL	1 mL	1 mL
0.6 M KCl	-	-	-	-	-	-	0.900 mL	-	-	-	-	-
1 M $MgSO_4 7\ H_2O$	-	-	1 mL	-	-	-	-	-	-	-	-	-
Oligo Solution	1 mL	1 mL	1 mL	1 mL	1 mL	1 mL	1 mL	0.562 mL	-	-	-	-
Oligo Solution -S	-	-	-	-	-	-	-	0.438 mL	-	-	-	-
Oligo Solution -Cu/ -Fe	-	-	-	-	-	-	-	-	1 mL	1 mL		
Oligo Solution -Mn/ -Zn	-	-	-	-	-	-	-	-	-	-	1 mL	1 mL
10 mM $FeSO_4.7\ H_2O$	-	-	-	-	-	-	-	-	1.8 mL	0.018 mL	-	-
1 mM $CuSO_4.5\ H_2O$	-	-	-	-	-	-	-	-	0.006 mL	6 mL	-	-
100mM $ZnSO_4.7H_2O$	-	-	-	-	-	-	-	-	-	-	0.765 mL	-
100mM $MnCl_2.4\ H_2O$	-	-	-	-	-	-	-	-	-	-	-	0.256 mL
Acetic acid	1 mL	-	-	1 mL	1 mL	1 mL	1 mL	1 mL	1 mL	1 mL	1 mL	1 mL

***After autoclaving

B. Initial phenotyping

Twenty-four *Chlamydomonas reinhardtii* (Chlamydomonas) strains were used for the initial characterization of phenotypic diversity of the species. The strains came from two backgrounds: lab strains and natural strains, and both mating types were represented in the set (**Table V.4**).

Table V.4 List of Chlamydomonas used for the project. Mating type, sampling year and origin are provided. Laboratory strains are highlighted.

#ULG	*mt*	Year	CC	Locality
1308	+	1945	CC-125	Laboratory, 137c derived from soil isolate near Amherst, USA
1396	-	2016	CC-5325	Laboratory (Jonikas) 4A- x D66+ (from thawed storage)
2030	+	1978	CC-503	Laboratory
2031	+	1983	CC-1690	Laboratory
2032	-	1986	CC-1952	Minnesota, USA
2033	-	1986/9	CC-2290	Minnesota, USA
2034	-	1989	CC-2342	Pittsburgh, PA, USA
2035	+	1989	CC-2343	Melbourne, FL, USA
2036	+	1989	CC-2344	Ralston, PA, USA
2037	-	1991	CC-2931	Durham, NC, USA
2038	-	1993	CC-2935	Quebec, Canada
2039	+	1993	CC-2936	Quebec, Canada
2040	+	1993	CC-2937	Quebec, Canada
2041	-	1993	CC-2938	Quebec, Canada
2042	+	2007	CC-4414	Breckenridge, CO, USA
2043	+	<1951	SAG 11-31	UK? Sample from Lever Broth. Ltd.
2044	-	1980	CC-1009	Laboratory, 137c derived from soil isolate near Amherst, USA
2045	+	1980	CC-1010	Laboratory, 137c derived from soil isolate near Amherst, USA
2046	-	1957	CC-410	Caroline Islands, South Pacific, soil from Jaluit, Australia
2047	-	1977	CC-1418	United States, Florida, from red tide (?)
2048	-	1945	CC-124	Laboratory
2049	+	1945	CC-1373	South Deerfield, MA, USA
2050	+	<1971	CC-3348	Japan ?
2051	+	<1981	CC-1374	France

1. Cell culture and maintenance

The strains were maintained mixotrophically in a room with controlled temperature (25°C) under 100 µmol photons.s^{-1}.cm^{-1} continuous light, on solid TAP medium

The cultures on solid media were refreshed every 2 weeks for 3 months, after which a new sample from a strain storage collection was taken out in order to minimize variation. Samples in the collection were kept in slants, at 18°C, 50 µmol.s^{-1}.cm^{-1} of light, with a photoperiod of 12/12 light/dark in order to reduce growth.

2. Single nutrient deficiency

Assays were performed in liquid media and conducted in GroBanks (GroBank BrightBoy Model BB-XXL.3, CLF PlantClimatics GmbH), with 100 µmol.s^{-1}.m^{-1} continuous light, at 25°C. Cells were agitated in an orbital shaker (Universal Shaker SM 30 A, Edmund Bühler GmbH) at 110 rpm to ensure uniform illumination and to prevent cell sinking.

Starter cultures of the strains were made by inoculating liquid TAP with cells from a culture on TAP agar medium. After 2 days of growth cell concentration was estimated using optical density at wavelength 750nm (OD_{750}), measured with a spectrophotometer (GENESYS™ 20 Visible Spectrophotometer Thermo Scientific™). An initial concentration of 10^4 cells.ml^{-1} was used for the assays, unless otherwise stated.

All flasks and bottles used for the deficiency assays were soaked in a 0.2 M HCl solution for 2 days prior to use, in order to remove any possible metal contamination.

a) Assay conditions

The growth and ionome of the twenty-four strains under nutrient deficiencies were studied. Starter cultures were made in 14 mL culture tube with two-position vent stopper filled with 2 mL of liquid TAP. The following deficiency conditions were assayed: acetate (CH_3COOH), calcium (Ca), magnesium (Mg), nitrogen (N), phosphate (P), sulphur (S), iron (Fe), copper (Cu), manganese (Mn), zinc (Zn) (**Table V.5**). Whenever possible, a complete removal of the nutrient was done, otherwise the lowest concentration that allowed enough biomass production for the phenotype analysis was selected.

Table V.5 Summary of the single nutrient deficiency conditions.

Nutrient	*Condition*	*Control (µM)*	*Deficiency (µM)*	*Ratio*
		Macronutrients		
Acetate	TMP	17416	0	0
Calcium	-Ca	387.6	0	0
Magnesium	-Mg	405.7	5.4	$^1/_{75}$
Nitrogen	-N	9478	2747.9	$^2/_7$
Sulphur	-S	506.5	56.6	$^1/_9$
Phosphate	-P	1000	100	$^1/_{10}$
		Micronutrients		
Iron	-Fe	17.95	1.8	$^1/_{100}$
Copper	-Cu	6.29	0.006	$^1/_{1000}$
Manganese	-Mn	25.6	0	0
Zinc	-Zn	76.5	0	0

A volume of 35 mL of autoclaved media was added to autoclaved flasks, inoculated with the starts culture and closed with a cellulose stopper. Growth was followed from day 3 until day 7, by measuring OD_{750}. At day 4, 10 mL of culture was sampled for ionome analysis.

3. ICP-AES sample preparation

Samples (10 ml of 4-day-old cultures) were centrifuged at 2,000 *g* to remove the culture media. The pellet was washed twice with 5 mL of 0.5 mM EDTA pH 8, to remove ions attached to the cell walls, and centrifuged at 2 000 *g*, for 5 min. The washed cells were then re-suspended in distilled water to remove traces of EDTA and centrifuged at 2 500 *g*, for 5 min. The pellet was then digested with 3 mL of >65% nitric acid for 2 days at 4°C. After digestion, samples were diluted to a final volume of 10 mL and 200 µL of >65% nitric acid is added to preserve the sample.

The elements Ca, Cu, Fe, potassium (K), sodium (Na), Mg, Mn, P and Zn were quantified using Inductively Coupled Plasma Atomic Emission Spectroscopy (ICP-AES) (vista AX CCD Simultaneous ICP-AES, Varian). The results were normalized using the OD_{750nm}.

4. qRT-PCR experiment

RNA was extracted using a genomic DNA extraction protocol followed by selective precipitation with LiCl (Loppes & Radoux, 2001; Newman et al., 1990).

a) Total RNA extraction and cDNA synthesis

On the 4th day of culture, approximately 10^7 cells were harvested and centrifuged at 2,000 *g* for 5 min. The pellet was frozen with liquid N_2 and kept at -80°C until extraction. Total RNA extraction was initiated by resuspending the cells in lysis buffer (2% SDS, 400 mM NaCl, 40 mM EDTA, 100mM Tris HCl pH 8.0), adding phenol/chloroform/isoamyl alcohol (25:24:1) and incubating 5 min in an agitator (50 rpm). The aqueous phase was separated by centrifugation 5 min at 15000 *g* and re-extracted with chloroform/isoamyl alcohol (24:1). Total RNA was selectively precipitated overnight at 4 °C in 8 M LiCl and collected by centrifugation 5 min at 15000 g. Pelleted RNA was then washed with 70% ethanol, centrifuged and diluted in RNase free H_2O. Concentration and quality were determined spectrophotometrically ($A_{260\ nm}/A_{280\ nm}$ ~2; $A_{260\ nm}/A_{230\ nm}$ = 2.0 – 2.2) using a NanoVue Plus Spectrophotometer (Cytiva) and the RNA quality was confirmed using agarose gel electrophoresis.

DNA contaminations were removed using the DNase Max kit (QIAGEN) and complementary DNA (cDNA) synthesis was performed using a RevertAid RT Reverse Transcription Kit (Thermo Fisher Scientific), both kits were used as instructed by the manufacturer.

b) Amplification

Quantitative reverse transcription-PCR (qRT-PCR) was performed using the QuantStudio™ 5 system (Thermo Fisher Scientific) and the Takyon™ Low ROX Probe 2X MasterMix dTTP blue (Eurogentec). Samples were amplified in triplicate and each reaction contained manufacturer's master mix, 125 nM of each primer and 1 µg of cDNA. Water was used as the negative control. The reaction conditions were as follows: (i) pre-PCR at 50 °C for 2 min, then 50 °C for 2 min, (ii) 40 cycles of PCR at 95 °C for 15 s and 60 °C for 1 min, (iii) melting curve at 95 °C for 15 s, 60 °C for 1 min and 95 °C for 15 s. Primers used are described in **Table V.6.**

Table V.6 Primers used for the qRT-PCR.

Gene	Gene ID (v5)	Name & Description	Primer sequences (5' - 3')	Length	Product length	Efficiency	Reference	Condition
RPL13 (R)	Cre14.g630100	Ribosomal protein L13, component of cytosolic 80S ribosome and 60S large subunit	TCAGCGTCTGAAGGCTTACC CTCGGCCAGAGGGGTCTCGA	20 20	88	1.91	Durante et al., 2019	TAP -Mn, -Fe
CBLP (R)	Cre06.g278222	Receptor of activated protein kinase C	GTGTCGTGCGTGCGCTTCT CACCAGGTTGTTCTTCAGCTTGC	19 23	117	1.93	Durante et al., 2019	TAP -Mn, -Fe
CTR2	Cre10.g434350	CTR type copper ion transporter	CACCAACAGCCTTTCCACAAG GACGCTGAACTGCGTAACCT	21 20	94	1.92	Allen et al., 2007b	TAP -Mn, -Fe
CYC6	Cre16.g651050	Cytochrome C oxidase, cbb3-type, subunit III. Cytochrome c6	AGGCTTGGGCCAGTACATTA GTGCAAAACCCGGTTGAAGC	20 20	150	1.92	Quinn & Merchant 1995	TAP -Fe
IRT1	Cre12.g530400	Iron Regulated Transporter1. Iron-nutrition responsive ZIP family transporter	CACAGTAGGGGCATGAGAGC CCCAATCCCAGTCCGTTAGG	20 20	81	1.90	Allen et al., 2007a	TAP -Mn, -Fe
FOX1	Cre09.g393150	Ferroxidase 1. Multicopper ferroxidase	TTGCGCTGCATGCAATAAGG GTTCGCGGCTCAACACAAAA	20 20	141	1.93	Allen et al., 2007a	TAP -Mn, -Fe
FRE1	Cre04.g227400	Ferric-chelate reductase/ oxidoreductase. Ferrireductase	CACTTCGCCAAGGACTCCAG GGGTCCAGGCATTGTACTTCT	20 21	124	1.915	Allen et al., 2007a	TAP -Mn, -Fe
FSD1	Cre10.g436050	Fe superoxide dismutase	CATGAACAAGCAGGTCGCTG GGCTTCATGCTCTCCCAGAA	20 20	150	1.91	Allen et al., 2007b	TAP -Mn, -Fe
MSD3	Cre16.g676150	Mn superoxide dismutase	GGACGCAATGCTGTGCTAAG TCTTGTCCGCAAAGCCTCAT	20 20	115	1.93	Allen et al., 2007b	TAP -Mn, -Fe
MTP4	Cre03.g160550	Metal Transport Protein (CDF transporter). Cation efflux transporter, membrane protein	CGTGATGAAGCCACTGCCTA CGATCTTGTCCCCCTCCTTT	20 20	108	1.92	Allen et al., 2007b	TAP -Mn
NRAMP1	Cre17.g707700	Natural Resistance Associated Macrophage-like Protein 1. Manganese/metal transporter NRAMP homolog	GCGGGTAATCCAGGGCTTTT GGAACCACCAGAGTGCAAGT	20 20	92	1.90	Allen et al., 2007b	TAP -Mn, -Fe
PTB2	Cre07.g325741	Phosphate transporter. Sodium/phosphate symporter	CTGCCCATGACCTTCAACCA GAAGTCAGCAACGCTTTCCC	20 20	145	1.90	Allen et al., 2007b	TAP -Mn
ZRT1	Cre07.g351950	Zn Regulator Transporter 1. Zinc-nutrition responsive transporter	CATTCTCAGTGCTCGCGTTG GAGCGCCACCTCTTCCTTAG	20 20	88	1.91	Allen et al., 2007b	TAP -Mn, -Fe
ZRT3	Cre13.g573950	Zinc-nutrition responsive transporter	GCGGCATTAATAGCGCTGAA CCGCCTACTTCCTGGTTTCT	20 20	86	1.96	Allen et al., 2007b	TAP -Mn, -Fe

c) Expression analysis

Amplification curve data was analysed in three steps (Nouet et al., 2015; Thiriet-Rupert et al., 2021b):

- first, cycle threshold (Ct) of each well was calculated using QuantStudio™ Design and Analysis Software Version 1.5.1 (Thermo Fisher Scientific) and exported to an Excel file, together with the amplification data;
- secondly, primer efficiency was calculated using the amplification data on the LinRegPCR Software Version 2020.2 (Amsterdam UMC, The Netherlands), with a minimum r^2=0.997 within the Window-of-Linearity;
- lastly, the qbase+ Software, Version 3.2 (Biogazelle, Zwijnaarde, Belgium) was used to handle gene expression analysis ($2^{-\Delta\Delta CT}$ method by Livak & Schmittgen (2001), using *RPL13* and *CBLP* as references and normalized to one of the replicate) and statistical analysis (One-way ANOVA for mean comparison).

5. Photosynthetic analysis

a) Pigment quantification

A volume of 1 mL of 4-day old culture was centrifuged at 2000 x *g* for 5 min and the lipophilic pigments were extracted using 1 mL of methanol. The supernatant was recovered after centrifuging the samples at 2000 x *g* for 5 min and the absorbance was measured at 470 nm, 652 nm and 665 nm. Chlorophyll *a* and *b*, carotenoid and concentrations were calculated as described in Wellburn (1994).

b) Chlorophyll fluorescence

From the sample used to measure OD_{750nm}, 100 µL were transferred to a white 96-well plate and dark adapted for 10 min min (Kalaji et al., 2014). Time-resolved chlorophyll fluorescence was then measured using a SpeedZen 200 fluorescence imaging system (Johnson et al., 2009) equipped with red LEDs (650-670nm) for actinic and saturating lighting, and blue LEDs (450-470 nm) as fluorescence detection lights. PSII variable fluorescence was monitored through a saturation curve composed of 7 light-steps (25, 50, 91, 130, 270, 420, 600 µmol of quanta m^{-2} s^{-1}) of 4 minutes each (one saturating pulse of 220ms every minute)., followed by a dark period of approximately 50 minutes (**Figure V.1**).

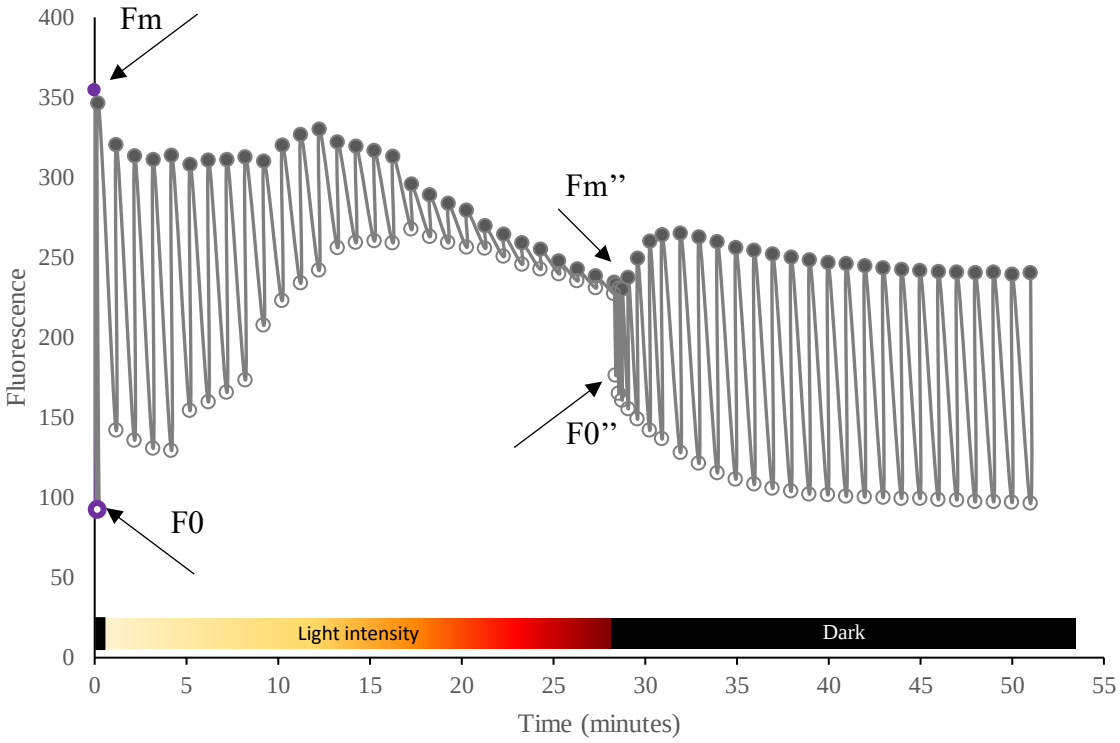

Figure V.1 Example of a 50-minute induction curve, plotting fluorescence in function of the time. Full circles indicate the maximum fluorescence (Fm'), and the empty circles represent steady-state fluorescence (Fs'). The maximum and minimum fluorescence of dark-adapted cells (Fm and F0, respectively), as well as maximum and minimum fluorescence of light-adapted cells (Fm'' and F0'', respectively) are indicated with arrows. Light intensity is indicated in the rectangle above the x-axis: black boxes represent absence of light, the box with a pale yellow to bordeaux gradient represents the growing light intensity (25, 50, 91, 130, 270, 420 and 600 µmol photons.$m^{-1}.s^{-1}$) used during the measurements. Each light intensity was used for four measurements (4 fm and 4 fs).

Four parameters were determined:

- Initial maximum quantum yield of PSII (Fv/Fm) was calculated using the expression *(Fm - F0)/Fm*, where Fm and F0 are the maximum and minimum fluorescence of dark-adapted cells, respectively;
- Recovery maximum quantum yield of PSII (Fv/Fm'') was calculated using the expression *(Fm'' – F0'')/Fm''*, where Fm' and F0' are the maximum and minimum fluorescence of light-adapted cells, respectively. Calculated after the transition from high light (600 µmol.$m^{-1}.s^{-1}$) to darkness;
- Relative electron transport (rETR) was calculated for each light intensity as *I*[(Fm'−Fs)/Fm']*, where I is the light intensity, Fm' is the maximum fluorescence of light-adapted cells and Fs is steady-state fluorescence.
- Non-photochemical quenching (NPQ) was calculated was calculated as Fm-Fm'/Fm'. The last two pulses at each light-step were averaged.

C. Multiparent Advanced Generation Inter-Cross (MAGIC)

1. Mating test ability test

Gametogenesis was induced by culturing cells in liquid nitrogen-free minimal media (M-N) (**Table V.3**). A small amount of cells (end of a 200 µL pipette tip) was taken from the solid TAP plates, older than 2 week, and resuspended in 3 mL of liquid M-N media, in 14 mL tubes.

After gametogenesis induction, strains were distributed in 96-well plates, *mt+* strains as columns and *mt-* strains as rows. In addition to the mating in liquid media, 50 µL of mix were spotted in 3% aga M-N media and placed in a GroBank, under low light (100 µmol photons.s^{-1}.cm^{-1} continuous light, covered with 1 sheet Tork^{TM} paper). Plates were left for 1 week to allow zygote maturation and encystation. To observe the zygotes under the binoculars, vegetative cells at the agar surface were scrapped out with a sterilized dull scalpel.

2. MAGIC design

a) Mating conditions and progeny selection

A small amount of cells (end of a 200 µL pipette tip) was taken from cultures growing on solid TAP plates and resuspended in 1 mL of liquid M-N media, in 24-well plates. After 1 day of differentiation in a GroBank (100 µmol photons.s^{-1}.cm^{-1} continuous light, 25°C), gametes of strains with different/opposing mating types were mixed and returned to the GroBank. Following 1h of agglutination, a 20 µL drop was plated on 3% agar nitrogen-reduced media (TAP 1/10 N), in duplicated plates. This process was repeated 3h and 6h after mating. Plates were wrapped in aluminium foil and kept in the GroBank. After one-week, vegetative cells were removed as described above and the encysted zygotes were retrieved by cutting a piece of agar containing approximately a dozen zygotes. The agar piece was placed on fresh 1.5% agar TAP media, followed by 30s exposition to chloroform vapours to kill any remaining vegetative cells. Zygotes were observed at the binoculars, under sterile condition, daily until germination. Upon germination, cells were spread around the plate with the help of 1 mL of TMP media and a spreader and the plates were placed in a GroBank under at 25°C and 100 µmol.s^{-1}.cm^{-1} of continuous light until colonies were visible with the naked eye. Upon visual confirmation of the colonies, 26 were collected with a 10 µL pipette tip and transferred to a new 1.5% agar TAP media plate, with numbered positions. Cells were picked at random, based on 3 criteria, in order of importance: (i) isolated colonies, (ii) colonies morphologically diverse, (iii) non-consecutive colonies.

b) Mating-type determination by colony PCR

DNA was extracted by sampling a small amount of cells from the numbered colonies, using a 10 µL pipette tip, and resuspending the cells into 25 µL of lysis buffer [15 µl of sterile ultra-pure water, 5 µl of proteinase K (20 $mg.ml^{-1}$) (VWR), 5 µL of 5x Colourless GoTaq reaction buffer (Promega)], in 200 µL 96-well PCR plates. After resuspending the cells, the plates were sealed with sealing film (Sealer AMPLIseal™, Greiner Bio-One International GmbH), and samples were incubated on a thermocycle at 58°C for 1h, followed by 1h at 96°C. Samples were stored at 4°C until further use.

Mating type was determined by adding 2.5 µL of extracted DNA to 22.5 µL of master mix containing 5 µL 5x Green GoTaq reaction buffer (Promega), 1.25 µL DMSO (100%), 0.5 µL dNTPs (10 mM) (Promega); 5 µL of primer mix (5 µM each), 0.13 µL GoTaq DNA Polymerase (Promega), 0.37 µL "home-made" GoTaq, and 10.25 µL ultra-pure water. Primer mix contained 1.25 µL of each 20 µM primer solution (Eurogentec): Fus1(+)_up: 5′-ATG CCT ATC TTT CTC ATT CT-3' and Fus1(+)_low : 5′-GCA AAA TAC ACG TCT GGA AG-3′, for the mating type *plus* locus (516 bp); Mid(-)_up: 5′- ATG GCC TGT TTC TTA GC-3′ and Mid(-)_low : 5′-CTA CAT GTG TTT CTT GAC G-3′ for the mating type *minus* locus (622 bp). Polymerase chain reaction was conducted according to the following program: 2 min pre-PCR at 94°C; 35 cycles of 30 s denaturation at 94°C, 30 s hybridization at 55°C, 30 s polymerisation at 72°C; 7 min post-PCR at 72°C.

c) Progeny maintenance

Progeny was divided into 96 square petri dishes, each containing 4 *families* of 8 strains issued of a single cross (4 *mt+* and 4 *mt-*), on 1.5% agar TAP media. The plates were kept in GroBanks, at 25°C, 50 $\mu mol.s^{-1}.cm^{-1}$ continuous light and refreshed once a month. Strains were also shared with Chlamydomonas Resource Center (University of Minnesota, https://www.chlamycollection.org/)

D. High Throughput Phenotyping

High throughput phenotyping assays were conducted in the same light, temperature, and agitation conditions as the initial phenotyping of the 24 Chlamydomonas strains (100 µmol.s^{-1}.cm^{-1} continuous light, at 25°C, 110 rpm). Given the increase in the number of samples, 24 well-plates were used to conduct the assays, instead of flasks. The 768 MAGIC strains were divided into batches, each containing one of the 8 strains of each *family*, totalling 8 batches of 96 strains. Several parameters were measured: growth, sedimentation, ionome quantification and photosynthetic response.

1. Assay conditions

For the progeny phenotyping, 6 conditions were assayed: control (TAP) and -Ca, -S, -Cu, -Fe and -Mn (cf **Table V.3**). Precultures were made in 24 well-plates filled with 2 mL of liquid TAP medium and adding the end of a 200 µL pipette tip of cells grown in solid media. After 2 days, the OD_{750nm} was measured and the precultures were all diluted 2.33x in 96 well-plates, by adding 200 µL of TAP media containing only Tris, Buffer II and acetate (pH = 7) to 150 µL of pre-culture. From this dilution, 25 µL were inoculated in 2 mL of TAP or of deficiency medium. At the 4^{th} day of growth, the cultures were harvested: 1.5 mL for ICP-AES analysis, 200 µL each for OD_{750nm} and for photosynthetic parameter measurements. Three traits were assessed by measuring the OD_{750nm} in 96-well plates with a plate reader (Victor Nivo, Perkin Elmer): (i) biomass at harvest time (OD_{750nm}); (ii) sedimentation, by calculating the difference between the OD_{750nm} measured after 10 min and the OD_{750nm} at harvest time; (iii) OD fold change, by dividing the biomass at harvest by the biomass inoculated at the start of the assay.

2. ICP-AES sample preparation

Sample preparation was done in 2 mL 96-deepwell MasterBlok®, with V-shaped bottom. A volume of 1.5 mL was sampled from each cultures, transferred to the deepwell block and centrifuged at 2 250 *g* for 7 minutes to remove the culture medium. The pellets were washed twice with 300 µL of 0.5 mM EDTA pH 8, to remove ions attached to the cell walls, and centrifuged at 2 250 *g*, for 7 min. The washed cells were then re-suspended in distilled water to remove traces of EDTA and centrifuged at 2 500 *g* for 10 min. The pellets were then digested with 300 µL of 70% nitric acid. After digestion, samples are diluted by adding 700 µL of distilled water and transferred to assay tubes containing 4 mL of distilled water (final volume = 5 mL) for analysis.

Element quantification (Ca, Cu, Fe, K, Na, Mg, Mn, P and Zn) was done by ICP-AES (5110 Visée Axiale, Agilent Technologies). The results were normalized using the OD_{750nm}.

3. Photosynthetic analysis

Photosynthetic analysis was performed as described above (*cf* V.B.5.b), however the photo induction period was shorter given the bigger number of samples (Figure V.3).

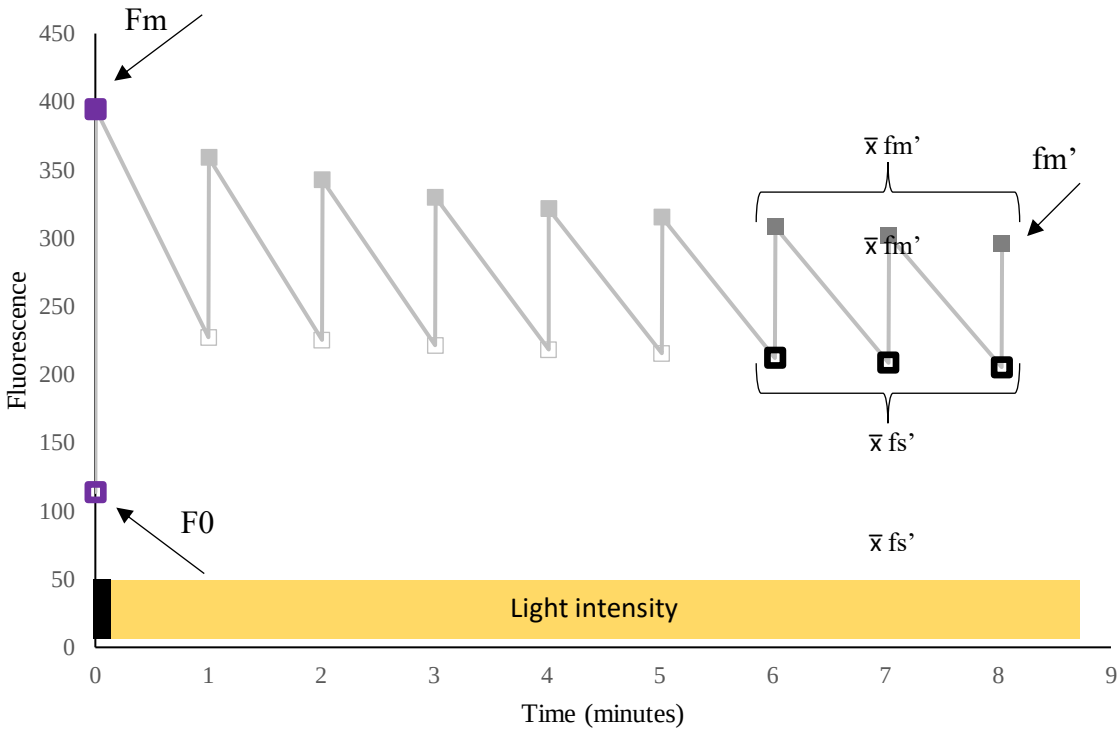

Figure V.2 Example of an 8-minute induction curve, plotting fluorescence in function of the time. Full squares indicate the maximum fluorescence (fm), and the empty squares represent steady-state fluorescence (fs). The maximum and minimum fluorescence of dark-adapted cells (Fm and F0, respectively), as well as the maximum fluorescence of light-adapted cells (fm') are indicated with arrows. Average fs (black border empty squares) and fm (dark grey squares) of light adapted samples ($\bar{x}$ fs' and $\bar{x}$ fm', respectively) are also represented Light intensity is indicated in the rectangle above the x-axis: the black box represent absence of light, the yellow coloured box represents the iluminated phase (91 µmol photons.m^{-1}.s^{-1}) used during the measurements.

Three parameters were determined:

- maximum quantum yield of PSII (Fv/Fm) was calculated using the expression *(Fm - F0)/Fm*, where Fm and F0 are the maximum and minimum fluorescence of dark-adapted cells, respectively;
- nonphotochemical quenching (NPQ) was calculated as *(Fm-Fm')/Fm'*, where Fm' and Fm are maximum fluorescence of light-adapted and dark-adapted cells, respectively;

- effective quantum yield of photosystem II (φPSII) was calculated as the difference between the averages of the last 3 *fm* and *fs* ($\bar{x}$ fm' and $\bar{x}$ fc, respectively), divided by $\bar{x}$ fm'[($\bar{x}$ fm'- $\bar{x}$ fc)/ $\bar{x}$ fm'].

E. Data analysis

Unless otherwise specified, data was analysed and plotted using R (R Core Team, 2022) and R Studio Desktop (RStudio Team, 2021). The employed packages are listed in **Table V.7**.

After data import, the data frames were cleaned and organized using the packages in the "Wrangling" column (**Table V.7**). Whenever necessary, data was summarized using the function *summarizeSE()* (Rmisc). Dunn's multiple comparisons using rank sums (Dunn, 1964) were used to test for statistical differences among strains in pairwise comparisons, *dunnTest()* (FSA). Statistical analysis results were summarized with the function *cldList()* (rcompanion), which uses letters to indicate significant differences in pairwise comparisons. Data was then plotted using the package *ggpubr* (barplots, boxplots) or ComplexHeatmap (heatmaps), with custom-made colour scales using *colorRamp2()* (circlize). Plots were exported in vector image format (.svg) using the svglite package or the function *ggsave*() (ggpubr).

Table V.7 Base R packages used for data analyses

Data		Figures	
Wrangling	Analysis	Plotting	Exporting
tidyverse v1.3.1 (Wickham et al., 2019) reshape2 v1.4.4 (Wickham, 2007) naniar v0.6.1 (Tierney et al., 2021)	rcompanion v2.4.1 (Mangiafico, 2021) Rmisc v1.5 (Hope, 2013) FSA v0.6.1 (Ogle et al., 2021)	ggpubr v0.4.0 (Kassambara, 2020) scales v1.1.1 (Wickham & Seidel, 2020) circlize v0.4.13 (Gu et al., 2014) ComplexHeatmap v2.8.0 (Gu et al., 2016)	svglite v2.0.0 (Wickham et al., 2021)

F. Quantitative Trait Loci (QTL) Analysis

1. Progeny genotyping

DNA extraction was performed using with NucleoMag® DNA Bacteria kit (Macherey-Nagel) and the supplied reagents, and a robot, the KingFisher™ Flex 96 Deep-Well Magnetic Particle Processor (Thermo Scientific). With exception of the lysis buffer and 80% ethanol, all the reagents used during the extraction were provided with the NucleoMag® kit.

a) Cell harvesting

Cells were harvested from 1.5% agar TAP plates using an inoculation loop and diluted in an Eppendorf tube filled with 1.5 mL of TAP media. After homogenization, half volume was transferred to a backup Eppendorf tube. Both tubes were centrifuged for 2 min, at 2000 x*g*. The supernatant was then removed, the pellets were frozen in liquid nitrogen and stored at -80°C until use.

b) DNA extraction

The harvested pellets were homogenized using 150 µL of 1x lysis buffer (diluted from 2x lysis buffer: 10 mM Tris-HCl, 10 mM NaCl, 10 mM EDTA pH=8 with NaOH, 0,5% SDS) and then transferred to 96-deepwell plates. Samples were incubated for 2h in a water bath at 58°C, after the addition of 13 µL of Proteinase K and plate vortexing. RNA was then removed by adding 2.5 µL of Liquid RNase, vortexing and incubating 10 min at room temperature. Binding condition was adjusted by adding 460 µL of IML buffer to each well and homogenising through vortexing. Plates were then centrifuged at 11 000 x*g* for 30 seconds. A volume of 600 µL of supernatant was transferred to a new 96-deepwell plate, to which 27 µL of paramagnetic B-Beads and 320 µL of IMB solution were added.

The plate was placed on the KingFisher™ robot, where the DNA washings and elution were performed. Plates were mixed with an up and down movement for 5 minutes, to allow DNA binding to the beads. The DNA-bound-beads were then transferred to a 96-deepwell plate, containing 600 µL of IMW buffer per well, and washed for 2 min. The beads were then washed twice with 600 µL of 80% ethanol, for 2 min. The beads were then dried for 10 min to remove the ethanol. Finally, the DNA was eluted from the beads using 50 µL of IME buffer, for 5 min, and the beads were removed.

After taking a 10 µL aliquot for DNA quality assessment, the plate was sealed and stocked at -20°C until use.

c) DNA quality assessment

DNA fragmentation was investigated via electrophoresis. Half of the aliquoted DNA (5 µL) was mixed with 2 µL of 5x Green GoTaq loading buffer (Promega) and loaded in a 0.5%

agarose gel (30 mL) stained with Midori Green (2.5 µL). The gel was run for 25 min at 100 V. DNA was quantified using the Quan-iT Picogreen dsDNA Assay kit (Thermo Fisher Scientific), and a minimum of 1 µg dsDNA was sent to the sequencing platform.

d) Library preparation and whole-genome sequencing

In addition to the F8 progeny, two previously non- sequenced founder strains were sequenced at the GIGA Genomics Platform (University of Liège). Libraries were prepared using the Illumina TruSeq DNA PCR-Free kit the founder strains and the Sopachem PlexWell kit (PW96 and PW384) was used for the progeny, using the manufacture's reagents and following their instructions. Libraries were then sequenced on an Illumina NovaSeq 6000. For the six additional founders, the sequencing data was downloaded from Flowers et al. (2015).

2. Bioinformatic analysis

The following bioinformatic analysis were performed by Dr. A. Misztak and Dr. T Druet. The corresponding protocols were written by Dr. T. Druet, which are reproduced here with a few minor modifications for completion.

a) Read mapping

The short reads sequencing data was mapped to the version 6 of the Chlamydomonas genome (Craig et al., 2022) to which the chloroplast and the mitochondria sequences available from Gallaher et al., (2018) were added. A workflow from the Broad Institute (Tutorial #6483) (*(How to) Map and Clean up Short Read Sequence Data Efficiently – GATK*, n.d.) was followed. First, unmapped BAM (uBAM) files were generated from FASTQ files with the FastqToSam command, marking adapter sequences using the MarkIlluminaAdapters command, and converting the resulting SAM files to FASTQ with the SamToFastq command. After application of these three commands from Picard tools 1.141, the FASTQ files were mapped with BWA-MEM (bwa v0.7.17) and mapped BAM and unmapped BAM files were then merged with MergeBamAlignment from Picard tools 1.141. Finally, potential duplicates were removed (MarkDuplicates) and the BAM file was sorted (SortSam) still with Picard tools 1.141. The depth of coverage for each sample was estimated using DepthOfCoverage with GATK (v3.2.2). A total of 21 lines with a cover below 4x, were re-sequenced. The distribution of the depth of coverage for the 768 F8 lines average coverage was equal to 9.2x (median = 8.7x, range from 4.2 to 19.4x). For the re-sequenced lines, the two BAM files were merged when their initial cover was > 1x and when genotypes were identical in the two BAM files for more than 99% of the called variants (for nine out of 21 re-sequenced lines).

b) Variant calling

Freebayes v1.2.0-17 (Garrison & Marth, 2012) was used to perform the variant calling in two steps. First, we called variants using the 20 strains sequenced in Flowers et al. (2015) and the two newly sequenced founders. Freebayes was run per chromosome, with ploidy set to 1 (*-p 1*) and with *--min-alternate-count* set to 5. To study the structure or relatedness among these 22 reference strains, we kept variants identified on the 17 chromosomes with *QUAL (quality) > 50*, with *DP (depth of coverage) > 499 or < 2350* (corresponding to approximately 2.5% and 97.5% quantiles), with *AO (alternate allele observation count) ≥ 20*. In that file, regions with extreme total coverage (> 10,000) were flagged to exclude them from later analyses.

The final variant calling was applied to the eight founders and the 768 F8 lines jointly. For this call, the genome was divided in small chunks around 500 kb long and high coverage regions previously flagged were excluded. Freebayes was run for haploid organisms (*-p 1*), with *--min-alternate-count set to 5*, and with the *--use-best-n-alleles 8* option to avoid computational issues and because we have theoretically only 8 alleles in our population. Note that similar intermediate runs were performed with control samples or with samples sequenced twice (to improve coverage). These intermediate runs allowed, for instance, to check whether replicate samples were identical as expected.

To obtain a set of high-quality variants for modelling the mosaic structure of the F8 lines, markers with *QUAL > 50*, with *DP < 2000* or *> 10250* (corresponding to 2.5% and 97.5% quantiles), with *AO < 20* were filtered out. In addition, markers with identical genotypes among all founders were also removed as these are non-informative. We also restricted our selection to variants covered by at least 1 read in each founder, with maximum eight alleles and for which founders had only one allele each (one allele accounted for at least 95% of the allele depth (AD)). These filters aimed to exclude regions covered by copy number variants and where genotyping calling is less accurate.

c) Genetic relatedness and identity-by-descent sharing among reference strains

As a measure of genetic distance, we counted the proportion of distinct genotypes d_{ij} among pairs of strains *i* and *j*. As in Flowers et al. (2015), a circular dendogram was constructed based on these distances to visualize relationships among the lines and plotted with the circlize_dendogram function in R. In addition, we also identified identity-by-descent (IBD) segments among the eight selected founders with the hidden Markov model (HMM) implemented in hmmIBD (Schaffner et al., 2018). We ran the program with default options on the filtered VCF files and using the 17 chromosomes.

d) Modeling the F8 lines as mosaic from the founders

A HMM describing F8 lines as mosaic from the eight founders was applied, similar to models applied in other MAGIC designs (e.g., Kover et al.,). In this model, at each marker position, the probability that the modeled F8 line inherited its chromosome segment from one of the founders was determined. The eight founders represented thus eight hidden states from the model. The transition probabilities $\tau_{l,l'}$ between successive markers *m* and *m+1* are inspired from Mott et al. (2000b):

$$\tau_{l,l'} = \begin{cases} e^{-Gd_m} + (1 - e^{-Gd_m})\frac{1}{K} & if\ l = l' \\ (1 - e^{-Gd_m})\frac{1}{K} & if\ l \neq l' \end{cases}$$

where G is the number of generations of crossing, equal to 8 in this design, d_m is the genetic distance between markers *m* and *m*+1 and *K* is the number of founders. 1 Mb was assumed to correspond to 10 cM in *C. reinhardtii*, close to the 1.2 x 10^{-5} cM/bp estimated by Liu et al. (2018). The emission probabilities were obtained by comparing genotypes in the F8 line with those in the founders. However, as the F8 lines were not sequenced at high coverage, the uncertainty in the genotype calling must be accounted for, and therefore rely on the genotype likelihoods (GL) estimated by Freebayes. The emission probability at marker *m* for founder *k* for the F8 line *i* can be computed as:

$$P(O_{im}|S_m = k) = \sum_{j=1}^{n_m} P(G_{im} = j)\, P(G_{km} = j)$$

Where O_{im} are the observations at marker *m* for F8 line *i* (its sequencing data, such as read counts), S_{im} is the state of F8 line *i* at marker *m*, n_m is the number of alleles at marker *m*, $P(G_{im} = j)$ is the probability that the genotype from line *i* at marker *m* corresponds to allele *j* and is obtained from the genotype likelihoods, $P(G_{km} = j)$ is the equivalent probability but for founder k. When the emission probability is lower than 0.0005, we set it equal to 0.0005 to accommodate for unaccounted genotype calling errors. The emission probabilities are set to 1.00 at marker positions not covered by any read. With such an HMM, the Viterbi algorithm provides the most likely mosaic (sequence of founder inheritance) for the modeled F8 line whereas the Forward-Backward algorithm provides at each markers position the founder probability corresponding to the probability that the modeled F8 line derives from one specific

founder (the IBD probability that line *i* derives from founder *k* at marker *m* noted as $P(S_{im} = k)$). For relatedness measures and QTL mapping, these IBD probabilities were averaged in 10 kb windows and noted as $\bar{P}(S_{iw} = k)$ where w indicates the window number.

e) Estimation of population structure and genetic relatedness in the experimental population

We used PLINK to perform a PCA based on the genotype data from the design (eight founders and 768 F8 lines). The relatedness among F8 lines was first estimated either based on a similarity index defined as the proportion of IBS genotypes $SI_{ii'}$ among lines *i* and *i*', or from IBD relationship with founder lines in 10 kb windows, averaged over the entire genome:

$$g_{ii'} = \frac{1}{N_W} \sum_{w=1}^{N_W} \sum_{k=1}^{8} \bar{P}(S_{iw} = k)\bar{P}(S_{i'w} = k)$$

where $g_{iu'}$ is the genetic relatedness between lines *i* and *i'* computed over the N_W 10kb windows.

f) Estimation of genetic parameters associated with recorded phenotypes

For each trait *t*, defined as a phenotype by growth condition combination, we relied on the following single-trait linear mixed model (LMM) to estimate the heritability and repeatability:

$$\boldsymbol{y}_{\mathrm{t}} = \boldsymbol{X}_{\mathrm{t}}\boldsymbol{\beta}_{\mathrm{t}} + \boldsymbol{Z}_{\mathrm{ut}}\boldsymbol{u}_{\mathrm{t}} + \boldsymbol{Z}_{\mathrm{pt}}\boldsymbol{p}_{\mathrm{t}} + \boldsymbol{e}_{\mathrm{t}}$$

where $\mathbf{y}_t$ is the vector of recorded observations for trait *t* (two replications before filtering), $\boldsymbol{\beta}_t$ is a vector of fixed effects (for trait *t*) including the design effect (3 levels) and the phenotyping batch (8 levels), $\mathbf{u}_t$ is the vector of random polygenic effects for trait t of each F8 line, $\mathbf{p}_t$ is the vector of random permanent environment effect of each F8 line, and $\mathbf{e}_t$ is a vector with residual error terms associated with each record. The random polygenic effect represents the combined effect of all individual loci of one F8 line, and are assumed to be normally distributed

$$\boldsymbol{u}_{\mathrm{t}} \sim \mathrm{N}\left(\mathbf{0}, \mathbf{G}\sigma^2_{\mathrm{g,t}}\right)$$

where **G** is the genomic relationship matrix (**GRM**) among F8 lines obtained from IBD probabilities and $\boldsymbol{\sigma}^{\mathbf{2}}_{\mathbf{g,t}}$ is the additive genetic variance associated to trait *t*. Note that F8 lines with a similarity > 0.95 where clustered, we considered that they had the same polygenic effect. The so-called random permanent environment effects correspond to random effects associated with a F8 line, these can be non-genetic effects but also genetic effects that are non-additive

(not captured through the GRM). They are used to model the fact that two repeated measures on the same line are correlated, the effects were normally distributed with

$$\boldsymbol{p}_{\mathrm{t}} \sim \mathrm{N}\left(\mathbf{0}, \mathbf{I}\sigma^2_{\mathrm{p,t}}\right))$$

where **I** is an identity matrix and $\sigma^2_{\mathrm{p,t}}$ is the variance associated to the random permanent environment effects. Finally, the random residual error terms are also normally distributed $\boldsymbol{e}_{\mathrm{t}} \sim \mathrm{N}\left(\mathbf{0}, \mathbf{I}\sigma^2_{\mathrm{e,t}}\right)$, with $\sigma^2_{\mathrm{e,t}}$ being the residual variance. The heritability for trait *t* can be computed as:

$$h^2_t = \frac{\sigma^2_{\mathrm{g,t}}}{\sigma^2_{\mathrm{g,t}} + \sigma^2_{\mathrm{p,t}} + \sigma^2_{\mathrm{e,t}}}$$

whereas the repeatability is obtained as:

$$r^2_t = \frac{\sigma^2_{\mathrm{g,t}} + \sigma^2_{\mathrm{p,t}}}{\sigma^2_{\mathrm{g,t}} + \sigma^2_{\mathrm{p,t}} + \sigma^2_{\mathrm{e,t}}}$$

A multiple trait model traits was subsequently applied to estimate the genetic correlations among T traits:

$$\mathbf{y} = \mathbf{X\beta} + \mathbf{Z}_{\mathrm{u}}\mathbf{u} + \mathbf{Z}_{\mathrm{p}}\mathbf{p} + \mathbf{e}$$

Where $\mathbf{y} = (\mathbf{y}_1, \mathbf{y}_2, \ldots, \mathbf{y}_T)$ is the vector of all phenotypes, $\boldsymbol{\beta} = (\boldsymbol{\beta}_1, \boldsymbol{\beta}_2, \ldots, \boldsymbol{\beta}_T)$ is a vector with fixed effects for different traits. Similarly, **u**, **p** and **e** are vectors of corresponding random effects for all the traits. The incidence matrices are obtained from the combination of trait-specific incidence matrices. For instance:

$$\mathbf{Z}_u = \begin{bmatrix} \mathbf{Z}_{u1} & 0 & \cdots & 0 \\ 0 & \mathbf{Z}_{u2} & \cdots & 0 \\ \vdots & \vdots & \ddots & \vdots \\ 0 & 0 & \cdots & \mathbf{Z}_{uT} \end{bmatrix}$$

In our model, var(**u**) = $\mathbf{G} \otimes \mathbf{V_u}$, where **G** is the genomic relationship matrix and $\mathbf{V}_{\mathrm{u}}$ is the matrix of genetic variances and covariances among traits. Similarly, var(**p**) = $\mathbf{I} \otimes \mathbf{V_p}$ and

var(**e**) = **I** $\otimes$ $\mathbf{V_e}$, with $\mathbf{V_p}$ and $\mathbf{V}_e$ are the (co)variances matrices among random permanent and residual effects, respectively. For computational reasons, the (co)variances among traits were estimated by subgroup of traits. For the 14 phenotypes related to mineral nutrition and recorded in six different conditions, the correlations were first estimated within conditions and then by pairs of conditions. In addition, we also estimated the variance components for the same measure, recorded in the 6 conditions to assess the magnitude of genotype-by-environment interactions (14 six-traits models). Genetic parameters were estimated with the REML and AI-REML algorithm as implement in REMLF90 and AIREMLF90 programs (Misztal et al., 2002). The standard deviations of heritabilities, repeatabilities and correlations were obtained by repeated sampling of parameters estimates from their asymptotic multivariate normal distribution (Meyer & Houle, 2013).

g) QTL mapping

We used a LMM approach to perform the association study (e.g., Runcie & Crawford, 2019; Wei & Xu, 2016). The QTL detection relied on a likelihood ratio test (LRT) comparing a model with QTL to a null model without QTL. The null model (H0) was identical to the model described above for the estimation of genetic parameters. The alternative model (H1) included an additional QTL effect. To reduce computational costs, and as successive positions are highly correlated, we defined non-overlapping 10-kb windows and performed one test per window using the average IBD probability of all the SNPs in the window. Windows without any polymorphic sites in our final VCF were excluded. As a result, we reduced the number of tests from 3,121,994 polymorphic sites to 10,599 windows. The model including the QTL effect was defined as:

$$\mathbf{y}_t = \mathbf{X}_t\boldsymbol{\beta}_t + \mathbf{Z}_{ut}\mathbf{u}_t + \mathbf{Z}_{pt}\mathbf{p}_t + \mathbf{Z}^{\mathbf{w}}_{qt}\mathbf{q}_{w,t} + \mathbf{e}_t$$

where $\mathbf{q}_{w,t}$ is the vector with the eight random founder haplotype effects (or QTL effects) for the tested window *w* for trait *t* that are assumed independently distributed with variance $\sigma^2_{q,t}$, and $\mathbf{Z}^{\mathbf{i}}_{qt}$ is the incidence matrix relating the founder haplotype effects for window *w* to the F8 lines. This incidence matrix has one row for each F8 line and 8 columns (one per founder). The element $z^{\mathbf{w}}_{qt}(i,k)$ from this matrix contains the probability that F8 line *i* derives from founder *k* in window *w*, based on the IBD probabilities estimated with the HMM (called founder probabilities). We applied a Leave-One-Chromosome-Out (LOCO) strategy (Lippert et al., 2011), meaning that in both models (H0 and H1) the GRM among polygenic effects were computed ignoring windows on the chromosome harboring the tested position *i*. To test for the

presence of a QTL, the log-likelihood of the two models are compared with a LRT (distributed as a χ^2 distribution with 1 degree of freedom). The log-likelihood of both LMM were estimated with the REML algorithm and using the remlf90 program.

The number of independent tests was estimated by an approach described in Druet et al. (2014). We performed a genome-wide scan with a simple linear model on a permuted phenotype (-Ca [Zn] (nmol.OD^{-1})). We repeated this 10,000 times and saved the best genome-wide p-value for each permutation, providing the distribution of best p-values under H0 (absence of QTL). Corrected p-values for each p-value were then obtained as their rank among the sorted best p-values. We estimated the number of independent tests to be 3348, based on the Sidak formula and the sets of corrected and uncorrected p-values. The number of independent phenotypes was evaluated to be equal to 63 using the meff function (method = Galwey) from the poolR R package (Cinar & Viechtbauer, 2022). In total, we performed thus 210,924 independent tests and used the Bonferroni correction to set the significance thresholds to 0.05/210,924 = 2.37e-7. Confidence intervals (CI) were obtained using the LOD drop-off approach. Here we used a conservative LOD drop-off value of 2. To estimate the variance associated to a QTL, we compared the estimated polygenic variance in model H0 and model H1. The polygenic variance reduction represents the variance explained by the QTL (Malosetti et al., 2008). In that case, we used the GRM estimated using all chromosomes. In addition, we estimated the variance among founder haplotype effects $\sigma^2_{q,t}$ (an approximation of the QTL variance if the founder alleles are homogeneously transmitted to F8 lines).

VI. Bibliography

Ågren, Wetterstedt, & Billberger. (2012). Nutrient limitation on terrestrial plant growth – modeling the interaction between nitrogen and phosphorus. *New Phytologist*, *194*(4), 953–960. https://doi.org/10.1111/J.1469-8137.2012.04116.X

Allen, del Campo, Kropat, & Merchant. (2007a). FEA1, FEA2, and FRE1, encoding two homologous secreted proteins and a candidate ferrireductase, are expressed coordinately with FOX1 and FTR1 in iron-deficient Chlamydomonas reinhardtii. *Eukaryotic Cell*, *6*(10), 1841–1852. https://doi.org/10.1128/EC.00205-07

Allen, Kropat, Tottey, del Campo, & Merchant. (2007b). Manganese deficiency in Chlamydomonas results in loss of photosystem II and MnSOD function, sensitivity to peroxides, and secondary phosphorus and iron deficiency. *Plant Physiology*, *143*(1), 263–277. https://doi.org/10.1104/pp.106.088609

Alonso-Blanco, & Koornneef. (2000). Naturally occurring variation in Arabidopsis: an underexploited resource for plant genetics. *Trends in Plant Science*, *5*(1), 22–29. https://doi.org/10.1016/S1360-1385(99)01510-1

Alonso-Blanco, Koornneef, & van Ooijen. (2006). QTL Analysis. In *Arabidopsis Protocols* (Vol. 323, pp. 79–100). Humana Press. https://doi.org/10.1385/1-59745-003-0:79

Altenhoff, Train, Gilbert, Mediratta, de Farias, Moi, Nevers, Radoykova, Rossier, Vesztrocy, Glover, & Dessimoz. (2021). OMA orthology in 2021: website overhaul, conserved isoforms, ancestral gene order and more. *Nucleic Acids Research*, *49*(D1), D373–D379. https://doi.org/10.1093/NAR/GKAA1007

Andreini, Bertini, Cavallaro, Holliday, & Thornton. (2008). Metal ions in biological catalysis: From enzyme databases to general principles. *Journal of Biological Inorganic Chemistry*, *13*(8), 1205–1218. https://doi.org/10.1007/s00775-008-0404-5

Aoyama, Saitoh, Kuroiwa, & Nakamura. (2014). Comparative analysis of zygospore transcripts during early germination in Chlamydomonas reinhardtii. *Journal of Plant Physiology*, *171*(18), 1685–1692. https://doi.org/10.1016/J.JPLPH.2014.07.016

Arnon, & Stout. (1939). The Essentiality of Certain Elements in Minute Quantity for Plants with Special Reference to Copper. *Plant Physiology*, *14*(2), 371–375. https://doi.org/10.1104/pp.14.2.371

Arrones, Vilanova, Plazas, Mangino, Pascual, Díez, Prohens, & Gramazio. (2020). The dawn of the age of multi-parent magic populations in plant breeding: Novel powerful next-generation resources for genetic analysis and selection of recombinant elite material. In *Biology* (Vol. 9, Issue 8, pp. 1–25). Multidisciplinary Digital Publishing Institute. https://doi.org/10.3390/biology9080229

Asif, Schilling, Tilbrook, Brien, Dowling, Rabie, Short, Trittermann, Garcia, Barrett-Lennard, Berger, Mather, Gilliham, Fleury, Tester, Roy, & Pearson. (2018). Mapping of novel salt tolerance QTL in an Excalibur × Kukri doubled haploid wheat population. *Theoretical and Applied Genetics 2018 131:10*, *131*(10), 2179–2196. https://doi.org/10.1007/S00122-018-3146-Y

Asins, Raga, Torrent, Roca, & Carbonell. (2020). QTL and candidate gene analyses of rootstock-mediated tomato fruit yield and quality traits under low iron stress. *Euphytica*, *216*(4), 1–19. https://doi.org/10.1007/S10681-020-02599-6/TABLES/3

Ates, Aldemir, Yagmur, Kahraman, Ozkan, Vandenberg, & Tanyolac. (2018). QTL mapping of genome regions controlling manganese uptake in Lentil Seed. *G3: Genes, Genomes, Genetics*, *8*(5), 1409–1416. https://doi.org/10.1534/G3.118.200259/-/DC1

Atwell, Huang, Vilhjálmsson, Willems, Horton, Li, Meng, Platt, Tarone, Hu, Jiang, Muliyati, Zhang, Amer, Baxter, Brachi, Chory, Dean, Debieu, … Nordborg. (2010). Genome-wide association study of 107 phenotypes in Arabidopsis thaliana inbred lines. *Nature 2010 465:7298*, *465*(7298), 627–631. https://doi.org/10.1038/nature08800

Axelsen, & Palmgren. (2001). Inventory of the Superfamily of P-Type Ion Pumps in Arabidopsis. *Plant Physiology*, *126*(2), 696–706. https://doi.org/10.1104/PP.126.2.696

Babst-Kostecka, Przybyłowicz, Seget, & Mesjasz-Przybyłowicz. (2020). Zinc allocation to and within Arabidopsis halleri seeds: Different strategies of metal homeostasis in accessions under divergent selection pressure. *Plant-Environment Interactions*, *1*(3), 207–220. https://doi.org/10.1002/PEI3.10032

Bajhaiya, Dean, Driver, Trivedi, Rattray, Allwood, Goodacre, & Pittman. (2016). High-throughput metabolic screening of microalgae genetic variation in response to nutrient limitation. *Metabolomics*, *12*(1), 1–14. https://doi.org/10.1007/S11306-015-0878-4/FIGURES/6

Balzano, Sardo, Blasio, Chahine, Dell'Anno, Sansone, & Brunet. (2020). Microalgal Metallothioneins and Phytochelatins and Their Potential Use in Bioremediation. *Frontiers in Microbiology*, *11*, 517. https://doi.org/10.3389/FMICB.2020.00517/BIBTEX

Bandillo, Raghavan, Muyco, Sevilla, Lobina, Dilla-Ermita, Tung, McCouch, Thomson, Mauleon, Singh, Gregorio, Redoña, & Leung. (2013). Multi-parent advanced generation inter-cross (MAGIC) populations in rice: Progress and potential for genetics research and breeding. *Rice*, *6*(1), 1–15. https://doi.org/10.1186/1939-8433-6-11/COMMENTS

Barghi, Hermisson, & Schlötterer. (2020). Polygenic adaptation: a unifying framework to understand positive selection. *Nature Reviews Genetics 2020 21:12*, *21*(12), 769–781. https://doi.org/10.1038/s41576-020-0250-z

Barreiro, & Hairston. (2013). The influence of resource limitation on the allelopathic effect of Chlamydomonas reinhardtii on other unicellular freshwater planktonic organisms. *Journal of Plankton Research*, *35*(6), 1339–1344. https://doi.org/10.1093/PLANKT/FBT080

Barzana, Rios, Lopez-Zaplana, Nicolas-Espinosa, Yepes-Molina, Garcia-Ibañez, & Carvajal. (2021). Interrelations of nutrient and water transporters in plants under abiotic stress. *Physiologia Plantarum*, *171*(4), 595–619. https://doi.org/10.1111/PPL.13206

Baxter. (2009). Ionomics: Studying the Social Network of Mineral Nutrients. *Current Opinion in Plant Biology*, *12*(3), 381. https://doi.org/10.1016/J.PBI.2009.05.002

Baxter. (2015). Should we treat the ionome as a combination of individual elements, or should we be deriving novel combined traits? *Journal of Experimental Botany*, *66*(8), 2127–2131. https://doi.org/10.1093/JXB/ERV040

Baxter, Brazelton, Yu, Huang, Lahner, Yakubova, Li, Bergelson, Borevitz, Nordborg, Vitek, & Salt. (2010). A Coastal Cline in Sodium Accumulation in Arabidopsis thaliana Is Driven by Natural Variation of the Sodium Transporter AtHKT1;1. *PLOS Genetics*, *6*(11), e1001193. https://doi.org/10.1371/JOURNAL.PGEN.1001193

Baxter, & Dilkes. (2012). Elemental profiles reflect plant adaptations to the environment. In *Science* (Vol. 336, Issue 6089, pp. 1661–1663). American Association for the Advancement of Science. https://doi.org/10.1126/science.1219992

Baxter, Hermans, Lahner, Yakubova, Tikhonova, Verbruggen, Chao, & Salt. (2012). Biodiversity of mineral nutrient and trace element accumulation in Arabidopsis thaliana. *PLoS ONE*, *7*(4), e35121. https://doi.org/10.1371/journal.pone.0035121

Baxter, Vitek, Lahner, Muthukumar, Borghi, Morrissey, Guerinot, & Salt. (2008). The leaf ionome as a multivariable system to detect a plant's physiological status. *Proceedings of the National Academy of Sciences of the United States of America*, *105*(33), 12081–12086. https://doi.org/10.1073/PNAS.0804175105

Bergström. (2010). The use of TN:TP and DIN:TP ratios as indicators for phytoplankton nutrient limitation in oligotrophic lakes affected by N deposition. *Aquatic Sciences*, *72*(3), 277–281. https://doi.org/10.1007/S00027-010-0132-0/

Bernardes, John, Woltermann, Valiadi, Hermann, & Becks. (2021). The evolution of convex trade-offs enables the transition towards multicellularity. *Nature Communications 2021 12:1*, *12*(1), 1–9. https://doi.org/10.1038/s41467-021-24503-z

Bhatt, Hossain, & Sharma. (2020). Zinc biofortification as an innovative technology to alleviate the zinc deficiency in human health: A review. *Open Agriculture*, *5*(1), 176–186.

https://doi.org/10.1515/OPAG-2020-0018/ASSET/GRAPHIC/J_OPAG-2020-0018_FIG_004.JPG

Blaby-Haas, & Merchant. (2012). The ins and outs of algal metal transport. *Biochimica et Biophysica Acta - Molecular Cell Research*, *1823*(9), 1531–1552. https://doi.org/10.1016/j.bbamcr.2012.04.010

Blaby-Haas, & Merchant. (2017a). Regulating cellular trace metal economy in algae. *Current Opinion in Plant Biology*, *39*, 88–96. https://doi.org/10.1016/j.pbi.2017.06.005

Blaby-Haas, & Merchant. (2017b). Regulating cellular trace metal economy in algae. *Current Opinion in Plant Biology*, *39*, 88–96. https://doi.org/10.1016/J.PBI.2017.06.005

Blair, Wu, Bhandari, & Astudillo. (2016). Genetic dissection of ICP-detected nutrient accumulation in the whole seed of common bean (Phaseolus vulgaris L.). *Frontiers in Plant Science*, *7*(MAR2016), 219. https://doi.org/10.3389/FPLS.2016.00219/

Boake. (1989). Repeatability: its role in evolutionary studies of mating behavior. *Evolutionary Ecology*, *3*, 173–182.

Borowitzka. (2016). Algal Physiology and Large-Scale Outdoor Cultures of Microalgae. In Borowitzka, Beardall, & Raven (Eds.), *The Physiology of Microalgae* (pp. 601–652). Springer International Publishing. https://doi.org/10.1007/978-3-319-24945-2_23

Borowitzka, Critchley, Kraan, Peters, Sjotun, & Notoya. (2016). *The Physiology of Microalgae* (Borowitzka, Beardall, & Raven, Eds.; Vol. 20, Issue 6). Springer International Publishing. https://doi.org/10.1007/978-3-319-24945-2

Brachi, Faure, Horton, Flahauw, Vazquez, Nordborg, Bergelson, Cuguen, & Roux. (2010). Linkage and Association Mapping of Arabidopsis thaliana Flowering Time in Nature. *PLOS Genetics*, *6*(5), e1000940. https://doi.org/10.1371/JOURNAL.PGEN.1000940

Britto, & Kronzucker. (2008). Cellular mechanisms of potassium transport in plants. *Physiologia Plantarum*, *133*(4), 637–650. https://doi.org/10.1111/J.1399-3054.2008.01067.X

Bruna, Kendra, Groisman, & Pontes. (2021). Limitation of phosphate assimilation maintains cytoplasmic magnesium homeostasis. *Proceedings of the National Academy of Sciences of the United States of America*, *118*(11), e2021370118. https://doi.org/10.1073/PNAS.2021370118

Buescher, Achberger, Amusan, Giannini, Ochsenfeld, Rus, Lahner, Hoekenga, Yakubova, Harper, Guerinot, Zhang, Salt, & Baxter. (2010a). Natural Genetic Variation in Selected Populations of Arabidopsis thaliana Is Associated with Ionomic Differences. *PLOS ONE*, *5*(6), e11081. https://doi.org/10.1371/JOURNAL.PONE.0011081

Buescher, Achberger, Amusan, Giannini, Ochsenfeld, Rus, Lahner, Hoekenga, Yakubova, Harper, Guerinot, Zhang, Salt, & Baxter. (2010b). Natural Genetic Variation in Selected Populations of Arabidopsis thaliana Is Associated with Ionomic Differences. *PLoS ONE*, *5*(6), 11081. https://doi.org/10.1371/JOURNAL.PONE.0011081

Burstrom. (1948). Mineral Nutrition of Plants. *Annual Review of Biochemistry*, *17*(1), 579–600. https://doi.org/10.1146/annurev.bi.17.070148.003051

Cailliatte, Schikora, Briat, Mari, & Curie. (2010). High-Affinity Manganese Uptake by the Metal Transporter NRAMP1 Is Essential for Arabidopsis Growth in Low Manganese Conditions. *The Plant Cell*, *22*(3), 904–917. https://doi.org/10.1105/TPC.109.073023

Calatrava, Chamizo-Ampudia, Sanz-Luque, Ocaña-Calahorro, Llamas, Fernandez, & Galvan. (2017). How Chlamydomonas handles nitrate and the nitric oxide cycle. *Journal of Experimental Botany*, *68*(10), 2593–2602. https://doi.org/10.1093/JXB/ERW507

Carstensen, Sánchez-Camacho, Duarte, Krause-Jensen, & Marbà. (2011). Connecting the dots: Responses of coastal ecosystems to changing nutrient concentrations. *Environmental Science and Technology*, *45*(21), 9122–9132. https://doi.org/10.1021/ES202351Y/SUPPL_FILE/ES202351Y_SI_001.PDF

Casella, Tuttolomondo, Høilund-Carlsen, & Mollenhauer. (2014). Natural pattern recognition mechanisms at epithelial barriers and potential use in nanomedicine. *European Journal of Nanomedicine*, *6*(3), 141–155. https://doi.org/10.1515/EJNM-2014-0020/

Castaings, Caquot, Loubet, & Curie. (2016). The high-affinity metal Transporters NRAMP1 and IRT1 Team up to Take up Iron under Sufficient Metal Provision. *Scientific Reports*, *6*. https://doi.org/10.1038/SREP37222

Castruita, Casero, Karpowicz, Kropat, Vieler, Hsieh, Yan, Cokus, Loo, Benning, Pellegrini, & Merchant. (2011). Systems Biology Approach in Chlamydomonas Reveals Connections between Copper Nutrition and Multiple Metabolic Steps. *Plant Cell*, *23*, 1273–1292. https://doi.org/10.1105/tpc.111.084400

Cavaiuolo, Kuras, Wollman, Choquet, & Vallon. (2017). Small RNA profiling in Chlamydomonas: insights into chloroplast RNA metabolism. *Nucleic Acids Research*, *45*(18), 10783. https://doi.org/10.1093/NAR/GKX668

Cavanagh, Morell, Mackay, & Powell. (2008). From mutations to MAGIC: resources for gene discovery, validation and delivery in crop plants. *Current Opinion in Plant Biology*, *11*(2), 215–221. https://doi.org/10.1016/j.pbi.2008.01.002

Chaiwong, Prom-U-thai, Bouain, Lacombe, & Rouached. (2018). Individual versus Combinatorial Effects of Silicon, Phosphate, and Iron Deficiency on the Growth of

Lowland and Upland Rice Varieties. *International Journal of Molecular Sciences*, *19*(3). https://doi.org/10.3390/IJMS19030899

Chang, Yin, Imanaka, Igarashi, Li, & Luo. (2020). The metal transporter CrNRAMP1 is involved in zinc and cobalt transports in Chlamydomonas reinhardtii. *Biochemical and Biophysical Research Communications*, *523*(4), 880–886. https://doi.org/10.1016/J.BBRC.2019.12.121

Chao, Silva, Baxter, Huang, Nordborg, Danku, Lahner, Yakubova, & Salt. (2012). Genome-Wide Association Studies Identify Heavy Metal ATPase3 as the Primary Determinant of Natural Variation in Leaf Cadmium in Arabidopsis thaliana. *PLOS Genetics*, *8*(9), e1002923. https://doi.org/10.1371/JOURNAL.PGEN.1002923

Chapin, Schulze, & Mooney. (1990). The Ecology and Economics of Storage in Plants. *Annual Review of Ecology and Systematics*, *21*(1), 423–447. https://doi.org/10.1146/annurev.es.21.110190.002231

Chen, Wang, Yang, Zeng, & Liu. (2019). NRAMP1 promotes iron uptake at the late stage of iron deficiency in poplars. *Tree Physiology*, *39*(7), 1235–1250. https://doi.org/10.1093/TREEPHYS/TPZ055

Chen, Wang, Zhai, Song, & Zhang. (2013). ZincExplorer: An accurate hybrid method to improve the prediction of zinc-binding sites from protein sequences. *Molecular BioSystems*, *9*(9), 2213–2222. https://doi.org/10.1039/c3mb70100j

Cheng, Show, Lau, Chang, & Ling. (2019). New Prospects for Modified Algae in Heavy Metal Adsorption. *Trends in Biotechnology*, *37*(11), 1255–1268. https://doi.org/10.1016/J.TIBTECH.2019.04.007

Chietera, & Chardon. (2014). *Natural Variation as a Tool to Investigate Nutrient Use Efficiency in Plants*. 29–50. https://doi.org/10.1007/978-3-319-10635-9_2

Choi, Hwang, Kim, Park, Jin, Choi, & Sim. (2021). Augmented CO2 tolerance by expressing a single H+-pump enables microalgal valorization of industrial flue gas. *Nature Communications 2021 12:1*, *12*(1), 1–15. https://doi.org/10.1038/s41467-021-26325-5

Choudhary, Baskaran, & Sharma. (2019). Reentrant Efficiency of Phototaxis in Chlamydomonas reinhardtii Cells. *Biophysical Journal*, *117*(8), 1508–1513. https://doi.org/10.1016/J.BPJ.2019.09.016

Chow, Melis, & Anderson. (1990). Adjustments of photosystem stoichiometry in chloroplasts improve the quantum efficiency of photosynthesis. *Proceedings of the National Academy of Sciences*, *87*(19), 7502–7506. https://doi.org/10.1073/pnas.87.19.7502

Churchill, Airey, Allayee, Angel, Attie, Beatty, Beavis, Belknap, Bennett, Berrettini, Bleich, Bogue, Broman, Buck, Buckler, Burmeister, Chesler, Cheverud, Clapcote, … Zou.

(2004). The Collaborative Cross, a community resource for the genetic analysis of complex traits. *Nature Genetics 2004 36:11*, *36*(11), 1133–1137. https://doi.org/10.1038/ng1104-1133

Cinar, & Viechtbauer. (2022). The poolr Package for Combining Independent and Dependent p Values. *Journal of Statistical Software*, *101*(1), 1–42. https://doi.org/10.18637/JSS.V101.I01

Clemens. (2001). Molecular mechanisms of plant metal tolerance and homeostasis. *Planta 2001 212:4*, *212*(4), 475–486. https://doi.org/10.1007/S004250000458

Clemens. (2006). Toxic metal accumulation, responses to exposure and mechanisms of tolerance in plants. *Biochimie*, *88*(11), 1707–1719. https://doi.org/10.1016/J.BIOCHI.2006.07.003

Clemens. (2021). The cell biology of zinc. *Journal of Experimental Botany*. https://doi.org/10.1093/jxb/erab481

Colina, Carbó, Cañal, & Valledor. (2020). A complex metabolic rearrangement towards the accumulation of glycerol and sugars consequence of a proteome remodeling is required for the survival of Chlamydomonas reinhardtii growing under osmotic stress. *Environmental and Experimental Botany*, *180*, 104261. https://doi.org/10.1016/J.ENVEXPBOT.2020.104261

Colvin, Holmes, Fontaine, & Maret. (2010). Cytosolic zinc buffering and muffling: Their role in intracellularzinc homeostasis. *Metallomics*, *2*(5), 306–317. https://doi.org/10.1039/B926662C

Cooper, Voss-Fels, Messina, Tang, & Hammer. (2021). Tackling G × E × M interactions to close on-farm yield-gaps: creating novel pathways for crop improvement by predicting contributions of genetics and management to crop productivity. *Theoretical and Applied Genetics*, *134*(6), 1625–1644. https://doi.org/10.1007/S00122-021-03812-3/

Corso, An, Jones, Gonzalez-Doblas, Schvartzman, Malkowski, Willats, Hanikenne, & Verbruggen. (2021). Adaptation of Arabidopsis halleri to extreme metal pollution through limited metal accumulation involves changes in cell wall composition and metal homeostasis. *New Phytologist*, *230*(2), 669–682. https://doi.org/10.1111/NPH.17173

Corso, Schvartzman, Guzzo, Souard, Malkowski, Hanikenne, & Verbruggen. (2018). Contrasting cadmium resistance strategies in two metallicolous populations of Arabidopsis halleri. *New Phytologist*, *218*(1), 283–297. https://doi.org/10.1111/NPH.14948

Craig, Gallaher, Shu, Salomé, Jenkins, Blaby-Haas, Purvine, O'Donnell, Barry, Grimwood, Strenkert, Kropat, Daum, Yoshinaga, Goodstein, Vallon, Schmutz, & Merchant. (2022).

The Chlamydomonas Genome Project, version 6: reference assemblies for mating type plus and minus strains reveal extensive structural mutation in the laboratory. *BioRxiv*, 2022.06.16.496473. https://doi.org/10.1101/2022.06.16.496473

Craig, Hasan, Ness, & Keightley. (2021). Comparative genomics of Chlamydomonas. *The Plant Cell*, *33*(4), 1016–1041. https://doi.org/10.1093/PLCELL/KOAB026

Cross, Umen, Frederick R. Cross, & Umen. (2015). The Chlamydomonas cell cycle. *The Plant Journal*, *82*(3), 370–392. https://doi.org/10.1111/tpj.12795

Crusio. (2007). An introduction to quantitative genetics. In B.C. Jones (Ed.), *Neurobehavioral Genetics: Methods and Applications* (2nd ed., pp. 37–54). CRC Press. https://doi.org/10.13140/RG.2.1.3723.1443

Cubillos. (2016). Exploiting budding yeast natural variation for industrial processes. *Current Genetics*, *62*(4), 745–751. https://doi.org/10.1007/s00294-016-0602-6

Daniel, & tom Dieck. (2004). Nutrient-gene interactions: A single nutrient and hundreds of target genes. *Biological Chemistry*, *385*(7), 571–583. https://doi.org/10.1515/BC.2004.071/

Davies, Flint, Myers, & Mott. (2016). Rapid genotype imputation from sequence without reference panels. *Nature Genetics 2016 48:8*, *48*(8), 965–969. https://doi.org/10.1038/ng.3594

de Baar. (1994). von Liebig's law of the minimum and plankton ecology (1899-1991). *Progress in Oceanography*, *33*(4), 347–386. https://doi.org/10.1016/0079-6611(94)90022-1

de Carpentier, Lemaire, & Danon. (2019). When Unity Is Strength: The Strategies Used by Chlamydomonas to Survive Environmental Stresses. *Cells*, *8*(11), 1307. https://doi.org/10.3390/cells8111307

de Mazancourt, & Schwartz. (2012). Starve a competitor: Evolution of luxury consumption as a competitive strategy. *Theoretical Ecology*, *5*(1), 37–49. https://doi.org/10.1007/S12080-010-0094-9/

del Campo, Quinn, & Merchant. (2004). Evaluation of Oxygen Response Involving Differential Gene Expression in Chlamydomonas reinhardtii. In *Methods in Enzymology* (Vol. 381, pp. 604–617). Academic Press Inc. https://doi.org/10.1016/S0076-6879(04)81039-5

Delker, & Quint. (2011). Expression level polymorphisms: heritable traits shaping natural variation. *Trends in Plant Science*, *16*(9), 481–488. https://doi.org/10.1016/J.TPLANTS.2011.05.009

Dell'acqua, Gatti, Pea, Cattonaro, Coppens, Magris, Hlaing, Aung, Nelissen, Baute, Frascaroli, Churchill, Inzé, Morgante, & Pè. (2011). *Genetic properties of the MAGIC maize population: a new platform for high definition QTL mapping in Zea mays*. https://doi.org/10.1186/s13059-015-0716-z

Dent, Han, & Niyogi. (2001). Functional genomics of plant photosynthesis in the fast lane using Chlamydomonas reinhardtii. *Trends in Plant Science*, *6*(8), 364–371. https://doi.org/10.1016/S1360-1385(01)02018-0

Des Marais, Hernandez, & Juenger. (2013). *Genotype-by-Environment Interaction and Plasticity: Exploring Genomic Responses of Plants to the Abiotic Environment*. https://doi.org/10.1146/annurev-ecolsys-110512-135806

Devadasu, Madireddi, Nama, & Subramanyam. (2016). Iron deficiency cause changes in photochemistry, thylakoid organization, and accumulation of photosystem II proteins in Chlamydomonas reinhardtii. *Photosynthesis Research*, *130*(1–3), 469–478. https://doi.org/10.1007/s11120-016-0284-4

Docampo, de Souza, Miranda, Rohloff, & Moreno. (2005). Acidocalcisomes - Conserved from bacteria to man. *Nature Reviews Microbiology*, *3*(3), 251–261. https://doi.org/10.1038/nrmicro1097

Doerge. (2002). Mapping and analysis of quantitative trait loci in experimental populations. *Nature Reviews Genetics*, *3*(1), 43–52. https://doi.org/10.1038/nrg703

Dohm. (2002). Repeatability Estimates Do Not Always Set an Upper Limit to Heritability Repeatability estimates do not always set a to heritability. *Functional Ecology*, *16*(2), 273–280.

Draghi, & Whitlock. (2012). Phenotypiv plasticity facilitates mutational variance, genetic variance, and evolvability along the major axis of environmental variation. *Evolution*, *66*(9), 2891–2902. https://doi.org/10.1111/j.1558-5646.2012.01649.x

Druet, Macleod, & Hayes. (2014). Toward genomic prediction from whole-genome sequence data: impact of sequencing design on genotype imputation and accuracy of predictions. *Heredity*, *112*(1), 39–47. https://doi.org/10.1038/hdy.2013.13

Du, Zeng, Wang, Qian, Zheng, & Ling. (2013). Environmental effects on mineral accumulation in rice grains and identification of ecological specific QTLs. *Environmental Geochemistry and Health*, *35*(2), 161–170. https://doi.org/10.1007/S10653-012-9473-Z/

Dubeaux, Neveu, Zelazny, & Vert. (2018). Metal Sensing by the IRT1 Transporter-Receptor Orchestrates Its Own Degradation and Plant Metal Nutrition. *Molecular Cell*, *69*(6), 953-964.e5. https://doi.org/10.1016/J.MOLCEL.2018.02.009

Dunn. (1964). Multiple comparisons using rank sums. *Technometrics*, *6*(3), 241–252.

Dutcher. (2000). Chlamydomonas reinhardtii: Biological Rationale for Genomics. *The Journal of Eukaryotic Microbiology*, *47*(4), 340–349. https://doi.org/10.1111/j.1550-7408.2000.tb00059.x

Ehret. (2010). Genome-Wide Association Studies: Contribution of Genomics to Understanding Blood Pressure and Essential Hypertension. *Current Hypertension Reports*, *12*(1), 17–25. https://doi.org/10.1007/s11906-009-0086-6

Elbaz, Wei, Meng, Zheng, & Yang. (2010). Mercury-induced oxidative stress and impact on antioxidant enzymes in Chlamydomonas reinhardtii. *Ecotoxicology*, *19*(7), 1285–1293. https://doi.org/10.1007/S10646-010-0514-Z/

Fakhimi, & Tavakoli. (2019). Improving hydrogen production using co-cultivation of bacteria with Chlamydomonas reinhardtii microalga. *Materials Science for Energy Technologies*, *2*(1), 1–7. https://doi.org/10.1016/J.MSET.2018.09.003

Falconer. (1960). *Introduction to quantitative genetics*. Oliver and Boyd.

Fan, Zhou, Chen, Tang, & Xie. (2021). Cross-Talks Between Macro- and Micronutrient Uptake and Signaling in Plants. *Frontiers in Plant Science*, *12*, 2076. https://doi.org/10.3389/FPLS.2021.663477/BIBTEX

Fang, de Los Reyes, & Umen. (2006). Cell Size Checkpoint Control by the Retinoblastoma Tumor Suppressor Pathway. *PLoS Genetics*, *2*(10), 1565–1579. https://doi.org/10.1371/JOURNAL.PGEN.0020167

Faralli, & Lawson. (2020). Natural genetic variation in photosynthesis: an untapped resource to increase crop yield potential? *Plant Journal*, *101*(3), 518–528. https://doi.org/10.1111/tpj.14568

Fei, Eriksson, Yang, & Deng. (2009). An Fe deficiency responsive element with a core sequence of TGGCA regulates the expression of FEA1 in Chlamydomonas reinharditii. *Journal of Biochemistry*, *146*(2), 157–166. https://doi.org/10.1093/jb/mvp056

Fei, Wilson, Mangan, Wingreen, & Jonikas. (2022). Modelling the pyrenoid-based CO2-concentrating mechanism provides insights into its operating principles and a roadmap for its engineering into crops. *Nature Plants 2022 8:5*, *8*(5), 583–595. https://doi.org/10.1038/s41477-022-01153-7

Feinleib, & Curry. (1971). The Relationship between Stimulus Intensity and Oriented Phototactic Response (Topotaxis) in Chlamydomonas. *Physiologia Plantarum*, *25*(3), 346–352. https://doi.org/10.1111/j.1399-3054.1971.tb01453.x

Fernandez, & Galvan. (2007). Inorganic nitrogen assimilation in Chlamydomonas. *Journal of Experimental Botany*, *58*(9), 2279–2287. https://doi.org/10.1093/JXB/ERM106

Fernandez, & Galvan. (2008). Nitrate assimilation in Chlamydomonas. *Eukaryotic Cell*, *7*(4), 555–559. https://doi.org/10.1128/EC.00431-07

Ferris, Goodenough, & Ferris. (1997). Mating Type in Chlamydomonas Is Specified by mid, the Minus-Dominance Gene. *Genetics*, *3*, 4–6. http://www.genetics.org/content/genetics/146/3/859.full.pdf

Ferris, Woessner, & Goodenough. (1996). A sex recognition glycoprotein is encoded by the plus mating-type gene fus1 of Chlamydomonas reinhardtii. *Molecular Biology of the Cell*, *7*(8), 1235–1248. https://doi.org/10.1091/MBC.7.8.1235

Figueroa-Torres, Pittman, & Theodoropoulos. (2017). Kinetic modelling of starch and lipid formation during mixotrophic, nutrient-limited microalgal growth. *Bioresource Technology*, *241*, 868–878. https://doi.org/10.1016/J.BIORTECH.2017.05.177

Fischer. (1930). *The genetical theory of natural selection.* The Clarendon Press.

Fisher. (1919). XV.—The correlation between relatives on the supposition of Mendelian inheritance. *Earth and Environmental Science Transactions of the Royal Society of Edinburgh*, *52*(2), 399–433.

Fisher, Badgley, & Blyth. (2012). Global nutrient limitation in terrestrial vegetation. *Global Biogeochemical Cycles*, *26*(3), 3007. https://doi.org/10.1029/2011GB004252

Flowers, Hazzouri, Pham, Rosas, Bahmani, Khraiwesh, Nelson, Jijakli, Abdrabu, Harris, Lefebvre, Hom, Salehi-Ashtiani, & Purugganan. (2015). Whole-Genome Resequencing Reveals Extensive Natural Variation in the Model Green Alga Chlamydomonas reinhardtii. *The Plant Cell*, *27*(9), 2353–2369. https://doi.org/10.1105/tpc.15.00492

Franco, Sánchez-Olea, Reyes-Reyes, & Panayiotidis. (2009). Environmental toxicity, oxidative stress and apoptosis: Ménage à Trois. *Mutation Research/Genetic Toxicology and Environmental Mutagenesis*, *674*(1–2), 3–22. https://doi.org/10.1016/J.MRGENTOX.2008.11.012

Frieden. (1984). A Survey of the Essential Biochemical Elements. *Biochemistry of the Essential Ultratrace Elements*, 1–15. https://doi.org/10.1007/978-1-4684-4775-0_1

Frunzo, Maharaj, Mattei, Frunzo, Hatzikioseyian, Van, Lens, & Esposito. (2019). Mathematical modelling of trace element dynamics in anaerobic digestion environments. In *Trace Elements in Anaerobic Biotechnologies* (Issue June). https://doi.org/10.2166/9781789060225_0101

Gallaher, Fitz-Gibbon, Glaesener, Pellegrini, Merchanta, & Merchant. (2015). Chlamydomonas Genome Resource for Laboratory Strains Reveals a Mosaic of Sequence Variation, Identifies True Strain Histories, and Enables Strain-Specific Studies. *The Plant Cell*, *27*(9), 2335–2352. https://doi.org/10.1105/tpc.15.00508

Gallaher, Fitz-Gibbon, Strenkert, Purvine, Pellegrini, & Merchant. (2018). High-throughput sequencing of the chloroplast and mitochondrion of Chlamydomonas reinhardtii to generate improved de novo assemblies, analyze expression patterns and transcript speciation, and evaluate diversity among laboratory strains and wild isolates. *The Plant Journal*, *93*(3), 545–565. https://doi.org/10.1111/TPJ.13788

Gao, Robe, Gaymard, Izquierdo, & Dubos. (2019). The transcriptional control of iron homeostasis in plants: A tale of bHLH transcription factors? *Frontiers in Plant Science*, *10*, 6. https://doi.org/10.3389/FPLS.2019.00006/BIBTEX

Gardner, & Latta. (2007). Shared quantitative trait loci underlying the genetic correlation between continuous traits. *Molecular Ecology*, *16*(20), 4195–4209. https://doi.org/10.1111/J.1365-294X.2007.03499.X

Garrison, & Marth. (2012). *Haplotype-based variant detection from short-read sequencing*. https://doi.org/10.48550/arxiv.1207.3907

Gasch, Payseur, & Pool. (2016). The Power of Natural Variation for Model Organism Biology. In *Trends in Genetics* (Vol. 32, Issue 3, pp. 147–154). Elsevier Ltd. https://doi.org/10.1016/j.tig.2015.12.003

Gerloff. (1963). Comparative Mineral Nutrition of Plants. *Annual Review of Plant Physiology*, *14*(1), 107–124. https://doi.org/10.1146/annurev.pp.14.060163.000543

Glaesener, Merchant, & Blaby-Haas. (2013). Iron economy in Chlamydomonas reinhardtii. *Frontiers in Plant Science*, *4*, 337. https://doi.org/10.3389/fpls.2013.00337

Glazier, Nadeau, & Aitman. (2002). Genetics: Finding genes that underline complex traits. *Science*, *298*(5602), 2345–2349. https://doi.org/10.1126/SCIENCE.1076641/SUPPL_FILE/GLAZIER.SOM.PDF

Goddard, Kemper, MacLeod, Chamberlain, & Hayes. (2016). Genetics of complex traits: prediction of phenotype, identification of causal polymorphisms and genetic architecture. *Proceedings of the Royal Society B: Biological Sciences*, *283*(1835). https://doi.org/10.1098/RSPB.2016.0569

Godhe, & Rynearson. (2017). The role of intraspecific variation in the ecological and evolutionary success of diatoms in changing environments. In *Philosophical Transactions of the Royal Society B: Biological Sciences* (Vol. 372, Issue 1728). Royal Society Publishing. https://doi.org/10.1098/rstb.2016.0399

González-Ballester, Casero, Cokus, Pellegrini, Merchant, & Grossman. (2010). RNA-Seq Analysis of Sulfur-Deprived *Chlamydomonas* Cells Reveals Aspects of Acclimation Critical for Cell Survival. *The Plant Cell*, *22*(6), 2058–2084. https://doi.org/10.1105/tpc.109.071167

Goodenough. (1992). Green Yeast. *Cell*, *70*, 533–538.

Goodenough, Heiss, Roth, Rusch, & Lee. (2019). Acidocalcisomes: Ultrastructure, Biogenesis, and Distribution in Microbial Eukaryotes. *Protist*, *170*(3), 287–313. https://doi.org/10.1016/J.PROTIS.2019.05.001

Goodstein, Shu, Howson, Neupane, Hayes, Fazo, Mitros, Dirks, Hellsten, Putnam, & Rokhsar. (2012). Phytozome: a comparative platform for green plant genomics. *Nucleic Acids Research*, *40*(D1), D1178–D1186. https://doi.org/10.1093/NAR/GKR944

Gorman, & Levine. (1965). Cytochrome f and plastocyanin: their sequence in the photosynthetic electron transport chain of Chlamydomonas reinhardi. *Proceedings of the National Academy of Sciences of the United States of America*, *54*(6), 1665–1669. http://www.ncbi.nlm.nih.gov/pubmed/4379719

Govorunova, & Sineshchekov. (2005). Chemotaxis in the Green Flagellate Alga Chlamydomonas. *Biochemistry (Moscow) 2005 70:7*, *70*(7), 717–725. https://doi.org/10.1007/S10541-005-0176-2

Gransee, & Führs. (2013). Magnesium mobility in soils as a challenge for soil and plant analysis, magnesium fertilization and root uptake under adverse growth conditions. *Plant and Soil*, *368*(1–2), 5–21. https://doi.org/10.1007/S11104-012-1567-Y/

Grossman, & Aksoy. (2018). Algae in a Phosphorus-Limited Landscape. *Annual Plant Reviews Online*, 337–374. https://doi.org/10.1002/9781119312994.APR0527

Grossman, Harris, Hauser, Lefebvre, Martinez, Rokhsar, Shrager, Silflow, Stern, Vallon, & Zhang. (2003). Chlamydomonas reinhardtii at the Crossroads of Genomics. In *Eukaryotic Cell* (Vol. 2, Issue 6, pp. 1137–1150). American Society for Microbiology (ASM). https://doi.org/10.1128/EC.2.6.1137-1150.2003

Gu, Eils, & Schlesner. (2016). Complex heatmaps reveal patterns and correlations in multidimensional genomic data. *Bioinformatics*. https://doi.org/10.1093/bioinformatics/btw313

Gu, Gu, Eils, Schlesner, & Brors. (2014). circlize implements and enhances circular visualization in R. *Bioinformatics*, *30*(19), 2811–2812. https://doi.org/10.1093/bioinformatics/btu393

Gulisija, Kim, & Plotkin. (2016). Phenotypic plasticity promotes balanced polymorphism in periodic environments by a genomic storage effect. *Genetics*, *202*(4), 1437–1448. https://doi.org/10.1534/GENETICS.115.185702/-/DC1

Gutu, Alvey, Bashour, Zingg, & Kehoe. (2011). Sulfate-Driven Elemental Sparing Is Regulated at the Transcriptional and Posttranscriptional Levels in a Filamentous

Cyanobacterium. *Journal of Bacteriology*, *193*(6), 1449. https://doi.org/10.1128/JB.00885-10

Hammani, Bonnard, Bouchoucha, Gobert, Pinker, Salinas, & Giegé. (2014). Helical repeats modular proteins are major players for organelle gene expression. *Biochimie*, *100*(1), 141–150. https://doi.org/10.1016/J.BIOCHI.2013.08.031

Han, Lee, Ro, Hur, Lee, Kwon, & Kang. (2018). QTL mapping and GWAS reveal candidate genes controlling capsaicinoid content in Capsicum. *Plant Biotechnology Journal*, *16*(9), 1546–1558. https://doi.org/10.1111/PBI.12894

Hanikenne. (2003). Chlamydomonas reinhardtii as a eukaryotic photosynthetic model for studies of heavy metal homeostasis and tolerance. *New Phytologist*, *159*(2), 331–340. https://doi.org/10.1046/j.1469-8137.2003.00788.x

Hanikenne, Esteves, Fanara, & Rouached. (2020). Coordinated homeostasis of essential mineral nutrients: a focus on iron. *Journal of Experimental Botany*. https://doi.org/10.1093/jxb/eraa483ï

Hanikenne, Krämer, Demoulin, & Baurain. (2005a). A comparative inventory of metal transporters in the green alga Chlamydomonas reinhardtii and the red alga Cyanidioschizon merolae. *Plant Physiology*, *137*(2), 428–446. https://doi.org/10.1104/pp.104.054189

Hanikenne, Merchant, & Hamel. (2009). Transition Metal Nutrition: A Balance Between Deficiency and Toxicity. In *The Chlamydomonas Sourcebook 3-Vol set* (Vol. 2, pp. 333–399). https://doi.org/10.1016/B978-0-12-370873-1.00018-6

Hanikenne, Motte, Wu, Wang, Loppes, & Matagne. (2005b). A mitochondrial half-size ABC transporter is involved in cadmium tolerance in Chlamydomonas reinhardtii. *Plant, Cell and Environment*, *28*(7), 863–873. https://doi.org/10.1111/j.1365-3040.2005.01335.x

Hanikenne, & Nouet. (2011). Metal hyperaccumulation and hypertolerance: a model for plant evolutionary genomics. *Current Opinion in Plant Biology*, *14*(3), 252–259. https://doi.org/10.1016/J.PBI.2011.04.003

Hänsch, & Mendel. (2009). Physiological functions of mineral micronutrients (Cu, Zn, Mn, Fe, Ni, Mo, B, Cl). *Current Opinion in Plant Biology*, *12*(3), 259–266. https://doi.org/10.1016/j.pbi.2009.05.006

Harris. (2001). Chlamydomonas as a model organism. *Annual Review of Plant Biology*, *52*(3), 363–406. https://doi.org/10.1146/annurev.arplant.52.1.363

Harris. (2009a). Chlamydomonas in the Laboratory. In *The Chlamydomonas Sourcebook* (Vol. 1, pp. 241–302). Elsevier. https://doi.org/10.1016/B978-0-12-370873-1.00008-3

Harris. (2009b). The Genus Chlamydomonas. In *The Chlamydomonas Sourcebook* (Vol. 1, pp. 1–24). Elsevier. https://doi.org/10.1016/B978-0-12-370873-1.00001-0

Hart, & Gardner. (2021). Lighting the way: Recent insights into the structure and regulation of phototropin blue light receptors. *Journal of Biological Chemistry*, *296*, 100594. https://doi.org/10.1016/J.JBC.2021.100594

Hasan, & Ness. (2020). Recombination Rate Variation and Infrequent Sex Influence Genetic Diversity in Chlamydomonas reinhardtii. *Genome Biology and Evolution*, *12*(4), 370–380. https://doi.org/10.1093/GBE/EVAA057

Hawkesford, Horst, Kichey, Lambers, Schjoerring, Møller, & White. (2012). Functions of Macronutrients. In *Marschner's Mineral Nutrition of Higher Plants* (pp. 135–189). Elsevier. https://doi.org/10.1016/B978-0-12-384905-2.00006-6

He, Rössner, Hoang, Alejandro, & Peiter. (2021). Transport, functions, and interaction of calcium and manganese in plant organellar compartments. *Plant Physiology*, *187*(4), 1940–1972. https://doi.org/10.1093/PLPHYS/KIAB122

He, Wu, Wei, Fu, Cui, Dong, Tan, & Qian. (2017). GWAS, QTL mapping and gene expression analyses in Brassica napus reveal genetic control of branching morphogenesis. *Scientific Reports*, *7*(1). https://doi.org/10.1038/S41598-017-15976-4

Heldt, Tyson, Cross, & Novák. (2020). A Single Light-Responsive Sizer Can Control Multiple-Fission Cycles in Chlamydomonas. *Current Biology*, *30*(4), 634-644.e7. https://doi.org/10.1016/J.CUB.2019.12.026

Hellemans, Mortier, de Paepe, Speleman, & Vandesompele. (2008). qBase relative quantification framework and software for management and automated analysis of real-time quantitative PCR data. *Genome Biology*, *8*(2), 1–14. https://doi.org/10.1186/GB-2007-8-2-R19

Herron, & Michod. (2008). Evolution of complexity in the volvocine algae: transitions in individuality through Darwin's eye. *Evolution; International Journal of Organic Evolution*, *62*(2), 436–451. https://doi.org/10.1111/j.1558-5646.2007.00304.x

Hope. (2013). *Rmisc: Rmisc: Ryan Miscellaneous*. https://cran.r-project.org/package=Rmisc

(How to) Map and clean up short read sequence data efficiently – GATK. (n.d.). https://gatk.broadinstitute.org/hc/en-us/articles/360039568932--How-to-Map-and-clean-up-short-read-sequence-data-efficiently

Howe, & Merchant. (1992). Heavy Metal-Activated Synthesis of Peptides in Chiamydomonas reinhardtii'. *Plant Physiol*, *98*, 127–136. https://academic.oup.com/plphys/article/98/1/127/6087687

Huang, George, Forrest, Kilian, Hayden, Morell, & Cavanagh. (2012). A multiparent advanced generation inter-cross population for genetic analysis in wheat. *Plant Biotechnology Journal*, *10*(7), 826–839. https://doi.org/10.1111/J.1467-7652.2012.00702.X

Huang, Hu, & Zhao. (2021). Molybdenum: More than an essential element. *Journal of Experimental Botany*. https://doi.org/10.1093/JXB/ERAB534

Huang, & Salt. (2016). Plant Ionomics: From Elemental Profiling to Environmental Adaptation. In *Molecular Plant* (Vol. 9, Issue 6, pp. 787–797). Cell Press. https://doi.org/10.1016/j.molp.2016.05.003

Huang, Verbyla, Verbyla, Raghavan, Singh, Gaur, Leung, Varshney, & Cavanagh. (2015). MAGIC populations in crops: current status and future prospects. *Theoretical and Applied Genetics*, *128*(6), 999–1017. https://doi.org/10.1007/s00122-015-2506-0

Hui, Schmollinger, Strenkert, Holbrook, Montgomery, Chen, Nelson, Weber, & Merchant. (2022). Simple steps to enable reproducibility: culture conditions affecting Chlamydomonas growth and elemental composition. *The Plant Journal*. https://doi.org/10.1111/tpj.15867

Hunter, & Provasoli. (1964). Nutrition of Algae. *Annual Review of Plant Physiology*, *15*(1), 37–56. https://doi.org/10.1146/annurev.pp.15.060164.000345

Hutner, Provasoli, Schatz, & Haskins. (1950). Some Approaches to the Study of the Role of Metals in the Metabolism of Microorganisms. *Proceedings of the American Philosophical Society*, *94*(2), 152–170.

Huynh, Ehlers, Huang, Muñoz-Amatriaín, Lonardi, Santos, Ndeve, Batieno, Boukar, Cisse, Drabo, Fatokun, Kusi, Agyare, Guo, Herniter, Lo, Wanamaker, Xu, … Roberts. (2018). A multi-parent advanced generation inter-cross (<scp>MAGIC</scp>) population for genetic analysis and improvement of cowpea (*Vigna unguiculata* L. Walp.). *The Plant Journal*, *93*(6), 1129–1142. https://doi.org/10.1111/tpj.13827

Iacono. (2023). *Natural variation in photosynthesis mechanisms of Chlamydomonas reinhardtii (provisional title)*. University of Liege.

Ibuot, Dean, McIntosh, & Pittman. (2017). Metal bioremediation by CrMTP4 over-expressing Chlamydomonas reinhardtii in comparison to natural wastewater-tolerant microalgae strains. *Algal Research*, *24*, 89–96. https://doi.org/10.1016/J.ALGAL.2017.03.002

Ibuot, Dean, & Pittman. (2020). Multi-genomic analysis of the cation diffusion facilitator transporters from algae. *Metallomics*, *12*(4), 617–630. https://doi.org/10.1039/D0MT00009D

Induri, Ellis, Slavov, Yin, Zhang, Muchero, Tuskan, & Difazio. (2012). Identification of quantitative trait loci and candidate genes for cadmium tolerance in Populus. *Tree Physiology*, *32*(5), 626–638. https://doi.org/10.1093/TREEPHYS/TPS032

Jamers, Lenjou, Deraedt, Bockstaele, Blust, & Coen. (2009). Flow cytometric analysis of the cadmium-exposed green alga Chlamydomonas reinhardtii (Chlorophyceae). *European Journal of Phycology*, *44*(4), 541–550. https://doi.org/10.1080/09670260903118214

Jang, & Ehrenreich. (2012). Genome-Wide Characterization of Genetic Variation in the Unicellular, Green Alga Chlamydomonas reinhardtii. *PLOS ONE*, *7*(7), e41307. https://doi.org/10.1371/JOURNAL.PONE.0041307

Jiang, & Stern. (2009). Mating and Tetrad Separation of Chlamydomonas reinhardtii for Genetic Analysis. *JoVE (Journal of Visualized Experiments)*, *30*, e1274. https://doi.org/10.3791/1274

Jin, Zhou, Chen, Zhu, Zhao, & Huang. (2013). The genetic architecture of zinc and iron content in maize grains as revealed by QTL mapping and meta-analysis. *Breeding Science*, *63*(3), 317–324. https://doi.org/10.1270/JSBBS.63.317

Johnson, Vandystadt, Bujaldon, Wollman, Dubois, Roussel, Alric, & Béal. (2009). A new setup for in vivo fluorescence imaging of photosynthetic activity. *Photosynthesis Research*, *102*(1), 85–93. https://doi.org/10.1007/S11120-009-9487-2

Jones, Wolf, & Mills. (1991). *Plant Analysis Handbook: A Practical Sampling, Preparation, Analysis, and Interpretation Guide*. Micro-Macro Pub. https://books.google.be/books?id=KkpFAQAAIAAJ

Jorde. (2000). Linkage Disequilibrium and the Search for Complex Disease Genes. *Genome Research*, *10*(10), 1435–1444. https://doi.org/10.1101/GR.144500

Kajikawa, & Fukuzawa. (2020). Algal Autophagy Is Necessary for the Regulation of Carbon Metabolism Under Nutrient Deficiency. *Frontiers in Plant Science*, *11*, 36. https://doi.org/10.3389/FPLS.2020.00036/

Kalaji, Schansker, Ladle, Goltsev, Bosa, Allakhverdiev, Brestic, Bussotti, Calatayud, Dąbrowski, Elsheery, Ferroni, Guidi, Hogewoning, Jajoo, Misra, Nebauer, Pancaldi, Penella, … Zivcak. (2014). Frequently asked questions about in vivo chlorophyll fluorescence: Practical issues. *Photosynthesis Research*, *122*(2), 121–158. https://doi.org/10.1007/S11120-014-0024-6

Kamalanathan, Pierangelini, Shearman, Gleadow, & Beardall. (2016). Impacts of nitrogen and phosphorus starvation on the physiology of Chlamydomonas reinhardtii. *Journal of Applied Phycology*, *28*(3), 1509–1520. https://doi.org/10.1007/s10811-015-0726-y

Kang, Zaitlen, Wade, Kirby, Heckerman, Daly, & Eskin. (2008). Efficient Control of Population Structure in Model Organism Association Mapping. *Genetics*, *178*(3), 1709–1723. https://doi.org/10.1534/GENETICS.107.080101

Kassambara. (2020). *ggpubr: "ggplot2" Based Publication Ready Plots*. https://cran.r-project.org/package=ggpubr

Kazmi, Khan, Willems, van Heusden, Ligterink, & Hilhorst. (2012). Complex genetics controls natural variation among seed quality phenotypes in a recombinant inbred population of an interspecific cross between Solanum lycopersicum × Solanum pimpinellifolium. *Plant, Cell & Environment*, *35*(5), 929–951. https://doi.org/10.1111/J.1365-3040.2011.02463.X

Khan, Singh, & Srivastava. (2018). Synthesis, nature and utility of universal iron chelator – Siderophore: A review. *Microbiological Research*, *212–213*, 103–111. https://doi.org/10.1016/J.MICRES.2017.10.012

Kirkby. (2011). Introduction, Definition and Classification of Nutrients. In *Marschner's Mineral Nutrition of Higher Plants: Third Edition* (pp. 3–5). https://doi.org/10.1016/B978-0-12-384905-2.00001-7

Kitayama, Kitayama, Osafune, & Togasaki. (1999). Subcellular localization of iron and manganese superoxide dismutase in Chlamydomonas reinhardtii (Chlorophyceae). *Journal of Phycology*, *35*(1), 136–142. https://doi.org/10.1046/j.1529-8817.1999.3510136.x

Kochoni, Aharchaou, Ohlund, Rosabal, Sleno, & Fortin. (2022). New insights in copper handling strategies in the green alga Chlamydomonas reinhardtii under low-iron condition. *Metallomics*, *14*(6), 33. https://doi.org/10.1093/MTOMCS/MFAC033

Kopriva, Mugford, Matthewman, & Koprivova. (2009). Plant sulfate assimilation genes: Redundancy versus specialization. *Plant Cell Reports*, *28*(12), 1769–1780. https://doi.org/10.1007/S00299-009-0793-0/FIGURES/3

Korte, & Farlow. (2013). *The advantages and limitations of trait analysis with GWAS: a review*. https://doi.org/10.1186/1746-4811-9-29

Kover, Valdar, Trakalo, Scarcelli, Ehrenreich, Purugganan, Durrant, & Mott. (2009). A Multiparent Advanced Generation Inter-Cross to Fine-Map Quantitative Traits in Arabidopsis thaliana. *PLoS Genetics*, *5*(7), e1000551. https://doi.org/10.1371/journal.pgen.1000551

Krämer. (2010). Metal Hyperaccumulation in Plants. *Annual Review of Plant Biology*, *61*(1), 517–534. https://doi.org/10.1146/annurev-arplant-042809-112156

Krämer, Talke, & Hanikenne. (2007). Transition metal transport. *FEBS Letters*, *581*(12), 2263–2272. https://doi.org/10.1016/J.FEBSLET.2007.04.010

Kroh, & Pilon. (2020). Regulation of iron homeostasis and use in chloroplasts. *International Journal of Molecular Sciences*, *21*(9), 3395. https://doi.org/10.3390/ijms21093395

Kropat, Gallaher, Urzica, Nakamoto, Strenkert, Tottey, Mason, & Merchant. (2015). Copper economy in Chlamydomonas: Prioritized allocation and eallocation of copper to respiration vs. Photosynthesis. *Proceedings of the National Academy of Sciences of the United States of America*, *112*(9), 2644–2651. https://doi.org/10.1073/PNAS.1422492112

Kropat, Hong-Hermesdorf, Casero, Ent, Castruita, Pellegrini, Merchant, & Malasarn. (2011). A revised mineral nutrient supplement increases biomass and growth rate in Chlamydomonas reinhardtii. *Plant Journal*, *66*(5), 770–780. https://doi.org/10.1111/j.1365-313X.2011.04537.x

Kruglyak. (1999). *Prospects for whole-genome linkage disequilibrium mapping of common disease genes* (Vol. 22). https://doi.org/10.1038/9642

Kumar, Kumar, & Mohapatra. (2021). Interaction Between Macro- and Micro-Nutrients in Plants. *Frontiers in Plant Science*, *12*, 753. https://doi.org/10.3389/FPLS.2021.665583/BIBTEX

la Fontaine, Quinn, Nakamoto, Dudley Page, Göhre, Moseley, Kropat, & Merchant. (2002). Copper-dependent iron assimilation pathway in the model photosynthetic eukaryote Chlamydomonas reinhardtii. *Eukaryotic Cell*, *1*(5), 736–757. https://doi.org/10.1128/EC.1.5.736-757.2002/FORMAT/EPUB

Lahner, Gong, Mahmoudian, Smith, Abid, Rogers, Guerinot, Harper, Ward, McIntyre, Schroeder, & Salt. (2003a). Genomic scale profiling of nutrient and trace elements in Arabidopsis thaliana. *Nature Biotechnology*, *21*(10), 1215–1221. https://doi.org/10.1038/nbt865

Lahner, Gong, Mahmoudian, Smith, Abid, Rogers, Guerinot, Harper, Ward, Mcintyre, Schroeder, & Salt. (2003b). Genomic scale profiling of nutrient and trace elements in Arabidopsis thaliana. *NATURE BIOTECHNOLOGY*, *21*. https://doi.org/10.1038/nbt865

Lander, & Botsteins. (1989). *Mapping Mendelian Factors Underlying Quantitative Traits Using RFLP Linkage Maps*.

Laurinavichene, Tolstygina, Galiulina, Ghirardi, Seibert, & Tsygankov. (2002). Dilution methods to deprive Chlamydomonas reinhardtii cultures of sulfur for subsequent hydrogen photoproduction. *International Journal of Hydrogen Energy*, *27*(11–12), 1245–1249. https://doi.org/10.1016/S0360-3199(02)00101-5

Lazarević, Horvat, & Poljak. (2014). Effect of Acid Aluminous Soil on Photosynthetic Parameters of Potato (Solanum tuberosum L.). *Potato Research*, *57*(1), 33–46. https://doi.org/10.1007/S11540-014-9251-7/

Lemaire, & Gastal. (2019). Crop Responses to Nitrogen. *Crop Science*, 159–184. https://doi.org/10.1007/978-1-4939-8621-7_385

Lin, Zhu, Yano, Gao, Liang, Su, Hu, Ren, & Chao. (2004). QTLs for Na+ and K+ uptake of the shoots and roots controlling rice salt tolerance. *Theoretical and Applied Genetics*, *108*(2), 253–260. https://doi.org/10.1007/S00122-003-1421-Y/TABLES/4

Lippert, Listgarten, Liu, Kadie, Davidson, & Heckerman. (2011). FaST linear mixed models for genome-wide association studies. *Nature Methods 2011 8:10*, *8*(10), 833–835. https://doi.org/10.1038/nmeth.1681

Liu, Huang, Sun, Li, Hu, Yu, Liti, Tian, Hurst, & Yang. (2018). Tetrad analysis in plants and fungi finds large differences in gene conversion rates but no GC bias. *Nature Ecology & Evolution*, *2*(1), 164. https://doi.org/10.1038/S41559-017-0372-7

Liu, Wang, Xiao, Luo, Qiao, Yang, Zhang, Meng, Sun, Yan, Peng, Niu, Jian, Song, Yan, Li, Zhao, Liu, Warburton, … Yan. (2020). CUBIC: An atlas of genetic architecture promises directed maize improvement. *Genome Biology*, *21*(1), 1–17. https://doi.org/10.1186/S13059-020-1930-X/

Livak, & Schmittgen. (2001). Analysis of Relative Gene Expression Data Using Real-Time Quantitative PCR and the 2−ΔΔCT Method. *Methods*, *25*(4), 402–408. https://doi.org/10.1006/meth.2001.1262

López-Paz, Liu, Geng, & Umen. (2017). Identification of Chlamydomonas reinhardtii endogenous genic flanking sequences for improved transgene expression. *The Plant Journal : For Cell and Molecular Biology*, *92*(6), 1232. https://doi.org/10.1111/TPJ.13731

Loppes, & Radoux. (2001). Identification of short promoter regions involved in the transcriptional expression of the nitrate reductase gene in Chlamydomonas reinhardtii. *Plant Molecular Biology*, *45*, 215–227.

Loudet, Saliba-Colombani, Camilleri, Calenge, Gaudon, Koprivova, North, Kopriva, & Daniel-Vedele. (2007). Natural variation for sulfate content in Arabidopsis thaliana is highly controlled by APR2. *Nature Genetics 2007 39:7*, *39*(7), 896–900. https://doi.org/10.1038/ng2050

Lucker, Temple, Panchy, Benning, Bibik, Neofotis, Weissman, Baxter, Shiu, & Kramer. (2022). Selection-enriched genomic loci (SEGL) reveals genetic loci for environmental

adaptation and photosynthetic productivity in Chlamydomonas reinhardtii. *Algal Research*, *64*, 102709. https://doi.org/10.1016/J.ALGAL.2022.102709

Ma, Salomé, Merchant, & Pellegrini. (2021). Single-cell RNA sequencing of batch Chlamydomonas cultures reveals heterogeneity in their diurnal cycle phase. *The Plant Cell*, *33*(4), 1042–1057. https://doi.org/10.1093/PLCELL/KOAB025

Macedo-Osorio, Martínez-Antonio, & Badillo-Corona. (2021). Pas de Trois: An Overview of Penta-, Tetra-, and Octo-Tricopeptide Repeat Proteins From Chlamydomonas reinhardtii and Their Role in Chloroplast Gene Expression. *Frontiers in Plant Science*, *12*. https://doi.org/10.3389/FPLS.2021.775366

Mackay, & Powell. (2007). Methods for linkage disequilibrium mapping in crops. *Trends in Plant Science*, *12*(2), 57–63. https://doi.org/10.1016/j.tplants.2006.12.001

Mackinnon, & Stone. (2022). The Ubiquitin Proteasome System and Nutrient Stress Response. *Frontiers in Plant Science*, *13*, 1373. https://doi.org/10.3389/FPLS.2022.867419/BIBTEX

Malasarn, Kropat, Hsieh, Finazzi, Casero, Loo, Pellegrini, Wollman, & Merchant. (2013). Zinc deficiency impacts CO2 Assimilation and disrupts copper homeostasis in Chlamydomonas Reinhardtii. *Journal of Biological Chemistry*, *288*(15), 10672–10683. https://doi.org/10.1074/jbc.M113.455105

Malcom, Hernandez, Likos, Wayne, Leibold, & Juenger. (2015). Extensive cross-environment fitness variation lies along few axes of genetic variation in the model alga, Chlamydomonas reinhardtii. *New Phytologist*, *205*(2), 841–851. https://doi.org/10.1111/NPH.13063

Maldonado, Allen, Chong, Lin, Leus, Karpenko, & Harris. (2006). Copper-dependent iron transport in coastal and oceanic diatoms. *Limnology and Oceanography*, *51*(4), 1729–1743. https://doi.org/10.4319/lo.2006.51.4.1729

Malosetti, Ribaut, Vargas, Crossa, & van Eeuwijk. (2008). A multi-trait multi-environment QTL mixed model with an application to drought and nitrogen stress trials in maize (Zea mays L.). *Euphytica*, *161*(1–2), 241–257. https://doi.org/10.1007/S10681-007-9594-0/FIGURES/3

Manenti, Galvan, Pettinicchio, Trincucci, Spada, Zolin, Milani, Gonzalez-Neira, & Dragani. (2009). Mouse Genome-Wide Association Mapping Needs Linkage Analysis to Avoid False-Positive Loci. *PLOS Genetics*, *5*(1), e1000331. https://doi.org/10.1371/JOURNAL.PGEN.1000331

Mangiafico. (2021). *rcompanion: Functions to Support Extension Education Program Evaluation*. https://cran.r-project.org/package=rcompanion

Marchand, Heydarizadeh, Schoefs, & Spetea. (2018). Ion and metabolite transport in the chloroplast of algae: lessons from land plants. *Cellular and Molecular Life Sciences*, *75*(12), 2153–2176. https://doi.org/10.1007/s00018-018-2793-0

Maret, & Copsey. (2012). Metallomics: whence and whither. *Metallomics*, *4*(10), 1017. https://doi.org/10.1039/c2mt90041f

Marschner (Ed.). (2011). *Marschner's Mineral Nutrition of Higher Plants* (3rd ed.). Academic Press.

Martínez, Moestrup, Holmskov, Mollenhauer, & Lozano. (2011). *The Conserved Scavenger Receptor Cysteine-Rich Superfamily in Therapy and Diagnosis*. https://doi.org/10.1124/pr.111.004523

Mauricio. (2001). Mapping quantitative trait loci in plants: uses and caveats for evolutionary biology. *Nature Reviews Genetics*, *2*(5), 370–381. https://doi.org/10.1038/35072085

Mengel, Kirkby, Kosegarten, & Appel. (2001a). Plant Nutrients. *Principles of Plant Nutrition*, 1–13. https://doi.org/10.1007/978-94-010-1009-2_1

Mengel, Kirkby, Kosegarten, & Appel. (2001b). Potassium. In *Principles of plant nutrition* (pp. 481–511). Springer.

Merchán, van den Ende, Fernández, & Beck. (2001). Low-expression genes induced by nitrogen starvation and subsequent sexual differentiation in Chlamydomonas reinhardtii, isolated by the differential display technique. *Planta*, *213*(2), 309–317. https://doi.org/10.1007/s004250100567

Merchant. (2010). The Elements of Plant Micronutrients. *Plant Physiology*, *154*(2), 512–515. https://doi.org/10.1104/pp.110.161810

Merchant, Allen, Kropat, Moseley, Long, Tottey, & Terauchi. (2006). Between a rock and a hard place: Trace element nutrition in Chlamydomonas. *Biochimica et Biophysica Acta (BBA) - Molecular Cell Research*, *1763*(7), 578–594. https://doi.org/10.1016/J.BBAMCR.2006.04.007

Merchant, & Bogorad. (1986a). Regulation by copper of the expression of plastocyanin and cytochrome c552 in Chlamydomonas reinhardi. *Molecular and Cellular Biology*, *6*(2), 462–469. https://doi.org/10.1128/mcb.6.2.462-469.1986

Merchant, & Bogorad. (1986b). Rapid degradation of apoplastocyanin in Cu(II)-deficient cells of Chlamydomonas reinhardtii. *Journal of Biological Chemistry*, *261*(34), 15850–15853. https://doi.org/10.1016/S0021-9258(18)66641-4

Merchant, & Bogorad. (1987). Metal ion regulated gene expression: use of a plastocyanin-less mutant of Chlamydomonas reinhardtii to study the Cu(II)-dependent expression of

cytochrome c-552. *The EMBO Journal*, *6*(9), 2531–2535. https://doi.org/10.1002/J.1460-2075.1987.TB02540.X

Merchant, & Helmann. (2012). Elemental Economy. In *Advances in microbial physiology* (Vol. 60, pp. 91–210). NIH Public Access. https://doi.org/10.1016/B978-0-12-398264-3.00002-4

Merchant, Prochnik, Vallon, Harris, Arpowicz, Witman, Terry, Salamov, Fritz-Laylin, Maréchal-Drouard, Marshall, Qu, Nelson, Sanderfoot, Spalding, Kapitonov, Ren, Ferris, Lindquist, … Grossman. (2007). The Chlamydomonas Genome Reveals the Evolution of Key Animal and Plant Functions. *Science*, *318*(5848), 245–250. https://doi.org/10.1126/science.1143609

Merchant, & Sawaya. (2005). The Light Reactions: A Guide to Recent Acquisitions for the Picture Gallery. *The Plant Cell*, *17*(3), 648–663. https://doi.org/10.1105/tpc.105.030676

Merchant, Schmollinger, Strenkert, Moseley, & Blaby-Haas. (2020). From economy to luxury: Copper homeostasis in Chlamydomonas and other algae. *Biochimica et Biophysica Acta (BBA) - Molecular Cell Research*, *1867*(11), 118822. https://doi.org/10.1016/J.BBAMCR.2020.118822

Meyer, & Houle. (2013). Sampling Based Approximation of Confidence Intervals for Functions of Genetic Covariance Matrices. *Proceedings of the Twentieth Conference of the Association for the Advancement of Animal Breeding and Genetics*.

Miramar, Inda, Saraiva, & Peleato. (2003). Plastocyanin/cytochrome c 6 interchange in Scenedesmus vacuolatus. *J. Plant Physiol*, *160*, 1483–1486. http://www.urbanfischer.de/journals/jpp

Misztal, Tsuruta, Strabel, Auvray, Druet, & Lee. (2002). BLUPF90 and related programs (BGF90). *7th World Congress on Genetics Applied to Livestock Production*. http://www.ozemail.com.au/~milleraj.

Mizushima, Yoshimori, & Ohsumi. (2011). The role of atg proteins in autophagosome formation. *Annual Review of Cell and Developmental Biology*, *27*, 107–132. https://doi.org/10.1146/annurev-cellbio-092910-154005

Moore, Mills, Arrigo, Berman-Frank, Bopp, Boyd, Galbraith, Geider, Guieu, Jaccard, Jickells, la Roche, Lenton, Mahowald, Marañón, Marinov, Moore, Nakatsuka, Oschlies, … Ulloa. (2013). Processes and patterns of oceanic nutrient limitation. *Nature Geoscience 2013 6:9*, *6*(9), 701–710. https://doi.org/10.1038/ngeo1765

Moroney, & Ynalvez. (2007). Proposed carbon dioxide concentrating mechanism in Chlamydomonas reinhardtii. *Eukaryotic Cell*, *6*(8), 1251–1259. https://doi.org/10.1128/EC.00064-07

Moseley, Allinger, Herzog, Hoerth, Wehinger, Merchant, & Hippler. (2002). Adaptation to Fe-deficiency requires remodeling of the photosynthetic apparatus. *The EMBO Journal*, *21*(24), 6709–6720. https://doi.org/10.1093/emboj/cdf666

Moseley, Chang, & Grossman. (2006). Genome-Based Approaches to Understanding Phosphorus Deprivation Responses and PSR1 Control in Chlamydomonas reinhardtii † ‡. *EUKARYOTIC CELL*, *5*(1), 26–44. https://doi.org/10.1128/EC.5.1.26-44.2006

Mott, Talbot, Turri, Collins, & Flint. (2000a). A method for fine mapping quantitative trait loci in outbred animal stocks. *Proceedings of the National Academy of Sciences*, *97*(23), 12649–12654. https://doi.org/10.1073/PNAS.230304397

Mott, Talbot, Turri, Collins, & Flint. (2000b). A method for fine mapping quantitative trait loci in outbred animal stocks. *Proceedings of the National Academy of Sciences of the United States of America*, *97*(23), 12649–12654. https://doi.org/10.1073/PNAS.230304397

Murchie, & Lawson. (2013). Chlorophyll fluorescence analysis: a guide to good practice and understanding some new applications. *Journal of Experimental Botany*, *64*(13), 3983–3998. https://doi.org/10.1093/jxb/ert208

Nakamura, Aoyama, & van Woesik. (2003). Strict paternal transmission of mitochondrial DNA of Chlamydomonas species is explained by selection against maternal nucleoids. *Protoplasma*, *221*(3), 205–210.

Nam, Shahzad, Dorone, Clowez, Zhao, Bouain, Lay-Pruitt, Cho, Rhee, & Rouached. (2021). Interdependent iron and phosphorus availability controls photosynthesis through retrograde signaling. *Nature Communications 2021 12:1*, *12*(1), 1–13. https://doi.org/10.1038/s41467-021-27548-2

Naumann, Busch, Allmer, Ostendorf, Zeller, Kirchhoff, & Hippler. (2007). Comparative quantitative proteomics to investigate the remodeling of bioenergetic pathways under iron deficiency in Chlamydomonas reinhardtii. *PROTEOMICS*, *7*(21), 3964–3979. https://doi.org/10.1002/PMIC.200700407

Neofotis, Temple, Tessmer, Bibik, Norris, Pollner, Lucker, Weraduwage, Withrow, Sears, Mogos, Frame, Hall, Weissman, & Kramer. (2021). The induction of pyrenoid synthesis by hyperoxia and its implications for the natural diversity of photosynthetic responses in Chlamydomonas. *ELife*, *10*. https://doi.org/10.7554/ELIFE.67565

Newman, Boynton, Gillham, Randolph-Anderson, Johnson, & Harris. (1990). *Transformation of Chloroplast Ribosomal RNA Genes in Chlamydomonas: Molecular and Genetic Characterization of Integration Events*.

Nishimura. (2010). Uniparental inheritance of cpDNA and the genetic control of sexual differentiation in Chlamydomonas reinhardtii. *Journal of Plant Research 2010 123:2*, *123*(2), 149–162. https://doi.org/10.1007/S10265-009-0292-Y

Nishimura. (2017). The Sexual Developmental Program of <Emphasis Type="Italic">Chlamydomonas reinhardtii</Emphasis>. In Hippler (Ed.), *Chlamydomonas: Biotechnology and Biomedicine* (pp. 127–148). Springer International Publishing. https://doi.org/10.1007/978-3-319-66360-9_6

Nishimura, Misumi, Kato, Inada, Higashiyama, Momoyama, & Kuroiwa. (2002). *An mt + gamete-specific nuclease that targets mt − chloroplasts during sexual reproduction in C. reinhardtii*. https://doi.org/10.1101/gad.979902

Nishimura, Misumi, Matsunaga, Higashiyama, Yokota, & Kuroiwa. (1999). The active digestion of uniparental chloroplast DNA in a single zygote of *Chlamydomonas reinhardtii* is revealed by using the optical tweezer. *Proceedings of the National Academy of Sciences*, *96*(22), 12577–12582. https://doi.org/10.1073/pnas.96.22.12577

Nishimura, Shikanai, Nakamura, Kawai-Yamada, & Uchimiya. (2012). Gsp1 Triggers the Sexual Developmental Program Including Inheritance of Chloroplast DNA and Mitochondrial DNA in Chlamydomonas reinhardtii. *The Plant Cell*, *24*(6), 2401–2414. https://doi.org/10.1105/tpc.112.097865

Noda, & Fujioka. (2015). Atg1 family kinases in autophagy initiation. *Cellular and Molecular Life Sciences*, *72*(16), 3083–3096. https://doi.org/10.1007/S00018-015-1917-Z/FIGURES/1

Nouet, Charlier, Carnol, Bosman, Farnir, Motte, & Hanikenne. (2015). Functional analysis of the three HMA4 copies of the metal hyperaccumulator Arabidopsis halleri. *Journal of Experimental Botany*, *66*(19), 5783–5795. https://doi.org/10.1093/JXB/ERV280

Ogle, Doll, Wheeler, & Dinno. (2021). *FSA: Fisheries Stock Analysis*. https://github.com/droglenc/FSA

Otero, & Goto. (2005). Microalgae: The "self-synchronized" eukaryotes. *Trends in Biotechnology*, *23*(9), 448–449. https://doi.org/10.1016/j.tibtech.2005.05.014

Page, Allen, Kropat, Urzica, Karpowicz, Hsieh, Loo, & Merchant. (2012). Fe Sparing and Fe Recycling Contribute to Increased Superoxide Dismutase Capacity in Iron-Starved Chlamydomonas reinhardtii. *The Plant Cell*, *24*(6), 2649–2665. https://doi.org/10.1105/TPC.112.098962

Page, Kropat, Hamel, & Merchant. (2009). Two Chlamydomonas CTR copper transporters with a novel cys-met motif are localized to the plasma membrane and function in copper assimilation. *Plant Cell*, *21*(3), 928–943. https://doi.org/10.1105/tpc.108.064907

Pascual, Desplat, Huang, Desgroux, Bruguier, Bouchet, Le, Chauchard, Verschave, & Causse. (2015). Potential of a tomato MAGIC population to decipher the genetic control of quantitative traits and detect causal variants in the resequencing era. *Plant Biotechnology Journal*, *13*(4), 565–577. https://doi.org/10.1111/PBI.12282

Paterson, Lander, Hewitt, Peterson, Lincoln, & Tanksley. (1988). Resolution of quantitative traits into Mendelian factors by using a complete linkage map of restriction fragment length polymorphisms. *Nature*, *335*(6192), 721–726. https://doi.org/10.1038/335721a0

Pedersen, Axelsen, Harper, & Palmgren. (2012). Evolution of plant P-type ATPases. *Frontiers in Plant Science*, *3*(FEB). https://doi.org/10.3389/FPLS.2012.00031/

Pelgas, Bousquet, Meirmans, Ritland, & Isabel. (2011). QTL mapping in white spruce: Gene maps and genomic regions underlying adaptive traits across pedigrees, years and environments. *BMC Genomics*, *12*(1), 1–23. https://doi.org/10.1186/1471-2164-12-145/

Pereira, Soriano Viana, Andrade, Fonseca e Silva, & Paes. (2018). Relevance of genetic relationship in GWAS and genomic prediction. *Journal of Applied Genetics*, *59*(1), 1–8. https://doi.org/10.1007/S13353-017-0417-2/

Pérez-Pérez, Couso, & Crespo. (2017). The TOR Signaling Network in the Model Unicellular Green Alga Chlamydomonas reinhardtii. *Biomolecules*, *7*(3). https://doi.org/10.3390/BIOM7030054

Pérez-Pérez, & Crespo. (2010). *Autophagy in the model alga Chlamydomonas reinhardtii*. https://doi.org/10.4161/auto.6.4.11822

Pierre, Stoeckel, & Wajnberg. (2022). The advantage of sex: Reinserting fluctuating selection in the pluralist approach. *PLOS ONE*, *17*(8), e0272134. https://doi.org/10.1371/JOURNAL.PONE.0272134

Pita-Barbosa, Ricachenevsky, & Flis. (2019). One "OMICS" to integrate them all: ionomics as a result of plant genetics, physiology and evolution. *Theoretical and Experimental Plant Physiology*, *31*(1), 71–89. https://doi.org/10.1007/s40626-019-00144-y

Pittman, Edmond, Sunderland, & Bray. (2009a). A cation-regulated and proton gradient-dependent cation transporter from chlamydomonas reinhardtii has a role in calcium and sodium homeostasis. *Journal of Biological Chemistry*, *284*(1), 525–533. https://doi.org/10.1074/JBC.M807173200/ATTACHMENT/3BCDF72A-4B2F-4F48-8065-C3FA66643E11/MMC1.PDF

Pittman, Edmond, Sunderland, & Bray. (2009b). A Cation-regulated and Proton Gradient-dependent Cation Transporter from Chlamydomonas reinhardtii Has a Role in Calcium and Sodium Homeostasis. *Journal of Biological Chemistry*, *284*(1), 525–533. https://doi.org/10.1074/jbc.M807173200

Platt, & Gordon. (1998). Scavenger receptors: diverse activities and promiscuous binding of polyanionic ligands. *Chemistry & Biology*, *5*(8), R193–R203. https://doi.org/10.1016/S1074-5521(98)90156-9

Plissonneau, Benevenuto, Mohd-Assaad, Fouché, Hartmann, & Croll. (2017). Using population and comparative genomics to understand the genetic basis of effector-driven fungal pathogen evolution. In *Frontiers in Plant Science* (Vol. 8, Issue FEBRUARY). Frontiers Media S.A. https://doi.org/10.3389/fpls.2017.00119

Plouviez, Oliveira da Rocha, & Guieysse. (2022). Intracellular polyphosphate is a P reserve in Chlamydomonas reinhardtii. *Algal Research*, *66*, 102779. https://doi.org/10.1016/J.ALGAL.2022.102779

Podar, & Maathuis. (2022). Primary nutrient sensors in plants. *IScience*, *25*(4), 104029. https://doi.org/10.1016/J.ISCI.2022.104029

Prinzenberg, Campos-Dominguez, Kruijer, Harbinson, & Aarts. (2020). Natural variation of photosynthetic efficiency in Arabidopsis thaliana accessions under low temperature conditions. *Plant, Cell & Environment*, *43*(8), 2000–2013. https://doi.org/10.1111/PCE.13811

Pritchard, & di Rienzo. (2010). Adaptation – not by sweeps alone. *Nature Reviews. Genetics*, *11*(10), 665. https://doi.org/10.1038/NRG2880

Quinn, & Merchant. (1995). Two copper-responsive elements associated with the Chlamydomonas Cyc6 gene function as targets for transcriptional activators. *The Plant Cell*, *7*(5), 623–628. https://doi.org/10.1105/tpc.7.5.623

R Core Team. (2022). *R: A Language and Environment for Statistical Computing*. https://www.r-project.org/

Rangarajan, Kapoor, Li, Drossopoulos, White, Madden, & Dohlman. (2020). Potassium starvation induces autophagy in yeast. *Journal of Biological Chemistry*, *295*(41), 14189–14202. https://doi.org/10.1074/JBC.RA120.014687

Ratcliff, Herron, Howell, Pentz, Rosenzweig, & Travisano. (2013). Experimental evolution of an alternating uni- and multicellular life cycle in Chlamydomonas reinhardtii. *Nature Communications*, *4*. https://doi.org/10.1038/NCOMMS3742

Redding, & Cole. (2008). Chlamydomonas : a sexually active, light-harvesting, carbon-reducing, hydrogen-belching 'planimal.' *EMBO Reports*, *9*(12), 1182–1187. https://doi.org/10.1038/embor.2008.205

Ricachenevsky, de Araújo Junior, Fett, & Sperotto. (2018). You shall not pass: Root vacuoles as a symplastic checkpoint for metal translocation to shoots and possible application to

grain nutritional quality. *Frontiers in Plant Science*, *9*, 412. https://doi.org/10.3389/FPLS.2018.00412/BIBTEX

Rochaix. (1995). Chlamydomonas reinhardtii as the photosynthetic yeast. In *Annual Review of Genetics* (Vol. 29, pp. 209–230). https://doi.org/10.1146/annurev.ge.29.120195.001233

Römheld. (2011). Diagnosis of Deficiency and Toxicity of Nutrients. In *Marschner's Mineral Nutrition of Higher Plants: Third Edition* (pp. 299–312). Elsevier Inc. https://doi.org/10.1016/B978-0-12-384905-2.00011-X

Rosakis, & Köster. (2005). Divalent metal transport in the green microalga Chlamydomonas reinhardtii is mediated by a protein similar to prokaryotic Nramp homologues. *Biometals 2005 18:1*, *18*(1), 107–120. https://doi.org/10.1007/S10534-004-2481-4

RStudio Team. (2021). *RStudio: Integrated Development Environment for R*. R Studio, PBC. http://www.rstudio.com/

Runcie, & Crawford. (2019). Fast and flexible linear mixed models for genome-wide genetics. *PLOS Genetics*, *15*(2), e1007978. https://doi.org/10.1371/JOURNAL.PGEN.1007978

Rupprecht. (2009). From systems biology to fuel-Chlamydomonas reinhardtii as a model for a systems biology approach to improve biohydrogen production. *Journal of Biotechnology*, *142*, 10–20. https://doi.org/10.1016/j.jbiotec.2009.02.008

Sager, & Granick. (1954). Nutritional control of sexuality in Chlamydomonas reinhardi. *Journal of General Physiology*, *37*(6), 729–742. https://doi.org/10.1085/jgp.37.6.729

Saito, Bertrand, Dutkiewicz, Bulygin, Moran, Monteiro, Follows, Valois, & Waterbury. (2011). Iron conservation by reduction of metalloenzyme inventories in the marine diazotroph Crocosphaera watsonii. *Proceedings of the National Academy of Sciences of the United States of America*, *108*(6), 2184–2189. https://doi.org/10.1073/PNAS.1006943108

Sallam, & Martsch. (2015). Association mapping for frost tolerance using multi-parent advanced generation inter-cross (MAGIC) population in faba bean (Vicia faba L.). *Genetica*, *143*(4), 501–514. https://doi.org/10.1007/s10709-015-9848-z

Salomé, & Merchant. (2019). A Series of Fortunate Events: Introducing Chlamydomonas as a Reference Organism. *The Plant Cell*, *31*(8), 1682–1707. https://academic.oup.com/plcell/article/31/8/1682/5985816

Salt, Baxter, & Lahner. (2008). Ionomics and the study of the plant ionome. In *Annual Review of Plant Biology* (Vol. 59, pp. 709–733). Annual Reviews. https://doi.org/10.1146/annurev.arplant.59.032607.092942

Salvi, & Tuberosa. (2015). The crop QTLome comes of age. *Current Opinion in Biotechnology*, *32*, 179–185. https://doi.org/10.1016/J.COPBIO.2015.01.001

Samantara, Reyes, Agrawal, Mohapatra, & Jena. (2021). Advances and trends on the utilization of multi-parent advanced generation intercross (MAGIC) for crop improvement. *Euphytica 2021 217:10*, *217*(10), 1–22. https://doi.org/10.1007/S10681-021-02925-6

Saroussi, Sanz-Luque, Kim, & Grossman. (2017). Nutrient scavenging and energy management: acclimation responses in nitrogen and sulfur deprived Chlamydomonas. *Current Opinion in Plant Biology*, *39*, 114–122. https://doi.org/10.1016/J.PBI.2017.06.002

Sasaki, Yamaji, & Ma. (2016). Transporters involved in mineral nutrient uptake in rice. *Journal of Experimental Botany*, *67*(12), 3645–3653. https://doi.org/10.1093/jxb/erw060

Sasso, Stibor, Mittag, & Grossman. (2018). The natural history of model organisms: From molecular manipulation of domesticated Chlamydomonas reinhardtii to survival in nature. *ELife*, *7*. https://doi.org/10.7554/eLife.39233

Sathe, & Durand. (2016). Cellular aggregation in Chlamydomonas (Chlorophyceae) is chimaeric and depends on traits like cell size and motility. *European Journal of Phycology*, *51*(2), 129–138. https://doi.org/10.1080/09670262.2015.1107759

Sawyer, Hankamer, & Ross. (2015). Sulphur responsiveness of the Chlamydomonas reinhardtii LHCBM9 promoter. *Planta*, *241*(5), 1287–1302. https://doi.org/10.1007/s00425-015-2249-9

Schaffner, Taylor, Wong, Wirth, & Neafsey. (2018). HmmIBD: Software to infer pairwise identity by descent between haploid genotypes. *Malaria Journal*, *17*(1), 1–4. https://doi.org/10.1186/S12936-018-2349-7/FIGURES/1

Schmidt, & Eckert. (1976). Calcium couples flagellar reversal to photostimulation in Chlamydomonas reinhardtii. *Nature*, *262*(5570), 713–715. https://doi.org/10.1038/262713a0

Schmidt, Hartung, Bennewitz, & Hans-Peter. (2019). Heritability in Plant Breeding on a Genotype-Difference Basis. *Genetics*, *212*(4), 991–1008. https://doi.org/10.1534/GENETICS.119.302134

Schmollinger, Chen, Strenkert, Hui, Ralle, & Merchant. (2021). Single-cell visualization and quantification of trace metals in *Chlamydomonas* lysosome-related organelles. *Proceedings of the National Academy of Sciences*, *118*(16), 2026811118. https://doi.org/10.1073/pnas.2026811118

Schoffman, Lis, Shaked, & Keren. (2016). Iron-nutrient interactions within phytoplankton. *Frontiers in Plant Science*, *7*(AUG2016), 12. https://doi.org/10.3389/fpls.2016.01223

Schroda, Hemme, & Mühlhaus. (2015). The Chlamydomonas heat stress response. *The Plant Journal*, *82*(3), 466–480. https://doi.org/10.1111/TPJ.12816

Schvartzman, Corso, Fataftah, Scheepers, Ecile Nouet, Bosman, Carnol, Motte, Verbruggen, & Hanikenne. (2018). Adaptation to high zinc depends on distinct mechanisms in metallicolous populations of Arabidopsis halleri. *New Phytologist*, *218*, 269–282. https://doi.org/10.1111/nph.14949

Scott, & Hayward. (1953). Metabolic factors influencing the sodium and potassium distribution in Ulva lactuca. *The Journal of General Physiology*, *36*(5), 659–671. https://doi.org/10.1085/jgp.36.5.659

Scott, Ladejobi, Amer, Bentley, Biernaskie, Boden, Clark, Dell'Acqua, Dixon, Filippi, Fradgley, Gardner, Mackay, O'Sullivan, Percival-Alwyn, Roorkiwal, Singh, Thudi, Varshney, … Mott. (2020). Multi-parent populations in crops: a toolbox integrating genomics and genetic mapping with breeding. *Heredity 2020 125:6*, *125*(6), 396–416. https://doi.org/10.1038/s41437-020-0336-6

Sekiguchi, Kameda, Kurosawa, Yoshida, & Yoshimura. (2018). Thermotaxis in Chlamydomonas is brought about by membrane excitation and controlled by redox conditions. *Scientific Reports*, *8*(1). https://doi.org/10.1038/s41598-018-34487-4

Shelton, Leslie, & Michod. (2017). Models of cell division initiation in Chlamydomonas: A challenge to the consensus view. *Journal of Theoretical Biology*, *412*, 186–197. https://doi.org/10.1016/j.jtbi.2016.10.018

Shen. (2015). The Structure of Photosystem II and the Mechanism of Water Oxidation in Photosynthesis PSII: photosystem II. *Annu. Rev. Plant Biol*, *66*, 23–48. https://doi.org/10.1146/annurev-arplant-050312-120129

Shih, Engel, Kocabas, Bilyard, Gennerich, Marshall, & Yildiz. (2013). Intraflagellar transport drives flagellar surface motility. *ELife*, *2013*(2). https://doi.org/10.7554/ELIFE.00744

Siao, Borner, Perkins, Deitsch, & Kirkman. (2020). Evolution of Host Specificity by Malaria Parasites through Altered Mechanisms Controlling Genome Maintenance. *MBio*, *11*(2). https://doi.org/10.1128/mBio.03272-19

Siaut, Cuiné, Cagnon, Fessler, Nguyen, Carrier, Beyly, Beisson, Triantaphylidès, Li-Beisson, & Peltier. (2011). Oil accumulation in the model green alga Chlamydomonas reinhardtii: Characterization, variability between common laboratory strains and relationship with starch reserves. *BMC Biotechnology*, *11*(7). https://doi.org/10.1186/1472-6750-11-7

Singh, & Singh. (2015). Mapping Populations. In *Marker-Assisted Plant Breeding: Principles and Practices* (pp. 125–150). Springer India. https://doi.org/10.1007/978-81-322-2316-0_5

Smith. (1946). The Nature of Sexuality in Chlamydomonas. *American Journal of Botany*, *33*(8), 625–630. https://doi.org/10.2307/2437342

Smith, & Regnery. (1950). Inheritance of Sexuality in Chlamydomonas Reinhardi. *Proceedings of the National Academy of Sciences*, *36*(4), 246–248. https://doi.org/10.1073/pnas.36.4.246

Snell. (1985). Cell-Cell Interactions in Chlamydomonas. *Annual Review of Plant Physiology*, *36*(1), 287–315. https://doi.org/10.1146/annurev.pp.36.060185.001443

Snell, Eskue, & Buchanan. (1989). Regulated Secretion of a Serine Protease that Activates an Extracellular Matrix-degrading Metalloprotease during Fertilization in Chlamydomonas. *J. Cell Biol*, *108*, 199–207. http://rupress.org/jcb/article-pdf/109/4/1689/1058389/1689.pdf

Socha, & Guerinot. (2014). Mn-euvering manganese: The role of transporter gene family members in manganese uptake and mobilization in plants. In *Frontiers in Plant Science* (Vol. 5, Issue APR). Frontiers Research Foundation. https://doi.org/10.3389/fpls.2014.00106

Sommer, Kropat, Malasarn, Grossoehme, Chen, Giedroc, & Merchant. (2010). The CRR1 Nutritional Copper Sensor in Chlamydomonas Contains Two Distinct Metal-Responsive Domains. *Plant Cell*, *22*, 4098–4113. https://doi.org/10.1105/tpc.110.080069

Srivastava, & Kumar. (2018). Prediction of zinc binding sites in proteins using sequence derived information. *Journal of Biomolecular Structure and Dynamics*, *36*(16), 4413–4423. https://doi.org/10.1080/07391102.2017.1417910/SUPPL_FILE/TBSD_A_1417910_SM7888.DOCX

Stadlmeier, Hartl, & Mohler. (2018). Usefulness of a multiparent advanced generation intercross population with a greatly reduced mating design for genetic studies in winter wheat. *Frontiers in Plant Science*, *871*, 1825. https://doi.org/10.3389/FPLS.2018.01825/BIBTEX

Stapley, Feulner, Johnston, Santure, & Smadja. (2017). Variation in recombination frequency and distribution across eukaryotes: patterns and processes. *Philosophical Transactions of the Royal Society B: Biological Sciences*, *372*(1736). https://doi.org/10.1098/RSTB.2016.0455

Subbarao, Ito, Berry, & Wheeler. (2003). Sodium - A Functional Plant Nutrient. In *Critical Reviews in Plant Sciences* (Vol. 22, Issue 5, pp. 391–416). https://doi.org/10.1080/07352680390243495

Sueoka. (1960). Mitotic replication of deoxyribonucleic acid in Chlamydomonas reinhardi. *Proceedings of the National Academy of Sciences*, *46*(1), 83–91. https://doi.org/10.1073/pnas.46.1.83

Sul, Martin, & Eskin. (2018). Population structure in genetic studies: Confounding factors and mixed models. *PLOS Genetics*, *14*(12), e1007309. https://doi.org/10.1371/JOURNAL.PGEN.1007309

Sutera, Tolone, Mastrangelo, di Gerlando, Sardina, Portolano, Pong-Wong, & Riggio. (2021). Detection of genomic regions underlying milk production traits in Valle del Belice dairy sheep using regional heritability mapping. *Journal of Animal Breeding and Genetics*, *138*(5), 552–561. https://doi.org/10.1111/JBG.12552

Sved, & Hill. (2018). One Hundred Years of Linkage Disequilibrium. *Genetics*, *209*(3), 629–636. https://doi.org/10.1534/GENETICS.118.300642

Tamás, & Martinoia. (2006). *Molecular Biology of Metal Homeostasis and Detoxification: From Microbes to Man*. Springer Berlin Heidelberg.

Tamiya. (1963). Synchronous Cultures of Algae. *Phycologia*, *2*(4), 135–147. https://doi.org/10.2216/i0031-8884-2-4-135.1

Tan, Smith, Hixson, Tan, McCarthy, Kustka, & Allen. (2020). The Importance of Protein Phosphorylation for Signaling and Metabolism in Response to Diel Light Cycling and Nutrient Availability in a Marine Diatom. *Biology 2020, Vol. 9, Page 155*, *9*(7), 155. https://doi.org/10.3390/BIOLOGY9070155

Teichler-Zallen. (1969). The Effect of Manganese on Chloroplast Structure and Photosynthetic Ability of *Chlamydomonas reinhardi*. *Plant Physiology*, *44*(5), 701–710. https://doi.org/10.1104/pp.44.5.701

Terauchi, Peers, Kobayashi, Niyogi, & Merchant. (2010). Trophic status of Chlamydomonas reinhardtii influences the impact of iron deficiency on photosynthesis. *Photosynthesis Research*, *105*(1), 39–49. https://doi.org/10.1007/s11120-010-9562-8

Theeuwen, Logie, Harbinson, & Aarts. (2022). Genetics as a key to improving crop photosynthesis. *Journal of Experimental Botany*, *73*(10), 3122–3137. https://doi.org/10.1093/JXB/ERAC076

Thiébaut, & Hanikenne. (2022). Zinc deficiency responses: bridging the gap between Arabidopsis and dicotyledonous crops. *Journal of Experimental Botany*, *73*(6), 1699–1716. https://doi.org/10.1093/JXB/ERAB491

Thiriet-Rupert, Gain, Jadoul, Vigneron, Bosman, Carnol, Motte, Cardol, Nouet, & Hanikenne. (2021a). Long-term acclimation to cadmium exposure reveals extensive phenotypic plasticity in Chlamydomonas. *Plant Physiology*, *187*(3), 1653–1678. https://doi.org/10.1093/plphys/kiab375

Thiriet-Rupert, Gain, Jadoul, Vigneron, Bosman, Carnol, Motte, Cardol, Nouet, & Hanikenne. (2021b). Long-term acclimation to cadmium exposure reveals extensive phenotypic plasticity in Chlamydomonas. *Plant Physiology*, *187*(3), 1653–1678. https://doi.org/10.1093/PLPHYS/KIAB375

Tierney, Cook, McBain, & Fay. (2021). *naniar: Data Structures, Summaries, and Visualisations for Missing Data*.

Tietel, Wikoff, Kind, Ma, & Fiehn. (2020). Hyperosmotic stress in Chlamydomonas induces metabolomic changes in biosynthesis of complex lipids. *European Journal of Phycology*, *55*(1), 11–29. https://doi.org/10.1080/09670262.2019.1637547/SUPPL_FILE/TEJP_A_1637547_SM1458.PNG

Tsednee, Castruita, Salomé, Sharma, Lewis, Schmollinger, Strenkert, Holbrook, Otegui, Khatua, Das, Datta, Chen, Ramon, Ralle, Weber, Stemmler, Pett-Ridge, Hoffman, & Merchant. (2019). Manganese co-localizes with calcium and phosphorus in Chlamydomonas acidocalcisomes and is mobilized in manganese-deficient conditions. *Journal of Biological Chemistry*, *294*(46), 17626–17641. https://doi.org/10.1074/jbc.RA119.009130

Umen, & Coelho. (2019). Algal Sex Determination and the Evolution of Anisogamy. *Https://Doi.Org/10.1146/Annurev-Micro-020518-120011*, *73*, 267–291. https://doi.org/10.1146/ANNUREV-MICRO-020518-120011

Umen, & Olson. (2012). Genomics of Volvocine Algae. *Advances in Botanical Research*, *64*, 185. https://doi.org/10.1016/B978-0-12-391499-6.00006-2

Urzica, Casero, Yamasaki, Hsieh, Adler, Karpowicz, Blaby-Haas, Clarke, Loo, Pellegrini, & Merchanta. (2012). Systems and Trans-system level analysis identifies conserved iron deficiency responses in the plant lineage. *Plant Cell*, *24*(10), 3921–3948. https://doi.org/10.1105/TPC.112.102491/DC1

Urzica, Vieler, Hong-Hermesdorf, Page, Casero, Gallaher, Kropat, Pellegrini, Benning, & Merchant. (2013). Remodeling of membrane lipids in iron-starved Chlamydomonas. *The Journal of Biological Chemistry*, *288*(42), 30246–30258. https://doi.org/10.1074/jbc.M113.490425

Valdar, Flint, & Mott. (2006a). Simulating the Collaborative Cross: Power of Quantitative Trait Loci Detection and Mapping Resolution in Large Sets of Recombinant Inbred Strains of Mice. *Genetics*, *172*(3), 1783–1797. https://doi.org/10.1534/GENETICS.104.039313

Valdar, Flint, & Mott. (2006b). Simulating the Collaborative Cross: Power of Quantitative Trait Loci Detection and Mapping Resolution in Large Sets of Recombinant Inbred Strains of Mice. *Genetics*, *172*(3), 1783–1797. https://doi.org/10.1534/GENETICS.104.039313

van Ooijen. (1999). LOD significance thresholds for QTL analysis in experimental populations of diploid species. *Heredity*, *83*(5), 613–624. https://doi.org/10.1038/sj.hdy.6886230

VanWallendael, Lowry, & Hamilton. (2022). One hundred years into the study of ecotypes, new advances are being made through large-scale field experiments in perennial plant systems. *Current Opinion in Plant Biology*, *66*, 102152. https://doi.org/10.1016/J.PBI.2021.102152

Verret, Wheeler, Taylor, Farnham, & Brownlee. (2010). Calcium channels in photosynthetic eukaryotes: implications for evolution of calcium-based signalling. *New Phytologist*, *187*(1), 23–43. https://doi.org/10.1111/J.1469-8137.2010.03271.X

Vert, Briat, & Curie. (2001). Arabidopsis IRT2 gene encodes a root-periphery iron transporter. *The Plant Journal*, *26*(2), 181–189. https://doi.org/10.1046/J.1365-313X.2001.01018.X

Ves-urai, Krobthong, Thongsuk, Roytrakul, & Yokthongwattana. (2021). Comparative secretome analysis between salinity-tolerant and control Chlamydomonas reinhardtii strains. *Planta*, *253*(3), 1–17. https://doi.org/10.1007/S00425-021-03583-7/FIGURES/5

Vilarrasa-Blasi, Vellosillo, Jinkerson, Fauser, Xiang, Minkoff, Wang, Kniazev, Guzman, Osaki, Sussman, Jonikas, & Dinneny. (n.d.). Identification of green lineage osmotic stress pathways. *BioRxiv*. https://doi.org/10.1101/2021.07.19.453009

Violle, Enquist, McGill, Jiang, Albert, Hulshof, Jung, & Messier. (2012). The return of the variance: Intraspecific variability in community ecology. *Trends in Ecology and Evolution*, *27*(4), 244–252. https://doi.org/10.1016/j.tree.2011.11.014

Wada, Oku, Nagano, Isobe, Suzuki, Mori, Takata, Hirata, Shimomura, Tsubone, Katayama, Hirashima, Uchimura, Ikegami, Sueyoshi, Obu, Hayashida, & Shibato. (2017). Development and characterization of a strawberry MAGIC population derived from crosses with six strawberry cultivars. *Breeding Science*, *67*(4), 370–381. https://doi.org/10.1270/JSBBS.17009

Wakao, Shih, Guan, Schackwitz, Ye, Patel, Shih, Dent, Chovatia, Sharma, Martin, Wei, & Niyogi. (2021a). Discovery of photosynthesis genes through whole-genome sequencing of acetate-requiring mutants of Chlamydomonas reinhardtii. *PLOS Genetics*, *17*(9), e1009725. https://doi.org/10.1371/JOURNAL.PGEN.1009725

Wakao, Shih, Guan, Schackwitz, Ye, Patel, Shih, Dent, Chovatia, Sharma, Martin, Wei, & Niyogi. (2021b). Discovery of photosynthesis genes through whole-genome sequencing of acetate-requiring mutants of Chlamydomonas reinhardtii. *PLoS Genetics*, *17*(9). https://doi.org/10.1371/JOURNAL.PGEN.1009725

Wang, Johnson, Cavaiuolo, Bohne, Nickelsen, & Vallon. (2015). Two Chlamydomonas OPR proteins stabilize chloroplast mRNAs encoding small subunits of photosystem II and cytochrome b6f. *The Plant Journal*, *82*(5), 861–873. https://doi.org/10.1111/TPJ.12858

Warringer, Zörgö, Cubillos, Zia, Gjuvsland, Simpson, Forsmark, Durbin, Omholt, Louis, Liti, Moses, Blomberg, Zö Rgö, Cubillos, Zia, & Gjuvsland. (2011). Trait variation in yeast is defined by population history. *PLoS Genetics*, *7*(6), e1002111. https://doi.org/10.1371/journal.pgen.1002111

Wei, & Xu. (2016). A random-model approach to QTL mapping in multiparent advanced generation intercross (MAGIC) populations. *Genetics*, *202*(2), 471–486. https://doi.org/10.1534/GENETICS.115.179945/-/DC1

Weigel. (2012). Natural Variation in Arabidopsis: From Molecular Genetics to Ecological Genomics. *Plant Physiology*, *158*(1), 2–22. https://doi.org/10.1104/PP.111.189845

Wellburn. (1994). The Spectral Determination of Chlorophylls a and b, as well as Total Carotenoids, Using Various Solvents with Spectrophotometers of Different Resolution. *Journal of Plant Physiology*, *144*(3), 307–313. https://doi.org/10.1016/S0176-1617(11)81192-2

Werner, & Mergenhagen. (1998). Mating Type Determination of Chlamydomonas reinhardtii by PCR. *Plant Molecular Biology Reporter*, *16*, 295–299.

Wheeler, Miranda-Saavedra, & Barton. (2008). Genome analysis of the unicellular green alga Chlamydomonas reinhardtii indicates an ancient evolutionary origin for key pattern recognition and cell-signaling protein families. *Genetics*, *179*(1), 193–197. https://doi.org/10.1534/genetics.107.085936

White, & Veneklaas. (2012). Nature and nurture: The importance of seed phosphorus content. *Plant and Soil*, *357*(1), 1–8. https://doi.org/10.1007/S11104-012-1128-4/TABLES/2

Wickham. (2007). Reshaping Data with the {reshape} Package. *Journal of Statistical Software*, *21*(12), 1–20. http://www.jstatsoft.org/v21/i12/

Wickham, Averick, Bryan, Chang, McGowan, François, Grolemund, Hayes, Henry, Hester, Kuhn, Pedersen, Miller, Bache, Müller, Ooms, Robinson, Seidel, Spinu, … Yutani. (2019). Welcome to the {tidyverse}. *Journal of Open Source Software*, *4*(43), 1686. https://doi.org/10.21105/joss.01686

Wickham, Henry, Pedersen, Luciani, Decorde, & Lise. (2021). *svglite: An "SVG" Graphics Device*. https://cran.r-project.org/package=svglite

Wickham, & Seidel. (2020). *scales: Scale Functions for Visualization*.

Williams. (2015). Plant Nutrition 3: Micronutrients and metals. *The Plant Cell*, *27*(5), tpc.115.tt0515. https://academic.oup.com/plcell/article/doi/10.1105/tpc.115.tt0515/6096522

Xu. (2013). *Principles of Statistical Genomics*. Springer New York. https://doi.org/10.1007/978-0-387-70807-2

Yadavalli, Jolley, Malleda, Thangaraj, Fromme, & Subramanyam. (2012). Alteration of Proteins and Pigments Influence the Function of Photosystem I under Iron Deficiency from Chlamydomonas reinhardtii. *PLOS ONE*, *7*(4), e35084. https://doi.org/10.1371/JOURNAL.PONE.0035084

Yan, Zhao, Yu, Wang, Khattak, & Tian. (2020). Development of a multiparent advanced generation intercross (MAGIC) population for genetic exploitation of complex traits in Brassica juncea: Glucosinolate content as an example. *Plant Breeding*, *139*(4), 779–789. https://doi.org/10.1111/PBR.12820

Yang, Edmondson, Piepho, Powell, & Mackay. (2021). Crafting for a better MAGIC: Systematic design and test for multiparental advanced generation inter-cross population. *G3: Genes, Genomes, Genetics*, *11*(11). https://doi.org/10.1093/g3journal/jkab295

Yildiz, Davies, & Grossman. (1994). Characterization of Sulfate Transport in Chlamydomonas reinhardtii during Sulfur-Limited and Sulfur-Sufficient Growth. *Plant Physiology*, *104*(3), 981. https://doi.org/10.1104/PP.104.3.981

Yoshimura, Matsuo, & Kamiya. (2003). Gravitaxis in Chlamydomonas reinhardtii Studied with Novel Mutants. *Plant and Cell Physiology*, *44*(10), 1112–1118. https://doi.org/10.1093/PCP/PCG134

Yu, Danku, Baxter, Kim, Vatamaniuk, Vitek, Ouzzani, & Salt. (2012). High-resolution genome-wide scan of genes, gene-networks and cellular systems impacting the yeast ionome. *BMC Genomics*, *13*(1). https://doi.org/10.1186/1471-2164-13-623

Zhang, Bendif, Zhou, Nevado, Shafiee, & Rickaby. (2022a). Declining metal availability in the Mesozoic seawater reflected in phytoplankton succession. *Nature Geoscience 2022*, 1–10. https://doi.org/10.1038/s41561-022-01053-7

Zhang, Pazouki, Nguyen, Jacobshagen, Bigge, Xia, Mattoon, Klebanovych, Sorkin, Nusinow, Avasthi, Czymmek, & Zhang. (2022b). Comparative Phenotyping of Two Commonly Used Chlamydomonas reinhardtii Background Strains: CC-1690 (21gr) and CC-5325 (The CLiP Mutant Library Background). *Plants 2022, Vol. 11, Page 585*, *11*(5), 585. https://doi.org/10.3390/PLANTS11050585

Zhao, Aranzana, Kim, Lister, Shindo, Tang, Toomajian, Zheng, Dean, Marjoram, & Nordborg. (2007). An Arabidopsis Example of Association Mapping in Structured Samples. *PLOS Genetics*, *3*(1), e4. https://doi.org/10.1371/JOURNAL.PGEN.0030004

VII. Annex

A. Review article

I contributed to the writing of this review by synthesizing known information on the interaction between iron (Fe) and other nutrients in algae. I thus wrote the entirety of the section entitled “Box1. Fe and nutrient interplay in eukaryotic algae”. I was interested in describing diversity of Fe uptake strategies in micro- and macroalgae, as well as the interaction of Fe with other nutrients [such as copper (Cu) and calcium (Ca)] in fresh and saltwater algae.

Journal of Experimental Botany, Vol. 72, No. 6 pp. 2136–2153, 2021
doi:10.1093/jxb/eraa483 Advance Access Publication 11 November 2020

REVIEW PAPER

Coordinated homeostasis of essential mineral nutrients: a focus on iron

Marc Hanikenne[1,*], Sara M. Esteves[1], Steven Fanara[1] and Hatem Rouached[2,3,4]

[1] InBioS – PhytoSystems, Functional Genomics and Plant Molecular Imaging, University of Liège, 4000 Liège, Belgium
[2] BPMP, Univ. Montpellier, CNRS, INRA, Montpellier SupAgro, Montpellier, France
[3] Department of Plant, Soil, and Microbial Sciences, Michigan State University, East Lansing, MI 48824, USA
[4] Plant Resilience Institute, Michigan State University, East Lansing, MI 48824, USA

* Correspondence: marc.hanikenne@uliege.be

Received 15 June 2020; Editorial decision 9 October 2020; Accepted 13 October 2020

Editor: Janneke Balk, John Innes Centre, UK

Abstract

In plants, iron (Fe) transport and homeostasis are highly regulated processes. Fe deficiency or excess dramatically limits plant and algal productivity. Interestingly, complex and unexpected interconnections between Fe and various macro- and micronutrient homeostatic networks, supposedly maintaining general ionic equilibrium and balanced nutrition, are currently being uncovered. Although these interactions have profound consequences for our understanding of Fe homeostasis and its regulation, their molecular bases and biological significance remain poorly understood. Here, we review recent knowledge gained on how Fe interacts with micronutrient (e.g. zinc, manganese) and macronutrient (e.g. sulfur, phosphate) homeostasis, and on how these interactions affect Fe uptake and trafficking. Finally, we highlight the importance of developing an improved model of how Fe signaling pathways are integrated into functional networks to control plant growth and development in response to fluctuating environments.

Keywords: Algae, ion signaling crosstalk, iron, iron deficiency, iron uptake, nicotianamine, nutrient interaction, mugineic acid, root growth

Introduction

Iron (Fe) is an essential element for all living organisms (Kobayashi and Nishizawa, 2012). Plants and algae are an important source of Fe entry into terrestrial and aquatic food webs, respectively. However, although it is abundant in the environment, Fe is poorly available to plants in soils (Marschner, 2012), and hence Fe deficiency is a major issue limiting crop productivity, as well as the quality of agricultural products. Similarly, algal primary productivity is severely impaired by low Fe availability in the open ocean (Sunda *et al.*, 1991; Strzepek and Harrison, 2004). Consequently, Fe deficiency threatens human health. Indeed, according to the World Health Organization (http://www.who.int/nutrition/en/), one-third of the human population worldwide is affected by Fe deficiency anemia. Therefore, there is an urgent need to better understand how photosynthetic organisms regulate Fe homeostasis.

In plant cells, while Fe can also be found in substantial amounts in the nucleolus (Roschzttardtz *et al.*, 2011), up to 80% of cellular Fe is found in chloroplasts in leaves (Terry and

Abadia, 1986), and Fe represents >60% of micronutrients in plant mitochondria (Tan *et al.*, 2010), where it is found associated to heme and iron–sulfur clusters or as a cation. Photosynthesis and respiration therefore require adequate Fe supply and are highly sensitive to Fe deficiency (Nouet *et al.*, 2011; Hanikenne *et al.*, 2014; Vigani and Hanikenne, 2018). Adequate Fe supply is also required for several developmental processes, including, for instance, root growth, flowering, and pollen production (Briat *et al.*, 2015*a*; Bouain *et al.*, 2019*b*). Fe deficiency is thus deleterious for the functioning of plant cells. In contrast, the redox properties that make Fe an essential cofactor of multiple biological processes can be harmful when Fe is delivered to cells in excessive amounts or if its interactions with biological macromolecules are uncontrolled (Stohs and Bagchi, 1995; Marschner, 2012). Therefore, plants possess sophisticated mechanisms, referred to as Fe homeostasis, to adjust, within a range of Fe supply, Fe uptake and distribution to needs throughout their development and upon changes in their environment (Kobayashi and Nishizawa, 2012; Thomine and Vert, 2013; and this special issue).

In addition to Fe, 13 mineral (micro- and macro-) elements are also essential for plant growth and development, and five others are considered beneficial (Marschner, 2012). Plants require an optimal and properly balanced supply of these elements. Nevertheless, in nature, plants can encounter multiple combinations of nutrient excesses and/or limitations. So far, the bulk of experimental studies have mainly focused on the responses of plants to variation in the supply of a single element. This enables the detailed dissection of the molecular homeostasis mechanisms for these elements, identifying transporters, chelators, assimilation pathways, as well as a number of (transcriptional) regulators and to a lesser extent sensing and signaling mechanisms. More recently, research has opened into the investigation of interactions between nutrient homeostatic networks at the molecular level, revealing (i) multiple kinds of nutrient inter-dependency—an element may be required for the proper uptake of another, deficiency or excess of one element impacts positively or negatively on the uptake of another, and elements share pathways (e.g. transporters or chelators with broad specificity) or regulatory processes—and (ii) hidden responses that are more than the addition of single stress responses (Bouain *et al.*, 2019*b*). Those networks need to be examined in more detail to better comprehend the challenges faced by plants in their natural environments during their lifetime. This will enable the design of integrated and sustainable approaches to ensure plant production and quality.

Here, we present recent findings on the role of Fe in regulating complex developmental processes in plants, with a focus on the regulation of primary root growth. We then review our current knowledge of the molecular mechanisms orchestrating homeostatic interactions of Fe with other micro- and macronutrients in vascular plants, pinpointing whenever possible commonalities and differences between monocots and dicots. Finally, we also present a brief overview of those interactions in algae in comparison with higher plants, highlighting originalities found in algae (Box 1). Gaining new insights into how plants regulate Fe homeostasis will likely help to improve crop production on Fe-poor soils and to meet the challenge of global population growth and increasing demand for biofortified food.

Regulation of primary root growth by iron availability

Fe uptake from the soil is mediated by the root system (Dubeaux *et al.*, 2015). Root-related processes are major targets of responses to changing Fe availability in the rhizosphere (Fig. 1). Fe deficiency or excess imposes drastic changes on the root system architecture, which varies within and between plant species (Gruber *et al.*, 2013). This supports the potential for discovering key genes and signaling pathways by screening for phenotypic diversity in Fe stress responses across plant ecotypes and accessions, using quantitative genetic approaches (Dubeaux *et al.*, 2015; Rouached and Rhee, 2017). Recently, genome-wide association studies (GWAS) were employed in the discovery of genes underpinning the root architecture in response to either Fe limitation or Fe excess, in the model plant *Arabidopsis thaliana* (Arabidopsis). *FERRIC REDUCTASE OXIDASE 2* (*FRO2*) was indeed identified as a gene responsible for the regulation of primary root growth in response to Fe deficiency (Satbhai *et al.*, 2017). Primary root growth variation in Fe-deficient conditions is explained by sequence variation of the *FRO2* locus that causes differential gene expression, as well as ferric-chelate reductase activity (Satbhai *et al.*, 2017). The same GWAS approaches were used more recently to identify additional genes involved in the control of root growth rate in response to Fe deficiency in Arabidopsis. Several candidate genes were identified, although their functional validation and the discovery of causal polymorphisms await future study (Bouain *et al.*, 2019*a*). GWAS has also been employed to identify loci associated with the natural variation of root growth in response to Fe toxicity. In this context, a causal gene named *S-NITROSOGLUTATHIONE-REDUCTASE* (*GSNOR*) was identified and characterized as essential in determining root growth in high Fe conditions (Li *et al.*, 2019). Plants with a non-functional *GSNOR* gene display higher Fe tolerance than plants with functional alleles. This mechanism appears to be related to the activities of a gaseous molecule, nitric oxide (NO). GSNOR likely plays a central role in NO metabolism and regulates the plant's ability to respond to cellular stress and damage (Li *et al.*, 2019). It has been proposed that in response to high Fe concentrations, the NO levels increase, impairing the tolerance of the plant roots (Li *et al.*, 2019). This mechanism is likely conserved between monocots and dicots, but it remains to be confirmed if this mechanism can be generalized to all higher plants. GSNOR and NO signaling contribute to salt stress response in the green alga *Chlamydomonas reinhardtii*, but have not been tied to Fe homeostasis (Chen *et al.*, 2016).

Box 1. Iron and nutrient interplay in eukaryotic algae

Land plants frequently come to mind when talking about photosynthetic organisms, and the heterogeneous group known as algae is often overlooked. 'Algae' is an umbrella term used to describe a polyphyletic group of (mostly aquatic and photosynthetic) eukaryotes (Prasanna and Kaushik, 2010; Brodie *et al.*, 2017) that acquired photosynthesis through primary or secondary endosymbiosis (Keeling, 2013; Brodie *et al.*, 2017). Algae produce ~50% of oxygen on earth and provide multiple ecosystem and economic services to humans (Brodie *et al.*, 2017). Their diverse evolutionary origins and diverse habitats, characterized by differences in Fe availability, give ample room for originality and innovation in homeostasis of Fe and its interactions with other nutrients. In this box, we will highlight a few examples of the peculiarities found in algae.

Fe is known to limit algal growth in marine environments (Sunda, 2012; Smetacek *et al.*, 2012; Brodie *et al.*, 2017) as well as in freshwater ecosystems (Liu *et al.*, 2018). Fe is a particularly limiting nutrient in the open ocean, the so-called high-nutrient, low-carbon areas (Boyd *et al.*, 2007; Morrissey and Bowler, 2012), leading to adaptation of the photosynthetic machinery in algae inhabiting those areas (Strzepek and Harrison, 2004; Cardol *et al.*, 2008). Fe uptake pathways are highly diversified in algae. In *Chlamydomonas reinhardtii* (Chlamydomonas), Fe^{3+} is first reduced by ferric chelate reductases, then high affinity Fe uptake is mediated by a multicopper ferroxidase that reoxidizes Fe^{2+} to Fe^{3+} and an Fe permease that transports Fe^{3+} into the cell, as occurs in yeast and mammals. This re-oxidation step, and subsequent uptake of Fe^{3+}, confers a high metal specificity to this high-affinity Fe uptake system (La Fontaine *et al.*, 2002; Herbik *et al.*, 2002; Merchant *et al.*, 2006). However, two ZIP homolog proteins, named IRT1 and IRT2, are also induced by Fe deficiency in Chlamydomonas and are expected to form a parallel pathway of Fe^{2+} transport (Hanikenne *et al.*, 2009; Urzica *et al.*, 2012). Cd exposure results in the strong induction of both uptake pathways, which enables limitation of the impact of Cd on Fe homeostasis but comes at the cost of higher Cd uptake (Thiriet-Rupert and Hanikenne, unpublished data). This response is in part controlled by the concerted action of a bHLH transcription factor and the main P_i transcriptional regulator, PHOSPHATE STARVATION RESPONSE 1 (PSR1) (Thiriet-Rupert and Hanikenne, unpublished data), an ortholog of the plant PHR1 transcription factor (Wykoff *et al.*, 1999; Rubio *et al.*, 2001; Moseley *et al.*, 2006; see main text). This indicates that, as in monocots, Fe homeostasis is impacted by other metal cations also in organisms relying partly on Fe^{3+} uptake.

Several other algal species also re-oxidize Fe^{2+} into Fe^{3+} and, in addition, possess, as in animals, transferrin-like proteins responsible for Fe^{3+} uptake (e.g. the halophyte alga *Dunaliella salina* and the sea weed *Ulva mutabilis*) (Paz *et al.*, 2007; Blaby-Haas and Merchant, 2017; De Clerck *et al.*, 2018). As with plants that export or secrete siderophores or phenolic compounds to mobilize and/or scavenge Fe^{3+} in the soil, algae also employ diverse strategies to capture Fe from their environment: using extracellular Fe-chelating proteins, such as the secreted Fe-Assimilation (FEA) 1 and FEA2 in Chlamydomonas or the plasmamembrane-anchored Fe Starvation-Inducible Protein (ISIP2a) in *Phaeodactylum tricornutum* (Allen *et al.*, 2007; Morrissey *et al.*, 2015; Blaby-Haas and Merchant, 2017); or relying on bacterial siderophores, as suggested in *U. mutabilis* and other species (Hopkinson and Morel, 2009; De Clerck *et al.*, 2018). *FEAs* and *ISIP2a* genes are induced by Fe deficiency (but not by deficiencies of other metals) (Allen *et al.*, 2007; Morrissey *et al.*, 2015), and ISIP2a was actually shown to bind Fe (Morrissey *et al.*, 2015). Whether these Fe scavenging strategies are influenced by interactions with other nutrients has not been examined in details.

Copper (Cu) and zinc (Zn) also play important roles in Fe homeostasis in algae. In several species, such as Chlamydomonas, *Thalassiosira oceanica*, and *D. salina*, multicopper oxidases (MCO) take part in high affinity Fe uptake (Maldonado *et al.*, 2006; Paz *et al.*, 2007; Blaby-Haas and Merchant, 2017). In contrast, in the marine alga *Ostreococcus tauri*, where Fe uptake is dependent on an IRT1-like protein, Zn, and not Cu, appears to be required for proper Fe-uptake and its regulation (Lelandais *et al.*, 2016). An interaction between Zn and the regulation of IRT1 also occurs in Chlamydomonas where an induction of IRT1 takes place under Zn deprivation (Blaby-Haas and Merchant, 2017). In addition, Cu-based plastocyanin and Fe-based cytochrome c_6 are interchangeable in the photosynthetic electron transfer chain in green algae such as Chlamydomonas. Upon Cu starvation, plastocyanin can be replaced by cytochrome c_6 as part of a Cu-saving program (Howe *et al.*, 2006; Merchant, 2007).

Box 1. Continued

An extreme example of this is the red alga *Cyanidioschizon merolae*, which inhabits acidic Fe-rich, low-Cu hot springs and completely lacks plactocyanin (Hanikenne *et al.*, 2005*a*). It also lacks MCOs, but possesses multiple Fe permeases (Blaby-Haas and Merchant, 2012; Hanikenne *et al.*, 2005*a*).

Cytosolic calcium (Ca) signaling was shown to be crucial for the response to changes of environmental Fe concentration in the diatom *P. tricornutum* (Falciatore *et al.*, 2000). Inside the cells, Ca interacts with Fe storage in vacuole-like acidocalcisomes in several algal species, including Chlamydomonas and the red alga *C. merolae* (Blaby-Haas and Merchant, 2014). In addition to Fe, these dense acidic organelles, made mostly of Ca and polyphosphate complexes, constitute the main storage compartment for divalent cations such as Zn, Mn, and Cd (Docampo *et al.*, 2005; Penen *et al.*, 2017; Tsednee *et al.*, 2019).

Although N availability is key for biomass production, most photosynthetic organisms cannot fix N from the massive reservoir that is atmospheric N_2 (Boyd and Peters, 2013). In soil, legumes can, however, form a symbiosis with a diazotrophic bacterium in order to fix N_2 (Mus *et al.*, 2016). Hence, the plant *Medicago truncatula* provides Fe to the symbiont, ensuring nitrogenase activity in the symbiont (González-Guerrero *et al.*, 2014; Escudero *et al.*, 2020). Algae can use different sources of N and their Fe requirement varies as a function of the N source (Raven, 1988). Indeed, diazotrophic cyanobacteria have a higher Fe requirement than algae growing on nitrate, which is superior to those growing on ammonia. Ammonia can be readily used from the medium, but nitrate reduction and N_2 fixation require Fe as cofactor and source of reductive power (Schoffman *et al.*, 2016).

Finally, P and Fe also interact both in fresh and marine water (Benitez-Nelson, 2000; Qiu *et al.*, 2020). In freshwater, both concentration and species of Fe have a significant impact on P uptake in *Scenedesmus quadricauda* (Qiu *et al.*, 2020). This contrasts with very acidic lakes, where pH is usually below 4 rendering Fe more bioavailable. There, by forming less bioavailable Fe–P complexes, Fe promotes P deficiency, even when P concentration is not limiting, possibly contributing to low primary productivity in Fe-rich acidic lakes (Spijkerman *et al.*, 2018). Algal species found in these habitats, such as *Chlamydomonas acidophila*, can tolerate an approximately 20 times higher amount of Fe compared with neutrophile species, such as Chlamydomonas (Spijkerman *et al.*, 2018).

Iron and micronutrient interactions: root uptake

The interactions of Fe homeostasis with other micronutrients, e.g. zinc (Zn) and manganese (Mn), or toxic and non-essential metal cations, e.g. cadmium (Cd), are strongly dependent on the Fe uptake mechanisms, which can come in two different flavors in plants (Fig. 2) and are even more diversified in algae (Box 1). In dicot plants such as Arabidopsis there exists a reduction-based strategy (or strategy I) where Fe^{2+} is taken-up by cells, whereas chelation and uptake of chelated Fe^{3+} (strategy II) is found in grasses (Marschner and Römheld, 1994). Both strategies, however, share many molecular actors (see below and Grillet and Schmidt, 2019). Unchelated Fe^{3+} is also taken up directly in many algae (Box 1; Blaby-Haas and Merchant, 2017). Both strategies of Fe^{2+} or Fe^{3+} uptake coexist in several species, rice and *C. reinhardtii* for instance (see below and Box 1; Blaby-Haas and Merchant, 2017; Kobayashi *et al.*, 2019). Divalent metal cations (Zn^{2+}, Mn^{2+}, Cd^{2+}) will therefore have a higher impact on Fe homeostasis in plants using the reduction strategy and Fe^{2+} uptake. For instance, Zn excess in Arabidopsis results in shoot chlorosis, reduced shoot Fe accumulation, and more generally in the induction of a secondary Fe deficiency. These Zn toxicity symptoms result from competition for uptake as well as for Fe binding sites in proteins (e.g. involved in respiration and photosynthesis), and are alleviated by elevated Fe supply (Fukao *et al.*, 2011; Shanmugam *et al.*, 2011; Zargar *et al.*, 2015; Lešková *et al.*, 2017). Conversely, Fe deficiency results in increased shoot accumulation of Zn, but also Mn and cobalt (Co) (Baxter *et al.*, 2008). Such interactions were also documented in multiple dicot species in addition to Arabidopsis (Foy *et al.*, 1978; Broadley *et al.*, 2007), for instance *Brassica rapa* (Li *et al.*, 2014) or poplar (Ariani *et al.*, 2015).

In Arabidopsis, upon acidification of the soil (Santi and Schmidt, 2009) and reduction of Fe^{3+} into Fe^{2+} by FRO2 (Robinson *et al.*, 1999), Fe^{2+} is taken up in root epidermal cells by IRON-REGULATED TRANSPORTER 1 (IRT1), a transporter of the ZINC-REGULATED AND IRON-REGULATED-LIKE PROTEINS (ZIP) family (Fig. 2A). IRT1 is a high affinity transporter but has a low specificity: in addition to Fe^{2+}, it transports a range of other divalent metal cations, including Zn^{2+}, Mn^{2+}, Co^{2+}, Ni^{2+}, and Cd^{2+} (Eide *et al.*, 1996; Vert *et al.*, 2002; Nishida *et al.*, 2011). IRT1 is a major contributor to the interaction of Fe homeostasis with other metal cations, in such a way that back-up systems are implemented in the Fe deficiency response to accommodate the IRT1-mediated non-specific uptake of non-Fe metal cations.

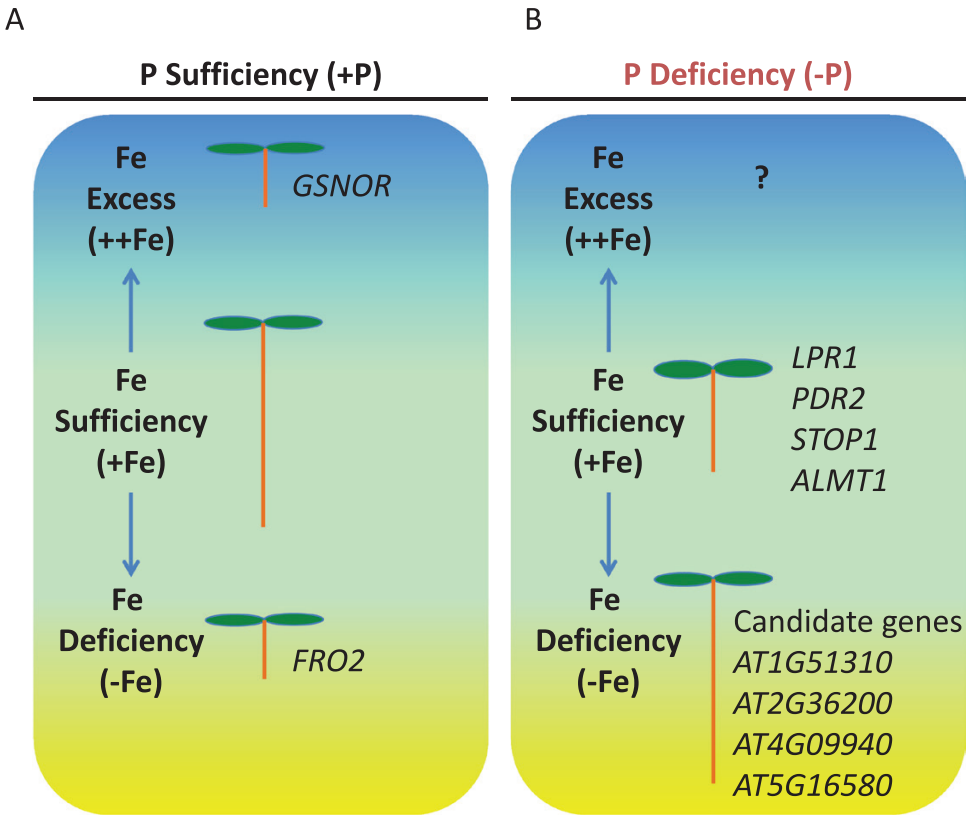

Fig. 1. Primary root growth in Arabidopsis depends on iron and phosphate availability. (A) Under phosphate sufficiency (+P), iron deficiency (–Fe) or excess (++Fe) inhibits primary root growth (PRG) compared with Fe sufficiency (+Fe). The PRG responses to –Fe and ++Fe involve the *FERRIC REDUCTASE OXIDASE 2* (*FRO2*) and *S-NITROSOGLUTATHIONE-REDUCTASE* (*GSNOR*) genes, respectively. (B) Simultaneous P deficiency (–P) and Fe sufficiency (+Fe) inhibits PRG compared with Fe sufficiency (+Fe). This response involves the cell wall-targeted FERROOXIDASE (*LPR1*), a P5-type ATPase (*PDR2*), *SENSITIVE TO PROTON RHIZOTOXICITY* (*STOP1*), encoding a transcription factor, and *ALUMINUM ACTIVATED MALATE TRANSPORTER 1* (*ALMT1*) genes. PRG is similar to Fe sufficiency upon simultaneous P (–P) and Fe (–Fe) deficiencies and this response may be controlled by the AT1G51310, AT2G36200, AT4G09940, and AT5G16580 candidate genes (Bouain *et al.*, 2019a). PRG under –P and Fe excess (++Fe) remains to be studied and is shown by a question mark.

Hence, up-regulation of *HEAVY METAL ATPASE 3* (*HMA3*; Morel *et al.*, 2009), *METAL TOLERANCE PROTEIN 3* (*MTP3*; Arrivault *et al.*, 2006), *MTP8* (Eroglu *et al.*, 2016), and *FERROPORTIN 2* (*FPN2*; Schaaf *et al.*, 2006; Morrissey *et al.*, 2009) upon Fe deficiency ensures increased vacuolar storage capacity of, respectively, Zn/Cd, Zn, Mn, and Co/Ni in root vacuoles, thus effectively limiting their toxicity in roots and their root-to-shoot translocation, whereas IRT2 ensures buffering of Fe itself in intracellular vesicles (Vert *et al.*, 2009). This back-up system is coordinated by the complex action of the master Fe deficiency regulator FER-LIKE IRON-DEFICIENCY-INDUCED TRANSCRIPTION FACTOR (FIT) and a multi-layer combination of additional transcription factors (e.g. more than 14 basic helix–loop–helix (bHLH) proteins, two MYELOBLASTOSIS (MYB)) and regulators (e.g. E3 ubiquitin ligase BRUTUS (BTS) and BTS-like targeting proteins for proteasome degradation), as well as hormonal control (e.g. by jasmonic acid, ethylene, or gibberellins) and NO signaling. These processes have been extensively detailed in recent reviews (see for instance Brumbarova *et al.*, 2015; Buet and Simontacchi, 2015; Rodríguez-Celma *et al.*, 2019; Kobayashi *et al.*, 2019; Wu and Ling, 2019; and this special issue). Recently, FIT-BINDING PROTEIN (FBP) was shown to control FIT activity, and to play an important role in fine-tuning Fe and Zn interactions (Chen *et al.*, 2018). In addition, the IRT1 protein itself is also subjected to a complex regulation by not only Fe but also by non-Fe metals (Zn, Mn, Co), at the transcriptional and post-transcriptional levels (Connolly *et al.*, 2002; Fukao *et al.*, 2011; Shanmugam *et al.*, 2011). Internalization of IRT1 from the plasma membrane upon ubiquitination followed by its recycling to the plasma membrane or its targeting for degradation in vacuoles is regulated by non-Fe metal (Zn, Mn, Co) availability to ensure proper balance between Fe uptake and the hazardous effects of excessive uptake of other divalent metals (Barberon *et al.*, 2011, 2014; Dubeaux *et al.*, 2018).

Evidence is accumulating that the broad specificity of IRT1 also plays a role in metal uptake in so-called metal hyperaccumulator plants (Krämer, 2010; Hanikenne and Nouet, 2011; Merlot *et al.*, 2018) and that IRT1 may be a major determinant of the intraspecific variation of the trait.

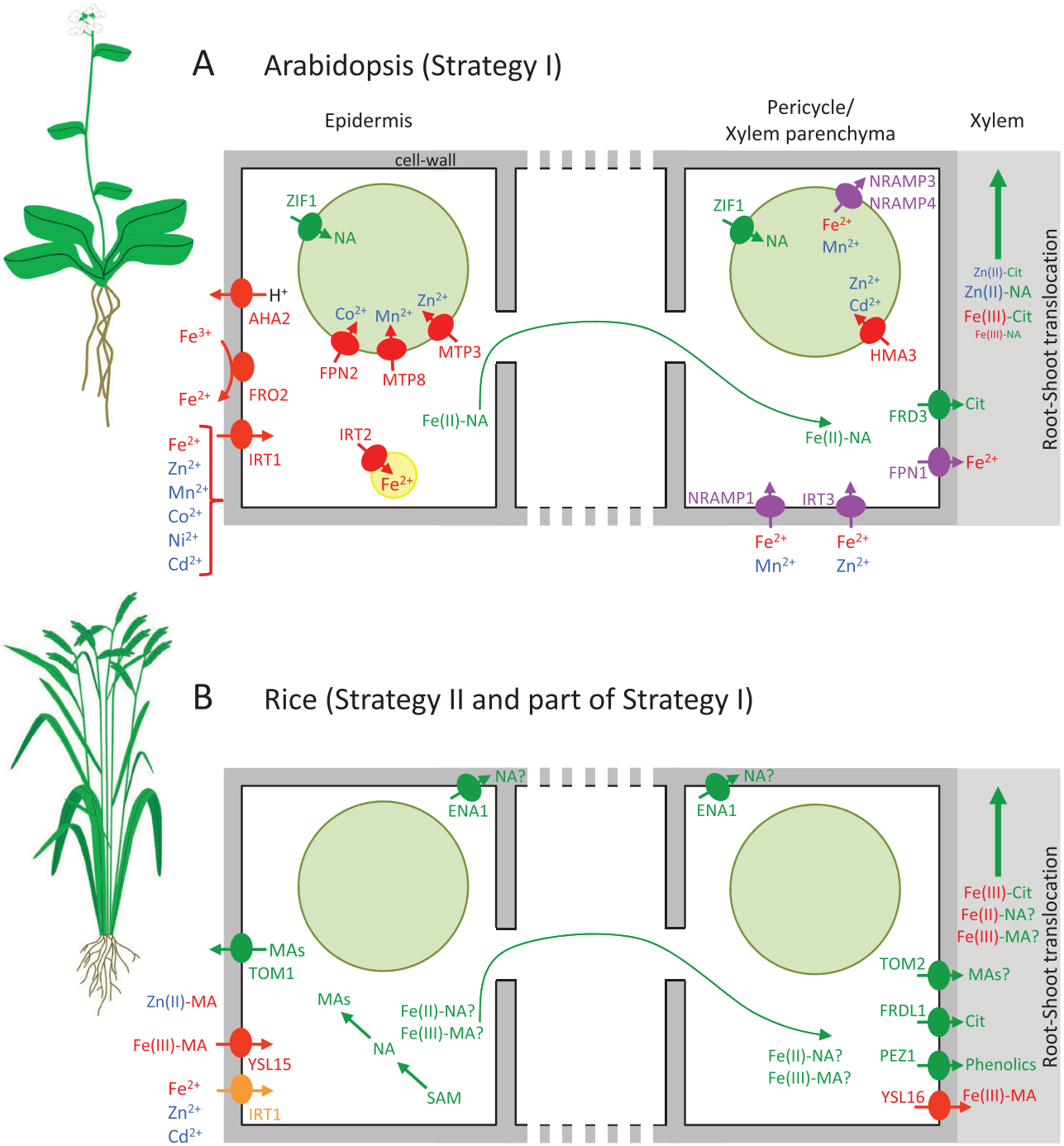

Fig. 2. Iron and micronutrient uptake and trafficking interactions in Arabidopsis and rice roots. Only the interface with the rhizosphere (left) and the xylem (right) is detailed. (A) Arabidopsis. In dicots, iron uptake from the soil relies on a reduction strategy (strategy I). The localization of IRT1 and NRAMP1 was shown to be dynamic, between plasma membrane and endo-membranes (see text). Metal ligands in the xylem, with their relative abundance represented by different font sizes, are based on data in *Pisum sativum* (Flis *et al.*, 2016). (B) Rice. In rice, as in grasses, iron uptake from the soil relies on a reduction strategy (strategy II). Rice is, however, an exception among grasses as it also uses part of strategy I. The mechanisms shared by all grasses for iron uptake are represented in red, and the function of IRT1 specific to rice is in orange. Note that the biosynthesis of mugineic acids (MAs) from *S*-adenosyl-L-methionine may take place in rough endoplasmic reticulum-derived vesicles, which are not represented here (Kobayashi *et al.*, 2019). Red: uptake processes taking place at the root epidermis, including processes related to the IRT1 lack of specificity in Arabidopsis (A); purple: intracellular and long distance trafficking processes; green: chelator- and chelator transporter-related processes. Vacuoles and vesicles are represented by green and yellow bubbles, respectively. The intracellular green arrow represents symplastic movements of metal chelates. Note that secretion of phenolics by roots into the

Indeed, variation of *IRT1* gene expression or function is linked to (i) variation in Zn and/or Cd shoot accumulation among populations of the Zn/Cd hyperaccumulators *Arabidopsis halleri* (Corso *et al.*, 2018; Schvartzman *et al.*, 2018) and *Noccaea caerulescens* (Halimaa *et al.*, 2019), and (ii) Ni shoot accumulation in Ni-hyperaccumulating populations of *N. caerulescens* (Halimaa *et al.*, 2014*a*,*b*) and in *Senecio coronatus* (Meier *et al.*, 2018). More generally, exposure to high metal levels and metal hyperaccumulation itself interfere with Fe homeostasis (Talke *et al.*, 2006; Krämer *et al.*, 2007; Lin *et al.*, 2009; Willems *et al.*, 2010; Sinclair and Krämer, 2012; Charlier *et al.*, 2015), and maintaining Fe homeostasis is thus key in hyperaccumulator species. This is achieved, in at least some populations or species, by inducing an Fe deficiency response, which mobilizes specific parts of the multi-layer regulation pathway found in Arabidopsis (Shanmugam *et al.*, 2011; Corso *et al.*, 2018; Schvartzman *et al.*, 2018).

If Fe deficiency results in Zn, Co, and Cd accumulation in Arabidopsis shoots (Col-0 accession), it has the opposite effect on shoot molybdenum (Mo) accumulation (Baxter *et al.*, 2008). Indeed, the acidification of the medium associated with strategy I Fe uptake limits Mo bioavailability (Marschner, 2012). In addition, several microRNAs initially identified as major players in Cu homeostasis (Pilon 2017) were recently shown to also be linked to Fe homeostasis, by controlling the oxidative stress response and oxidative metabolic processes (Waters *et al.*, 2012; Carrió-Seguí *et al.*, 2019).

In grasses, Fe acquisition involves the secretion of mugineic acid family (MA) phytosiderophores, high affinity Fe^{3+} chelators able to solubilize Fe from the soil (Fig. 2B) (Marschner and Römheld, 1994; Kobayashi and Nishizawa, 2012). Upon synthesis from *S*-adenosyl-L-methionine (SAM), with nicotianamine (NA, see below) as intermediate, MAs are secreted into the soil by TRANSPORTER OF MUGINEIC ACID FAMILY PHYTOSIDEROPHORES 1 (TOM1) (Nozoye *et al.*, 2011). MA–Fe(III) complexes are then taken-up by YELLOW-STRIPE 1/YS-LIKE (YS1/YSL) transporters (Curie *et al.*, 2001; Inoue *et al.*, 2009). This strategy is particularly advantageous on calcareous soils where high pH reduces strongly Fe availability (Marschner and Römheld, 1994). Many commonalities have been found between the regulation of the Fe deficiency response in dicots and grasses, including the involvement of bHLH transcription factors and E3 ubiquitin ligases, but with also some differences, including the key role of IRON DEFICIENCY-RESPONSIVE ELEMENT BINDING FACTOR 1 (IDEF1) and IDEF2 transcription factors in transcriptional regulation and Fe status sensing in rice (for detailed reviews, see Kobayashi and Nishizawa, 2012, 2015; Kobayashi *et al.*, 2019).

Rice (*Oryza sativa*) has been the most used model to uncover metal homeostasis mechanisms in grasses. However, in contrast to other graminaceous plants, it uses an Fe uptake strategy, which possibly evolved prior to rice domestication (Wairich *et al.*, 2019), combining elements of both reduction and chelation strategies, and this may have biased our view on how Fe homeostasis takes place in grasses. Indeed, OsIRT1 and OsIRT2, two proteins related to the Arabidopsis IRT1 protein (Evens *et al.*, 2017), are involved in Fe^{2+} uptake, in the absence of both acidification by H^+-ATPase and ferric-chelate reductase activity. The two corresponding genes are highly induced upon Fe deficiency. In addition to the chelation strategy, direct uptake of Fe^{2+} comes in handy in paddy fields, which have low oxygen and high Fe^{2+} levels (Ishimaru *et al.*, 2006; Cheng *et al.*, 2007). It possibly comes at a cost of specificity as overexpression of OsIRT1 in rice not only results in increased accumulation of Fe, but also of Zn and Cd in root and shoot tissues, and in higher sensitivity to high Zn and Cd exposure (Lee and An, 2009). OsIRT1 and OsIRT2 were suggested to contribute to higher Cd accumulation upon Fe deficiency (Nakanishi *et al.*, 2006). In contrast to its Arabidopsis homolog, however, the *OsIRT1* transcript level is not induced by Zn excess, suggesting a distinct impact of Zn in the two species (Ishimaru *et al.*, 2008). The combined strategy of Fe uptake is limited to rice and a few relatives (Ishimaru *et al.*, 2008; Wairich *et al.*, 2019). Although its genome contains an *IRT1* homolog (Li *et al.*, 2013; Evens *et al.*, 2017) and genes putatively encoding an H^+-ATPase and a ferric-chelate reductase (Li *et al.*, 2018), maize (*Zea mays*) is indeed strictly dependent on MA–Fe(III) uptake for Fe acquisition and survival, whereas rice plants unable to synthetize MAs are healthy when supplied with Fe^{2+} (Cheng *et al.*, 2007). An IRT1 homolog is also found in barley (Evens *et al.*, 2017), but is important for uptake of Mn, not Fe (Pedas *et al.*, 2008).

Grasses are more sensitive to Zn toxicity than dicots, especially on calcareous soils. This observation can be linked to the Fe deficiency-induced production of phytosiderophores by roots that also strongly solubilizes Zn (Chaney, 1993). MAs were indeed shown to contribute to chelation and uptake of non-Fe metals, including Zn upon Zn deficiency in the form of MA–Zn(II), in barley and maize (von Wirén *et al.*, 1996; Suzuki *et al.*, 2006). In rice, secretion of MAs upon Zn deficiency is low compared with other grasses (Suzuki *et al.*,

rhizosphere is not represented (Kobayashi *et al.*, 2019). Most of these processes are induced by iron deficiency under the control of complex and multi-layer regulatory mechanisms (see text). Hypothetical processes are labelled with a question mark. AHA2, ARABIDOPSIS H^+-ATPASE 2; Cit, citrate; ENA1, EFFLUX TRANSPORTER OF NA 1; FRD(L), FERRIC REDUCTASE DEFECTIVE(-LIKE); FPN, FERROPORTIN; FRO2, FERRIC REDUCTASE-OXIDASE 2; HMA3, HEAVY METAL ATPASE 3; IRT, IRON-REGULATED TRANSPORTER; MA: mugineic acid family phytosiderophores; MTP: METAL TOLERANCE PROTEIN; NA, nicotianamine; NRAMP: NATURAL RESISTANCE-ASSOCIATED MACROPHAGE PROTEIN; PEZ1: PHENOLICS EFFLUX ZERO 1; SAM: *S*-adenosyl-L-methionine; TOM: TRANSPORTER OF MUGINEIC ACID family phytosiderophores; YSL: YELLOW-STRIPE-LIKE; ZIF1: ZINC-INDUCED FACILITATOR 1.

2008), but appears to be sufficient to account for Zn uptake in these conditions (Arnold *et al.*, 2010; Ptashnyk *et al.*, 2011; Marković *et al.*, 2017). MAs are also involved in Zn translocation to shoot tissues in rice (Suzuki *et al.*, 2008). In many cases, overexpression of elements of the MA synthesis, secretion, uptake, or translocation pathways results in an increased Fe but also Zn content in rice grains (Bashir *et al.*, 2013).

Iron and micronutrient interactions: intracellular and long distance trafficking

In addition to uptake, Fe and micronutrient intracellular trafficking and long distance distribution within the plant is mediated by common metal chelators and (chelated) metal transporters (Fig. 2). For instance, the ZIP transporter IRT3 is a plasma membrane-located Zn and Fe transporter in Arabidopsis, and was therefore suggested to contribute to cellular uptake of Fe and Zn (Lin *et al.*, 2009). The *IRT3* gene is induced by Zn deficiency (Talke *et al.*, 2006) but not by Fe deficiency (Yang *et al.*, 2010), and its expression level, together with that of *ZIP4*, has been linked to variation of Zn deficiency tolerance among Arabidopsis accessions (Campos *et al.*, 2017). *IRT3* is also associated with a quantitative trait locus (QTL) for Fe accumulation in shoots of *A. halleri*, suggesting that it may contribute to maintenance of Fe homeostasis in the Zn/Cd hyperaccumulator (Willems *et al.*, 2010). Several other Arabidopsis ZIP transporters were shown to transport Fe and Zn (ZIP3) or to be regulated by both the Fe and Zn status of the plant (ZIP10, ZIP11, ZIP12) (Shanmugam *et al.*, 2013), but as for most ZIP transporters in plants, their individual contributions to metal homeostasis remain largely unknown (Ricachenevsky *et al.*, 2015).

Transporters of the NATURAL RESISTANCE-ASSOCIATED MACROPHAGE PROTEIN (NRAMP) family also tie Fe to other microelements, such as Mn and Zn. Indeed, the Arabidopsis NRAMP1 was shown to transport Mn and Fe in yeast (Thomine *et al.*, 2000; Curie *et al.*, 2000), and to be the main Mn uptake system in plant roots (Cailliatte *et al.*, 2010; Bian *et al.*, 2018). NRAMP1 also contributes to Fe uptake together with IRT1 (Castaings *et al.*, 2016). As with IRT1 (see above), NRAMP1 undergoes intracellular trafficking, involving a phosphatidylinositol 3-phosphate-binding protein, with a localization on endomembranes or the plasma membrane, possibly enabling the fine-tuning of Fe and Mn uptake (Agorio *et al.*, 2017). Higher expression of NRAMP1 has been associated with higher shoot Cd accumulation among rice (Takahashi *et al.*, 2011*a*,*b*) or *N. caerulescens* (Milner *et al.*, 2014) accessions. In rice and possibly other monocots, NRAMP5, primarily a Mn transporter, is a major determinant of Cd accumulation in grains (reviewed in Clemens, 2019).

NRAMP3 and NRAMP4 are two additional Fe and Mn transporters, localized in the vacuolar membrane in Arabidopsis. Together, they are essential for Fe mobilization from vacuoles during seed germination (Lanquar *et al.*, 2005), and for providing sufficient Mn for the photosynthetic apparatus in mature leaves (Lanquar *et al.*, 2010). Both proteins, furthermore, contribute to Zn and Cd tolerance by mediating appropriate Fe and Mn supply to chloroplasts, thus maintaining the photosynthetic function when exposed to Zn excess or Cd (Molins *et al.*, 2013). *NRAMP3* is overexpressed in *A. halleri* and *N. caerulescens*, suggesting a contribution to Zn/Cd hypertolerance or hyperaccumulation (Talke *et al.*, 2006; van de Mortel *et al.*, 2006; Oomen *et al.*, 2009). The *NRAMP3* gene is further associated with a Zn-tolerance QTL for photosynthetic yield in an F_2 progeny of an intraspecific cross in *A. halleri* (Karam *et al.*, 2019). The counterpart of NRAMP3 and NRAMP4 in Arabidopsis is VIT1, which is key for Fe vacuolar storage in seeds (Kim *et al.*, 2006*b*). In rice, two VIT1 homologs (OsVIT1 and OsVIT2) are vacuolar transporters of Fe and Zn, and are responsible for vacuolar storage of these metals in flag leaf blade and sheath, and consequently for controlling the transfer of both elements to grains (Zhang *et al.*, 2012).

Both inter- and intra-cellular movements of Fe and other metals (e.g. Zn, Mn) are facilitated by the production of common chelating compounds such as the organic acid citrate and NA, with which these metals form soluble complexes (Morrissey and Guerinot, 2009; Sinclair and Krämer, 2012; Flis *et al.*, 2016). In grasses, MA phytosiderophores additionally contribute to these processes (Suzuki *et al.*, 2008; Kobayashi and Nishizawa, 2012). The production and subcellular distribution of these metal chelator molecules are affected by metal availability. It is indeed well known that Fe deficiency and Zn excess both result in increased concentration of citrate in roots (i.e. in the xylem sap) (López-Millán *et al.*, 2000; Sarret *et al.*, 2002). Citrate has an optimum chelating capacity and forms more stable complexes at acidic pH (ranging from 5.5 to 6), a pH similar to that of the xylem sap (López-Millán *et al.*, 2000; Ryan *et al.*, 2001; Yoneyama *et al.*, 2015). At this pH range, Fe is transferred from cytoplasmic NA to citrate upon loading in the xylem sap as $[FeCitrateOH]^-$ and $[FeCitrate_2]^{3-}$ complexes (López-Millán *et al.*, 2000; Ryan *et al.*, 2001; Yoneyama *et al.*, 2015). Similarly, Zn–citrate complexes are also largely present in the xylem sap (Cornu *et al.*, 2015; Flis *et al.*, 2016). Citrate loading into the xylem results from the activity of the citrate effluxer FERRIC REDUCTASE DEFECTIVE 3 (FRD3), a member of the MULTIDRUG AND TOXIC EFFLUX (MATE) family (Durrett *et al.*, 2007), whose expression in Arabidopsis is induced not only upon Fe deficiency but also upon Zn excess in roots and Zn deficiency in shoots (Pineau *et al.*, 2012; Charlier *et al.*, 2015). *frd3* mutant plants are small and chlorotic, and display constitutive overexpression of the strategy I Fe uptake machinery (see above) as well accumulation of Fe, Mn, and Zn in tissues (Delhaize, 1996; Rogers and Guerinot, 2002; Green and Rogers, 2004; Durrett *et al.*, 2007). In addition to severe Fe deficiency in shoot tissues, the growth

defect of the *frd3* mutant results from Mn toxicity as well as Fe accumulation-induced reactive oxygen species production and biotic stress response (Scheepers *et al.*, 2020). Zn excess partially restores growth of the mutant, by abolishing Mn accumulation in shoot and Fe accumulation in the cell wall in roots (Scheepers *et al.*, 2020). This depicts not only the cross-talk between Fe and Zn homeostasis but also the role of FRD3 as an essential regulator of this interplay (Pineau *et al.*, 2012; Scheepers *et al.*, 2020). A homolog of FRD3 has been characterized in rice (OsFRDL1, FRD-like 1) and shares a similar function in citrate efflux to the root xylem for Fe translocation to the shoots and in Fe distribution in panicles (Inoue *et al.*, 2004; Yokosho *et al.*, 2009, 2016; Yoneyama *et al.*, 2015). However, *osfrdl1* mutants do not display severe growth phenotypes as an Arabidopsis *frd3* mutant (Yokosho *et al.*, 2009), suggesting that chelators, in addition to citrate, are important for Fe translocation to shoot in rice. Hence, PHENOLICS EFFLUX ZERO 1 (PEZ1), a MATE transporter, is responsible for phenolic compound release into the xylem in rice roots contributing to Fe mobilization and long distance Fe translocation (Ishimaru *et al.*, 2011). TOM2 (Nozoye *et al.*, 2015) and EFFLUX TRANSPORTER OF NA 1 (ENA1) (Nozoye *et al.*, 2019) are additionally required for efflux of 2′-deoxymugeneic acid and NA into the apoplasm, respectively, and also contribute to Fe mobilization in this compartment.

NA has a key function in the control of cellular metal levels in both monocots and dicots. The formation and the stability of the NA–metal complexes are optimal at pH above 6.5, suggesting that NA serves as a chelator predominately enriched within cells and phloem sap where it contributes to compartmentalization of metals and long distance transport (von Wirén *et al.*, 1999). NA is synthesized from SAM by NA SYNTHASE (NAS) enzymes (Pianelli *et al.*, 2005; Haydon and Cobbett, 2007*a*). The Arabidopsis genome contains four *NAS* genes (*AtNAS1–4*), whose expression is upregulated upon Fe or Zn deficiency, as well as Zn excess (Colangelo and Guerinot, 2004; van de Mortel *et al.*, 2006; Klatte *et al.*, 2009; Chen *et al.*, 2018). *nas4x-1* and *nas4x-2* quadruple mutants are sensitive to Fe deficiency but not Zn deficiency, and are unable to properly distribute Fe and Zn to flowers due to the drastic reduction in NA levels, thereby resulting in sterility (Klatte *et al.*, 2009; Schuler *et al.*, 2011, 2012). NA levels are a key element controlling radial movements of metals in the roots, favoring either vacuolar storage or translocation to the shoots, two processes in which Fe and Zn compete as well (Arrivault *et al.*, 2006; Haydon *et al.*, 2012; Chen *et al.*, 2018). NA overaccumulation in Arabidopsis results in increased sensitivity to Fe deficiency, but Ni resistance, as well as decreased levels of Fe in roots resulting from enhanced translocation of Fe to shoots, and Zn elevation in both roots and shoots (Pianelli *et al.*, 2005; Kim *et al.*, 2005; Cassin *et al.*, 2009, Chen *et al.*, 2018). It was also shown that an elevated production of NA is a key factor for Zn hyperaccumulation in *A. halleri* (Weber *et al.*, 2004; Uraguchi *et al.*, 2019).

Numerous proteins are involved in both the partitioning and the long distance transport of NA–metal complexes. Two major facilitator superfamily transporters, ZINC-INDUCED FACILITATOR 1 (ZIF1) and ZIF2, localize to the tonoplast where they control the vacuolar storage of NA-chelated metals (i.e. Fe^{2+}, Fe^{3+}, Zn^{2+}) in Arabidopsis (Beneš *et al.*, 1983; von Wirén *et al.*, 1999). ZIF1 plays a critical role in Zn detoxification under Fe deficiency (Haydon and Cobbett, 2007*b*), and omission of Zn from the medium partially suppresses the growth defect of the Fe-deficient *zif1-3* mutant (Haydon *et al.*, 2012). *ZIF1* expression is induced upon Zn excess (Haydon and Cobbett, 2007*b*) or Fe limitation (Haydon *et al.*, 2012). Increased vacuolar partitioning of NA through *ZIF1* overexpression leads to vacuolar Zn sequestration in roots and ultimately to decreased Zn shoot levels as a result of the impairment of both Zn symplastic mobility and xylem loading (Haydon *et al.*, 2012). *ZIF1* overexpressing plants also display reduced leaf cell-to-cell mobility of Fe, leading to constitutive symptoms of Fe deficiency (Haydon *et al.*, 2012). Higher expression of *ZIF2* upon Zn excess leads to increased Zn tolerance thanks to favored root vacuolar Zn sequestration and prevention of NA–Zn translocation to shoots (Remy *et al.*, 2014). In contrast to non-accumulator species that achieve root vacuolar sequestration of excessive metals when exposed to increased amounts of chelating compounds, hyperaccumulator species tend to favor the mobility of NA-chelated metal (i.e. Zn) towards the xylem (Deinlein *et al.*, 2012; Cornu *et al.*, 2015).

Involved in the transport of both NA–metal and MA–metal complexes in monocots, the YSL function is restricted to the mobilization of NA-chelated metals (NA–Fe, –Zn, –Ni or –Cu) in dicots (Schaaf *et al.*, 2004; Waters *et al.*, 2006; Sinclair and Krämer, 2012). In Arabidopsis, the eight YSL genes display differential patterns of regulation of Fe, Zn, and Cu deficiency and/or excess (DiDonato *et al.*, 2004; Schaaf *et al.*, 2005; Le Jean *et al.*, 2005; Waters *et al.*, 2006; Conte *et al.*, 2013). Single (*ysl1*) or double mutant (*ysl1ysl3* and *ysl4ysl6*) plants mainly display alterations of NA and metal concentrations in tissues, characterized by increased levels of Zn, Mn, and Cu, but reduced amount of Fe, in leaves, as well as a subsequent deficiency of Fe, Zn, and Cu in seeds, leading to a low fertility (Le Jean *et al.*, 2005; Waters *et al.*, 2006; Chu *et al.*, 2010; Conte *et al.*, 2013).

In addition to citrate and NA, glutathione (GSH) is known to contribute to the crosstalk between Zn and Fe homeostasis in Arabidopsis. GSH is an antioxidant contributing to the ascorbate–glutathione cycle that plays a role in Fe-mediated Zn tolerance. Indeed, a loss-of-function mutation in *GSH1*, which encodes a γ-glutamylcysteine synthetase involved in the biosynthesis of GSH, leads to increased sensitivity to Zn excess in the concomitant presence of additional Fe (Shanmugam *et al.*, 2012). GSH also links Fe and Mo homeostasis. Indeed, ABC TRANSPORTER OF THE MITOCHONDRIA 3 (ATM3) exports GSH-polysulfide out of the mitochondria and is

required for the maturation of Fe–S cytosolic enzymes and for Mo cofactor (Moco) biosynthesis (Schaedler *et al.*, 2014; Teschner *et al.*, 2010). *atm3* mutants are moreover sensitive to Cd (Hanikenne *et al.*, 2005*b*; Kim *et al.*, 2006*a*).

Interaction between iron and sulfur homeostasis

Evidence at the molecular and morphological levels in support of the interplay between Fe and sulfur (S) homeostasis is constantly growing. It has been shown that despite the presence of sufficient S in the medium, conditions of Fe deficiency lead to a S deficiency response at the molecular level in durum wheat (*Triticum turgidum* L.; Ciaffi *et al.*, 2013). Grasses (strategy II plants) respond to Fe deficiency by secreting phytosiderophores into the rhizosphere, which are required for chelation as well as for Fe uptake (see above). Interestingly, the release of these molecules is modulated by S availability: S deficiency reduces their release, whereas sulfate resupply enhances it in barley (*Hordeum vulgare* L.) (Astolfi *et al.*, 2010; Ciaffi *et al.*, 2013). On the other hand, Fe nutrition appears to affect S transport in plants, with Fe starvation increasing the expression of sulfate transporters, which enhances S uptake from the soil and influences S remobilization from the vacuole (Schuler *et al.*, 2011; Couturier *et al.*, 2013; Paolacci *et al.*, 2014; Kaur *et al.*, 2019). Fe also affects the S distribution between roots and shoots. In leaves, Fe and S are known to interact in the building of Fe–S clusters, which are a major sink for Fe and are known to be essential for photosynthetic electron transfer, chlorophyll metabolism, respiration, and many cellular enzymatic reactions (Couturier *et al.*, 2013; Kaur *et al.*, 2019). This suggests a tight coordination between the metabolisms of these two nutrients in support of vital plant biological processes. However, the mechanisms regulating the integrated homeostasis of these two elements remains to be deciphered.

While Fe limitation strongly reduces the total S content in both shoots and roots of tomato (*Solanum lycopersicum*) plants (Zuchi *et al.*, 2015), S limitation causes a decrease in the Fe concentration in leaves. For instance, tomatoes grown under S-deficient conditions display a reduction in Fe concentrations in comparison to plants grown under S-sufficient conditions. This low Fe accumulation could be explained by the reduction in Fe uptake capacity associated with a decrease in the expression and activity of the Fe uptake machinery. In dicots such as Arabidopsis, S deficiency strongly represses the expression of the high affinity Fe transporter *IRT1* (Forieri *et al.*, 2013). Interestingly, when challenged with both S and Fe starvation, the expression of *IRT1* is induced but to a lower extent compared with Fe-deficient conditions, which can be explained by a decreased requirement of Fe for Fe–S cluster synthesis under S deficiency (Forieri *et al.*, 2013). Finally, in tomato plants, the activity of Fe transporters is reduced suggesting that S deficiency prevents the typical responses to Fe deficiency (Zuchi *et al.*, 2009).

Beyond ion transport activity, Fe nutrition profoundly impacts S assimilation in both graminaceous and non-graminaceous plants (Forieri *et al.*, 2013; Briat *et al.*, 2015*b*; Bouain *et al.*, 2019*b*). For instance, in Arabidopsis, gene expression profiling has revealed that a number of genes involved in the S assimilation pathway are co-expressed with Fe-deficient genes in response to Fe deficiency (Schuler *et al.*, 2011), suggesting that Fe availability partially controls the S assimilation-related genes. This control is visible at the transcriptional, post-transcriptional, and protein activity levels. Altogether, these findings provide physiological and molecular evidence for a crosstalk between the Fe and S pathways in different plant species, with marked species specificities. These findings also reveal the presence of many transcriptional and post-transcriptional regulatory mechanisms that plants can use to adapt to Fe fluctuation by modulating their S homeostasis, and vice versa. Further investigations are now needed to decipher the molecular details of these mechanisms.

Interaction between iron and phosphate homeostasis

The interaction between Fe and phosphate (P_i) is well-recognized in soil as well as in plants (Müller *et al.*, 2007; Thibaud *et al.*, 2010; Briat *et al.*, 2015*b*; Bouain *et al.*, 2019*b*). Indeed, the complexing of Fe by P_i in the soil leads to the formation of precipitates, which decreases the availability of these two elements for plants (Briat *et al.*, 2020). While low P_i availability in soil leads to the Fe overaccumulation in plants, the converse is also true (Misson *et al.*, 2005; Hirsch *et al.*, 2006; Müller *et al.*, 2007; Thibaud *et al.*, 2010). Indeed, plants have evolved a coordinated gene expression network in order to respond jointly to element deficiencies and/or excesses. For instance, gene expression profiling of P_i-deficient plants revealed an increase in abundance of transcripts of both P_i starvation-related and Fe excess-responsive genes (Misson *et al.*, 2005; Müller *et al.*, 2007; Thibaud *et al.*, 2010). Such examples can be seen in the remarkable induction of expression of *AtFER1–4* mRNAs, which encode the Fe storage protein ferritin, accurately reflecting the increase in available Fe under P_i starvation conditions (Hirsch *et al.*, 2006). Interestingly, higher *AtFER1* expression appears to be mediated by PHOSPHATE RESPONSE 1 (PHR1) and PHR1-LIKE 1 (PHL1), key regulators of the phosphate starvation response (PSR) in plants, thus revealing a role for these transcription factors in the overall control of Fe homeostasis that is integrated with the P_i status of the plant (Bournier *et al.*, 2013; Bouain *et al.*, 2019*b*; see also Box 1). Decades of research have helped in understanding how plants respond to P_i deficiency, mainly in the roots, leading to the identification of a mechanism that is tightly linked to variation in Fe accumulation. Key genes involved in this process include those for the cell wall-targeted FERROOXIDASE (LPR1), a P5-type ATPase (PDR2), as well as the SENSITIVE TO PROTON RHIZOTOXICITY (STOP1) transcription factor and its target *ALUMINUM ACTIVATED MALATE*

TRANSPORTER 1 (*ALMT1*) (Fig. 1). PDR2 controls LPR1 activity, which mediates Fe accumulation in the root tip. STOP1 upregulates *ALMT1*, which modulates exudation of malate (Müller *et al.*, 2007; Thibaud *et al.*, 2010; Balzergue *et al.*, 2017; Mora-Macías *et al.*, 2017), consequently promoting Fe deposition in the root. Thus these genes could be considered as Fe-responsive genes, and they form two modules that act in concert to provoke Fe overaccumulation in roots, which is likely a primary cause of primary root growth inhibition under P_i deficiencies (Müller *et al.*, 2007; Ward *et al.*, 2008; Ticconi *et al.*, 2009; Thibaud *et al.*, 2010; Briat *et al.*, 2015*b*; Bouain *et al.*, 2019*b*). This is consistent with the fact that simultaneous Fe and P_i deficiencies restore primary root growth in Arabidopsis. This observation reveals that plants respond to the combined Fe and P_i stress in a manner distinct from individual Fe or P_i deficiencies (Bouain *et al.*, 2019*b*). Key genes associated with this phenotype were recently identified and include *VARIANT IN METHYLATION 1*, *FORMIN-LIKE-PROTEIN-6*, and *VOLTAGE-DEPENDENT ANION-SELECTIVE CHANNEL PROTEIN 3* (Fig. 1; Bouain *et al.*, 2019*b*). Additional candidate genes to regulate root growth under co-occurring Fe and P deficiency stress have been identified (AT1G51310, AT2G36200, AT4G09940, and AT5G16580) and await functional validation (Bouain *et al.*, 2019*b*). It is worth mentioning that a recent study showed, unexpectedly, that if P_i deficiency stimulates early root growth rate of most accessions, Fe deficiency reduces it (Bouain *et al.*, 2019*a*). The combination of both P_i and Fe deficiency leads to a suppression of the growth inhibition exerted by Fe deficiency alone. Surprisingly, the Arabidopsis accession Columbia (Col-0) is not representative of the species under P_i deficiency (Bouain *et al.*, 2019*a*), and therefore used inappropriately as reference for these stresses in the literature. Both discoveries go against the main stream of thinking and will have an impact on future research aimed at understanding plant response to nutrient deficiency. Finally, it is clear that Fe content plays not only a nutritional role in plants but also a central 'signaling' role in controlling different aspects of plant growth under other nutrient deficiencies. For example, recent work has revealed a role for Fe in regulating the number of lateral roots in response to potassium deficiency via a complex mechanism involving auxin and changes in DNA methylation (Shahzad *et al.*, 2020). In short, Arabidopsis roots exhibit increased numbers of lateral roots in response to this stress, and this response is dependent on the Fe status (Shahzad *et al.*, 2020).

Once taken up by the roots, Fe can interact with P_i, leading to a reduction in their translocation to the shoots (Cumbus *et al.*, 1977; Mathan and Amberger, 1977). In shoots, these nutrients are stored in vacuoles or distributed among organelles such as the chloroplast. It is well known that photosynthesis is severely affected by either Fe or P_i deficiency (Chen and Barak, 1982; Carstensen *et al.*, 2018). For instance, leaf Fe content correlates well with photosynthetic capacity (Terry and Abadia, 1986; Shikanai *et al.*, 2003) and Fe deficiency causes chlorosis. Intriguingly, even if the leaf Fe level is sufficient, leaves with high P_i content still show chlorosis (Dekock *et al.*, 1979). This provides further support for the interplay between Fe and P_i homeostasis in shoots. Remarkably, plants grown under a combined limitation of Fe and P_i do not show any chlorotic phenotype (Saenchai *et al.*, 2016; Shi *et al.*, 2018). Despite the importance of this phenomenon in agronomy, the characterization of Fe and P_i interactions involved in regulating photosynthesis is still in its infancy, and more research is needed to understand the complexity of how the various pathways involved are integrated. Systems genetics approaches can be used to screen for the phenotypic diversity of Fe and P_i stress responses across plant ecotypes and accessions, and would help in better understanding how plants integrate nutrient deficiency signals to control photosynthesis (Rouached and Rhee, 2017). At the end of the plant life cycle, Fe is accumulated in the seed vacuoles, where it is mainly chelated and stored via its close interaction with P_i ions from phytate (Lanquar *et al.*, 2005). Phytate content is one of the key factors in Fe remobilization during germination and seedling establishment. It has been shown that transgenic plants overexpressing bacterial phytase, an enzyme that degrades phytate, remobilize Fe faster during germination than wild type plants (Belgaroui *et al.*, 2014). From a dietary point of view for humans, phytate limits Fe, and also Zn, absorption in the intestinal tract, thereby contributing to mineral deficiencies (Gibson *et al.*, 2018). Finally, whereas it is known that Fe and P_i interact throughout the plant life cycle, our understanding of how this interaction, and the underlying molecular basis, varies between stages of plant growth and development remains limited.

Conclusion and perspectives

Fe deficiency or excess impacts plant metabolic functions, resulting in major physiological disorders that can adversely affect growth and development. We have discussed here, furthermore, that Fe homeostatic mechanisms are engaged in a wide range of interactions with other nutrients. The reductionist view of ion homeostasis regulation, in which each ion's level is controlled by its own mechanisms and signaling pathways, therefore needs to be revised (Bouain *et al.*, 2019*b*). This is even clearer when we consider the mitigated success rate of research efforts focused on improving Fe content in plants (Shahzad *et al.*, 2014). Investigating the precise molecular mechanisms coordinating Fe response pathways that shape plant developmental programs (i.e. root and shoot growth) in response to single or multiple nutrient deficiencies is topical. In this context, the existence of a tight coordination between the homeostasis of Fe and other mineral nutrients offers the potential to identify new mechanisms for Fe uptake and transport. A good example is the recent discovery of a new route for P_i transport and accumulation by the activation of a Zn deficiency signaling pathway (Bouain *et al.*, 2014; Khan *et al.*, 2014; Pal *et al.*, 2017; Kisko *et al.*, 2018). Similar to the effect of Zn deficiency on P_i accumulation, it

has been shown that Fe accumulation strongly increases in response to combined nitrogen (N) and P_i deficiencies, as compared with the small increase observed under either single P_i or single N starvation stress (Kellermeier *et al.*, 2014). Moreover, other micronutrient deficiencies (Zn or Mn for instance) often cause increased Fe uptake (and vice versa), likely because micronutrients share transport and chelation systems with lax specificities, and mechanisms ensuring the tight coordination of micronutrient homeostasis are only starting to be uncovered. In addition to proteins involved in Fe uptake, transport, and storage, genetic manipulation of mechanisms recently shown to play a role in Fe dynamics in plants is of equal importance. For example, autophagy, i.e. the recycling of cytoplasmic components via encapsulation in vesicles and subsequent degradation in the vacuole (recently reviewed in Chen *et al.*, 2019), influences Fe (and also N, Zn, and Mn) remobilization to seeds during leaf senescence (Pottier *et al.*, 2014, 2019; Shinozaki *et al.*, 2020). Hence, genetic inactivation of *AuTophaGy 5* (*ATG5*) results in a 30% reduction of Fe, as well as a 10–40% reduction of N, in Arabidopsis seeds (Pottier *et al.*, 2019; Chen *et al.*, 2019). Taken together, it is clear that designing research strategies to examine how Fe accumulation in plants is concomitantly influenced by the crosstalk of N, P_i, and other micronutrient signals will help in identifying new players involved in Fe uptake and transport. Future research efforts need to focus on the molecular basis of the coordinated Fe, micro- and macronutrient homeostatic mechanisms, which will enable integrated approaches to improving Fe accumulation in crops.

Acknowledgements

Research in the authors' laboratories is funded by the 'Fonds de la Recherche Scientifique–FNRS' (MIS-F.4511.16, CDR J.0009.17, and PDR-T0120.18 to MH), the University of Liège (ARC GreenMagic to MH) and the 'Agence Nationale de la Recherche (ANR)' (ANR-19-CE13-0007 to HR). The Michigan State University also supports HR. MH is Senior Research Associate of the FRS–FNRS and SF was a doctoral fellow of the FRIA.

Author contributions

MH and HR conceptualized the manuscript. MH, HR, SE, and SF wrote the draft manuscript. MH, HR, and SF made the figures. MH and HR reviewed and edited the manuscript.

References

Agorio A, Giraudat J, Bianchi MW, Marion J, Espagne C, Castaings L, Lelièvre F, Curie C, Thomine S, Merlot S. 2017. Phosphatidylinositol 3-phosphate-binding protein AtPH1 controls the localization of the metal transporter NRAMP1 in *Arabidopsis*. Proceedings of the National Academy of Sciences, USA **114**, E3354–E3363.

Allen MD, del Campo JA, Kropat J, Merchant SS. 2007. *FEA1*, *FEA2*, and *FRE1*, encoding two homologous secreted proteins and a candidate ferrireductase, are expressed coordinately with *FOX1* and *FTR1* in iron-deficient *Chlamydomonas reinhardtii*. Eukaryotic Cell **6**, 1841–1852.

Ariani A, Di Baccio D, Romeo S, Lombardi L, Andreucci A, Lux A, Horner DS, Sebastiani L. 2015. RNA sequencing of *Populus* × *canadensis* roots identifies key molecular mechanisms underlying physiological adaptation to excess zinc. PLoS One **10**, e0117571.

Arnold T, Kirk GJ, Wissuwa M, Frei M, Zhao FJ, Mason TF, Weiss DJ. 2010. Evidence for the mechanisms of zinc uptake by rice using isotope fractionation. Plant, Cell & Environment **33**, 370–381.

Arrivault S, Senger T, Krämer U. 2006. The Arabidopsis metal tolerance protein AtMTP3 maintains metal homeostasis by mediating Zn exclusion from the shoot under Fe deficiency and Zn oversupply. The Plant Journal **46**, 861–879.

Astolfi S, Zuchi S, Hubberten HM, Pinton R, Hoefgen R. 2010. Supply of sulphur to S-deficient young barley seedlings restores their capability to cope with iron shortage. Journal of Experimental Botany **61**, 799–806.

Balzergue C, Dartevelle T, Godon C, *et al.* 2017. Low phosphate activates STOP1-ALMT1 to rapidly inhibit root cell elongation. Nature Communications **8**, 15300.

Barberon M, Dubeaux G, Kolb C, Isono E, Zelazny E, Vert G. 2014. Polarization of IRON-REGULATED TRANSPORTER 1 (IRT1) to the plant-soil interface plays crucial role in metal homeostasis. Proceedings of the National Academy of Sciences, USA **111**, 8293–8298.

Barberon M, Zelazny E, Robert S, Conéjéro G, Curie C, Friml J, Vert G. 2011. Monoubiquitin-dependent endocytosis of the iron-regulated transporter 1 (IRT1) transporter controls iron uptake in plants. Proceedings of the National Academy of Sciences, USA **108**, E450–E458.

Bashir K, Takahashi R, Nakanishi H, Nishizawa NK. 2013. The road to micronutrient biofortification of rice: progress and prospects. Frontiers in Plant Science **4**, 15.

Baxter IR, Vitek O, Lahner B, Muthukumar B, Borghi M, Morrissey J, Guerinot ML, Salt DE. 2008. The leaf ionome as a multivariable system to detect a plant's physiological status. Proceedings of the National Academy of Sciences, USA **105**, 12081–12086.

Belgaroui N, Zaidi I, Farhat A, *et al.* 2014. Over-expression of the bacterial phytase US417 in *Arabidopsis* reduces the concentration of phytic acid and reveals its involvement in the regulation of sulfate and phosphate homeostasis and signaling. Plant & Cell Physiology **55**, 1912–1924.

Beneš I, Schreiber K, Ripperger H, Kircheiss A. 1983. Metal complex formation by nicotianamine, a possible phytosiderophore. Experientia **39**, 261–262.

Benitez-Nelson CR. 2000. The biogeochemical cycling of phosphorus in marine systems. Earth-Science Reviews **51**, 109–135.

Bian B, Kageshima S, Yano K, Fujiwara T, Kamiya T. 2018. Screening *Arabidopsis thaliana* mutants for low sensitivity to manganese identifies novel alleles of *NRAMP1* and *PGSIP6*. Journal of Experimental Botany **69**, 1795–1803.

Blaby-Haas CE, Merchant SS. 2012. The ins and outs of algal metal transport. Biochimica et Biophysica Acta **1823**, 1531–1552.

Blaby-Haas CE, Merchant SS. 2014. Lysosome-related organelles as mediators of metal homeostasis. The Journal of Biological Chemistry **289**, 28129–28136.

Blaby-Haas CE, Merchant SS. 2017. Regulating cellular trace metal economy in algae. Current Opinion in Plant Biology **39**, 88–96.

Bouain N, Korte A, Satbhai SB, Nam HI, Rhee SY, Busch W, Rouached H. 2019*a*. Systems genomics approaches provide new insights into *Arabidopsis thaliana* root growth regulation under combinatorial mineral nutrient limitation. PLoS Genetics **15**, e1008392.

Bouain N, Krouk G, Lacombe B, Rouached H. 2019*b*. Getting to the root of plant mineral nutrition: combinatorial nutrient stresses reveal emergent properties. Trends in Plant Science **24**, 542–552.

Bouain N, Shahzad Z, Rouached A, Khan GA, Berthomieu P, Abdelly C, Poirier Y, Rouached H. 2014. Phosphate and zinc transport and signalling in plants: toward a better understanding of their homeostasis interaction. Journal of Experimental Botany **65**, 5725–5741.

Bournier M, Tissot N, Mari S, Boucherez J, Lacombe E, Briat JF, Gaymard F. 2013. *Arabidopsis* ferritin 1 (*AtFer1*) gene regulation by the phosphate starvation response 1 (AtPHR1) transcription factor reveals a direct molecular link between iron and phosphate homeostasis. The Journal of Biological Chemistry **288**, 22670–22680.

Boyd ES, Peters JW. 2013. New insights into the evolutionary history of biological nitrogen fixation. Frontiers in Microbiology **4**, 201.

Boyd PW, Jickells T, Law CS, *et al.* 2007. Mesoscale iron enrichment experiments 1993-2005: synthesis and future directions. Science **315**, 612–617.

Briat J-F, Dubos C, Gaymard F. 2015*a*. Iron nutrition, biomass production, and plant product quality. Trends in Plant Science **20**, 33–40.

Briat J-F, Gojon A, Plassard C, Rouached H, Lemaire G. 2020. Reappraisal of the central role of soil nutrient availability in nutrient management in light of recent advances in plant nutrition at crop and molecular levels. European Journal of Agronomy **116**, 126069.

Briat J-F, Rouached H, Tissot N, Gaymard F, Dubos C. 2015*b*. Integration of P, S, Fe, and Zn nutrition signals in *Arabidopsis thaliana*: potential involvement of PHOSPHATE STARVATION RESPONSE 1 (PHR1). Frontiers in Plant Science **6**, 290.

Broadley MR, White PJ, Hammond JP, Zelko I, Lux A. 2007. Zinc in plants. New Phytologist **173**, 677–702.

Brodie J, Chan CX, De Clerck O, *et al.* 2017. The algal revolution. Trends in Plant Science **22**, 726–738.

Brumbarova T, Bauer P, Ivanov R. 2015. Molecular mechanisms governing *Arabidopsis* iron uptake. Trends in Plant Science **20**, 124–133.

Buet A, Simontacchi M. 2015. Nitric oxide and plant iron homeostasis. Annals of the New York Academy of Sciences **1340**, 39–46.

Cailliatte R, Schikora A, Briat JF, Mari S, Curie C. 2010. High-affinity manganese uptake by the metal transporter NRAMP1 is essential for *Arabidopsis* growth in low manganese conditions. The Plant Cell **22**, 904–917.

Campos ACAL, Kruijer W, Alexander R, Akkers RC, Danku J, Salt DE, Aarts MGM. 2017. Natural variation in *Arabidopsis thaliana* reveals shoot ionome, biomass, and gene expression changes as biomarkers for zinc deficiency tolerance. Journal of Experimental Botany **68**, 3643–3656.

Cardol P, Bailleul B, Rappaport F, *et al.* 2008. An original adaptation of photosynthesis in the marine green alga *Ostreococcus*. Proceedings of the National Academy of Sciences, USA **105**, 7881–7886.

Carrió-Seguí À, Ruiz-Rivero O, Villamayor-Belinchón L, Puig S, Perea-García A, Peñarrubia L. 2019. The altered expression of *microRNA408* influences the Arabidopsis response to iron deficiency. Frontiers in Plant Science **10**, 324.

Carstensen A, Herdean A, Schmidt SB, Sharma A, Spetea C, Pribil M, Husted S. 2018. The impacts of phosphorus deficiency on the photosynthetic electron transport chain. Plant Physiology **177**, 271–284.

Cassin G, Mari S, Curie C, Briat JF, Czernic P. 2009. Increased sensitivity to iron deficiency in *Arabidopsis thaliana* overaccumulating nicotianamine. Journal of Experimental Botany **60**, 1249–1259.

Castaings L, Caquot A, Loubet S, Curie C. 2016. The high-affinity metal Transporters NRAMP1 and IRT1 team up to take up iron under sufficient metal provision. Scientific Reports **6**, 37222.

Chaney RL. 1993. Zinc phytotoxicity. In: Robson AD, eds. Zinc in soils and plants. Developments in Plant and Soil Sciences, vol 55. Dordrecht: Springer, 135–150.

Charlier JB, Polese C, Nouet C, Carnol M, Bosman B, Krämer U, Motte P, Hanikenne M. 2015. Zinc triggers a complex transcriptional and post-transcriptional regulation of the metal homeostasis gene *FRD3* in *Arabidopsis* relatives. Journal of Experimental Botany **66**, 3865–3878.

Chen CL, Cui Y, Cui M, Zhou WJ, Wu HL, Ling HQ. 2018. A FIT-binding protein is involved in modulating iron and zinc homeostasis in *Arabidopsis*. Plant, Cell & Environment **41**, 1698–1714.

Chen Q, Shinozaki D, Luo J, *et al*. 2019. Autophagy and nutrients management in plants. Cells **8**, 1426.

Chen X, Tian D, Kong X, Chen Q, E F AA, Hu X, Jia A. 2016. The role of nitric oxide signalling in response to salt stress in *Chlamydomonas reinhardtii*. Planta **244**, 651–669.

Chen Y, Barak P. 1982. Iron nutrition of plants in calcareous soils. In: Brady NC, ed. Advances in Agronomy. Academic Press, 217–240.

Cheng L, Wang F, Shou H, *et al.* 2007. Mutation in nicotianamine aminotransferase stimulated the Fe(II) acquisition system and led to iron accumulation in rice. Plant Physiology **145**, 1647–1657.

Chu HH, Chiecko J, Punshon T, Lanzirotti A, Lahner B, Salt DE, Walker EL. 2010. Successful reproduction requires the function of Arabidopsis Yellow Stripe-Like1 and Yellow Stripe-Like3 metal-nicotianamine transporters in both vegetative and reproductive structures. Plant Physiology **154**, 197–210.

Ciaffi M, Paolacci AR, Celletti S, Catarcione G, Kopriva S, Astolfi S. 2013. Transcriptional and physiological changes in the S assimilation pathway due to single or combined S and Fe deprivation in durum wheat (*Triticum durum* L.) seedlings. Journal of Experimental Botany **64**, 1663–1675.

Clemens S. 2019. Metal ligands in micronutrient acquisition and homeostasis. Plant, Cell & Environment **42**, 2902–2912.

Colangelo EP, Guerinot ML. 2004. The essential basic helix-loop-helix protein FIT1 is required for the iron deficiency response. The Plant Cell **16**, 3400–3412.

Connolly EL, Fett JP, Guerinot ML. 2002. Expression of the IRT1 metal transporter is controlled by metals at the levels of transcript and protein accumulation. The Plant Cell **14**, 1347–1357.

Conte SS, Chu HH, Rodriguez DC, Punshon T, Vasques KA, Salt DE, Walker EL. 2013. *Arabidopsis thaliana* Yellow Stripe1-Like4 and Yellow Stripe1-Like6 localize to internal cellular membranes and are involved in metal ion homeostasis. Frontiers in Plant Science **4**, 283.

Cornu JY, Deinlein U, Höreth S, Braun M, Schmidt H, Weber M, Persson DP, Husted S, Schjoerring JK, Clemens S. 2015. Contrasting effects of nicotianamine synthase knockdown on zinc and nickel tolerance and accumulation in the zinc/cadmium hyperaccumulator *Arabidopsis halleri*. New Phytologist **206**, 738–750.

Corso M, Schvartzman MS, Guzzo F, Souard F, Malkowski E, Hanikenne M, Verbruggen N. 2018. Contrasting cadmium resistance strategies in two metallicolous populations of *Arabidopsis halleri*. New Phytologist **218**, 283–297.

Couturier J, Touraine B, Briat JF, Gaymard F, Rouhier N. 2013. The iron-sulfur cluster assembly machineries in plants: current knowledge and open questions. Frontiers in Plant Science **4**, 259.

Cumbus IP, Hornsey DJ, Robinson LW. 1977. The influence of phosphorus, zinc and manganese on absorption and translocation of iron in watercress. Plant and Soil **48**, 651–660.

Curie C, Alonso JM, Le Jean M, Ecker JR, Briat JF. 2000. Involvement of NRAMP1 from *Arabidopsis thaliana* in iron transport. The Biochemical Journal **347**, 749–755.

Curie C, Panaviene Z, Loulergue C, Dellaporta SL, Briat JF, Walker EL. 2001. Maize *yellow stripe1* encodes a membrane protein directly involved in Fe(III) uptake. Nature **409**, 346–349.

De Clerck O, Kao SM, Bogaert KA, *et al.* 2018. Insights into the evolution of multicellularity from the sea lettuce genome. Current Biology **28**, 2921–2933.e5.

Deinlein U, Weber M, Schmidt H, *et al.* 2012. Elevated nicotianamine levels in *Arabidopsis halleri* roots play a key role in zinc hyperaccumulation. The Plant Cell **24**, 708–723.

Dekock PC, Hall A, Inkson RHE. 1979. Active iron in plant leaves. Annals of Botany **43**, 737–740.

Delhaize E. 1996. A metal-accumulator mutant of *Arabidopsis thaliana*. Plant Physiology **111**, 849–855.

DiDonato RJ Jr, Roberts LA, Sanderson T, Eisley RB, Walker EL. 2004. Arabidopsis *Yellow Stripe-Like2* (*YSL2*): a metal-regulated gene encoding a plasma membrane transporter of nicotianamine-metal complexes. The Plant Journal **39**, 403–414.

Docampo R, de Souza W, Miranda K, Rohloff P, Moreno SNJ. 2005. Acidocalcisomes? Conserved from bacteria to man. Nature Reviews. Microbiology **3**, 251–261.

Dubeaux G, Neveu J, Zelazny E, Vert G. 2018. Metal sensing by the IRT1 transporter-receptor orchestrates its own degradation and plant metal nutrition. Molecular Cell **69**, 953–964.e5.

Dubeaux G, Zelazny E, Vert G. 2015. Getting to the root of plant iron uptake and cell-cell transport: Polarity matters! Communicative & Integrative Biology **8**, e1038441.

Durrett TP, Gassmann W, Rogers EE. 2007. The FRD3-mediated efflux of citrate into the root vasculature is necessary for efficient iron translocation. Plant Physiology **144**, 197–205.

Eide D, Broderius M, Fett J, Guerinot ML. 1996. A novel iron-regulated metal transporter from plants identified by functional expression in yeast. Proceedings of the National Academy of Sciences, USA **93**, 5624–5628.

Eroglu S, Meier B, von Wirén N, Peiter E. 2016. The vacuolar manganese transporter mtp8 determines tolerance to iron deficiency-induced chlorosis in Arabidopsis. Plant Physiology **170**, 1030–1045.

Escudero V, Abreu I, Tejada-Jiménez M, *et al*. 2020. *Medicago truncatula* Ferroportin2 mediates iron import into nodule symbiosomes. New Phytologist **228**, 194–209.

Evens NP, Buchner P, Williams LE, Hawkesford MJ. 2017. The role of ZIP transporters and group F bZIP transcription factors in the Zn-deficiency response of wheat (*Triticum aestivum*). The Plant Journal **92**, 291–304.

Falciatore A, d'Alcalà MR, Croot P, Bowler C. 2000. Perception of environmental signals by a marine diatom. Science **288**, 2363–2366.

Flis P, Ouerdane L, Grillet L, Curie C, Mari S, Lobinski R. 2016. Inventory of metal complexes circulating in plant fluids: a reliable method based on HPLC coupled with dual elemental and high-resolution molecular mass spectrometric detection. New Phytologist **211**, 1129–1141.

Forieri I, Wirtz M, Hell R. 2013. Toward new perspectives on the interaction of iron and sulfur metabolism in plants. Frontiers in Plant Science **4**, 357.

Foy CD, Chaney RL, White MC. 1978. The physiology of metal toxicity in plants. Annual Review of Plant Physiology **29**, 511–566.

Fukao Y, Ferjani A, Tomioka R, Nagasaki N, Kurata R, Nishimori Y, Fujiwara M, Maeshima M. 2011. iTRAQ analysis reveals mechanisms of growth defects due to excess zinc in Arabidopsis. Plant Physiology **155**, 1893–1907.

Gibson RS, Raboy V, King JC. 2018. Implications of phytate in plant-based foods for iron and zinc bioavailability, setting dietary requirements, and formulating programs and policies. Nutrition Reviews **76**, 793–804.

González-Guerrero M, Matthiadis A, Sáez Á, Long TA. 2014. Fixating on metals: new insights into the role of metals in nodulation and symbiotic nitrogen fixation. Frontiers in Plant Science **5**, 45.

Green LS, Rogers EE. 2004. FRD3 controls iron localization in Arabidopsis. Plant Physiology **136**, 2523–2531.

Grillet L, Schmidt W. 2019. Iron acquisition strategies in land plants: not so different after all. New Phytologist **224**, 11–18.

Gruber BD, Giehl RF, Friedel S, von Wirén N. 2013. Plasticity of the Arabidopsis root system under nutrient deficiencies. Plant Physiology **163**, 161–179.

Halimaa P, Blande D, Aarts MG, Tuomainen M, Tervahauta A, Kärenlampi S. 2014*a*. Comparative transcriptome analysis of the metal hyperaccumulator *Noccaea caerulescens*. Frontiers in Plant Science **5**, 213.

Halimaa P, Blande D, Baltzi E, *et al.* 2019. Transcriptional effects of cadmium on iron homeostasis differ in calamine accessions of *Noccaea caerulescens*. The Plant Journal **97**, 306–320.

Halimaa P, Lin YF, Ahonen VH, *et al.* 2014*b*. Gene expression differences between *Noccaea caerulescens* ecotypes help to identify candidate genes for metal phytoremediation. Environmental Science & Technology **48**, 3344–3353.

Hanikenne M, Bernal M, Urzica E-I. 2014. Ion homeostasis in the chloroplast. In: Theg S, Wollman FA, eds. Plastid biology. Advances in Plant Biology, vol 5. New York: Springer, 465–514.

Hanikenne M, Krämer U, Demoulin V, Baurain D. 2005*a*. A comparative inventory of metal transporters in the green alga *Chlamydomonas reinhardtii* and the red alga *Cyanidioschizon merolae*. Plant Physiology **137**, 428–446.

Hanikenne M, Merchant SS, Hamel P. 2009. Transition metal nutrition. The Chlamydomonas Sourcebook **2**, 333–399.

Hanikenne M, Motte P, Wu MCS, Wang T, Loppes R, Matagne RF. 2005*b*. A mitochondrial half-size ABC transporter is involved in cadmium tolerance in *Chlamydomonas reinhardtii*. Plant, Cell & Environment **28**, 863–873.

Hanikenne M, Nouet C. 2011. Metal hyperaccumulation and hypertolerance: a model for plant evolutionary genomics. Current Opinion in Plant Biology **14**, 252–259.

Haydon MJ, Cobbett CS. 2007*a*. Transporters of ligands for essential metal ions in plants. New Phytologist **174**, 499–506.

Haydon MJ, Cobbett CS. 2007*b*. A novel major facilitator superfamily protein at the tonoplast influences zinc tolerance and accumulation in Arabidopsis. Plant Physiology **143**, 1705–1719.

Haydon MJ, Kawachi M, Wirtz M, Hillmer S, Hell R, Krämer U. 2012. Vacuolar nicotianamine has critical and distinct roles under iron deficiency and for zinc sequestration in *Arabidopsis*. The Plant Cell **24**, 724–737.

Herbik A, Bölling C, Buckhout TJ. 2002. The involvement of a multicopper oxidase in iron uptake by the green algae *Chlamydomonas reinhardtii*. Plant Physiology **130**, 2039–2048.

Hirsch J, Marin E, Floriani M, Chiarenza S, Richaud P, Nussaume L, Thibaud MC. 2006. Phosphate deficiency promotes modification of iron distribution in *Arabidopsis* plants. Biochimie **88**, 1767–1771.

Hopkinson BM, Morel FM. 2009. The role of siderophores in iron acquisition by photosynthetic marine microorganisms. Biometals **22**, 659–669.

Howe CJ, Schlarb-Ridley BG, Wastl J, Purton S, Bendall DS. 2006. The novel cytochrome c_6 of chloroplasts: a case of evolutionary bricolage? Journal of Experimental Botany **57**, 13–22.

Inoue H, Kobayashi T, Nozoye T, Takahashi M, Kakei Y, Suzuki K, Nakazono M, Nakanishi H, Mori S, Nishizawa NK. 2009. Rice OsYSL15 is an iron-regulated iron(III)-deoxymugineic acid transporter expressed in the roots and is essential for iron uptake in early growth of the seedlings. The Journal of Biological Chemistry **284**, 3470–3479.

Inoue H, Mizuno D, Takahashi M, Nakanishi H, Mori S, Nishizawa NK. 2004. A rice *FRD3-like* (*OsFRDL1*) gene is expressed in the cells involved in long-distance transport. Soil Science and Plant Nutrition **50**, 1133–1140.

Ishimaru Y, Kakei Y, Shimo H, Bashir K, Sato Y, Sato Y, Uozumi N, Nakanishi H, Nishizawa NK. 2011. A rice phenolic efflux transporter is essential for solubilizing precipitated apoplasmic iron in the plant stele. The Journal of Biological Chemistry **286**, 24649–24655.

Ishimaru Y, Suzuki M, Ogo Y, Takahashi M, Nakanishi H, Mori S, Nishizawa NK. 2008. Synthesis of nicotianamine and deoxymugineic acid is regulated by OsIRO2 in Zn excess rice plants. Soil Science and Plant Nutrition **54**, 417–423.

Ishimaru Y, Suzuki M, Tsukamoto T, *et al.* 2006. Rice plants take up iron as an Fe^{3+}-phytosiderophore and as Fe^{2+}. The Plant Journal **45**, 335–346.

Karam MJ, Souleman D, Schvartzman MS, Gallina S, Spielmann J, Poncet C, Bouchez O, Pauwels M, Hanikenne M, Frérot H. 2019. Genetic architecture of a plant adaptive trait: QTL mapping of intraspecific variation for tolerance to metal pollution in *Arabidopsis halleri*. Heredity **122**, 877–892.

Kaur G, Shukla V, Kumar A, *et al.* 2019. Integrative analysis of hexaploid wheat roots identifies signature components during iron starvation. Journal of Experimental Botany **70**, 6141–6161.

Keeling PJ. 2013. The number, speed, and impact of plastid endosymbioses in eukaryotic evolution. Annual Review of Plant Biology **64**, 583–607.

Kellermeier F, Armengaud P, Seditas TJ, Danku J, Salt DE, Amtmann A. 2014. Analysis of the root system architecture of *Arabidopsis* provides a quantitative readout of crosstalk between nutritional signals. The Plant Cell **26**, 1480–1496.

Khan GA, Bouraine S, Wege S, Li Y, de Carbonnel M, Berthomieu P, Poirier Y, Rouached H. 2014. Coordination between zinc and phosphate

homeostasis involves the transcription factor PHR1, the phosphate exporter PHO1, and its homologue PHO1;H3 in *Arabidopsis*. Journal of Experimental Botany **65**, 871–884.

Kim DY, Bovet L, Kushnir S, Noh EW, Martinoia E, Lee Y. 2006*a*. AtATM3 is involved in heavy metal resistance in Arabidopsis. Plant Physiology **140**, 922–932.

Kim S, Takahashi M, Higuchi K, Tsunoda K, Nakanishi H, Yoshimura E, Mori S, Nishizawa NK. 2005. Increased nicotianamine biosynthesis confers enhanced tolerance of high levels of metals, in particular nickel, to plants. Plant & Cell Physiology **46**, 1809–1818.

Kim SA, Punshon T, Lanzirotti A, Li L, Alonso JM, Ecker JR, Kaplan J, Guerinot ML. 2006*b*. Localization of iron in *Arabidopsis* seed requires the vacuolar membrane transporter VIT1. Science **314**, 1295–1298.

Kisko M, Bouain N, Safi A, *et al*. 2018. LPCAT1 controls phosphate homeostasis in a zinc-dependent manner. eLife **7**, e32077.

Klatte M, Schuler M, Wirtz M, Fink-Straube C, Hell R, Bauer P. 2009. The analysis of Arabidopsis nicotianamine synthase mutants reveals functions for nicotianamine in seed iron loading and iron deficiency responses. Plant Physiology **150**, 257–271.

Kobayashi T, Nishizawa NK. 2012. Iron uptake, translocation, and regulation in higher plants. Annual Review of Plant Biology **63**, 131–152.

Kobayashi T, Nishizawa NK. 2015. Intracellular iron sensing by the direct binding of iron to regulators. Frontiers in Plant Science **6**, 155.

Kobayashi T, Nozoye T, Nishizawa NK. 2019. Iron transport and its regulation in plants. Free Radical Biology & Medicine **133**, 11–20.

Krämer U. 2010. Metal hyperaccumulation in plants. Annual Review of Plant Biology **61**, 517–534.

Krämer U, Talke IN, Hanikenne M. 2007. Transition metal transport. FEBS Letters **581**, 2263–2272.

La Fontaine S, Quinn JM, Nakamoto SS, Page MD, Göhre V, Moseley JL, Kropat J, Merchant S. 2002. Copper-dependent iron assimilation pathway in the model photosynthetic eukaryote *Chlamydomonas reinhardtii*. Eukaryotic Cell **1**, 736–757.

Lanquar V, Lelièvre F, Bolte S, *et al.* 2005. Mobilization of vacuolar iron by AtNRAMP3 and AtNRAMP4 is essential for seed germination on low iron. The EMBO Journal **24**, 4041–4051.

Lanquar V, Ramos MS, Lelièvre F, Barbier-Brygoo H, Krieger-Liszkay A, Krämer U, Thomine S. 2010. Export of vacuolar manganese by AtNRAMP3 and AtNRAMP4 is required for optimal photosynthesis and growth under manganese deficiency. Plant Physiology **152**, 1986–1999.

Lee S, An G. 2009. Over-expression of *OsIRT1* leads to increased iron and zinc accumulations in rice. Plant, Cell & Environment **32**, 408–416.

Le Jean M, Schikora A, Mari S, Briat JF, Curie C. 2005. A loss-of-function mutation in *AtYSL1* reveals its role in iron and nicotianamine seed loading. The Plant Journal **44**, 769–782.

Lelandais G, Scheiber I, Paz-Yepes J, *et al.* 2016. *Ostreococcus tauri* is a new model green alga for studying iron metabolism in eukaryotic phytoplankton. BMC Genomics **17**, 319.

Lešková A, Giehl RFH, Hartmann A, Fargašová A, von Wirén N. 2017. Heavy metals induce iron deficiency responses at different hierarchic and regulatory levels. Plant Physiology **174**, 1648–1668.

Li B, Sun L, Huang J, Göschl C, Shi W, Chory J, Busch W. 2019. GSNOR provides plant tolerance to iron toxicity via preventing iron-dependent nitrosative and oxidative cytotoxicity. Nature Communications **10**, 3896.

Li J, Liu B, Cheng F, Wang X, Aarts MG, Wu J. 2014. Expression profiling reveals functionally redundant multiple-copy genes related to zinc, iron and cadmium responses in *Brassica rapa*. New Phytologist **203**, 182–194.

Li S, Zhou X, Chen J, Chen R. 2018. Is there a strategy I iron uptake mechanism in maize? Plant Signaling & Behavior **13**, e1161877.

Li S, Zhou X, Huang Y, Zhu L, Zhang S, Zhao Y, Guo J, Chen J, Chen R. 2013. Identification and characterization of the zinc-regulated transporters, iron-regulated transporter-like protein (ZIP) gene family in maize. BMC Plant Biology **13**, 114.

Lin YF, Liang HM, Yang SY, Boch A, Clemens S, Chen CC, Wu JF, Huang JL, Yeh KC. 2009. Arabidopsis IRT3 is a zinc-regulated and plasma membrane localized zinc/iron transporter. New Phytologist **182**, 392–404.

Liu J, Tan K, He L, Qiu Y, Tan W, Guo Y, Wang Z, Sun W. 2018. Effect of limitation of iron and manganese on microalgae growth in fresh water. Microbiology **164**, 1514–1521.

López-Millán AF, Morales F, Abadía A, Abadía J. 2000. Effects of iron deficiency on the composition of the leaf apoplastic fluid and xylem sap in sugar beet. Implications for iron and carbon transport. Plant Physiology **124**, 873–884.

Maldonado MT, Allen AE, Chong JS, Lin K, Leus D, Karpenko N, Harris SL. 2006. Copper-dependent iron transport in coastal and oceanic diatoms. Limnology and Oceanography **51**, 1729–1743.

Marković T, Manzoor S, Humphreys-Williams E, Kirk GJ, Vilar R, Weiss DJ. 2017. Experimental determination of zinc isotope fractionation in complexes with the phytosiderophore 2′-deoxymugeneic acid (DMA) and its structural analogues, and implications for plant uptake mechanisms. Environmental Science & Technology **51**, 98–107.

Marschner P. 2012. Marschner's mineral nutrition of higher plants. London: Academic Press.

Marschner H, Römheld V. 1994. Strategies of plants for acquisition of iron. Plant and Soil **165**, 261–274.

Mathan KK, Amberger A. 1977. Influence of iron on the uptake of phosphorus by maize. Plant and Soil **46**, 413–422.

Meier SK, Adams N, Wolf M, Balkwill K, Muasya AM, Gehring CA, Bishop JM, Ingle RA. 2018. Comparative RNA-seq analysis of nickel hyperaccumulating and non-accumulating populations of *Senecio coronatus* (Asteraceae). The Plant Journal **95**, 1023–1038.

Merchant SS. 2007. Trace metal utilization in chloroplasts. In Wise RR, Hoober JK, eds. The structure and function of plastids. Advances in Photosynthesis and Respiration, vol 23. Dordrecht: Springer, 199–218.

Merchant SS, Allen MD, Kropat J, Moseley JL, Long JC, Tottey S, Terauchi AM. 2006. Between a rock and a hard place: trace element nutrition in *Chlamydomonas*. Biochimica et Biophysica Acta **1763**, 578–594.

Merlot S, de la Torre VSG, Hanikenne M. 2018. Physiology and molecular biology of trace element hyperaccumulation. In: Van der Ent A, Echevarria G, Baker A, Morel J, eds. Agromining: farming for metals. Mineral Resource Reviews. Cham: Springer, 93–116.

Milner MJ, Mitani-Ueno N, Yamaji N, Yokosho K, Craft E, Fei Z, Ebbs S, Clemencia Zambrano M, Ma JF, Kochian LV. 2014. Root and shoot transcriptome analysis of two ecotypes of *Noccaea caerulescens* uncovers the role of NcNramp1 in Cd hyperaccumulation. The Plant Journal **78**, 398–410.

Misson J, Raghothama KG, Jain A, *et al.* 2005. A genome-wide transcriptional analysis using *Arabidopsis thaliana* Affymetrix gene chips determined plant responses to phosphate deprivation. Proceedings of the National Academy of Sciences, USA **102**, 11934–11939.

Molins H, Michelet L, Lanquar V, Agorio A, Giraudat J, Roach T, Krieger-Liszkay A, Thomine S. 2013. Mutants impaired in vacuolar metal mobilization identify chloroplasts as a target for cadmium hypersensitivity in *Arabidopsis thaliana*. Plant, Cell & Environment **36**, 804–817.

Mora-Macías J, Ojeda-Rivera JO, Gutiérrez-Alanís D, Yong-Villalobos L, Oropeza-Aburto A, Raya-González J, Jiménez-Domínguez G, Chávez-Calvillo G, Rellán-Álvarez R, Herrera-Estrella L. 2017. Malate-dependent Fe accumulation is a critical checkpoint in the root developmental response to low phosphate. Proceedings of the National Academy of Sciences, USA **114**, E3563–E3572.

Morel M, Crouzet J, Gravot A, Auroy P, Leonhardt N, Vavasseur A, Richaud P. 2009. AtHMA3, a P1B-ATPase allowing Cd/Zn/Co/Pb vacuolar storage in Arabidopsis. Plant Physiology **149**, 894–904.

Morrissey J, Baxter IR, Lee J, Li L, Lahner B, Grotz N, Kaplan J, Salt DE, Guerinot ML. 2009. The ferroportin metal efflux proteins function in iron and cobalt homeostasis in *Arabidopsis*. The Plant Cell **21**, 3326–3338.

Morrissey J, Bowler C. 2012. Iron utilization in marine cyanobacteria and eukaryotic algae. Frontiers in Microbiology **3**, 43.

Morrissey J, Guerinot ML. 2009. Iron uptake and transport in plants: the good, the bad, and the ionome. Chemical Reviews **109**, 4553–4567.

Morrissey J, Sutak R, Paz-Yepes J, *et al.* 2015. A novel protein, ubiquitous in marine phytoplankton, concentrates iron at the cell surface and facilitates uptake. Current Biology **25**, 364–371.

Moseley JL, Chang CW, Grossman AR. 2006. Genome-based approaches to understanding phosphorus deprivation responses and PSR1 control in *Chlamydomonas reinhardtii*. Eukaryotic Cell **5**, 26–44.

Müller R, Morant M, Jarmer H, Nilsson L, Nielsen TH. 2007. Genome-wide analysis of the Arabidopsis leaf transcriptome reveals interaction of phosphate and sugar metabolism. Plant Physiology **143**, 156–171.

Mus F, Crook MB, Garcia K, *et al.* 2016. Symbiotic nitrogen fixation and the challenges to its extension to nonlegumes. Applied and Environmental Microbiology **82**, 3698–3710.

Nakanishi H, Ogawa I, Ishimaru Y, Mori S, Nishizawa NK. 2006. Iron deficiency enhances cadmium uptake and translocation mediated by the Fe^{2+} transporters OsIRT1 and OsIRT2 in rice. Soil Science and Plant Nutrition **52**, 464–469.

Nishida S, Tsuzuki C, Kato A, Aisu A, Yoshida J, Mizuno T. 2011. AtIRT1, the primary iron uptake transporter in the root, mediates excess nickel accumulation in *Arabidopsis thaliana*. Plant & Cell Physiology **52**, 1433–1442.

Nouet C, Motte P, Hanikenne M. 2011. Chloroplastic and mitochondrial metal homeostasis. Trends in Plant Science **16**, 395–404.

Nozoye T, Nagasaka S, Kobayashi T, Sato Y, Uozumi N, Nakanishi H, Nishizawa NK. 2015. The phytosiderophore efflux transporter TOM2 is involved in metal transport in rice. The Journal of Biological Chemistry **290**, 27688–27699.

Nozoye T, Nagasaka S, Kobayashi T, Takahashi M, Sato Y, Sato Y, Uozumi N, Nakanishi H, Nishizawa NK. 2011. Phytosiderophore efflux transporters are crucial for iron acquisition in graminaceous plants. The Journal of Biological Chemistry **286**, 5446–5454.

Nozoye T, von Wirén N, Sato Y, Higashiyama T, Nakanishi H, Nishizawa NK. 2019. Characterization of the nicotianamine exporter ENA1 in rice. Frontiers in Plant Science **10**, 502.

Oomen RJ, Wu J, Lelièvre F, Blanchet S, Richaud P, Barbier-Brygoo H, Aarts MG, Thomine S. 2009. Functional characterization of NRAMP3 and NRAMP4 from the metal hyperaccumulator *Thlaspi caerulescens*. New Phytologist **181**, 637–650.

Pal S, Kisko M, Dubos C, Lacombe B, Berthomieu P, Krouk G, Rouached H. 2017. TransDetect identifies a new regulatory module controlling phosphate accumulation. Plant Physiology **175**, 916–926.

Paolacci AR, Celletti S, Catarcione G, Hawkesford MJ, Astolfi S, Ciaffi M. 2014. Iron deprivation results in a rapid but not sustained increase of the expression of genes involved in iron metabolism and sulfate uptake in tomato (*Solanum lycopersicum* L.) seedlings. Journal of Integrative Plant Biology **56**, 88–100.

Paz Y, Katz A, Pick U. 2007. A multicopper ferroxidase involved in iron binding to transferrins in *Dunaliella salina* plasma membranes. The Journal of Biological Chemistry **282**, 8658–8666.

Pedas P, Ytting CK, Fuglsang AT, Jahn TP, Schjoerring JK, Husted S. 2008. Manganese efficiency in barley: identification and characterization of the metal ion transporter HvIRT1. Plant Physiology **148**, 455–466.

Penen F, Isaure MP, Dobritzsch D, Bertalan I, Castillo-Michel H, Proux O, Gontier E, Le Coustumer P, Schaumlöffel D. 2017. Pools of cadmium in *Chlamydomonas reinhardtii* revealed by chemical imaging and XAS spectroscopy. Metallomics **9**, 910–923.

Pianelli K, Mari S, Marquès L, Lebrun M, Czernic P. 2005. Nicotianamine over-accumulation confers resistance to nickel in *Arabidopsis thaliana*. Transgenic Research **14**, 739–748.

Pilon M. 2017. The copper microRNAs. New Phytologist **213**, 1030–1035.

Pineau C, Loubet S, Lefoulon C, Chalies C, Fizames C, Lacombe B, Ferrand M, Loudet O, Berthomieu P, Richard O. 2012. Natural variation at the *FRD3* MATE transporter locus reveals cross-talk between Fe homeostasis and Zn tolerance in *Arabidopsis thaliana*. PLoS Genetics **8**, e1003120.

Pottier M, Dumont J, Masclaux-Daubresse C, Thomine S. 2019. Autophagy is essential for optimal translocation of iron to seeds in Arabidopsis. Journal of Experimental Botany **70**, 859–869.

Pottier M, Masclaux-Daubresse C, Yoshimoto K, Thomine S. 2014. Autophagy as a possible mechanism for micronutrient remobilization from leaves to seeds. Frontiers in Plant Science **5**, 11.

Prasanna R, Kaushik BD. 2010. Evolutionary relationships among cyanobacteria, algae and plants: Revisited in the light of Darwinism. In: Sharma VP, eds. Nature at work: ongoing saga of evolution. New Delhi: Springer, 119–140.

Ptashnyk M, Roose T, Jones DL, Kirk GJ. 2011. Enhanced zinc uptake by rice through phytosiderophore secretion: a modelling study. Plant, Cell & Environment **34**, 2038–2046.

Qiu Y, Wang Z, Liu F, Wu Z, Chen H, Tang D, Liu J. 2020. Effect of complex iron on the phosphorus absorption by two freshwater algae. Environmental Technology, doi: 10.1080/09593330.2020.1745294.

Raven JA. 1988. The iron and molybdenum use efficiencies of plant growth with different energy, carbon and nitrogen sources. New Phytologist **109**, 279–287.

Remy E, Cabrito TR, Batista RA, Hussein MA, Teixeira MC, Athanasiadis A, Sá-Correia I, Duque P. 2014. Intron retention in the 5′UTR of the novel ZIF2 transporter enhances translation to promote zinc tolerance in *Arabidopsis*. PLoS Genetics **10**, e1004375.

Ricachenevsky FK, Menguer PK, Sperotto RA, Fett JP. 2015. Got to hide your Zn away: Molecular control of Zn accumulation and biotechnological applications. Plant Science **236**, 1–17.

Robinson NJ, Procter CM, Connolly EL, Guerinot ML. 1999. A ferric-chelate reductase for iron uptake from soils. Nature **397**, 694–697.

Rodríguez-Celma J, Chou H, Kobayashi T, Long TA, Balk J. 2019. Hemerythrin E3 ubiquitin ligases as negative regulators of iron homeostasis in plants. Frontiers in Plant Science **10**, 98.

Rogers EE, Guerinot ML. 2002. FRD3, a member of the multidrug and toxin efflux family, controls iron deficiency responses in Arabidopsis. The Plant Cell **14**, 1787–1799.

Roschzttardtz H, Grillet L, Isaure MP, Conéjéro G, Ortega R, Curie C, Mari S. 2011. Plant cell nucleolus as a hot spot for iron. The Journal of Biological Chemistry **286**, 27863–27866.

Rouached H, Rhee SY. 2017. System-level understanding of plant mineral nutrition in the big data era. Current Opinion in Systems Biology **4**, 71–77.

Rubio V, Linhares F, Solano R, Martín AC, Iglesias J, Leyva A, Paz-Ares J. 2001. A conserved MYB transcription factor involved in phosphate starvation signaling both in vascular plants and in unicellular algae. Genes & Development **15**, 2122–2133.

Ryan P, Delhaize E, Jones D. 2001. Function and mechanism of organic anion exudation from plant roots. Annual Review of Plant Physiology and Plant Molecular Biology **52**, 527–560.

Saenchai C, Bouain N, Kisko M, Prom-U-Thai C, Doumas P, Rouached H. 2016. The involvement of OsPHO1;1 in the regulation of iron transport through integration of phosphate and zinc deficiency signaling. Frontiers in Plant Science **7**, 396.

Santi S, Schmidt W. 2009. Dissecting iron deficiency-induced proton extrusion in Arabidopsis roots. New Phytologist **183**, 1072–1084.

Sarret G, Saumitou-Laprade P, Bert V, Proux O, Hazemann JL, Traverse A, Marcus MA, Manceau A. 2002. Forms of zinc accumulated in the hyperaccumulator *Arabidopsis halleri*. Plant Physiology **130**, 1815–1826.

Satbhai SB, Setzer C, Freynschlag F, Slovak R, Kerdaffrec E, Busch W. 2017. Natural allelic variation of *FRO2* modulates *Arabidopsis* root growth under iron deficiency. Nature Communications **8**, 15603.

Schaaf G, Honsbein A, Meda AR, Kirchner S, Wipf D, von Wirén N. 2006. *AtIREG2* encodes a tonoplast transport protein involved in iron-dependent nickel detoxification in *Arabidopsis thaliana* roots. The Journal of Biological Chemistry **281**, 25532–25540.

Schaaf G, Ludewig U, Erenoglu BE, Mori S, Kitahara T, von Wirén N. 2004. ZmYS1 functions as a proton-coupled symporter for phytosiderophore- and nicotianamine-chelated metals. The Journal of Biological Chemistry **279**, 9091–9096.

Schaaf G, Schikora A, Häberle J, Vert G, Ludewig U, Briat JF, Curie C, von Wirén N. 2005. A putative function for the *Arabidopsis* Fe-phytosiderophore transporter homolog AtYSL2 in Fe and Zn homeostasis. Plant & Cell Physiology **46**, 762–774.

Schaedler TA, Thornton JD, Kruse I, Schwarzländer M, Meyer AJ, van Veen HW, Balk J. 2014. A conserved mitochondrial ATP-binding cassette transporter exports glutathione polysulfide for cytosolic metal cofactor assembly. The Journal of Biological Chemistry **289**, 23264–23274.

Scheepers M, Spielmann J, Boulanger M, Carnol M, Bosman B, De Pauw E, Goormaghtigh E, Motte P, Hanikenne M. 2020. Intertwined metal homeostasis, oxidative and biotic stress responses in the Arabidopsis *frd3* mutant. The Plant Journal **102**, 34–52.

Schoffman H, Lis H, Shaked Y, Keren N. 2016. Iron-nutrient interactions within phytoplankton. Frontiers in Plant Science **7**, 1223.

Schuler M, Keller A, Backes C, Philippar K, Lenhof HP, Bauer P. 2011. Transcriptome analysis by GeneTrail revealed regulation of functional categories in response to alterations of iron homeostasis in *Arabidopsis thaliana*. BMC Plant Biology **11**, 87.

Schuler M, Rellán-Álvarez R, Fink-Straube C, Abadía J, Bauer P. 2012. Nicotianamine functions in the phloem-based transport of iron to sink organs, in pollen development and pollen tube growth in *Arabidopsis*. The Plant Cell **24**, 2380–2400.

Schvartzman MS, Corso M, Fataftah N, Scheepers M, Nouet C, Bosman B, Carnol M, Motte P, Verbruggen N, Hanikenne M. 2018. Adaptation to high zinc depends on distinct mechanisms in metallicolous populations of *Arabidopsis halleri*. New Phytologist **218**, 269–282.

Shahzad Z, Eaglesfield R, Carr C, Amtmann A. 2020. Cryptic variation in RNA-directed DNA-methylation controls lateral root development when auxin signalling is perturbed. Nature Communications **11**, 218.

Shahzad Z, Rouached H, Rakha A. 2014. Combating mineral malnutrition through iron and zinc biofortification of cereals. Comprehensive Reviews in Food Science and Food Safety **13**, 329–346.

Shanmugam V, Lo JC, Wu CL, Wang SL, Lai CC, Connolly EL, Huang JL, Yeh KC. 2011. Differential expression and regulation of iron-regulated metal transporters in *Arabidopsis halleri* and *Arabidopsis thaliana* – the role in zinc tolerance. New Phytologist **190**, 125–137.

Shanmugam V, Lo JC, Yeh KC. 2013. Control of Zn uptake in *Arabidopsis halleri*: a balance between Zn and Fe. Frontiers in Plant Science **4**, 281.

Shanmugam V, Tsednee M, Yeh KC. 2012. ZINC TOLERANCE INDUCED BY IRON 1 reveals the importance of glutathione in the cross-homeostasis between zinc and iron in *Arabidopsis thaliana*. The Plant Journal **69**, 1006–1017.

Shi R, Melzer M, Zheng S, Benke A, Stich B, von Wirén N. 2018. Iron retention in root hemicelluloses causes genotypic variability in the tolerance to iron deficiency-induced chlorosis in maize. Frontiers in Plant Science **9**, 557.

Shikanai T, Müller-Moulé P, Munekage Y, Niyogi KK, Pilon M. 2003. PAA1, a P-type ATPase of Arabidopsis, functions in copper transport in chloroplasts. The Plant Cell **15**, 1333–1346.

Shinozaki D, Merkulova EA, Naya L, Horie T, Kanno Y, Seo M, Ohsumi Y, Masclaux-Daubresse C, Yoshimoto K. 2020. Autophagy increases zinc bioavailability to avoid light-mediated reactive oxygen species production under zinc deficiency. Plant Physiology **182**, 1284–1296.

Sinclair SA, Krämer U. 2012. The zinc homeostasis network of land plants. Biochimica et Biophysica Acta **1823**, 1553–1567.

Smetacek V, Klaas C, Strass VH, *et al.* 2012. Deep carbon export from a Southern Ocean iron-fertilized diatom bloom. Nature **487**, 313–319.

Spijkerman E, Behrend H, Fach B, Gaedke U. 2018. Decreased phosphorus incorporation explains the negative effect of high iron concentrations in the green microalga *Chlamydomonas acidophila*. The Science of the Total Environment **626**, 1342–1349.

Stohs SJ, Bagchi D. 1995. Oxidative mechanisms in the toxicity of metal ions. Free Radical Biology & Medicine **18**, 321–336.

Strzepek RF, Harrison PJ. 2004. Photosynthetic architecture differs in coastal and oceanic diatoms. Nature **431**, 689–692.

Sunda WG. 2012. Feedback interactions between trace metal nutrients and phytoplankton in the ocean. Frontiers in Microbiology **3**, 204.

Sunda WG, Swift DG, Huntsman SA. 1991. Low iron requirement for growth in oceanic phytoplankton. Nature **351**, 55–57.

Suzuki M, Takahashi M, Tsukamoto T, *et al.* 2006. Biosynthesis and secretion of mugineic acid family phytosiderophores in zinc-deficient barley. The Plant Journal **48**, 85–97.

Suzuki M, Tsukamoto T, Inoue H, Watanabe S, Matsuhashi S, Takahashi M, Nakanishi H, Mori S, Nishizawa NK. 2008. Deoxymugineic acid increases Zn translocation in Zn-deficient rice plants. Plant Molecular Biology **66**, 609–617.

Takahashi R, Ishimaru Y, Nakanishi H, Nishizawa NK. 2011*a*. Role of the iron transporter OsNRAMP1 in cadmium uptake and accumulation in rice. Plant Signaling & Behavior **6**, 1813–1816.

Takahashi R, Ishimaru Y, Senoura T, Shimo H, Ishikawa S, Arao T, Nakanishi H, Nishizawa NK. 2011*b*. The OsNRAMP1 iron transporter is involved in Cd accumulation in rice. Journal of Experimental Botany **62**, 4843–4850.

Talke IN, Hanikenne M, Krämer U. 2006. Zinc-dependent global transcriptional control, transcriptional deregulation, and higher gene copy number for genes in metal homeostasis of the hyperaccumulator *Arabidopsis halleri*. Plant Physiology **142**, 148–167.

Tan YF, O'Toole N, Taylor NL, Millar AH. 2010. Divalent metal ions in plant mitochondria and their role in interactions with proteins and oxidative stress-induced damage to respiratory function. Plant Physiology **152**, 747–761.

Terry N, Abadia J. 1986. Function of iron in chloroplasts. Journal of Plant Nutrition **9**, 609–646.

Teschner J, Lachmann N, Schulze J, Geisler M, Selbach K, Santamaria-Araujo J, Balk J, Mendel RR, Bittner F. 2010. A novel role for *Arabidopsis* mitochondrial ABC transporter ATM3 in molybdenum cofactor biosynthesis. The Plant Cell **22**, 468–480.

Thibaud MC, Arrighi JF, Bayle V, Chiarenza S, Creff A, Bustos R, Paz-Ares J, Poirier Y, Nussaume L. 2010. Dissection of local and systemic transcriptional responses to phosphate starvation in Arabidopsis. The Plant Journal **64**, 775–789.

Thomine S, Vert G. 2013. Iron transport in plants: better be safe than sorry. Current Opinion in Plant Biology **16**, 322–327.

Thomine S, Wang R, Ward JM, Crawford NM, Schroeder JI. 2000. Cadmium and iron transport by members of a plant metal transporter family in *Arabidopsis* with homology to *Nramp* genes. Proceedings of the National Academy of Sciences, USA **97**, 4991–4996.

Ticconi CA, Lucero RD, Sakhonwasee S, Adamson AW, Creff A, Nussaume L, Desnos T, Abel S. 2009. ER-resident proteins PDR2 and LPR1 mediate the developmental response of root meristems to phosphate availability. Proceedings of the National Academy of Sciences, USA **106**, 14174–14179.

Tsednee M, Castruita M, Salomé PA, *et al.* 2019. Manganese co-localizes with calcium and phosphorus in *Chlamydomonas* acidocalcisomes and is mobilized in manganese-deficient conditions. The Journal of Biological Chemistry **294**, 17626–17641.

Uraguchi S, Weber M, Clemens S. 2019. Elevated root nicotianamine concentrations are critical for Zn hyperaccumulation across diverse edaphic environments. Plant, Cell & Environment **42**, 2003–2014.

Urzica EI, Casero D, Yamasaki H, *et al.* 2012. Systems and trans-system level analysis identifies conserved iron deficiency responses in the plant lineage. The Plant Cell **24**, 3921–3948.

van de Mortel JE, Almar Villanueva L, Schat H, Kwekkeboom J, Coughlan S, Moerland PD, Ver Loren van Themaat E, Koornneef M, Aarts MGM. 2006. Large expression differences in genes for iron and zinc homeostasis, stress response, and lignin biosynthesis distinguish roots

of *Arabidopsis thaliana* and the related metal hyperaccumulator *Thlaspi caerulescens*. Plant Physiology **142**, 1127–1147.

Vert G, Barberon M, Zelazny E, Séguéla M, Briat JF, Curie C. 2009. *Arabidopsis* IRT2 cooperates with the high-affinity iron uptake system to maintain iron homeostasis in root epidermal cells. Planta **229**, 1171–1179.

Vert G, Grotz N, Dédaldéchamp F, Gaymard F, Guerinot ML, Briat JF, Curie C. 2002. IRT1, an Arabidopsis transporter essential for iron uptake from the soil and for plant growth. The Plant Cell **14**, 1223–1233.

Vigani G, Hanikenne M. 2018. Metal homeostasis in plant mitochondria. Annual Plant Reviews Online **50**, 111–142.

von Wirén N, Klair S, Bansal S, Briat JF, Khodr H, Shioiri T, Leigh RA, Hider RC. 1999. Nicotianamine chelates both FeIII and FeII. Implications for metal transport in plants. Plant Physiology **119**, 1107–1114.

von Wirén N, Marschner H, Romheld V. 1996. Roots of iron-efficient maize also absorb phytosiderophore-chelated zinc. Plant Physiology **111**, 1119–1125.

Wairich A, de Oliveira BHN, Arend EB, Duarte GL, Ponte LR, Sperotto RA, Ricachenevsky FK, Fett JP. 2019. The Combined Strategy for iron uptake is not exclusive to domesticated rice (*Oryza sativa*). Scientific Reports **9**, 16144.

Ward JT, Lahner B, Yakubova E, Salt DE, Raghothama KG. 2008. The effect of iron on the primary root elongation of Arabidopsis during phosphate deficiency. Plant Physiology **147**, 1181–1191.

Waters BM, Chu HH, Didonato RJ, Roberts LA, Eisley RB, Lahner B, Salt DE, Walker EL. 2006. Mutations in Arabidopsis *yellow stripe-like1* and *yellow stripe-like3* reveal their roles in metal ion homeostasis and loading of metal ions in seeds. Plant Physiology **141**, 1446–1458.

Waters BM, McInturf SA, Stein RJ. 2012. Rosette iron deficiency transcript and microRNA profiling reveals links between copper and iron homeostasis in *Arabidopsis thaliana*. Journal of Experimental Botany **63**, 5903–5918.

Weber M, Harada E, Vess C, Roepenack-Lahaye Ev, Clemens S. 2004. Comparative microarray analysis of *Arabidopsis thaliana* and *Arabidopsis halleri* roots identifies nicotianamine synthase, a ZIP transporter and other genes as potential metal hyperaccumulation factors. The Plant Journal **37**, 269–281.

Willems G, Frérot H, Gennen J, Salis P, Saumitou-Laprade P, Verbruggen N. 2010. Quantitative trait loci analysis of mineral element concentrations in an *Arabidopsis halleri* × *Arabidopsis lyrata petraea* F_2 progeny grown on cadmium-contaminated soil. New Phytologist **187**, 368–379.

Wu H, Ling HQ. 2019. FIT-binding proteins and their functions in the regulation of Fe homeostasis. Frontiers in Plant Science **10**, 844.

Wykoff DD, Grossman AR, Weeks DP, Usuda H, Shimogawara K. 1999. Psr1, a nuclear localized protein that regulates phosphorus metabolism in *Chlamydomonas*. Proceedings of the National Academy of Sciences, USA **96**, 15336–15341.

Yang TJ, Lin WD, Schmidt W. 2010. Transcriptional profiling of the Arabidopsis iron deficiency response reveals conserved transition metal homeostasis networks. Plant Physiology **152**, 2130–2141.

Yokosho K, Yamaji N, Ma JF. 2016. *OsFRDL1* expressed in nodes is required for distribution of iron to grains in rice. Journal of Experimental Botany **67**, 5485–5494.

Yokosho K, Yamaji N, Ueno D, Mitani N, Ma JF. 2009. OsFRDL1 is a citrate transporter required for efficient translocation of iron in rice. Plant Physiology **149**, 297–305.

Yoneyama T, Ishikawa S, Fujimaki S. 2015. Route and regulation of zinc, cadmium, and iron transport in rice plants (*Oryza sativa* L.) during vegetative growth and grain filling: metal transporters, metal speciation, grain Cd reduction and Zn and Fe biofortification. International Journal of Molecular sciences **16**, 19111–19129.

Zargar SM, Kurata R, Inaba S, Oikawa A, Fukui R, Ogata Y, Agrawal GK, Rakwal R, Fukao Y. 2015. Quantitative proteomics of *Arabidopsis* shoot microsomal proteins reveals a cross-talk between excess zinc and iron deficiency. Proteomics **15**, 1196–1201.

Zhang Y, Xu YH, Yi HY, Gong JM. 2012. Vacuolar membrane transporters OsVIT1 and OsVIT2 modulate iron translocation between flag leaves and seeds in rice. The Plant Journal **72**, 400–410.

Zuchi S, Cesco S, Varanini Z, Pinton R, Astolfi S. 2009. Sulphur deprivation limits Fe-deficiency responses in tomato plants. Planta **230**, 85–94.

Zuchi S, Watanabe M, Hubberten H-M, *et al*. 2015. The interplay between sulfur and iron nutrition in tomato. Plant Physiology **169**, 2624–2639.